

**AN ANALYSIS OF SEASONAL THUNDERSTORM
CLOUD DISTRIBUTION AND ITS RELATION TO
RAINFALL OCCURRENCE IN THAILAND
USING REMOTELY-SENSED DATA**

Pornthip Bumrungklang

**A Thesis Submitted in Partial Fulfillment of the Requirements for the
Degree of Doctor of Philosophy in Geoinformatics
Suranaree University of Technology
Academic Year 2008**

การวิเคราะห์การกระจายตัวของเมฆพายุฟ้าคะนองตามฤดูกาล
และความสัมพันธ์กับการเกิดฝนในประเทศไทย
โดยใช้ข้อมูลจากการสำรวจระยะไกล

นางสาวพรทิพย์ บำรุงกลาง

วิทยานิพนธ์นี้เป็นส่วนหนึ่งของการศึกษาตามหลักสูตรปริญญาวิทยาศาสตรดุษฎีบัณฑิต
สาขาวิชาภูมิสารสนเทศ
มหาวิทยาลัยเทคโนโลยีสุรนารี
ปีการศึกษา 2551

**AN ANALYSIS OF SEASONAL THUNDERSTORM CLOUD
DISTRIBUTION AND ITS RELATION TO RAINFALL
OCCURRENCE IN THAILAND
USING REMOTELY-SENSED DATA**

Suranaree University of Technology has approved this thesis submitted in partial fulfillment of the requirements for a Degree of Doctor of Philosophy.

Thesis Examining Committee

(Asst. Prof. Dr. Sunya Sarapirome)

Chairperson

(Asst. Prof. Dr. Songkot Dasananda)

Member (Thesis Advisor)

(Dr. Dusadee Sukawat)

Member

(Assoc. Prof. Dr. Kaew Nualchawee)

Member

(Dr. Surachai Ratanasermpong)

Member

(Prof. Dr. Pairote Sattayatham)

Vice Rector for Academic Affairs

(Assoc. Prof. Dr. Prapan Manyam)

Dean of Institute of Science

พรทิพย์ บำรุงกลาง : การวิเคราะห์การกระจายตัวของเมฆพายุฟ้าคะนองตามฤดูกาล และความสัมพันธ์กับการเกิดฝนในประเทศไทย โดยใช้ข้อมูลจากการสำรวจระยะไกล (AN ANALYSIS OF SEASONAL THUNDERSTORM CLOUD DISTRIBUTION AND ITS RELATION TO RAINFALL OCCURRENCE IN THAILAND USING REMOTELY-SENSED DATA) อาจารย์ที่ปรึกษา : ผู้ช่วยศาสตราจารย์ ดร.ทรงกิต ทัศนานนท์, 179 หน้า.

วัตถุประสงค์หลักของการศึกษานี้ คือการวิเคราะห์ความสัมพันธ์ระหว่างความรุนแรงของฝนและคุณสมบัติของเมฆที่เกี่ยวข้อง คืออุณหภูมิยอดเมฆ (Cloud top temperature: CTT) และพื้นที่ของเมฆในประเทศไทย อิงตามบางกรณีศึกษาที่เลือกมาระหว่างปี ค.ศ. 2006 และปี ค.ศ. 2007 นอกจากนี้ แผนที่เมฆที่จำแนกได้ยังถูกใช้ในการวิเคราะห์การกระจายตัวตามฤดูกาลของเมฆและฝนระหว่างปีที่เลือกมาด้วย

เพื่อช่วยในการสร้างแผนที่อุณหภูมิยอดเมฆที่มีประสิทธิภาพ ได้มีการพัฒนาแบบจำลองเพื่อการจำแนกเมฆโดยอัตโนมัติสำหรับภาพช่วงอินฟราเรดความร้อนของดาวเทียม MTSAT-1R ขึ้น และใช้เป็นเครื่องมือหลักในการจัดทำแผนที่อุณหภูมิยอดเมฆในการศึกษาครั้งนี้ และเพื่อลดแนวโน้มของความสับสนระหว่างเมฆระดับบนและเมฆฝน (คิวโมโลนิมบัส) เมฆระดับบนจึงถูกกรองออกก่อนเป็นลำดับแรก โดยใช้เทคนิค Split-window ภายใต้เงื่อนไขของค่าวิกฤติที่กำหนดให้แผนที่อุณหภูมิยอดเมฆ (Cloud top temperature map) ที่จำแนกได้ จะรวมเมฆทุกชนิดที่มีอุณหภูมิยอดเมฆต่ำกว่า 10°C เอาไว้ ดังนั้นเมฆอุ่นและเมฆเย็นเกือบทั้งหมดจึงถูกแสดงไว้บนแผนที่ที่ได้รับดังกล่าว

การวิเคราะห์การกระจายตัวของเมฆตามฤดูกาลและปริมาณฝน บ่งชี้ว่ารูปแบบการกระจายตัวของเมฆเป็นผลมาจากการกระทำของปัจจัยกระตุ้นหลักหลายตัวรวมกัน โดยในฤดูร้อนปัจจัยดังกล่าว คือระบบการพาความร้อนระดับท้องถิ่น มวลอากาศเย็น ร่องมรสุม กระแสลมตะวันตก และบริเวณความกดอากาศต่ำจากมหาสมุทร สำหรับในฤดูฝนคือ ร่องมรสุม ลมมรสุมตะวันตกเฉียงใต้ พายุหมุนเขตร้อน และบริเวณความกดอากาศต่ำจากมหาสมุทร ส่วนในฤดูหนาวคือ มวลอากาศเย็น ลมมรสุมตะวันออกเฉียงเหนือ (สำหรับภาคใต้) และ ระบบการพาความร้อนระดับท้องถิ่น

การวิเคราะห์ความสัมพันธ์ระหว่างปริมาณฝนที่ตรวจวัดได้รายวันทั่วประเทศ และอุณหภูมิยอดเมฆที่สอดคล้องกัน บ่งชี้ว่าความสัมพันธ์ระหว่างปริมาณฝนและอุณหภูมิยอดเมฆที่ตรวจวัดได้จากสถานีตรวจวัด 116 สถานี ไม่ปรากฏรูปแบบที่เด่นชัดมากนัก โดยค่าสหสัมพันธ์สูงสุดที่ได้คือ 0.6277 ซึ่งพบในช่วงฤดูฝน ส่วนในฤดูร้อนและฤดูหนาว ระดับค่าสหสัมพันธ์จะค่อนข้างต่ำ (น้อยกว่า 0.5) ซึ่งหมายความว่า ค่าอุณหภูมิยอดเมฆเพียงประการเดียว ไม่เพียงพอในการเป็นตัวบ่งบอกปริมาณฝนที่ตรวจวัดได้ในแต่ละวัน

นอกจากนั้น ยังเห็นได้ชัดจากการศึกษาว่า ค่าสหสัมพันธ์ของปริมาณฝนรายวันและปริมาณของพื้นที่เมฆรายวันปรากฏอยู่ในระดับสูง โดยมี $r^2 > 0.8$ ในทุกกรณี โดยเฉพาะกับฝนที่ตกหนัก (ตัวอย่างเช่น > 80 mm) หรือในวันที่ลูกเห็บเกิดขึ้น (มีค่า $r^2 = 0.8915$)

สาขาวิชาการรับรู้จากระยะไกล
ปีการศึกษา 2551

ลายมือชื่อนักศึกษา _____
ลายมือชื่ออาจารย์ที่ปรึกษา _____
ลายมือชื่ออาจารย์ที่ปรึกษาร่วม _____

PORNTHIP BUMRUNGKLANG : AN ANALYSIS OF SEASONAL
THUNDERSTORM CLOUD DISTRIBUTION AND ITS RELATION TO
RAINFALL OCCURRENCE IN THAILAND USING REMOTELY-SENSED
DATA. THESIS ADVISOR : ASST. PROF. SONGKOT DASANANDA, Ph.D.
179 PP.

SATELLITE CLOUD CLASSIFICATION/ THUNDERSTORM CLOUD
DISTRIBUTION/ ESTIMATE RAINFALL/ MTSAT-1R/ SPLIT WINDOWS

The main objective of this study is to analyze the relationship between rainfall intensity and the associated cloud properties which are cloud top temperature (CTT) and cloud cover in Thailand based on some selected case studies during years 2006 and 2007. In addition, the classified cloud data were also applied to the investigation of seasonal cloud and rainfall distribution during those specified years.

To assist the efficient derivation of cloud top temperature maps, the automatic cloud classification model for the TIR images of MTSAT-1R satellite was developed and applied as main tool for CTT mapping in the study. And to reduce possible confusion between high clouds and rain clouds (cumulonimbus), the high clouds were filtered off first using split-window technique under the given thresholds. The classified CTT maps include all clouds with CTT less than 10°C and, as a consequence, most warm clouds and cold clouds are depicted on the obtained maps.

The analysis of seasonal cloud and rainfall distribution indicates that patterns of their distribution in Thailand are product of the combined effects among several main driving factors. In summer, these are the local convective system, the cold airmass, the monsoon trough, the westerly wind, and the low pressure area from the ocean. In rainy

season, these are the monsoon trough, the southwest monsoon, the tropical cyclone and low pressure area from the ocean. And in winter, these are the cold air mass, northeast monsoon (for the south), and local convection.

The analysis on relationship between daily measured rainfall across the country and the corresponding cloud top temperature indicated that the relationships between rainfall amount from 116 rain-gauge stations and observed CTT found still did not exhibit a clear pattern where the highest correlation of 0.6277 was seen in rainy season but in summer and winter, the correlation level was still rather low (less than 0.5). This means the CTT value alone cannot be used as sole indicator of the rainfall amount observed each day.

In addition, it was clearly seen from the study that amount of total daily rainfall has high correlation with the amount of cloud cover area seen each day, with $r^2 > 0.8$ in all cases especially heavy rainfall (e.g. > 80 mm) or on the hail days (with $r^2 = 0.8915$).

School of Remote Sensing

Academic Year 2008

Student's Signature _____

Advisor's Signature _____

Co-advisor's Signature _____

ACKNOWLEDGEMENTS

Completing a Remote Sensing Ph.D. thesis was a challenging task, but working on an interesting topic was enjoyable. Numerous people who have contributed to the studies are described here. I would like to thank all people who made this thesis possible. My last remaining task is to acknowledge all these people that have contributed to the work described in this thesis. This could be an impossible task without any help from them to design, implement, apply, criticize, and sponsor my work. I am going to try anyway, and if your name is not listed, rest assured that my gratitude is not less than for those listed below.

Foremost, it is difficult to overstate my gratitude to my Ph.D. advisor, Assistant Professor Dr. Songkot Dasananda. With his enthusiasm, his inspiration, and his great efforts to explain things clearly and simply, he made Remote Sensing an enjoyable subject for me. Throughout my thesis writing period, he provided encouragement, sound advice, good teaching, fine companionship, and lot of excellent ideas. His adjustment on my research methods helped this study more valuable. He also helped me a lot to review and have been adjusted this dissertation. He's great. I would have been lost without him.

My deepest gratitude to my co-advisor, Dr. Dusadee Sukawat from whom I learn to design experiments in a scientific way, to present data in a logical way, and to write papers in a precise way. His suggestions and guidance have encouraged me throughout the study. I am very much appreciated for his supervision, discussion, supports and understanding in various aspects. He taught me a lot about meteorology and had me interested in this research topic. He has been actively interested in my work and has been

available to advise me. I am grateful for his patience, motivation, enthusiasm, and immense knowledge in meteorology and implementation of satellite data in meteorology. His willpower helped me feel better when I was tired. He is my excellent teacher. Honestly, I have learnt a lot from my advisor and co-advisors. I promise that I will not forget to give back to the next generation.

I wish to express my warm and sincere thanks to all teachers in the School of Remote Sensing. I got lot of knowledge about this study from them.

Moreover, I would like to express my appreciation to the thesis committees, Asst. Prof. Dr. Sunya Sarapirome, Assoc. Prof. Dr. Kaew Nualchawee and Dr. Surachai Ratanasermpong for their comments. Their comments help my research more valuable.

I gratefully acknowledge my former supervisors and colleagues since I studied the master degree in the School of Remote Sensing, Mr. Manu Omakupt, Dr. Pannee Waraasawapati, Dr. Surachai Ratanasermpong, Assoc. Prof. Dr. Kaew Nualchawee and Mr. Teerawong Laosuwan. I began to feel interested in the Remote Sensing field from then and still now. They taught and helped me a lot; not only the knowledge but also the beneficial experience for my life.

I am grateful to the secretaries and administrative staffs in the School of Remote Sensing, Penkhae, Warunee, Ratchaneekorn, Fiat and Winai for their assistance to help me complete the documents.

I wish to thank my teachers and my student colleagues in the School of Remote Sensing. Their comments and their suggestions in seminar classes, in progression report, and in proposal presentations helped me learnt and provided me a lot of excellent ideas. I would like to thank my friends here, e.g., Vi, Joe, Oui, Keng, Lek, P'Add, Por, Joy, Gif, P'Nung, P'Pooky, P'So, Ake, Nong-dee, Anek, Sil, Poo and also those whose names are not mentioned here for their kind help and moral support to me.

Thank you to Thai Meteorological Department (TMD) for supporting the raw data, i.e., rainfall and other meteorological documents, especially Mr. Saman Prakarnrat; he has been a very good support and kindness.

Thank you to Department of Environmental Quality Promotion (DEQP) for supporting the landuse data, especially Mr. Jakchai Chumjit who provided excellent suggestions. He always gives the good for me.

Lastly and most importantly, I wish to thank my parents, Huad and Huay. I wouldn't have today without my lovely father and mother, my grandmother, my aunt, my husband, my family, my adoptive father (Prof. Dr. Paisarn Laosuwan), my adoptive mother (Mrs. Bulan Laosuwan) and my lovely friends. Most of my studied attention came from them. I dedicate the usefulness from this dissertation to them.

Pornthip Bumrungrang

CONTENTS

	Page
ABSTRACT IN THAI.....	I
ABSTRACT IN ENGLISH.....	III
ACKNOWLEDGEMENT.....	V
CONTENTS.....	VIII
LIST OF TABLES.....	XII
LIST OF FIGURES.....	XIV
LIST OF ABBREVIATIONS.....	XIX
LIST OF SYMBOLS.....	XXIV
CHAPTER	
I INTRODUCTION.....	1
1.1 Background problem and significance of the study.....	1
1.2 Objectives of the study.....	2
1.3 Scope and limitations of the study.....	2
1.4 Study area.....	2
1.5 Expected results.....	5
II LITERATURE REVIEW.....	6
2.1 Height and structure of the atmosphere.....	6
2.1.1 Variation of air density and pressure with height.....	6
2.1.2 Layers of the atmosphere.....	7
2.2 Cloud classification and formation.....	9

CONTENTS (Continued)

	Page
2.2.1 Cloud classification.....	10
2.2.2 Cloud formation.....	14
2.2.3 Cumulus and cumulonimbus clouds.....	16
2.3 Rain and hail formation.....	17
2.3.1 Rain formation.....	17
2.3.2 Precipitation in clouds.....	22
2.3.3 Thunderstorm and hail formation.....	23
2.3.3.1 Ordinary thunderstorms.....	24
2.3.3.2 Severe thunderstorms.....	26
2.3.4 Mesoscale Convective Complexes (MCCs).....	27
2.3.5 Hail formation.....	28
2.3.6 Rainfall characteristics in Thailand.....	29
2.3.7 Regional rainfall characteristics.....	34
2.4 Weather satellites.....	34
2.4.1 Low earth orbit satellites.....	35
2.4.2 Geostationary orbit satellites.....	41
2.5 Relationship between cloud and rain.....	45
2.5.1 Cloud classification techniques.....	46
2.5.1.1 Bi-spectral technique.....	48
2.5.1.2 Split window technique.....	49
2.5.2 Rain and cloud relationship.....	52
2.5.2.1 Visible and infrared techniques.....	53

CONTENTS (Continued)

	Page
2.5.2.2 Passive microwave techniques.....	57
2.5.2.3 Active microwave techniques.....	59
2.5.2.4 Hybrid method.....	59
2.5.3 Studies of cloud-rainfall relationship in Thailand.....	61
III METHODOLOGY.....	64
3.1 Conceptual framework.....	64
3.2 Data collection and data map preparation.....	66
3.2.1 Rainfall map.....	67
3.2.2 Cloud cover map.....	69
3.3 Analyzing process.....	71
3.4 Development of automatic cloud classification model.....	74
3.4.1 Cropping and geometric correction of Thailand portion.....	74
3.4.2 Radiance conversion for BT mapping.....	78
3.4.2.1 Classified CTT maps.....	81
3.4.3 Cloud classification scheme.....	83
3.4.3.1 High cloud filtering.....	85
3.4.3.2 Development of the classification model.....	89
IV RESULTS AND DISCUSSION.....	91
4.1 Seasonal rainfall and cloud cover distribution patterns.....	91
4.1.1 Seasonal rainfall distribution.....	91
4.1.1.1 First quarter: February to April.....	96
4.1.1.2 Second quarter: May to July.....	99

CONTENTS (Continued)

	Page
4.1.1.3 Third quarter: August to October.....	104
4.1.1.4 Fourth quarter: November to January.....	106
4.1.2 Seasonal cloud distribution.....	108
4.1.2.1 Cloud/rainfall in winter.....	108
4.1.2.2 Cloud/rainfall in summer.....	115
4.1.2.3 Cloud/rainfall in monsoon season.....	121
4.2 Relationship between rainfall and cloud properties.....	127
4.2.1 Rainfall intensity and CTT.....	128
4.2.2 Rainfall estimation using lowest CTT.....	130
4.2.3 Rainfall intensity and cloud cover area.....	133
V CONCLUSION.....	135
5.1 Conclusions and recommendation.....	135
REFERENCES.....	138
APPENDICES.....	149
APPENDIX A USER MANUAL OF CLOUD MODEL.....	150
APPENDIX B SAMPLE OF MATLAB CROP PROGRAMMING.....	161
APPENDIX C DATA PREPARATION AND MANIPULATION.....	167
CURRICULUM VITAE.....	179

LIST OF TABLES

Table	Page
2.1 Cloud groups, their members, and heights of cloud base.....	13
2.2 Seasonal rainfall amount (in mm) and annual rainy days in different regions of Thailand.....	31
2.3 Classification scheme for rainfall distributing pattern in Thailand.....	33
2.4 Classification scheme for 24-hr rainfall intensity in Thailand.....	34
2.5 NOAA-AVHRR spectral ranges.....	37
2.6 TRMM-VIS/PR/TMI and DMSP-SSM/I data.....	39
2.7 GOES-Imager instrument characteristics.....	42
2.8 SEVIRI instrument characteristics.....	43
2.9 GMS-VISSR instrument characteristics.....	44
2.10 Rainfall-CCD relationship in Mohammedberhan (1998).....	56
2.11 Rainfall-CCT relationship in Udomchoke and Aungsuratana (1995).....	62
2.12 Rainfall-CCT relationship in วีระพงษ์ เสาวภาคย์ (2539).....	62
2.13 Rainfall-CCD relationship in ธนิต ชัยบุญหาญ (2545) and มณฑล จิตเอื้ออารีกุล (2546).....	63
2.14 Rainfall-CCT relationship in Budhakooncharoen (2004).....	63
3.1 Information of the data usage.....	66
3.2 Reports of hail events in 2006 and 2007 from the TMD and DDPM.....	73
3.3 Values of the constants a_1 and a_2 for each MTSAT-1R band.....	79
3.4 Example of the conversion table for TIR images of MTSAT-1R.....	79

LIST OF TABLES (Continued)

Table	Page
3.5 The classification scheme of cloud top temperature map.....	83
3.6 BT and ΔT statistics for the high cloud and cumulonimbus cloud over Thailand.....	86
4.1 Monthly accumulated rainfall amount in 2006 and 2007.....	95
4.2 Reports of severe floods and number of casualties in 2006 and 2007	100
4.3 Variation of CTT area coverage during 6-7 January 2007.....	114
4.4 Variation of CTT area coverage during 18-19 April 2007.....	121
4.5 Variation of CTT area coverage during 16-17 August 2007.....	127
4.6 Statistics of the lowest CTT for seasonal and hail events.....	130
4.7 Application of the cloud/rainfall relationship.....	133

LIST OF FIGURES

Figure	Page
1.1 Location map of Thailand	3
1.2 Main influencing factors of weather variation in Thailand.....	5
2.1 Layers of the atmosphere defined by the vertical temperature structure.....	8
2.2 Generalized illustration of basic cloud types based on cloud base heights.....	12
2.3 The distribution of ice and water in a cumulonimbus cloud.....	13
2.4 Four basic air-lifting processes in the formulation of cloud.....	14
2.5 The Bergeron process in which ice crystal grows at the expense of cloud droplets until they are large enough to fall as snow or rain.....	19
2.6 The collision-coalescence process in which collisions between liquid droplets (with different sizes) play important role in producing precipitation	21
2.7 Stages in the development of an ordinary thunderstorm.....	25
2.8 Structure and air movements within the severe thunderstorm.....	27
2.9 Annual rainfalls (millimeter) in Thailand (30-year average, 1971-2000).....	30
2.10 Viewing structure of the PR instrument.....	37
2.11 Structure of the hurricane in both 2D and 3D as seen by the PR instrument.....	39
2.12 Rainfall pattern from TRMM satellite during 21-28 May 2006.....	40
2.13 GMS-5 VIS/TIR satellite image over the Pacific Ocean on 31 August 2002.....	45

LIST OF FIGURES (Continued)

Figure	Page
2.14 Three main forms of cloud: cirrifom, stratiform and cumuliform.....	47
2.15 Cloud classification table proposed by Inoue (1987) for NOAA AVHRR.....	52
2.16 Relationship between radar rainfall rate and cloud brightness temperature given in Vicente <i>et al.</i> (1998) where dots represents mean radar derived rainfall for each one degree temperature interval from 195 K to 260 K.....	61
3.1 Flow chart of the study divided into 4 principal parts: (a) data collection (b) data map preparation, (c) cloud model development and (d) analysis and reporting.....	65
3.2 Location map of the 116 TMD weather stations in use.....	68
3.3 Example of the used rainfall data files (before re-formatting).....	68
3.4 Structure of the MTSAT-1R filename.....	69
3.5 MTSAT-1R VIS image over the Pacific Ocean on 25 April 2007.....	70
3.6 Original area cover of MTSAT-1R image.....	75
3.7 Cropping area cover of MTSAT-1R image.....	75
3.8 Examples of the cropped MTSAT-1R satellite image for Thailand portion in (a) visible band (at 0.55-0.90 μm), (b) IR1 band (at 10.3-11.3 μm), (c) IR2 band (at 11.5-12.5 μm), (d) IR3 band (at 6.5-7.0 μm) and (e) IR4 band (at 3.5-4.0 μm).....	76

LIST OF FIGURES (Continued)

Figure	Page
3.9 Examples of the MTSAT TIR image (a) before conversion-displayed as radiance image and (b) after conversion-displayed as equivalent BT image (in Kevin unit).....	80
3.10 The GUI appearance of the derived radiance/BT conversion module.....	82
3.11 Examples of the classified CTT map over Thailand based on the MTSAT image of (a) band IR1 and (b) band IR 2 as shown in Figure 3.8. (Apr 25, 2007 UTC00 images).....	84
3.12 Scatter plots of IR1/IR2 BT and IR1/ ΔT of high cloud samples.....	87
3.13a Examples of cloud images (a) with and (b) without high cloud appearance, example on Apr 19, 2007 (h1).....	87
3.13b Example of cloud image after the high-cloud filtering process (without high cloud appearance) on April 19, 2007 (h1).....	88
3.14 Step-by-step GUI of derive ERDAS module for cloud classification.....	90
4.1 Pattern of rainfall distribution in periods: (a) February-April, (b) May-July, (c) August-October and (d) November-January.....	92
4.2 Annual rainfall maps for (a) 2006 and (b) 2007.....	94
4.3 Rainfall map on 3 January 2006 when the strong northeast monsoon generated widespread rainfall in the south, especially on the eastern side and in the far south.....	97
4.4 Rainfall map on 13 February 2006 when the strong upper westerly wind was moving across the south which caused heavy rainfall and flooding in some areas.....	98

LIST OF FIGURES (Continued)

Figure	Page
4.5 Rainfall map on 2 July 2006 when the strong southwest monsoon induced the widespread heavy rainfall and flooding in several places across the country.....	101
4.6 Rainfall map on 22 May 2006 when the strong monsoon trough induced the widespread heavy rainfall and flooding in several places in the lower-northern region.....	102
4.7 Rainfall map on 4 October 2007 when the tropical cyclone “Lekima” moved into the country and induced widespread heavy rainfall and flooding in several places in the lower-northern and northeastern regions of the country.....	103
4.8 Rainfall map on 2 May 2007 as the low depression area from the Gulf of Thailand moved inland and induced widespread heavy rainfall in several regions of the country.....	105
4.9 Rainfall map on 13 March 2006 when large cold mass moved to occupy upper part of the country and induced widespread rainfall along the weather front.....	107
4.10 Rainfall map for 7 January 2007 when strong northeast monsoon generated widespread rainfall in the south, especially on the eastern side and in the far south. And, there was no record of rainfall measured in the upper part of the country.....	109

LIST OF FIGURES (Continued)

Figure	Page
4.11 Hourly CTT maps (derived from MTSAT-1R images) for 6-7 January 2007 taken within 24 hours during 7.00 am (6 th Jan) to 6.00 am (7 th Jan).....	110
4.12 Rainfall map for 19 April 2007 when strong current of warm/moist air from the Thai Gulf and Andaman Sea to move into the central and lower northeastern region that had resulted of widespread rainfall within that area.....	116
4.13 Hourly CTT maps (derived from MTSAT-1R images) for 18-19 April 2007 taken within 24 hours during 7.00 am (18 ^h Apr) to 6.00 am (19 th Apr).....	117
4.14 Rainfall map for 17 August 2007.....	122
4.15 Hourly CTT maps (derived from MTSAT-1R images) for 16-17 August 2007 taken within 24 hours during 7.00 am (16 th Aug) to 6.00 am (17 th Aug).....	123
4.16 Data of the minimum hourly CCT on the used MTSAT-1R satellite images on different season and also for the chosen “hail” days in 2006 and 2007.....	129
4.17 Relationship between rainfall amounts and lowest CTT in different season based on data from several stations across Thailand.....	132
4.18 The relationship between average daily cloud cover and the total amount of observed rainfall for different levels of rainfall intensity and the hail days.....	134

LIST OF ABBREVIATIONS

Ac	Alto cumulus
As	Alto stratus
AMS	American Meteorological Society
BT	Brightness temperature
BTD	Brightness temperature difference
Cb	Cumulonimbus cloud or Thunderstorm cloud
Cc	Cirrocumulus
CCD	Cold cloud duration
CCN	Cloud condensation nuclei
Ci	Cirrus
Cs	Cirrostratus
CST	Convective Stratiform Technique
CTT	Cloud top temperature
Cu	Cumulus
DDPM	Department of Disaster Prevention and Mitigation
DEQP	Department of Environmental Quality Promotion
DMSP	Defense Meteorological Satellite Program
EML	ERDAS Macro Language
EOS	Earth Observation System
ERDAS	ERDAS IMAGINE software

LIST OF ABBREVIATIONS (Continued)

EUMETSAT	The European Organisation for the Exploitation of Meteorological Satellites
FAR	False alarm ratio
FOV	Field of view
GARP	Global Atmosphere Research Programme
GEO	Geostationary Orbit
GIS	Geographic Information System
GMS	Geosynchronous Meteorological Satellite
GOES	Geostationary Operational Environmental Satellite
GPCP	Global Precipitation Climatology Project
GPI	GOES Precipitation Index
GUI	Graphic User Interface
HRV	High Resolution Visible sensor
IDW	Inverse Distance Weighted
IFOV	Instantaneous field of view IFOV
IR1	Infrared 1
IR2	Infrared 2
IR3	Infrared 3
IR4	Infrared 4
ITCZ	Inter Tropical Convergence Zone
JAXA	Japan Aerospace Exploration Agency
JMA	Japan Meteorological Agency

LIST OF ABBREVIATIONS (Continued)

Lao PDR	Lao People's Democratic Republic
LEO	Low Earth Orbit
LULC	Land use Land Cover
MATLAB	Language of Technical Computing
MCCs	Mesoscale Convective Complexes
MCS	Mesoscale Convective System
METEOSAT	European Organization for the Exploitation of Meteorological Satellites
MI	The Ministry of Interior
MIR	Mid-infrared
MODIS	Modulate Resolution Imaging Spectro-Radiometer
MSC	Meteorological Satellite Center
MSG	Meteosat Second Generation
MSL	Mean sea level
MTP	Meteosat Transition Program
MTSAT	Multi-functional Transport Satellite
MW	Microwave
MUSIC	Multiple-Sensor Precipitation Measurements, Integration, Calibration and Flood Forecasting
NASA	National Aeronautics and Space Administration
NESDIS	NOAA satellite Data and Information Service
NCEP	National Center for Environmental Predictions

LIST OF ABBREVIATIONS (Continued)

NGDC	National Geophysical Data Center
NIR	Near infrared
NOAA-AVHRR	NOAA- Advanced Very High Resolution Radiometer
Ns	Nimbostratus
US-NWS	United State-National Weather Service
RMSE	Root Mean Square Error
PR	Precipitation Radar
RS	Remote Sensing
Sc	Stratocumulus
SEVIRI	Spinning Enhanced Visible and Infrared Imager
SLP	Pressure at mean sea level
SML	Spatial Modeler Language
SSM/I	Microwave Imager
St	Stratus
SWIR	Shortwave infrared
TAMSAT	Tropical Applications of Meteorology using satellite
TIR	Thermal infrared
TIROS-1	Television Infrared Observation Satellites
TMI	TRMM Microwave Imager
TMD	Thai Meteorological Department
TRMM	Tropical Rainfall Measurement Mission

LIST OF ABBREVIATIONS (Continued)

USGS-AVHRR	United State Geological Survey-Advanced Very High Resolution Radiometer
UTC	Universal Time Coordinate
UV	Ultraviolet
VIS	Visible
VISSR	Visible and Infrared Spin Scan Radiometer
WCRP	World Climate Research Program
WGS-84	World Geodetic System 1984
WMO	World Meteorological Organization

LIST OF SYMBOLS

°C	Celsius degree
cm	centimeter
GHz	gigahertz
hr(s)	hour(s)
hPa (or mb)	hetero Pascal
K	Kevin degree
kg/m ³	kilogram per cubic meter
km/hr	kilometer per hour
km	kilometer
μm	micrometer
m ²	square meter
m ³ /s	cubic meter per second
mm	millimeter
mm/h	millimeter per hour
r ²	coefficient of determination
sg.km or km ²	square kilometer
T _b	brightness temperatures

CHAPTER I

INTRODUCTION

1.1 Background problem and significance of the study

Cloud and rain are considered key components of the global hydrologic cycle that regulates circulating mechanism of water in nature. Clouds are the original source of rain which is crucial for the daily living of the majority of population on the Earth, especially the farmers. As a result, knowledge of cloud structure and distribution is essential for the understanding of rainfall pattern and climate changes in the interested area. At present, the most effective method to study cloud and rainfall distribution in regional or country scale is using observed data from the weather satellites. These satellites have been specifically designed for the observation and measurement about structure and gaseous components of the Earth's atmosphere as well as the important atmospheric phenomena such as rain, cloud, wind, thunderstorm, or the hurricane.

Typically, the application of satellite imagery to weather study in Thailand is still rare and mostly focused on the prediction of rain rate from cloud top temperature derived from the thermal infrared (TIR) satellite images. However, most studies mainly focused on the analysis of cloud/rainfall relationship base on data at few selected stations. Therefore, in principle, their obtained results still can not explain the variety of the cloud and rainfall relationship in the country as a whole. To gain more knowledge of the relationship in wider scope, data from more stations covering wider area and in longer time-span of rain/cloud record are needed, which is significantly

fulfilled in this study. In addition, in this thesis, the cloud data derived from TIR satellite images are also applied to the study of seasonal weather variation observed in years 2006 and 2007.

1.2 Objectives of the study

This study comprises of three main objectives as follows:

1.2.1 To develop a computer-based automatic cloud classification program for the use with satellite TIR imagery.

1.2.2 To apply the classified satellite cloud images for the study of seasonal rainfall and cloud distribution during years 2006 and 2007.

1.2.3 To find proper relationship between observed rainfall amount and some cloud properties (cloud top temperature and cloud cover area).

1.3 Scope and limitations of the study

1.3.1 Study area covers the whole Thailand all during period 2006 and 2007.

1.3.2 Daily rainfall data collected by the TMD and hourly satellite TIR image are valid for the analysis of rainfall and cloud distribution.

1.3.3 Only clouds with cloud top temperature less than 10°C are considered.

1.4 Study area

Thailand is located in the tropical zone within latitude of 05° 37' to 20° 27'N and longitude 97° 22' to 105° 37'E with approximately 513,115 km² in area cover. It is bordered with Myanmar and Laos PDR in the north, with Lao PDR, Cambodia and the Gulf of Thailand in the east, with Malaysia in the south, and with Andaman Sea and Myanmar in the west (Figure 1.1).



Figure 1.1 Location map of Thailand

Source: TMD website (<http://www.tmd.go.th>)

The country is geographically divided into four natural regions: the North, the Central (or the Chao Phraya River Basin), the Northeast (or the Korat Plateau) and the South (or the Southern Peninsula). The northern region is mountainous area prone to flood, earthquake, landslides, the northeast region is arid area on the Korat Plateau, frequently faces sudden flood during rainy season, severe drought and cold during hot and cold season. The Central region is the fertile area but often inundated during rainy season. The Southern region is hilly to mountainous and several offshore islands. The severe disasters in this region are floods, tropical storms, landslides and forest fires.

Its seasonal climate is largely under influence of regional monsoon wind especially the southwest and northeast monsoons. From the meteorological aspect, climate of Thailand can be divided into three seasons (see also Figure 1.2).

(1) Summer or pre-monsoon season (mid-February to mid-May) during which weather is generally hot and dry as the whole country is exposed to the sun the most and it is still lack of strong monsoon winds to influence weather otherwise.

(2) Rainy or southwest-monsoon season (mid-May to mid-October). During this period, the southwest monsoon mostly prevails over Thailand and it brings huge amount of moisture from the Indian Ocean to form abundant rain all over the country. Weather is usually hot and humid and the wettest period is August to September.

(3) Winter or northeast-monsoon season (mid-October to mid-February). At this time, the weather pattern is mostly under the influence of northeast monsoon that brings cold and dry air from the Siberian High to govern the whole country, especially in the middle and upper part. But in the south, it will bring more rain to the area.

Upper Thailand usually experiences dry weather in winter due to the influence of the northeast monsoon but in summer, amount of rainfall gradually increases as well as the thunderstorms. The onset of the southwest monsoon leads to an intensive rainfall from mid-May till early October with peak in August or September. However, dry spells commonly occur for 1 to 2 weeks or more during June to early July.

Rainy season in the south is different as abundant rainfall occurs during both the southwest (for the western coast) and northeast monsoon (for the eastern coast) periods. Amount of rainfall on the western side reaches its peak in September but the eastern side in November and remains high until January of the following year.

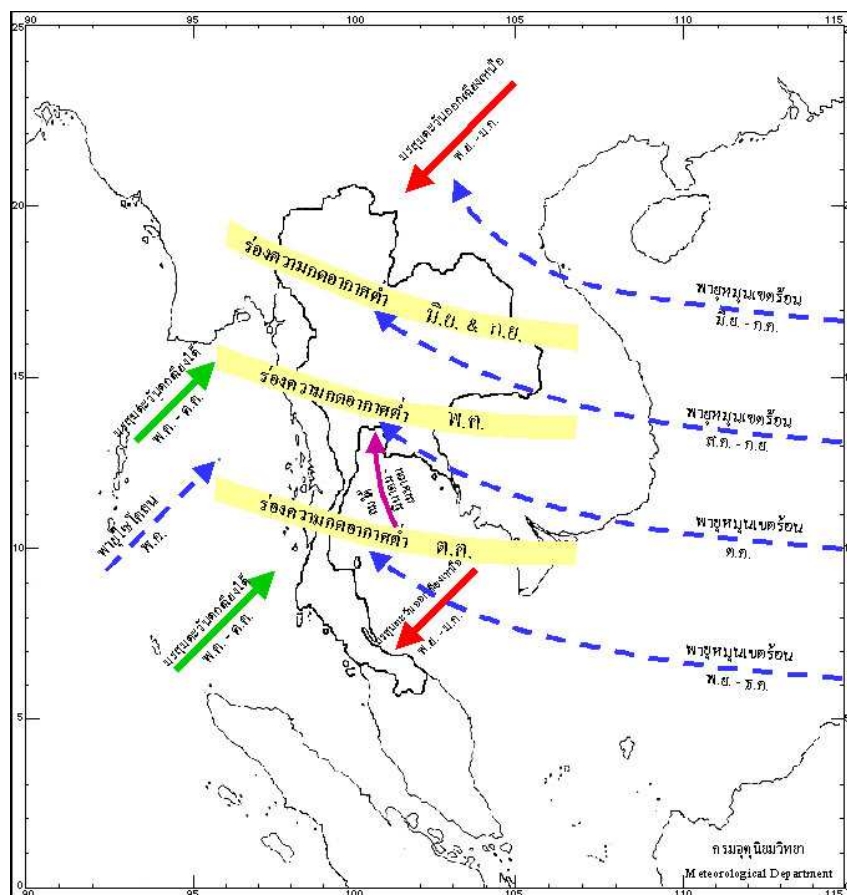


Figure 1.2 Main influencing factors of weather variation in Thailand

Source: TMD website (<http://www.tmd.go.th>)

1.5 Expected results

1.5.1 Automatic cloud classification module from satellite TIR image base on the derived cloud top temperature map.

1.5.2 Knowledge about seasonal cloud and rainfall distribution in the country during years 2006 and 2007, and associated the main influencing factors.

1.5.3 Proper relationship pattern between rainfall amount and cloud properties (cloud top temperature and cloud cover area).

1.5.4 Better understanding on the potential applications of TIR satellite images to the study about cloud and rainfall issues in Thailand.

CHAPTER II

LITERATURE REVIEW

This chapter mainly focuses on a review of literature related to main objectives of the dissertation. It begins with data of the background theory, theories, definitions and related documents.

2.1 Height and structure of the atmosphere

Principally, the Earth comprises of four major components which are the atmosphere (or Earth's gaseous envelope), the solid Earth (or Earth's core, mantle and crust), the hydrosphere (or Earth's water portion), and the biosphere (where all bio-organisms live). Literally, the atmosphere extends from the Earth's surface upward to the outer space and no clear boundary set for the end of its territory. Most atmospheric particles concentrate in the lower portion of the atmosphere close to the surface due to the gravity. About 50 percents of the atmosphere by mass lies below an altitude of 5.6 km and about 90 percents lie below 16 km altitude. Most dominant gases in normal air are nitrogen (78 percents) and oxygen (21 percents).

2.1.1 Variation of air density and pressure with height

Air density normally decreases rapidly with height above Earth's surface as follows:

$$D(z) = D_0 e^{-z/H_d} \tag{2.1}$$

Here, $D(z)$ is the air density at height z above mean sea level (msl), $D_0 = 1.225 \text{ kg/m}^3$ is the reference density at mean sea level and $H_D = 8.55 \text{ km}$ is the constant called scale height for density. As air density decreases, air pressure also decreases in a similar manner which can be described as follows:

$$P(z) = P_0 e^{-z/H_p} \quad (2.2)$$

$P(z)$ is the air pressure at height z above msl, $P_0 = 1,013.25 \text{ mb}$ (or hPa) is the reference pressure at mean sea level (SLP) and $H_p = 7.29 \text{ km}$ is called scale height for pressure.

However, in real atmosphere, the surface air pressure can vary dramatically with place and time, and this knowledge is necessary for the understanding of climate change. For example, area with low pressure (e.g. lower than SLP) normally indicates warm and turbulent weather while area with high pressure (e.g. higher than SLP) is associated with cold and more static weather (Ahrens, 2000; Stull, 2000).

2.1.2 Layers of the atmosphere

Air temperature can vary dramatically with height and the tendency of its vertical variation has been used to define atmosphere's layers as follow: troposphere (0-12 km), stratosphere (12-50 km), mesosphere (50-85 km), and thermosphere (> 85 km) (Figure 2.1).

Among these layers, the troposphere is most important as it contains most gases necessary for the living of human being (and all other living organisms). The temperature tends to decrease with height in the troposphere, from about 20°C at

the surface to -60°C at altitude of about 12 km. This temperature decreasing rate is called the environmental lapse rate where its average value is 6.5°C per kilometer, a figure known as normal lapse rate. However, this lapse rate is not constant and can vary during the course of a day with fluctuations of the weather, as well as seasonally and from place to place.

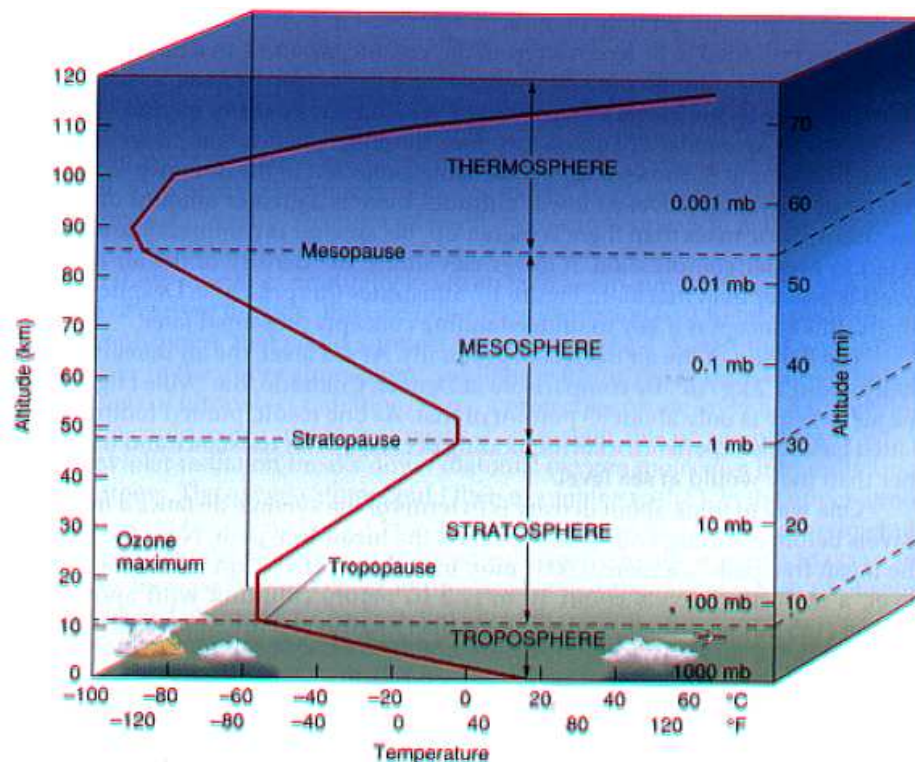


Figure 2.1 Layers of the atmosphere defined by the vertical temperature structure.

Source: Figure 1.9 in Ahrens (2000)

The troposphere is being chief focus of meteorologists, because in this layer that essentially all important weather phenomena occur. Almost all cloud and precipitation, as well as all violent storms, are born in this lowermost layer of the atmosphere. As a result, sometimes it is named the “weather sphere”.

Beyond the troposphere lies the stratosphere in which it has the boundary between the troposphere and the stratosphere known as the tropopause. In this boundary layer, the weather is considerably calm (much contrary to situation in troposphere) and temperature is relatively constant throughout (at about -60°C). Normally, height of the tropopause varies significantly with place and time, but in average, it is higher in summer and lower in winter. The temperature starts to rise sharply with height at an altitude near 20 km and continues until it reaches stratopause at a height of about 50 km above the Earth's surface. Higher temperatures present in this layer due to the absorption of high energy UV ray in sunlight by the thick ozone layer situated at altitude 15-30 km.

Above the stratosphere is the mesosphere where temperature continue to decrease with height again until the mesopause, at 85 km above the surface with the temperature about -90°C , is encountered. The outermost layer is thermosphere which contains only a minute of the atmosphere's mass and has no well-defined upper limit. Here, temperature increases with height to some extremely high values of more than $1,000^{\circ}\text{C}$. The rise owes to the strong absorption of very-short wave, high-energy solar radiation by atoms of oxygen and nitrogen gases (Lutgens and Tarbuck, 1998).

2.2 Cloud classification and formation

In this section, general concepts of cloud formation and its classification scheme are presented. The special interest is given to the thunderstorm cloud which is the main source of heavy rainfall observed in nature. Most content described here is summarized from two main sources; Lutgens and Tarbuck (1998) and Ahrens (2000), unless stated otherwise.

2.2.1 Cloud classification

Cloud is the natural phenomenon that is familiar to most people on the Earth. In essence, it is a visible form of the highly packed water droplets and/or ice particles in the atmosphere above the Earth's surface (AMS Glossary of Meteorology, 2009). Clouds can appear in different shapes and sizes depending on the formulating process and the then influencing environment. To distinguish different patterns of the cloud appearances into some definite categories, several cloud classification schemes have been proposed so far. But the most widely-used one was developed by Luke Howard (1772-1864), the English amateur meteorologist in 1803 (Hamblyn, 2001). The system was later adopted by the WMO (World Meteorological Organization) and used in the writing of International Cloud Atlas (WMO, 1956). In this system, Howard employed Latin words to describe clouds as they appear to a ground observer in which four basic cloud forms were identified, which are, a sheet-like cloud *stratus* (from Latin for "layer"), a puffy cloud *cumulus* ("heep"), a wispy cloud *cirrus* ("curl of hair"), and a rain cloud *nimbus* ("violent rain"). All other clouds can be described by combination of these basic types. For example, nimbostratus is a rain cloud that shows layering form, while cumulonimbus is a rain cloud having pronounced vertical development. Based on Howard's system, five fundamental properties of clouds were categorized which are (AMS Glossary of Meteorology, 2000):

- (1) Genera: Main characteristic forms of clouds,
- (2) Species: Peculiarities in shape and differences in internal structure of clouds,
- (3) Varieties: Special characteristics of arrangement and transparency of clouds,

(4) Supplementary features: Appended and associated minor cloud forms, and

(5) Mother-clouds, the origin of clouds if formed from other clouds.

Based on these criteria, ten cloud genera have been identified, which are cirrus, cirrocumulus, cirrostratus, altocumulus, stratus, altostratus, nimbostratus, stratocumulus, cumulus, and cumulonimbus. The fourteen cloud species are fibratus, uncinus, spissatus, castellanus, floccus, stratiform, nebulosus, lenticularis, fractus, humilis, mediocris, congestus, calvus, and capillatus. The nine cloud varieties are intortus, vertebratus, undulatus, radiatus, lacunosus, duplicatus, translucidus, perlucidus and opacus. The nine supplementary features and accessory clouds are incus, mamma, virga, praecipitatio, arcus, tuba, pileus, velum, and pannus.

Another popular classification scheme was developed based on the usual altitudes of observed clouds in which ten principal cloud forms are divided into four primary cloud groups, high, middle, low, and vertically-developed clouds. The first three categories are identified by height of the cloud's base above the surface whereas fourth group contains clouds showing more vertical than horizontal development. And within each group, cloud types are identified by their appearance. High clouds include cirrus (Ci), cirrocumulus (Cc), cirrostratus (Cs) while middle clouds are altocumulus (Ac) and altostratus (As), and low clouds are nimbostratus (Ns), stratocumulus (Sc) and stratus (St). Finally, the clouds with vertical development are cumulus (Cu) and cumulonimbus (Cb) (Figure 2.2). Table 2.1 lists these cloud groups, their members and approximate based height. Note that the altitude separating high and middle clouds overlaps and varies with latitude.

In addition, clouds are also divided according to their particulate composition, namely, the water clouds, ice-crystal clouds, and mixed clouds. Among these, the first compose entirely of water droplets (ordinary and/or supercooled states), the second entirely of ice crystals, and the third a combination of the first two. Only cirrostratus and cirrus that are always ice-crystal clouds, cirrocumulus can be mixed, and only cumulonimbus is always mixed (Figure 2.3). Altostratus is nearly always mixed, but can occasionally be water. All the rest (cumulus, stratus, stratocumulus, nimbostratus, and altocumulus) are usually water clouds but can be occasionally mixed.

Typically, cloud which has only liquid components (even at temperature less than 0°C) is referred to as “warm cloud”, and the precipitation that results is said to be due to warm-cloud process. Cloud that contains ice crystal is referred to as “cold cloud”, and the resulting precipitation is said to be product of the cold-cloud process, which is normally referred to as the Bergeron mechanism.

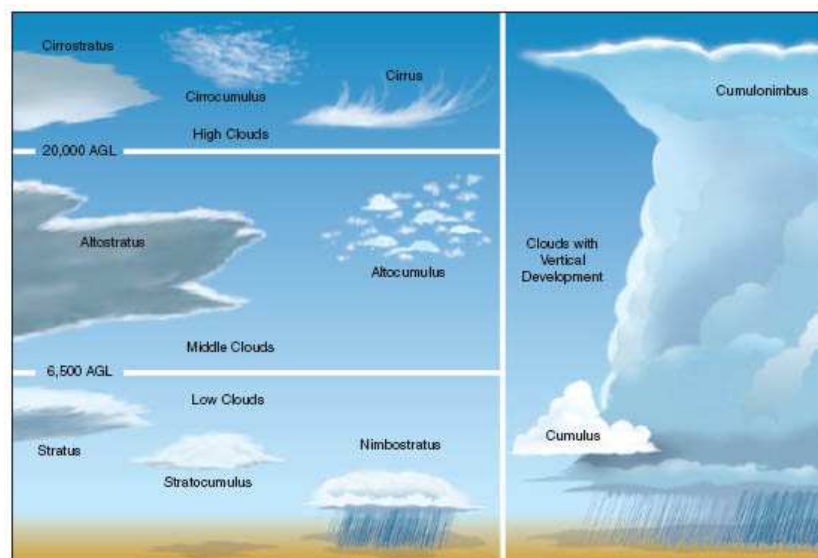
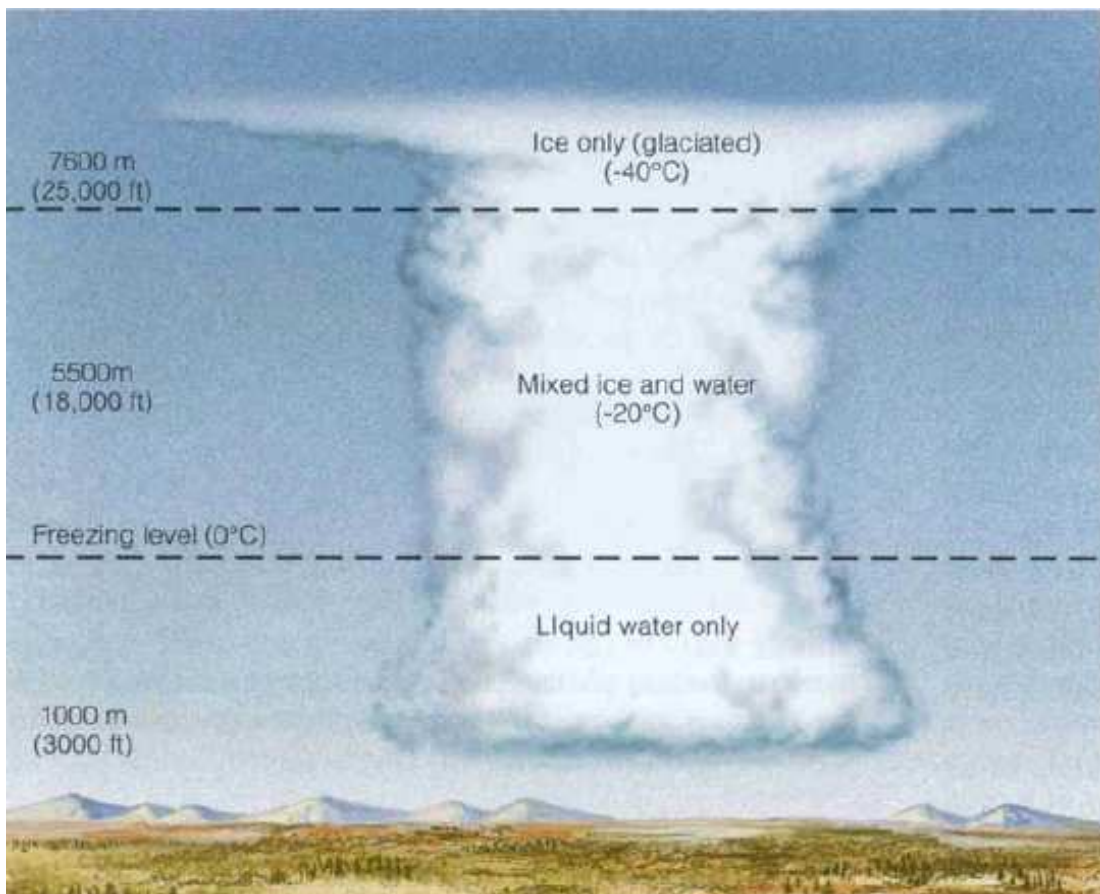


Figure 2.2 Generalized illustration of basic cloud types based on cloud base heights.

Source: website <http://www.ilmutrans-udara.com>

Table 2.1 Cloud groups, their members, and heights of cloud base (Ahrens, 2000)

Cloud group	Cloud type	Height of cloud bases (m)		
		Tropical	Mid-latitude	Polar region
High clouds	Cirrus (Ci), Cirrocumulus (Cc), Cirrostratus (Cs)	6,000-18,000	5,000-13,000	3,000-8,000
Middle clouds	Altostratus (As), Altostratus (As)	2,000-8,000	2,000-7,000	2,000-4,000
Low clouds	Stratus (Sc), Stratocumulus (St) , Nimbostratus (Ns)	0-2,000	0-2,000	0-2,000
Vertical development	Cumulus (Cu) Cumulonimbus (Cb)	-	-	-

**Figure 2.3** The distribution of ice and water in a cumulonimbus cloud.**Source:** Figure 8.6 in Ahrens (2000)

2.2.2 Cloud formation

Normally, clouds develop in the atmosphere as a result of the condensation of water vapor in the rising currents of warm moist air (above the condensation level) under four basic processes, convective lifting, orographic lifting, frontal wedging, and convergence (as shown in Figure 2.4). Most of the observed clouds and precipitation result from one or a combination of these mechanisms.

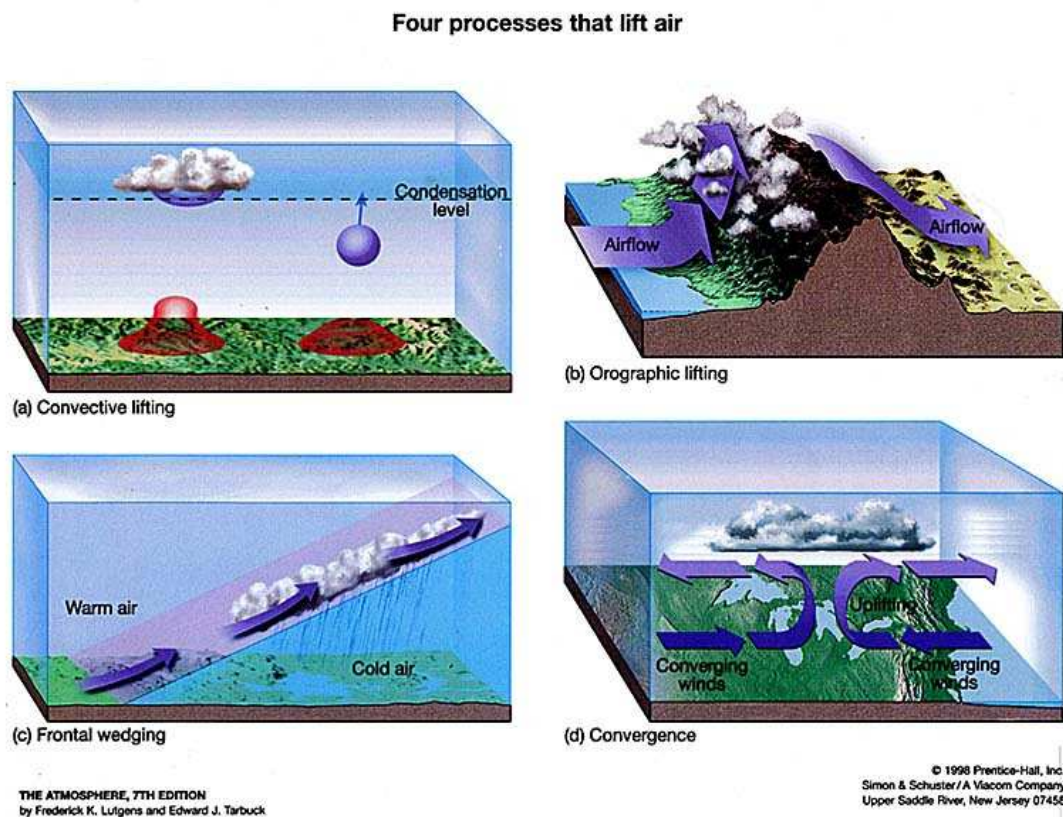


Figure 2.4 Four basic air-lifting processes in the formulation of cloud.

Source: Figure 4-21 in Lutgens and Tarbuck (1998)

In the convective lifting process, the warmer near-ground air parcel (due to higher surface heat absorption) rises naturally by the atmospheric buoyancy force. During this ascending, it is expanding and cooling. And if this rising air cools to

its saturation point, at a height called the lifting condensation level, its moisture content will condense and be visible as cloud. Precipitation associated to convective lifting is normally isolated and of short duration. In orographic lifting, the air is forced to lift along the topographic barrier such as a mountain (Figure 2.4b). As air ascends a mountain slope pass the condensation level, adiabatic cooling often generates clouds and copious precipitation. In reality, many of the rainiest places in the world are located on windward mountain slopes like the Himalaya Mountain in Nepal. In this case, the type of cloud that is formed depends on the air's stability and moisture content. On the leeward side of the mountain, as the air moves downhill, it warms. This sinking air is now drier, since much of its moisture was removed in forms of clouds and precipitation on the windward side. As a result, this region on the leeward side, where precipitation is noticeable less, is called a rain shadow.

Clouds also frequently occur along the boundary where cold and warm air masses collide (called "weather front") by a process called frontal wedging where the cooler (and denser air) acts as a barrier over which the warmer (and less dense) air rises until reaches the condensation level. The stability of the rising air determines to a great extent the type of clouds that form and the amount of precipitation that may be expected. The merging of air flows (from different directions) in lower troposphere can result in air-lifting that generates cloud. This phenomenon is called convergence and is regarded as being major contributor to the stormy weather associated with the middle-latitude cyclones and hurricanes.

To achieve the referred condensation mechanism, the rising air must be saturated and there must be surface on which the water vapor can condense. This is provided by the tiny particles known as "cloud condensation nuclei, CCN" which

generally include the microscopic dust, smoke, and salt particles, which are abundant in the lower atmosphere. CCN are important because, if they are absent, a relative humidity well in excess of 100 percents is needed to produce clouds. Initially, the growth rate of cloud droplets is rapid but this will diminish in a short time as the available water vapor is rapidly consumed by a large number of competing droplets. The result is formation of many tiny water droplets (at micrometer scale), that be remain suspended in the air and seen as clouds.

Particles that make the most effective cloud condensation nuclei are hygroscopic, which means they are water-absorbent material. Some of the most common hygroscopic condensation nuclei are minute crystals of sulfate and nitrate compounds. Hygroscopic nuclei are released into the atmosphere mainly as a by-product of consumption (burning), from such sources as forest fires, automobiles, and coal-burning furnaces. In addition, salt from breaking ocean waves and some particles found in ordinary dust can serve as cloud condensation nuclei.

2.2.3 Cumulus and cumulonimbus clouds

Most of the observed heavy rainfall in nature can be normally associated with the formation of vertically-developed clouds, cumulus and cumulonimbus. Cumulus clouds are individual masses that develop into vertical domes or towers, the tops of which often resemble cauliflower (Figure 2.2). They most usually form on clear days when unequal surface heating causes parcels of air to rise upward through the lifting condensation level. This level is often apparent to an observer as the flat cloud bottoms clearly define it.

Although cumulus clouds are normally associated with fair weather, under proper circumstances, they may grow dramatically in height, and the clouds

with great vertical extent are formed called a *cumulus congestus*. Eventually, when the cloud becomes even more towering and rains begin to occur, it becomes a cumulonimbus. Cumulonimbus is dark, dense, billowy, cloud of gigantic vertical extent in form of huge tower (Figure 2.2). In later stages of development, the upper part of a cumulonimbus turns to ice and appears fibrous (cirrus form). Furthermore, the tops of these clouds frequently spread out in shape of an anvil under the influence of the strong upper wind. Cumulonimbus towers extend from a few hundred meters above the Earth's surface upward to about 10-15 kilometers. These huge cloud towers can produce heavily precipitation, lightening, and thunder and occasionally hail.

2.3 Rain and hail formation

Rain and hail are two most common features of the precipitation usually found in the tropical countries like Thailand. In this section, the formation process of rain and hail is described along with the rainfall characteristics in Thailand. This knowledge is crucial for the further study on the relationship between cloud and rain. Most content given here is gained from Lutgens and Tarbuck (1998) and Ahrens (2000) unless stated otherwise.

2.3.1 Rain formation

In theory, a raindrop normally develops from the combination of millions of cloud droplets through two fundamental mechanisms, the Bergeron process and the collision-coalescence process. The first one is applied specifically to the formation of cold-cloud (or icy cloud) precipitation and the second one is typically used to explain the occurrence of warm-cloud (or water cloud) precipitation.

(1) Bergeron process

Most rain and snow found in the mid-latitude region originate from the formation of ice crystal under the “Bergeron process”, which is named after its key discoverer, Tor Bergeron, the famous Swedish meteorologist. The working principle of the process relies on two specific properties of the liquid cloud droplets which are (1) it can remain in the liquid state at subzero temperature (below 0°C) called “supercooled” state until it reaches a temperature of nearly -40°C and (2) the saturation vapor pressure above ice crystals is much lower than above supercooled liquid droplets.

In general, the supercooled droplets and ice crystals are major component of most clouds situated at subzero temperature. However, these supercooled droplets are usually very sensitive to the agitation and it will freeze on contact with solid particles that have a crystal form closely that of ice (silver iodide is an example) to form ice crystal. These materials have been termed freezing nuclei. The need for freezing nuclei to stimulate the freezing process is similar to the requirement for condensation nuclei in the condensing process mentioned earlier. However, in contrast to condensation nuclei, freezing nuclei are sparse in the atmosphere and they do not generally become active until temperature reach -10°C or below. Thus, at temperatures between 0 and -10°C , clouds consist mainly of supercooled water droplets. Between -10 and -20°C , liquid droplets coexist with the ice crystals, and below -20°C , clouds are generally composed entirely of the ice crystals, for example, high altitude cirrus cloud.

The coexistence of supercooled water droplet and ice crystal can generate snow and then rainfall if situation provide. This is because when air is

saturated (100 percents relative humidity) with respect to liquid droplets, it is supersaturated (over 100 percents) with respect to ice crystals. As a result of this supersaturated condition, the ice crystal can collect more water molecules than they lose by sublimation process. This result in much lower saturation vapor pressure over ice crystal than above supercooled liquid droplet and water content thus continues to evaporate from the liquid drops and provides a key source of water vapor to feed the growth of ice crystals nearby (Figure 2.5).

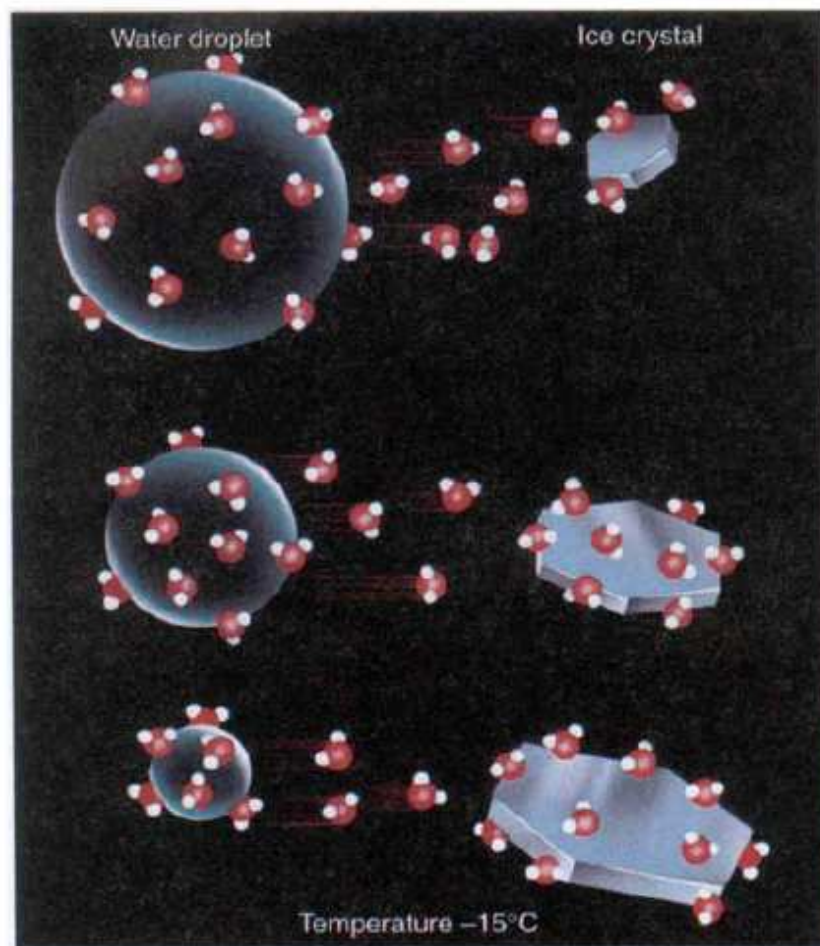


Figure 2.5 The Bergeron process in which ice crystal grows at the expense of cloud droplets until they are large enough to fall as snow or rain.

Source: Figure 8.9 in Ahrens (2000)

If the process lasts long enough, the growth of ice crystals is normally sufficient to generate snow crystals large enough to fall. During their descent, these crystals enlarge as they intercept cloud drops that freeze on them. But air movement will sometimes break up these delicate crystals and the fragments will serve as freezing nuclei for other liquid droplets. This can result in many snow crystals, which, by accretion, will form into larger masses called snowflakes. Large snowflake may consist of 10 to 30 individual crystals. However, when the surface temperature is above 4°C, the snowflakes usually melt before they reach the ground and continue their descent as rain. Even a summer rain may have begun as a snowstorm in the clouds overhead. Cloud seeding normally uses the Bergeron process as a mean to stimulate rainfall by adding freezing nuclei (usually silver iodide) to supercooled clouds which can significantly change the growth of these clouds.

(2) Collision-coalescence process

A few decades ago, the Bergeron process was believed as sole resource of most observed precipitation except for light drizzle. But later, it was found that copious rainfall seen in the tropics normally form under the influence of different triggering mechanism called “collision-coalescence process”. In this process, collisions between liquid droplets (especially in warm clouds) play important role in producing precipitation (Figure 2.6).

This begins with the formation of the very large cloud droplets at the presence of gigantic condensation nuclei, or hygroscopic particles (such as salt particles), or through random collision of smaller droplets. These giant droplets eventually fall through lower cloud layer by their own weight and, along the way, they may collide with some smaller and slower droplets and then merge together (coalesce)

to form bigger droplet. Becoming larger in the process, they fall even more rapidly (or, in an updraft, they rise more slowly) and increase their chances of collision and a rate of growth. After collecting a million or so cloud droplets, they are large enough to fall to the surface without evaporating as rain.

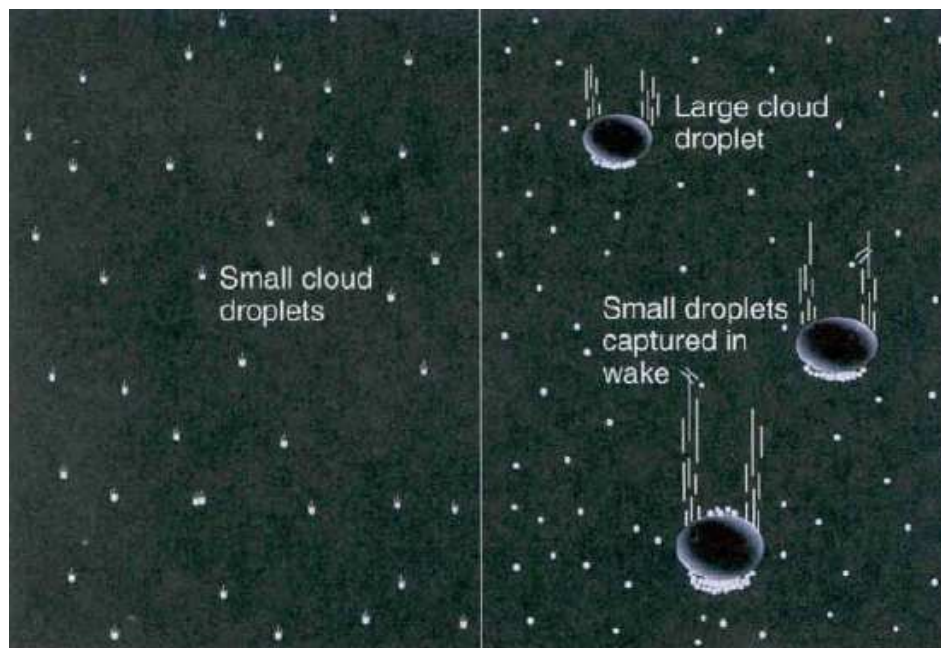


Figure 2.6 The collision-coalescence process in which collisions between liquid droplets (with different sizes) play important role in producing precipitation.

Source: Figure 8.4 in Ahrens (2000)

Coalescence appears to be enhanced if colliding droplets have opposite electrical charges. An important factor that influences cloud droplet growth by the collision process is amount of time the droplets spend in the clouds. In this case, rising warm air currents (updrafts) in forming cloud can slow the rate at which droplets fall towards the ground. Consequently, thick cloud with strong updrafts maximizes time

that cloud droplets spend in the cloud and, hence, the size to which they can grow (maximum is about 5 mm).

The collision and coalescence process dominate the forming of raindrop within warm clouds, sometimes called “warm rain”. The most important factor in the production of the raindrop here is amount of liquid water in the cloud where other accessory factors are, for examples, range of droplet sizes, cloud thickness, updrafts of the cloud, electric charge of the droplets. Relatively thin stratus clouds with slow, upward air currents are, at best, only able to produce drizzle, whereas the towering cumulus clouds associated with rapidly rising air can cause heavy showers (Ahrens, 2000). From the preceding discussion, it is apparent that large condensation nuclei are required if warm clouds are to generate any appreciable precipitation. This fact has led to the attempt to “seed” these clouds by adding “giant” nuclei. One material used is table salt but water can also be sprayed into the target clouds and acts as giant particles to initiate the collision process.

2.3.2 Precipitation in clouds

In cold, strongly convective clouds, precipitation may begin only minutes after the cloud forms and may be initiated by either the collision-coalescence process or the Bergeron process. Once either process begins, most precipitation further growth is by accretion. Although precipitation is commonly absent in warmed-layer clouds, such as stratus, it is often associated with such cold-layered clouds, such as nimbostratus and also stratus. This precipitation is thought to form principally by the Bergeron process because the liquid water content of these clouds is generally lower than that in convective clouds, thus making the collision-coalescence process much less effective. Nimbostratus clouds are normally thick enough to extend to

levels where air temperatures are quite low, and they usually last long enough for the Bergeron process to initiate precipitation.

Raindrop may fall from a cloud and not reach ground, if they encounter rapidly rising air. But if the updraft weakens or changes direction and becomes a downdraft, the suspended drops will eventually fall to the ground as a sudden rain shower. The showers falling from cumuliform clouds (e.g. cumulus) are usually brief and sporadic, as the cloud moves overhead and then drift on by. But continuous rain, on the other rain, usually falls from a layered cloud that covers a large area and has smaller vertical air currents. These conditions are normally associated to nimbostratus clouds. Typically, rains generated from cumulonimbus clouds are heavy and can last for hours due to the strong long-lasting moist updrafts that fuel such incidence.

And by definition given by meteorologists, to be considered as “rain”, the falling liquid drops must have diameter equal to, or greater than, 0.5 mm. Fine uniform drops of water whose diameters less than 0.5 mm are called “drizzle”. Most drizzle falls from the stratus clouds, however, small raindrops may fall through air that is unsaturated, partially evaporate, and reach the ground as drizzle.

2.3.3 Thunderstorm and hail formation

Thunderstorms are the well-known phenomena to most people especially ones living in the tropical region where the unstable atmosphere dominates. Thunderstorms activity is associated with cumulonimbus clouds that generate heavy rainfall, thunder, lightening, and occasionally hail. The greatest number of events occurs in association with the short-lived cumulonimbus clouds which produce local rainfall. Occasionally, however, thunderstorms may grow much larger and remain active for a few hours. As a result, they can produce frequent lightening accompanied

by the locally damaging winds or hails. Due to some differences in the forming process, the thunderstorms can be divided into two types:

(1) Isolated (or ordinary) thunderstorms, produced by a single storm cell and

(2) Severe thunderstorm produced by several storm cells.

2.3.3.1 Ordinary thunderstorms

Several studies indicate that a thunderstorm goes through a cycle of development from birth, to maturity, to decay (Figure 2.7). The first stage is known as cumulus stage. This begins with the rising of the humid air along which it cools and then condenses into single cumulus or cluster of clouds above the local condensation level. Once the forming cloud passes beyond the freezing level, the Bergeron process begins to produce precipitation. Usually within an hour of its inception, the accumulation of precipitation in the cloud is too great for the updrafts to support and start to fall. The falling precipitation causes drag on the air and initiates a downdraft.

The downdraft strength is further aided by the influx of cool, dry air surrounding the cloud, a process termed “entrainment”. This process intensifies the downdraft because the added air is mostly cool and dry, it thus causes some of the falling precipitation to evaporate (a cooling process), thereby cooling the air within the downdraft.

As the downdraft leaves the base of cloud, precipitation is released which marks the beginning of the cloud’s mature stage. Approaching the surface, the cool downdraft spreads laterally and can be felt before the actual precipitation reaches the ground. The sharp cool gusts at the surface are indicative of the downdrafts aloft. During the mature stage, updrafts exist side by side with downdrafts and then continue

to enlarge the cloud. This coexistence of updraft and downdraft in the growing cloud constitute a storm cell. Most thunderstorms have several storm cells, each of which may last for an hour or more. When the cloud expands to the top of the unstable region, often located at the base of the warmer stratosphere, the updrafts spread laterally under the influencing of strong upper wind and produce the characteristic anvil top. Generally, cirrus clouds make up the cloud top and are spread downwind by the rapid winds aloft. The mature stage is the most active period of a thunderstorm life-cycle where gusty wind, lightening, heavy rain, and sometimes hail are experienced.

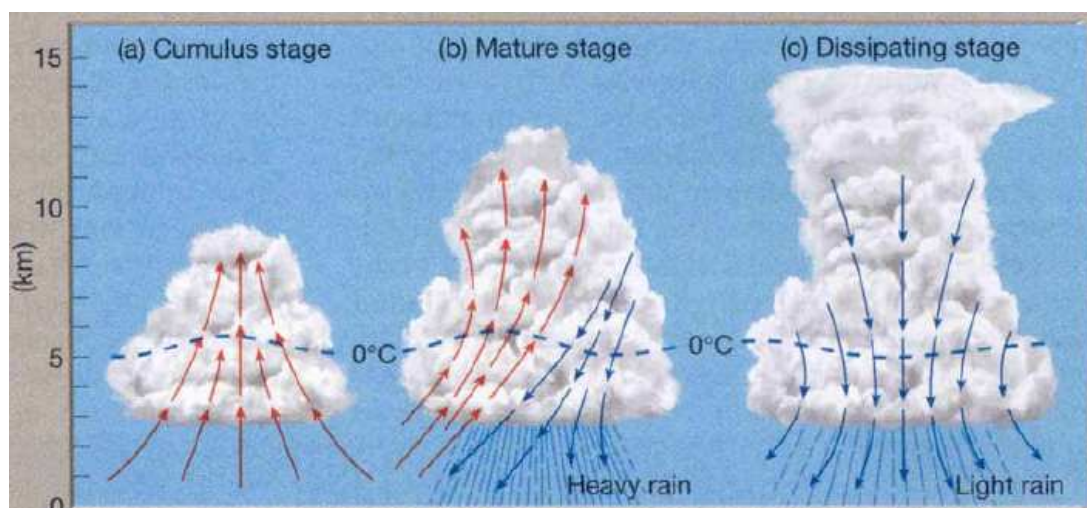


Figure 2.7 Stages in the development of an ordinary thunderstorm.

Source: Figure 10-4 in Lutgens and Tarbuck (1998)

Once downdraft begins, the vacating air encourages more entrainment of the cool, dry air surrounding the cloud. Eventually, the downdrafts dominate throughout the cloud and initiate the dissipating stage. The cooling effect of falling precipitation and the influx of colder air aloft mark the end of the thunderstorm

activity. Without a supply of moisture, the cloud will eventually evaporate sometimes leaving just only cirrus anvil as the reminder of once mighty presence. The lifespan of a single cumulonimbus cell within a thunderstorm complex is less than an hour or two, but as a storm moves, fresh supplies of warm, water-laden air might generate new cells to those that are dissipating.

In addition, upon reaching the surface, the cold downdraft has another effect. It may force warm, moist surface air upward. This rising air then condenses and gradually builds into a new thunderstorm. Thus, it is entirely possible for a series of thunderstorm to appear in a line, one next to the other, each in a different stage of the development. These are termed multi-cell storms. Most ordinary thunderstorms are multi-cell storms, as are most sever thunderstorms.

2.3.3.2 Severe thunderstorms

Severe thunderstorms are frequent natural hazard capable of producing large hail, strong and gusty surface wind, flash flood, and tornado. Just like ordinary thunderstorm, severe thunderstorms form when moist air rises into a conditionally unstable atmosphere and produce rain clouds but size and air movement of the cloud in this case can be greatly enhanced by the existing of a strong vertical wind sheer in the area. Due to massive size of many severe thunderstorms, they are often called supercell storms.

Strong winds aloft may cause the updrafts in a severe thunderstorm to tilt in its mature stage, as seen in Figure 2.8. The storm is moving from left to right and the upper- level winds cause the system to tilt so that the updrafts move up and over the downdrafts. This situation will allow the updraft to remain strong for an extended period of time. The updrafts in a severe thunderstorm may be so strong that

the cloud top is able to intrude well into the stable atmosphere (called overshooting). In some cases, the top of the cloud may extend to more than 18 km above the surface.

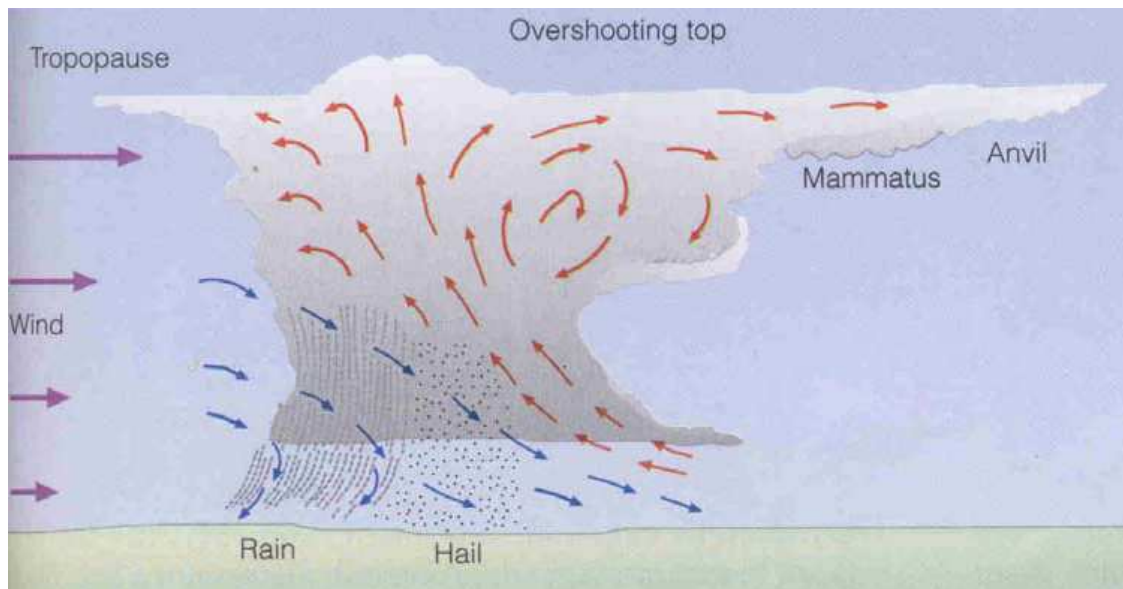


Figure 2.8 Structure and air movements within the severe thunderstorm.

Source: Figure 15.6 in Ahrens (2000)

2.3.4 Mesoscale Convective Complexes (MCCs)

In mid-latitude zone, where conditions are favorable for the strong convection, a number of individual thunderstorms may exceptionally develop in size and organize into large convective system called Mesoscale Convective System (MCS) which may be round or linear in shape. MCS includes systems such as tropical cyclones, squall lines, and Mesoscale Convective Complexes (MCCs), among others.

MCC is a unique kind of the MCS which, by definition, must have area of cloud top at -32°C or less greater than 100,000 square kilometers, and area at -52°C or less greater than 50,000 square kilometers or more. And these size criteria must be met for at least 6 hours. MCCs typically form during afternoon and evening in the

form of several isolated thunderstorms. Within the MCC, the individual storms apparently work together to generate a long-lasting weather system that moves slowly (usually less than 40 km/hr) and often exists for periods exceeding 12 hours. The circulation of the MCC supports the growth of new thunderstorms as well as a region of widespread precipitation. They can also produce a wide variety of severe weather, including hail, strong winds, destructive flash floods, and tornado. Typically, the word “MCS” is usually used to describe a cluster of thunderstorms that does not satisfy size, shape, or duration criteria of an MCC.

2.3.5 Hail formation

Hail is precipitation in the form of hard, rounded pellets or irregular lumps of ice. Hailstones mostly have diameters range between 1 and 5 cm, although some can be as big as an orange or even bigger. Hail is produced only in large cumulonimbus clouds where updrafts can sometimes reach speeds of 160 km/hr and abundant supply of supercooled water is available. Hailstones begin as small embryonic ice pellets that grow by collecting supercooled droplets as they fall through the cloud.

If they encounter strong updraft, they may be carried upward again and begin the downward journey anew. Each trip through the supercooled portion of the cloud may be represented by an additional layer of ice. If this process lasts long enough, the hailstones may grow to considerable size. However, hailstones may also form from a single descent through updraft. Either way, the process continues until encounters downdraft or grows too heavy to remain suspended by the thunderstorm’s updraft.

2.3.6 Rainfall characteristics in Thailand

Thailand is located in the tropical zone between latitudes 5° 37' to 20° 27'N and longitudes 97° 22' to 105° 37'E with total area of 513,115 km². Its seasonal climate is largely under influence of regional monsoon wind especially the southwest and northeast monsoons. General knowledge of weather and rainfall patterns in Thailand is given in the Thai Meteorological Department website (TMD, 2009) and some data are concluded here. From the meteorological aspect, climate of Thailand can be divided into three seasons:

(1) Summer or pre-monsoon season (mid-February to mid-May) during which weather is generally hot and dry as the whole country is exposed to the sun the most and it is still lack of strong monsoon winds to influence weather otherwise,

(2) Rainy or southwest-monsoon season (mid-May to mid-October). During this period, the southwest monsoon mostly prevails over Thailand and it brings huge amount of moisture from the Indian Ocean to form abundant rain all over the country. Weather is usually hot and humid and the usual wettest period is August to September, and

(3) Winter or northeast-monsoon season (mid-October to mid-February). At this time, the weather pattern is mostly under the influence of northeast monsoon that brings cold and dry air from the Siberian High to govern the whole country, especially in the middle and upper part. But in the south, it will bring more rain to the area.

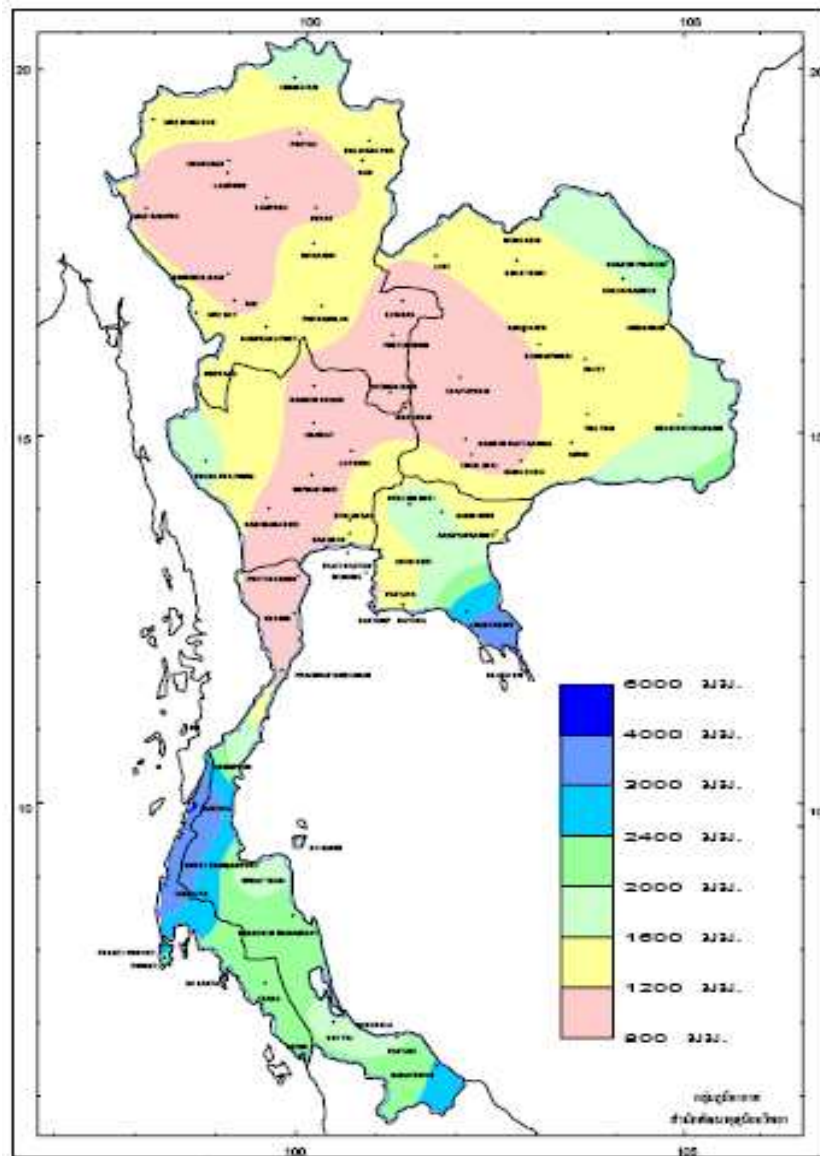


Figure 2.9 Annual rainfalls (millimeter) in Thailand (30-year average, 1971-2000).

Source: Thai Meteorological Department website (TMD, 2009)

In general, most rainfall in Thailand occurs during rainy season but few can still be seen in summer and winter (mostly convective rain). According to an average annual rainfall pattern (Figure 2.9 and Table 2.2), most areas have 1,200-1,600 mm a year. But some areas (on the windward side), particularly Trat Province in the East and Ranong Province in the South have more than 4,000 mm annually.

Typically, annual rainfall less than 1,200 mm occurs in the leeward-side areas (rain shadow), such as the central valleys and the uppermost portion of the South.

Table 2.2 Seasonal rainfall amount (in mm) and annual rainy days in different regions of Thailand (30-year average, 1971-2000) (TMD, 2009)

Region	Winter	Summer	Rainy	Total	Rainy days
North	105.5	182.5	952.1	1240.1	123
Northeast	71.9	214.2	1,085.8	1371.9	117
Central	124.4	187.1	903.3	1214.8	113
East	187.9	250.9	1,417.6	1856.4	131
South, East Coast	759.3	249.6	707.3	1716.2	148
South, West Coast	445.9	383.7	1,895.7	2725.3	176

Normally, there are 5 important factors that are believed to contribute most to the observed rainfall in the country, which are:

(1) The southwest monsoon which starts in May and brings warm moist air from the Indian Ocean inland causing abundant rain over the country, especially in the south (west-side) and in the far west. This situation could last until September,

(2) The monsoon trough, or the Intertropical Convergence Zone (ITCZ), which is a prominent belt of low pressure situating close to the equator. It is formed by the vertical ascent of warm, moist air from the latitudes north and south of the equator. However, the belt actual location varies over time where, over land, it moves back and forth across the equator following the sun's zenith point. Every year, it moves up north from the equator passing Thailand around May to June towards southern China and then moves back south through the country again from August to

October. During these times, it can initiate huge amount of cloud and rainfall along its border which makes more rain being observed than usual. Local flash flood and landslide often occur during the passing of the ITCZ also.

In general, dry spells commonly occur for 1-2 weeks or more during June to early July when the ITCZ leaves the country to southern China.

(3) The northeast monsoon which starts in October and lasts until February. Not only carrying cold and dry air from the China mainland to most parts of the country, it can also propel warm and moist air over the Thai Gulf inland causing abundant rainfall along the eastern coast of the south. This makes the provinces located under the influence of the monsoon have exceptionally high rainfall during this period (Table 2.2).

(4) The tropical cyclone which enters Thailand from time to time during monsoon season from the western North Pacific Ocean or the South China Sea. And based on its measured strength, three main forms of tropical cyclone are identified which are tropical depression, tropical storm, and typhoon (or hurricane).

However, only its depression form that is mostly seen in Thailand as the country situates very farther inland with respect to the originating zone of the cyclone, therefore, it is usually much weaken when entering the country's territory. However, several places in the south sometimes still suffered from the mighty tropical storms and typhoon that invaded their area. For examples, tropical storm "Harriet" that hit Nakhon Si Thammarat in October 1962 and typhoon "Gay" that hit Chumphon Province in November 1989.

(5) Cold airmass which is descending from the China mainland into the country during November to April. This large and dense airmass might collide with

the less-dense warm air flowing inland from the Thai Gulf that can induce instability weather and strong thunderstorm to be seen along the collision boundary.

Apart from these five influencing factors, rain and thunderstorms in Thailand can sporadically happen across the country as a result of the local convection process and the confluence of ocean air streams inland. Thunderstorms in the upper Thailand often occur from April to October (but most frequent in May) while those occur in the south usually seen in March to November. The afternoon and evening thunderstorms (especially in summer and winter) normally arise from convection process while the others from the confluence of different airstreams. The classification schemes for rain scattering and intensity by the TMD are shown in Table 2.3 and 2.4 respectively.

Table 2.3 Classification scheme for rainfall pattern in Thailand (TMD, 2009)

Class	Rainfall distribution	Meaning (of the total area)
Isolated	0-20% or 0/5-1/5	Raining less than 20%
Wildly scattered	20-40% or 1/5-2/5	Raining more than 20% but < 40%
Scattered	40-60% or 2/5-3/5	Raining more than 40% but < 60%
Almost widespread	60-80% or 3/5-4/5	Raining more than 60% but < 80%
Widespread	80-100% or 4/5-5/5	Raining more than 80% but < 100%

Table 2.4 Classification scheme for 24-hr rainfall intensity in Thailand (TMD, 2009)

Class	Rainfall amount
Not traceable	0-0.1 mm
Light rain	0-10.0 mm
Moderate rain	10.1-35.0 mm
Heavy rain	35.1-90.0 mm
Very heavy rain	90.1 mm up

2.3.7 Regional rainfall characteristics

Upper Thailand usually experiences dry weather in winter due to the influence of the northeast monsoon but in summer, amount of rainfall gradually increases as well as the thunderstorms. The onset of the southwest monsoon leads to an intensive rainfall from mid-May till early October with peak in August or September. However, dry spells commonly occur for 1 to 2 weeks or more during June to early July.

Rainy season in the south is different as abundant rainfall occurs during both the southwest (for the western coast) and northeast monsoon (for the eastern coast) periods. Amount of rainfall on the western side reaches its peak in September but the eastern side in November and remains high until January of the following year.

2.4 Weather satellites

Weather satellites are satellites that have been specifically designed and made for the observation and measurement about structure and gaseous components of the Earth's atmosphere as well as the important atmospheric phenomena such as rain, cloud, wind, thunderstorm, or the hurricane. First weather satellite called "TIROS-1" (Television Infrared Observation Satellites) was launched on 1 April 1960 by NASA

and in operation until July 2, 1965. The satellite has two TV cameras onboard for taking television footage of weather patterns (mostly cloud and large-scale cyclone) from an almost circular orbit, at an altitude ranging from 700 to 750 km. The success of the TIROS-1 operation led to the development of several more weather satellites later on by the NASA and the most successful programs from 1970 up to present are NOAA and GOES satellites in which 19 NOAA and 13 GOES satellites were already made so far (Davis, 2007).

2.4.1 Low earth orbit satellites

The weather satellites can be separated into two main categories according to their orbital altitude, the low earth orbit (LEO) and the geostationary orbit (GEO). The first group comprises of weather satellites that orbit the Earth's surface at altitude approximately 300 to 1,000 km and most of them operate along the near polar orbit. Therefore, sometimes they are called polar-orbiting satellites. Examples of the well-known LEO satellites at present are NOAA, DMSP, TRMM and Terra/Aqua.

NOAA satellites operate at altitudes of 800-850 km along which they take approximately 100 minutes to complete a full orbit. The most important instrument onboard is AVHRR (Advanced Very High Resolution Radiometer) sensor which has 4 or 5 channels scanning radiometer, measuring in the visible, near-infrared, and thermal infrared portions of the electromagnetic spectrum (see Table 2.5 for more information) (USGS-AVHRR, 2009). The latest satellite in this program, NOAA-19, was launched on 6 February 2009.

Like NOAA, DMSP (Defense Meteorological Satellite Program) satellites also operate at altitude 800-850 km. They usually have several instruments

onboard but most useful one is SSM/I-Microwave Imager. The SSM/I is a seven channels, four frequency, linearly-polarized, passive microwave radiometric system which measures atmospheric, ocean and terrain microwave brightness temperatures at 19.35, 22.235, 37.0 and 85.5 GHz (Table 2.6). SSM/I data are used to derive geophysical parameters, notably, ocean surface wind speed, ice properties, precipitation over land, cloud liquid water, soil moisture, land/sea surface temperature, and snow cover (NGDC, 2006).

Tropical Rainfall Measuring Mission (TRMM) satellite is a joint mission between NASA and Japan Aerospace Exploration Agency (JAXA). It was primarily designed to monitor tropical rainfall between latitudes 30°N and 30°S at orbital altitude 350 km and was successfully launched on 27 November 1997. There are five instruments onboard but the most well-recognized are Visible/Infrared Scanner (VIS), Precipitation Radar (PR) and the TRMM-Microwave Imager (TMI) (JAXA, 2009).

Precipitation Radar is weather radar working at frequency 13.8 GHz and is the first spaceborne instrument designed to investigate three-dimensional maps of the severe storm structure (Figure 2.11). The measurements yield information on the intensity and distribution of rainfall, on the rain type, on the storm depth and on the height at which the snow transforms into rain (see Table 2.6, Figure 2.10 and Figure 2.12 for more information). Major objectives of PR are (Adhikari and Nakamura, 2002):

- (1) Provide 3-dimensional rainfall structure,
- (2) Achieve quantitative rainfall measurement over land and ocean, and

(3) Improve the accuracy of TRMM Microwave Imager (TMI) measurement by providing the rain structure information.

Table 2.5 NOAA-AVHRR spectral ranges (USGS-AVHRR, 2009)

Spectral Band	Band spectral ranges (in micrometers)			IFOV (in milliradians)
	NOAA 6, 8, 10	NOAA 7, 9, 11,12,14	NOAA 15, 16, 17	
1	0.58-0.68	0.58	0.68	1.39
2	0.725-1.10	0.725-1.10	0.725-1.10	1.41
3(A)	-	-	0.58-1.64	1.30
3(B)	3.55-3.93	3.55-3.93	3.55-3.93	1.51
4	10.50-11.50	10.30-11.30	10.30-11.30	1.41
5	10.50-11.50	11.50-12.50	11.50-12.50	1.30

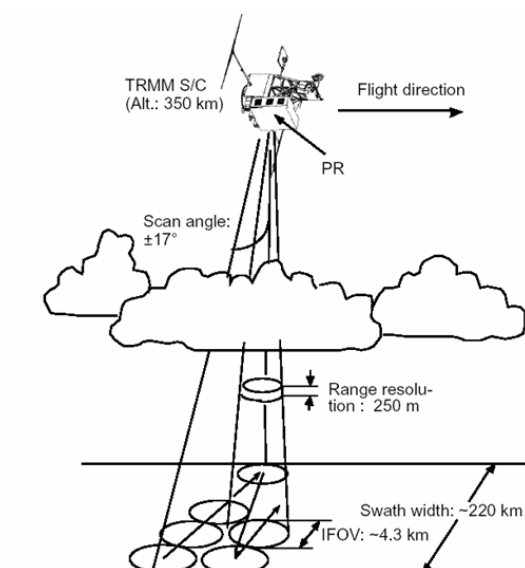


Figure 2.10 Viewing structure of the PR instrument.

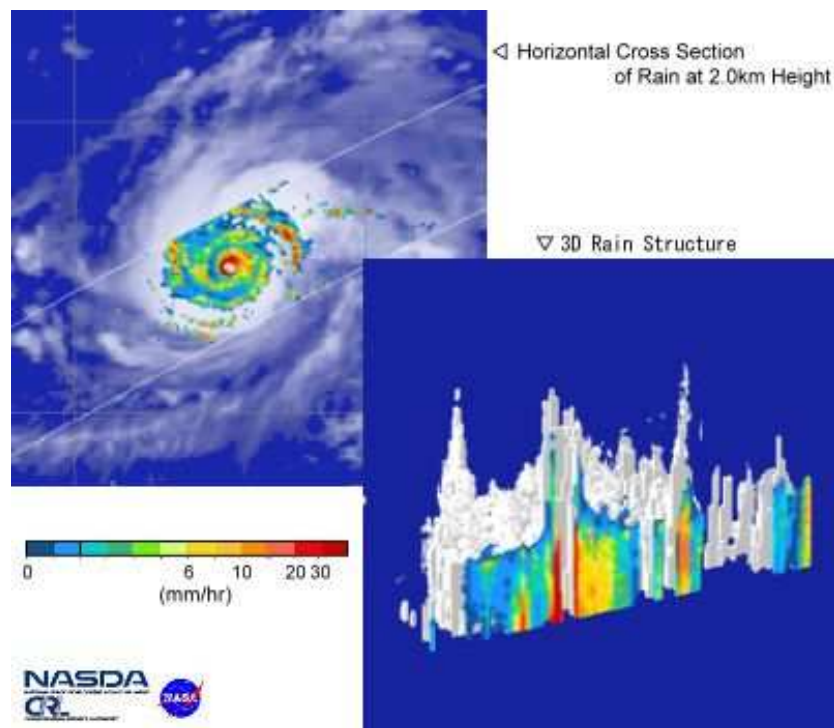
Source: JAXA (2009)

The TRMM Microwave Imager (TMI) is a passive microwave sensor designed to provide quantitative rainfall information over a wide swath under the TRMM satellite. By carefully measuring minute amounts of microwave energy emitted by the Earth and its atmosphere, TMI is able to quantify water vapor, cloud water, and rainfall intensity in the atmosphere. TMI is a multi-channel/dual-polarized microwave radiometer that measures radiation at frequency, 10.7, 19.4, 21.3, 37.0 and 85.5 GHz. The obtained information will provide data related to rainfall rates over the oceans. The TMI data together with PR data will be the primary data set of precipitation measurement. Up-to-date rainfall data from TRMM are provided in the website.

Terra and Aqua are two recent satellites in the Earth Observation System (EOS) of the US government launched in 1999 and 2002 respectively. One of their prime sensor is Modulate Resolution Imaging Spectro-Radiometer (MODIS) which have 36 spectral bands in the visible, NIR, Mid-IR, and TIR. The observation in the visible can provide cloud pattern and in TIR for the CTT (NASA-MODIS, 2009).

Table 2.6 TRMM-VIS/PR/TMI and DMSP-SSM/I data (JAXA, 2009)

Characteristic	VIS	PR	TMI	SSM/I
Frequency/ Wavelength	0.63, 1.6, 3.75, 10.8, 12 μm	13.8 GHz	10.65, 19.35, 21.3, 37.0, 85.5 GHz	19.35, 21.235, 21.3, 37.0, 85.5 GHz
Scanning Mode	Cross track	Cross track	Conical	Conical
Ground Resolution	2.1 km	4.3 km at nadir	7x5 km at 85.5 GHz to 63x37 km at 10.65 GHz	16x14 km at 85.5 GHz to 70x45 km at 10.65 GHz
Swath Width	720 km	220 km	760 km	1,400 km

**Figure 2.11** Structure of the hurricane in both 2D and 3D as seen by the PR instrument.

Source: NASA-TRMM website (<http://trmm.gsfc.nasa.gov>)

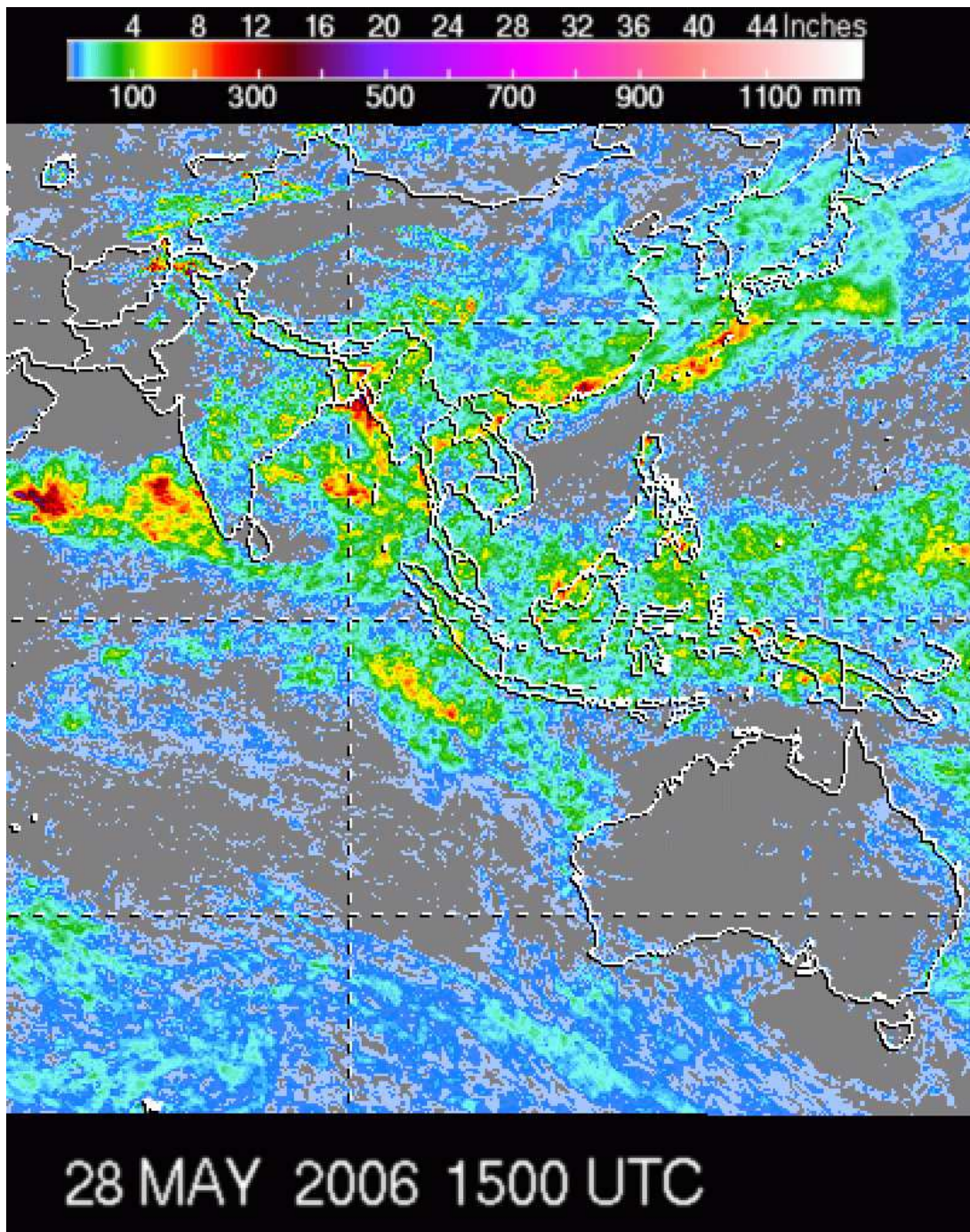


Figure 2.12 Rainfall pattern from TRMM satellite during 21-28 May 2006.

Source: NASA-TRMM website (<http://trmm.gsfc.nasa.gov>)

2.4.2 Geostationary orbit satellites

The second group of weather satellite contains satellites that are located above the equatorial line with similar orbital altitude at about 35,786 km. In this orbit, satellites will complete the orbit once every 24 hours, in accordance with the Earth's rotation rate. Therefore, their apparent locations are not changing with time as seen by the observers on the Earth's surface (which is the origin of name "GEO"). Examples of well-known GEO satellites are GOES, Meteosat, GMS and MTSAT.

The advantages of the LEO to GEO satellites are their better spatial resolution and the continuous observation along the orbit path, however, their temporal resolution is not as good as the GEO (mostly having about 15-20 days revisiting period). On the contrary, GEO satellites can observe Earth's atmosphere continuously during both daytime and nighttime (with about 15-30 minutes gap between each look), and with area cover of about 1/4 of the earth's surface but with rather coarse spatial resolution (usually 1-10 km).

The Geostationary Operational Environmental Satellite (or GOES) program is key component in the US-National Weather Service (NWS) operation as being main resource for the needed atmospheric data (e.g. from the satellite images or atmospheric soundings) necessary in global weather forecasting and meteorological research. First GOES satellite was launched on 16 October 1975 and the latest one in series, GOES-13, was launched on 24 May 2006. At present, there are four GOES satellites in the operation, GOES-10 (at 60°W over the South America), GOES-11 or GOES-West (at 135°W over the Pacific Ocean), GOES-12 or GOES-East (at 75°W over the Amazon River and provides most of the U.S. weather information) and GOES-13 which is still in on-orbit storage at 105°W. The most important instrument

onboard is GOES-Imager which has 5 spectral bands (1 in visible and 4 in IR regions) as described in Table 2.7 (NOAA-GOES, 2009).

Table 2.7 GOES-Imager instrument bands (GOES 8-12) (NOAA-GOES, 2009)

Channel	1 (Visible)	2 (SWIR)	3 (Moisture)	4 (TIR-1)	5 (TIR-2)
Wavelength (μm)	0.55-0.75	3.80-4.00	6.50-7.00	10.2-11.2	11.5-12.5
Ifov (nadir)	1 km	4 km	8 km	4 km	4 km

The Meteosat satellites are operated by the EUMETSAT under the Meteosat Transition Program (MTP) in which the first one, Meteosat-1, was launched in 1977 and the last of the first generation, Meteosat-7, was launched in 1997. Their main operational location is at 0° longitude above the Equator. However, two more Meteosat satellites in the second generation of the program (called MSG-1 and MSG-2) have been launched in 2002 and 2005 respectively to accompany and eventually replace the Meteosat-7 satellite. At present, the main operating satellite is MSG-2 (or Meteosat-9) at location 0° longitude while MSG-1 (or Meteosat-8) operates as a back-up at 9.5°E (EUMETSAT, 2009).

The SEVIRI (Spinning Enhanced Visible and Infrared Imager) radiometer is the main element of the MSG satellite. It will scan the Earth's surface sufficiently quickly to permit a repeat cycle of 15 minutes, using its 12 spectral bands that can provide daylight images of the weather patterns and thermal information with 1-km and 3 km spatial resolution in the visible and IR bands respectively (8 of which are in the TIR) (Table 2.8).

Table 2.8 SEVIRI instrument characteristics (MSG) (EUMETSAT, 2009)

Channel (Center)	Spectral Band (μm)	Resolution (km)	Principal target
HRV (0.75)	0.6-0.9	1 km	cloud texture, winds
VIS (0.64)	0.56-0.71	3 km	cloud over land, winds
VIS (0.81)	0.74-0.88	3 km	cloud over water, vegetation
NIR (1.6)	1.50-1.78	3 km	cloud over snow
MIR (3.8)	3.48-4.36	3 km	low cloud
IR (6.2)	5.35-7.15	3 km	high water vapor
IR (7.3)	6.85-7.85	3 km	middle water vapor
IR (8.7)	8.30-9.10	3 km	total water vapor
IR (9.7)	9.38-9.94	3 km	total ozone
IR (10.8)	9.80-11.80	3 km	surface/cloud top temp., winds
IR (12.0)	11.00-13.00	3 km	surface temp. correction
IR (13.4)	12.40-13.40	3 km	higher clouds

The Geostationary Meteorological Satellites (GMSs) program is operated by the Meteorological Satellite Center (MSC) of Japan Meteorological Agency (JMA) and a series of the GMS satellite (called “Himawari” in Japanese) have been launched since 1977 where the most recent one, GMS-5, was launched on 18 March 1995 into the GEO orbit at 140°E. It carries instrument called VISSR (Visible and Infrared Spin Scan Radiometer) that has four channels, one in the visible and three in the infrared regions (Table 2.9). The ground resolution (at nadir) is 1.25 km in the visible band and 5 km in the infrared.

The MTSAT-1R (Multi-functional Transport Satellite), or Himawari-6, is the first satellite in this series being launched into orbit on 26 February 2005 as a replacement to the old GMS-5. It has new infrared channel that was added to improve

the detection of fog at nighttime and also the accuracy of sea surface temperature observation (Table 2.9). During the MTSAT-1R operation, the MTSAT-2 (launched in 2006) has been placed in standby mode at 145°E to continue the mission if MTSAT-1R fails to work properly.

Table 2.9 GMS-VISSR instrument characteristics (MSC, 2009)

Title	GMS 1-4	GMS-5	MTSAT-1R	MTSAT-2
Channel and Wavelength (all in μm)	IR (Infrared) (10.5-12.5)	IR1 (10.5-11.5)	IR1 (10.3-11.3)	
			IR2 (11.5-12.5)	
		IR3 (6.5-7.0) (Water vapor)		
			IR4 (3.5-4.0)	
	Visible (0.50-0.70)		Visible (0.55-0.90)	

Imager spatial resolution: Visible: 1 km (nadir), IR 1-4: 4 km (nadir)
Imager quantization levels: Visible: 10 bits, IR 1-4: 10 bits

MTSAT observes cloud and water-vapor distribution continuously during day and night as well as the land/sea surface and cloud-top temperatures. By analyzing these data, a range of useful information, such as cloud top height, cloud distribution, cloud types (e.g. cumulus, stratus, cirrus, and cumulonimbus), fog and winds in the atmosphere can be obtained. Further, the development of typhoons, depressions and fronts, as well as the sea ice and volcanic ash clouds can also be observed by MTSAT. Example of the VIS/TIR GMS-5 satellite images are shown in Figure 2.13.

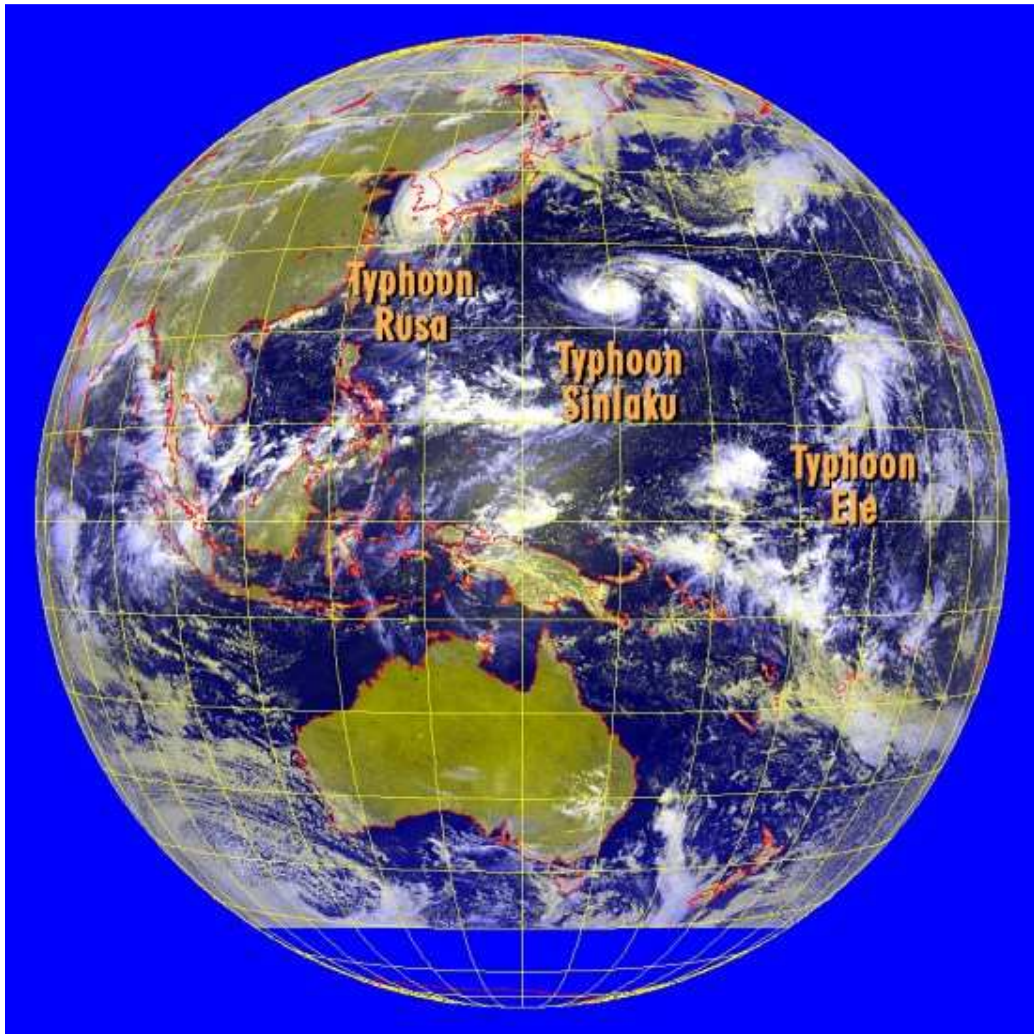


Figure 2.13 GMS-5 VIS/TIR satellite image over Pacific Ocean on 31 August 2002. Major features appeared include deep/thick cloud (white), high/thin cloud (light blue), low clouds (pale yellow), land (yellowish green) and sea (dark). Note that, there are three typhoons appeared in the upper part of the images (as names seen).

Source: Hong Kong Observatory website (<http://www.hko.gov.hk>)

2.5 Relationship between cloud and rain

Cloud and rain are the key components of the global hydrologic cycle that regulates circulating mechanism of water around the world. Clouds are the original

source of rain which is crucial for the daily living of the majority of population on the Earth, especially the farmers. The important role of clouds is not only producing rain but also maintaining the Earth's energy balance system. Thick clouds can reflect a considerable amount of the incoming sunlight back to space during daytime while high thin clouds can absorb some of the outgoing infrared radiation emitted from the Earth surface, especially at nighttime, and radiate it back downward. As a result, knowledge of cloud structure and distribution is essential for the understanding of rainfall pattern, climate changes, and energy balance characteristics of the interested area (NASA-Cloud and Radiation, 2009).

2.5.1 Cloud classification techniques

The cloud structure depends greatly on stability level of air in which it forms from which three groups of cloud cluster are usually identified: cirriform, stratiform and cumuliform. Cirriform clouds usually form in the upper troposphere and compose principally of ice crystals. It is normally thin and transparent, wispy and white in appearance but sometimes it can be seen in the form of a very dense patch which is left over from the anvil cloud of a cumulonimbus which has disappeared.

Stratiform clouds mostly form in the stable air in which vertical movement of air parcels is strongly suppressed, as a result, the growing clouds have to mostly extend horizontally. This makes them have sheet-like layers with a large horizontal out reach. On the contrary, the cumuliform clouds mostly happen in the unstable air in which the vertical movement of the air parcels is strongly enhanced. This situation leads to the developing clouds often have vertical extent that is larger than their horizontal outstretch, for examples, the cumulus or cumulonimbus clouds.

Generally, the cirriform clouds cannot produce rain whereas the stratiform clouds may cause some light rainfall. But the heavy rainfall is always associated with the deep and thick clouds like cumulonimbus. Figure 2.14 shows different cloud types as normally seen in the tropical summer time.



Figure 2.14 Three main forms of cloud: cirriform, stratiform and cumuliform.

Source: <http://www.carlwozniak.com/clouds/Graphics/New%20Pix/clouds25.jpg>

Cloud classification is the process of identifying type of clouds based mainly on their appearances or the observed properties. In feature selection, 6 criteria of appearance: brightness, texture, area cover, shape, organization and shadow, are often considered for cloud identification by NASA and NOAA Weather Satellite Programs (like NOAA). In addition, cloud motions are sometimes added to provide the information of how rain moves. At present, cloud classification is typically utilized

based on the satellite images taken in the visible, mid-infrared (MIR), thermal infrared (TIR), and microwave portions of the electromagnetic spectrum.

Images of cloud in visible region can provide useful information about cloud size, shape, texture and context while images in the infrared region can inform about the water content and surface temperature of the cloud. The active microwave images can be used to identify cloud structure and its water content. Several techniques have been proposed to identify different types of cloud in the satellite imagery (mostly for rainfall estimation) but they can be divided into three broad categories, which are:

- (1) Spectral-based methods: e.g. the bi-spectral or split window techniques,
- (2) Texture-based methods: e.g. the texture analysis or fractal analysis,
- (3) Structure-based methods: e.g. spatial clustering or component identification.

2.5.1.1 Bi-spectral technique

Among these described methods, the most popular one is the bi-spectral technique which classified cloud types based on their appearance in the visible and thermal infrared satellite images (see Figure 3.4 for example). Naturally, bright clouds in visible images represent dense and thick cumuliform clouds (with high albedo like cumulonimbus) that are more likely to precipitate while less dense or high thin clouds (like cirrus) normally appear in the gray tone. However, cold clouds (like cumulonimbus cloud top and all high cloud) shall appear as bright area in the thermal infrared images due to their low surface temperature, but low and middle clouds that have warmer surface typically appear in gray tone. If cloud images in these

two spectral regions are jointly considered, some specific criteria, or thresholds, may be reached to identify types of the clouds embedded in those associated images (Dioszeghy and Fejes, 1995; Masson *et al.*, 1996; Fan *et al.*, 1997).

For examples, cirrus or other high thin clouds appear gray in the visible image but are very bright in the TIR image, whereas cumulonimbus appear bright both in the visible or infrared images. In addition, thick low/middle clouds with high albedo (like cumulus) usually appear bright in the visible but grey tone in the infrared image (see Figure 3.8 for example).

2.5.1.2 Split-window technique

Other technique widely-used for the identification of cumulonimbus cloud from the surrounding high clouds is called the “split-window” approach. The method was initially proposed by Inoue (1985, 1987a, b) for the automatic delineation of convective rainfall areas in the NOAA-AVHRR images. This method uses two infrared brightness temperatures (T_b) observed at infrared bands e.g. at 10.5-11.5 (T_{11}) and 11.5-12.5 (T_{12}) μm measured from weather satellites (like NOAA, GOES, GMS, or MTSAT). These data are available during both daytime and nighttime.

The basis of the split-window technique for cloud detection lies in property of the infrared window region from 8 to 12 μm , in which, the refractive index of water and ice (particularly its imaginary part) varies significantly with wavelength. This variation results in the difference in transmissivity and emissivity of the cloud. In case of thick clouds, the clouds can achieve their blackbody state so that the brightness temperature observed from space does not change with respect to their wavelength. On the other hand, in case of thin clouds such as cirrus clouds, the clouds are usually far from being in the blackbody state, as a result, radiation from the

underlying surface and atmosphere passes through the cloud and a part of radiation thermally emitted from cloud body itself is added to upward radiation above clouds. Therefore, BT of optically thin clouds changes with wavelength, and the clouds can be detectable by means of two channels in the IR window region (Hayasaka, 1996).

The technique is developed based on the data of brightness temperature observed in the two TIR bands (center at 11 and 12 μm) given in terms of T_{11} and $\Delta T = T_{11} - T_{12}$ (Cooper *et al.*, 2003). In addition, at night, the difference between BTs measured in the shortwave (at 3.75 μm) and longwave (11 μm) IR ($T_{B_{3.75}} - T_{B_{11}}$) can be used to detect partial cloud or thin cloud within the sensor's field of view (FOV). The small or negative differences are seen only when opaque scene (such as thick cloud or the surface) fills the FOV and negative differences occur at night over extended cloud due to lower cloud emissivity at 3.75 μm channel.

At nighttime, the 6.7 μm TIR channels could also be employed to identify the thick cumulonimbus cloud. The idea is that low clouds are buried in the water vapor, and since the 6.7 μm channel sees temperature of the cooler water vapor present above the cloud (as temperature decreases with height), the satellite-measured temperature will be lower than the actual cloud top temperature. But, the same cloud when observed at 11 μm will yield temperature much closer to the true cloud top temperature. Therefore, the difference between the two measurements will be large. Conversely, for high and thick cloud, there is not much water vapor above it to depress the relative difference between two channels so the values in this case are small (Kurino, 1997a, b).

Based on these facts, extensive algorithms have been developed to classify clouds and estimate the cloud-top height and optical thickness using split-

window measurement with various thresholds. For examples, Inoue (1987; 1989) used this technique to classify cirrus and blackbody clouds in the AVHRR images in which two-dimensional histograms of brightness temperature of the 11 μm channel and BT difference (BTD) between split window data were constructed. By selecting proper thresholds in the histogram, cirrus, dense cirrus, cumulonimbus, and cumulus clouds can be identified over the tropical ocean (Figure 2.15).

The technique was also used in Inoue *et al.* (1997) for the GMS-5 satellite images and in Inoue (2004) for the GOES-West satellite image. In the latter work, the BT of 253 K (-20°C) was used as a cloud threshold of deep convection, and the BTD of 1 K was applied for the cirrus/cumulonimbus type cloud classification. A deep convection is defined as the cloud area that is colder than 253 K.

According to Inoue (1989), the height of the cloud top can be classified by two thresholds. If the brightness temperature value was below (above) -20°C , then the cloud type should be classified as being low) level cloud. In general, -20°C roughly corresponds to the air temperature around 400 hPa in the tropics. Similarly, Inoue *et al.* (2004) applied split-window method to examine spatiotemporal structures of cloud properties over the Bay of Bengal during the period 1986-1993. In this work, six cloud types including low-level cumulus, cumulus, thin cirrus, thick cirrus, dense cirrus, and cumulonimbus type were classified where the 0.75°C threshold was used to distinguish optically thick clouds (cumulonimbus) from dense cirrus and the -20°C threshold to separate between low level cumulus and cumulonimbus.

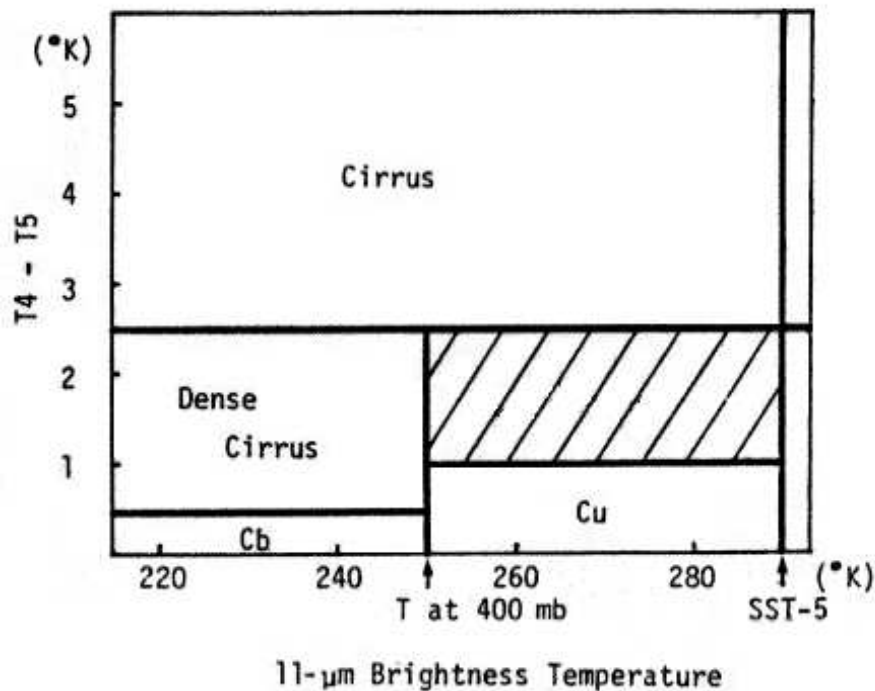


Figure 2.15 Cloud classification table proposed by Inoue (1987) for NOAA AVHRR. The abscissa and ordinate show $11\text{-}\mu\text{m}$ BT and the difference between $11\text{-}\mu\text{m}$ and $12\text{-}\mu\text{m}$ BT, respectively. The 0.5 K threshold was applied to separate cumulonimbus from dense cirrus. The clear-sky region (over sea) is defined as $T_{11} > \text{SST}-5$ K.

2.5.2 Rain and cloud relationship

The effective quantitative determination of the rain rate from the knowledge cloud type and its distributing pattern is still one of the most difficult and changeling problems facing science and technology of satellite remote sensing (see for reviews in Barrett and Martin, 1981; Petty, 1995; Levizzani, 1999; Levizzani *et al.*, 2002). The viewpoint varies substantially from the relatively simple methods used for climatic-scale analyses (Arkin, 1979; Arkin and Janowiak, 1991) down to the instantaneous rain rate estimations for the research and nowcasting (e.g. Bellon *et al.*, 1980; Scofield, 1987; Adler and Negri, 1988; Turk *et al.*, 1998a, b) and the unified

perspective on satellite precipitation estimates still not unanimously exists. In the past, mostly used satellite data for rainfall estimation were from the visible, infrared and water vapor bands of the weather satellites.

However, in the last decade, several passive and active microwave instruments have been sent to space for the measurement of cloud property and the resulting rainfall but the technical deficiencies delimit the use of the microwave sensors to only for the low earth orbit satellites not for the geostationary satellite.

2.5.2.1 Visible and infrared techniques

Visible and infrared satellite imagery are the common resource for the analysis of rainfall amount based on many proposed methods that can be broadly divided into four categories which are (1) cloud indexing, (2) bi-spectral, (3) life history and (4) cloud model-based. Each category stresses a particular aspect of the sensing of cloud physical properties using satellite imagery (Barrett and Martin, 1981; Levizzani 1999, 2000).

Cloud indexing techniques normally assign a specific rain rate value to each cloud type identified on the satellite imagery. The simplest and perhaps mostly used one was invented by Arkin (1979) based on high correlation between radar estimated precipitation and fraction of area associated to temperatures lower than 235 K in the TIR cloud images.

This method, named GOES Precipitation Index (GPI), assigns these areas with a constant rain rate of 3 mm/hr, which is appropriate for measuring tropical precipitation over $2.5^{\circ} \times 2.5^{\circ}$ boxes (Arkin and Meisner, 1987). GPI has become standard and regularly applied for the simple rainfall estimation in large area (e.g. in Kumar and Prasad, 1997 and Islam and Wahid, 2003). The linear form of the GPI is:

$$\text{GPI (mm)} = K \times \text{FC} \times P \quad (2.3)$$

where K is a constant rain rate, taken as 3 mm/hr by Arkin and Meissner (1987), FC is the fractional coverage of cloud, and P is the average raining period (in hr).

Rain days could be identified from the occurrence of IR brightness temperatures below a threshold at a given location. Estimated rain days are combined with rain daily means that are spatially variable to produce rainfall estimations for extended periods. The World Climate Research Program (WCRP) along with Global Precipitation Climatology Project (GPCP) has started estimating precipitation at this scale over the globe for periods from five days to a month (World Climate Research Program, 1996). A family of cloud indexing algorithms was developed at the University of Bristol, originally for the NOAA satellites and recently adapted to geostationary satellite imagery, and has been applied by Todd *et al.* (1995) to rainfall estimation in River Nile catchment while Tucker and Sear (2001) applied it for the whole Kenya in 1996-1998.

Bi-spectral methods are based on very simple, though not automatic, relationship between cold and bright clouds and high probability of the precipitation as it frequently happens for cumulonimbus. Lower probabilities are associated to cold but dark (cirrus) or bright but warm (stratus) clouds. Tsonis and Isaac (1985) and Tsonis (1987) developed clustering methods similar to bi-spectral cloud classification. Rain areas are determined by classifying pixel clusters in the VIS/IR histogram of the cloudy scene and radar data are used as the validation ground truth.

The role of VIS data in improving IR rainfall estimates was also examined by King *et al.* (1995) and their results show a higher correlation with validation data using VIS/IR over the IR alone for a case of warm, orographically

induced rainfall. O'Sullivan *et al.* (1990) used CTT and textural characteristics during daytime along with TIR temperature patterns to estimate rainfall over a 10x10 pixel array in three categories: no rain, light rain, and moderate/heavy rain.

The life-history methods, like Griffith-Woodley technique (Griffith *et al.*, 1978), are oriented towards the convective cloud system. It relies upon a detailed analysis of the cloud's life cycle, which is particularly relevant for convective clouds. The used formula for rainfall determination is normally described as (Sumner, 1988):

$$R(t) = aA(t) + b(dA/dt) \quad (2.4)$$

where $R(t)$ is the rain rate at time t (m^3/s), $A(t)$ is the area of cloud cover at time t (m^2), a and b are constants of the system. A major problem arises in presence of cirrus anvils of neighboring clouds which often screen the cloud life cycle underneath leading to possible underestimates early in the day and overestimates towards the evening.

Cloud model techniques incorporate mechanisms of cloud formation process into the retrieval of associated rainfall amount. A 1D-cloud model has been usually adopted to relate cloud top temperature (CTT) to rain rate and rain area (Adler and Negri, 1988). Precipitation is assigned to convective areas by means of the derived cloud model from which the relationship between CTT and rain rate are determined and described in form of some chosen mathematical formula. The most popular one is in the form:

$$P = aT^b \quad (2.5)$$

where P is the rainfall amount and T is the associated cloud top temperature, a and b are appropriate constants of the calculation derived from the reference data.

In addition, apart from the CTT, the duration of rain cloud existing was also used for the estimation of rainfall in the tropics, mostly in Africa, as seen in Mohammedberhan (1998), Thorne *et al.* (2001), and Grimes *et al.* (1999). All works used same technique called “TAMSAT” (Tropical Applications of Meteorology using Satellite data) to predict the amount of rainfall which can be described as

$$P = aCCD + b \quad (2.6)$$

where P is the rainfall amount, CCD is the associated rain (or cold) cloud duration, while a and b are appropriate constants derived from the referenced rain data. Results found in Mohammedberhan (1998) are shown, for example, in Table 2.10.

Table 2.10 Rain-CCD relationship used by Mohammedberhan (1998)

Month	Formula	r ²	Threshold
May	P = 0.075CCD + 4.38	0.42	-40°C
July	P = 0.98CCD + 17.19	0.74	-30°C
August	P = 0.55CCD + 20.72	0.48	-30°C
September	P = 0.88CCD + 1.71	0.52	-50°C

Note: P = Rainfall amount (in mm) and CCD = Cold Cloud Duration (in hr)

In addition, the aforementioned split-window technique can also be used for the instantaneous delineation of the convective rainfall areas using data in the 10.5-11.5 and 11.5-12.5 μm channel (Inoue 1987; 1989; 1997). The content of the two channels partially corrects erroneous rainfall area (and consequent frequent rainfall

overestimate) of simple IR techniques producing better false alarm ratios (FAR). Kurino (1997a, b) has applied a split-window technique to data from the Japanese Geostationary Meteorological Satellite (GMS) from which three parameters: the 11 μm brightness temperature, the difference between 11 and 12 μm , and the difference between 11 and 6.7 μm were extracted.

2.5.2.2 Passive microwave techniques

In the VIS and IR spectral range, clouds are frequently opaque and precipitation is inferred from the cloud top structure only. However, at passive microwave frequencies, precipitation particles are the main source of attenuation of the upwelling radiation and, therefore, the passive microwave technique can provide physically more direct than those based on VIS/IR radiation. The emission of radiation from atmospheric particles results in an increase of the received signal at the instrument. But at the same time, the scattering due to hydrometeors reduces radiation streams whereas type and size of the influencing hydrometeors depend on the frequency of the upwelling radiation (Levizzani, 1999).

Above 60 GHz, ice scattering dominates and the radiometers can only sense ice while rain is not detected. Below about 22 GHz, absorption is the primary mechanism affecting the transfer of microwave radiation and ice above rain is virtually transparent. Between 19.3 and 85.5 GHz, the common passive microwave frequency range, radiation interacts with the main types of hydrometeors, water particles or droplets (liquid/frozen). Scattering and emission happen at the same time with radiation undergoing multiple transformations within cloud column in the sensor's FOV. At different frequencies, the radiometers observe different parts of the rain column. As for other parts of the spectrum, microwave radiation is absorbed (but

not scattered) by cloud droplets, water vapor and oxygen. This can make precipitation estimates based on absorption potentially difficult.

Precipitation drops strongly interact with microwave radiation and are detected by radiometers without the IR strong biases. The biggest disadvantage is the poor spatial and temporal resolution; the first due to diffraction and the latter to the fact that microwave sensors are presently only mounted on polar orbiters. The situation is further complicated by the differences in radiative characteristics of sea and land surfaces that lie underneath. A sea surface has a relatively constant low emissivity ($e = 0.4$) so that the radiation emitted from it is small and precipitation ($e = 0.8$) will increase the amount of radiation detected by the sensor through emission. The high polarization of sea surface also contrasts very much with the low polarization of rain. Land surfaces have a high and variable emissivity ($e = 0.7-0.9$) close to that of the precipitation and low polarization.

The emissivity depends upon characteristics of the surface including vegetation cover and moisture content. Rainfall overland increases the upwelling radiation stream but, at the same time, absorbs radiation inducing errors in the identification of rain areas. Scattering is thus the key to microwave rainfall estimation techniques over land and the 85.5 GHz channel of the Special Sensor Microwave/Imager (SSM/I) is very sensitive to scattering from small particles. The applicability of passive microwave rainfall retrieval methods needs to be clearly defined, especially when operational applications are at stake (Ferraro *et al.*, 1994; Berg *et al.*, 1998). Wilheit *et al.* (1994) provide a fairly complete overview of the field and Petty (1995) concentrates on rainfall estimation over land.

2.5.2.3 Active microwave techniques

A new perspective in tropical rainfall measurements from space is available since November 1997 with the launch of the Tropical Rainfall Measuring Mission (TRMM) satellite. The main objectives of its three-year mission are to measure rainfall and energy (i.e. latent heat of condensation) exchanges of tropical and subtropical regions for a better initialization of global weather and climate models. The passive microwave instrument TMI is a follow-up of SSM/I with a new 10.7 GHz channel installed and horizontally polarized and the water vapor channel shifted from 22.235 to 21.3 GHz. The most important improvement is the double frequency (13.796 and 13.802 GHz) PR instrument, the first of its kind to be flown on board a spacecraft. The instrument aims at providing the vertical distribution of rainfall for the investigation of its three-dimensional structure, obtaining quantitative measurements over land and sea.

2.5.2.4 Hybrid method

Accurate and rapidly-updated precipitation products can be drawn from the use of multiple satellite sensors on geostationary and polar orbits. Sensors such as the GOES's Imager and Meteosat's VISSR rapidly update imagery taken in the IR spectrum, which corresponds to emitted cloud top radiation for optically thick clouds. The SSM/I provides a global coverage of precipitation from polar orbit. The method of Turk *et al.* (1998a, b) attempts to statistically fuse these two types of satellite data in real time for the retrieval of instantaneous and accumulated rain rates at the geostationary time scale, i.e. half an hour or less. A probability matching is performed between the SSM/I rain rates from the closest passage in time and the geostationary TIR brightness temperatures. The matching is automatically updated as new SSM/I

data are ingested in real time. The technique can work in principle for all current GEO satellites (GOES-8/9, GMS-5, METEOSAT-7) and adaptation is also applied for the assimilation of rain rates from the TMI.

Several other IR/MW methods have been proposed trying to take advantage of the higher physical content of microwave measurements and the spatial/temporal coverage of geostationary satellites. Among them are Jobard and Desbois (1992), Laing *et al.* (1994) and Vicente and Anderson (1994). All these methods have to properly consider about the necessity of a constantly ongoing and non-static calibration procedure as being outlined by Levizzani *et al.* (1996) and incorporate it in some kind of probability matching method like one described above.

A different approach based on the synergetic use of GOES-8/9 thermal IR data, radar instantaneous rainfall estimates and model output is the Auto-Estimator technique of NOAA satellite Data and Information Service (NESDIS) (Vicente *et al.*, 1998). The method has been developed using power-law regression algorithm to compute real-time precipitation values. The regression is based on a statistical matching between radar-derived rainfall estimates and observed satellite brightness temperature field. Adjustments are performed for different moisture regimes using real-time fields of precipitable water and relative humidity as computed by the Eta Model of the National Center for Environmental Predictions (NCEP).

Vicente *et al.* (1998) reported the comparison results between mean radar-derived estimated rainfall and cloud top temperature from 195 K to 260 K as seen in Figure 2.16. The solid curve represents the regression fit given by:

$$R = 1.1183 \times 10^{11} \times \text{Exp}(-3.6382 \times 10^{-2} \times T^{1.2}) \quad (2.7)$$

where R is the rainfall rate in mm/hr and T is the cloud top temperature in Kelvin (K). Both rain and non-rain pixels are considered in the computation of the regression fit.

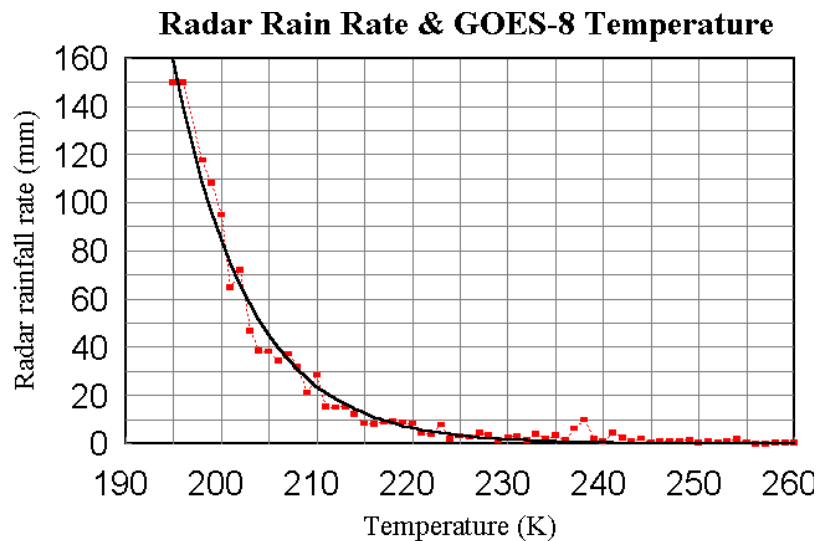


Figure 2.16 Relationship between radar rainfall rate and cloud brightness temperature given in Vicente *et al.* (1998) where dots represents mean radar derived rainfall for each one degree temperature interval from 195 K to 260 K. The solid curve represents the power law fit between radar derived rainfall estimates and cloud top temperature.

2.5.3 Studies of cloud-rainfall relationship in Thailand

In recent years, there are several efforts to investigate the arithmetic relationship between rainfall rate and cloud top temperature (CTT) with various results. For examples, Udomchoke and Aungsuratana (1995) compared the amount of rainfall collected from 20 weather stations in the north with their corresponding CTT above the used station derived from GMS-4 satellite. Results were shown in Table 2.11. This is normally called the power-law P-T relationship.

Table 2.11 Rainfall-CCT relationship in Udomchoke and Aungsuratana (1995)

Period	Formula	r^2	Season
March–May	$P = 4.3932 \times 10^{58} T^{-24.80}$	0.97	Hot season 1993
August–September	$P = 1.8462 \times 10^{22} T^{-8.93}$	0.62	Rainy season 1994

Note: P = Rainfall amount (mm), T = Cloud top temperature (K)

ธีระพงษ์ เสาวภาคย์ (2539) found that the amount of daily rainfall that produced flash-flood in different regions of Thailand could be estimated from the CCT in term of the non-linear regression equations as seen in Table 2.12.

Table 2.12 Rainfall-CCT relationship in ธีระพงษ์ เสาวภาคย์ (2539)

Region	Formula	r^2
North	$P = 1.1102 \times 10^{13} T^{-4.8288}$	0.71
North Eastern	$P = 4.4905 \times 10^{10} T^{-3.8012}$	0.73
East	$P = 5.2384 \times 10^{12} T^{-4.6683}$	0.70
South	$P = 2.4916 \times 10^{11} T^{-4.0804}$	0.71

Note: P = Rainfall amount (mm), T = Cloud top temperature (in K)

In addition, ธนิต ธีญญหาญ (2545) and มณฑล จิตเธื่ออารีกุล (2546) have used the TAMSAT technique and cloud top temperature to estimate rainfall in Bangkok Metropolitan during the southwest monsoon (May-October) and northeast monsoon (October-March) season, respectively and the results are shown in Table 2.13.

Table 2.13 Rainfall-CCD relationship in ชนิด ัญญาหาญ (2545) and มณฑล จิตเอื้ออารีกุล (2546)

Period	Formula	r^2	Threshold
May-October (2001) ชนิด (2545)	$P = 8.8333\text{CCD} - 30.875$ $P = 6.854 \times 10^5 T^{-1.7474}$	0.742 (-30°C) 0.745	-30, -40, -50°C $P > 40 \text{ mm}$
Oct (2000)-Mar (2001) มณฑล (2546)	$P = 0.616\text{CCD} + 14.488$	0.7 (-40°C)	0 to -60°C

Note: P = Rainfall amount (in mm), CCD = Cold Cloud Duration (in hr), T = CTT (in °C)

Also, Budhakooncharoen (2004) used the 3 hrs rainfall data observed at 3 ground stations in the Petchabun Province (Muang, Lomsak and Wichianburi) to investigate their relationship with CTT data over the station extracted from the GMS5 satellite imagery. The data were collected during May-October in 1997 and 1998 and the obtained results were described in the P-T form as seen in Table 2.14.

Table 2.14 Rainfall-CCT relationship in Budhakooncharoen (2004)

Station	Formula	r^2
Muang	$P = 2.52 \times 10^{28} T^{-11.141}$	0.7527
Lomsak	$P = 7.57 \times 10^{24} T^{-9.555}$	0.6829
Wichianburi	$P = 1.796 \times 10^{26} T^{-10.525}$	0.8149

Note: P = Rainfall amount (in mm/3 hr), T = CTT (in K)

CHAPTER III

METHODOLOGY

3.1 Conceptual framework

The main objective of this study is to analyze the relationship between rainfall intensity and the associated cloud properties (cloud top temperature and cloud cover area) in Thailand based on the selected case studies occurring in 2006 and 2007. To achieve this goal, three main steps of the work procedure were planned and implemented:

(1) Development of the automatic cloud mapping and classification model for the use with MTSAT-1R imagery,

(2) Examination of the seasonal rainfall and cloud cover distributing patterns during the selected years, and

(3) Analysis on the relationship between rainfall intensity and cloud properties (cloud top temperature and cloud cover area) based on the chosen case studies.

Figure 3.1 presents diagram of the work procedure mentioned above where its first part (model development) is described in detail in this chapter while information of the other two parts are further described in Chapter IV. Information about all used data and their original source is given in Table 3.1.

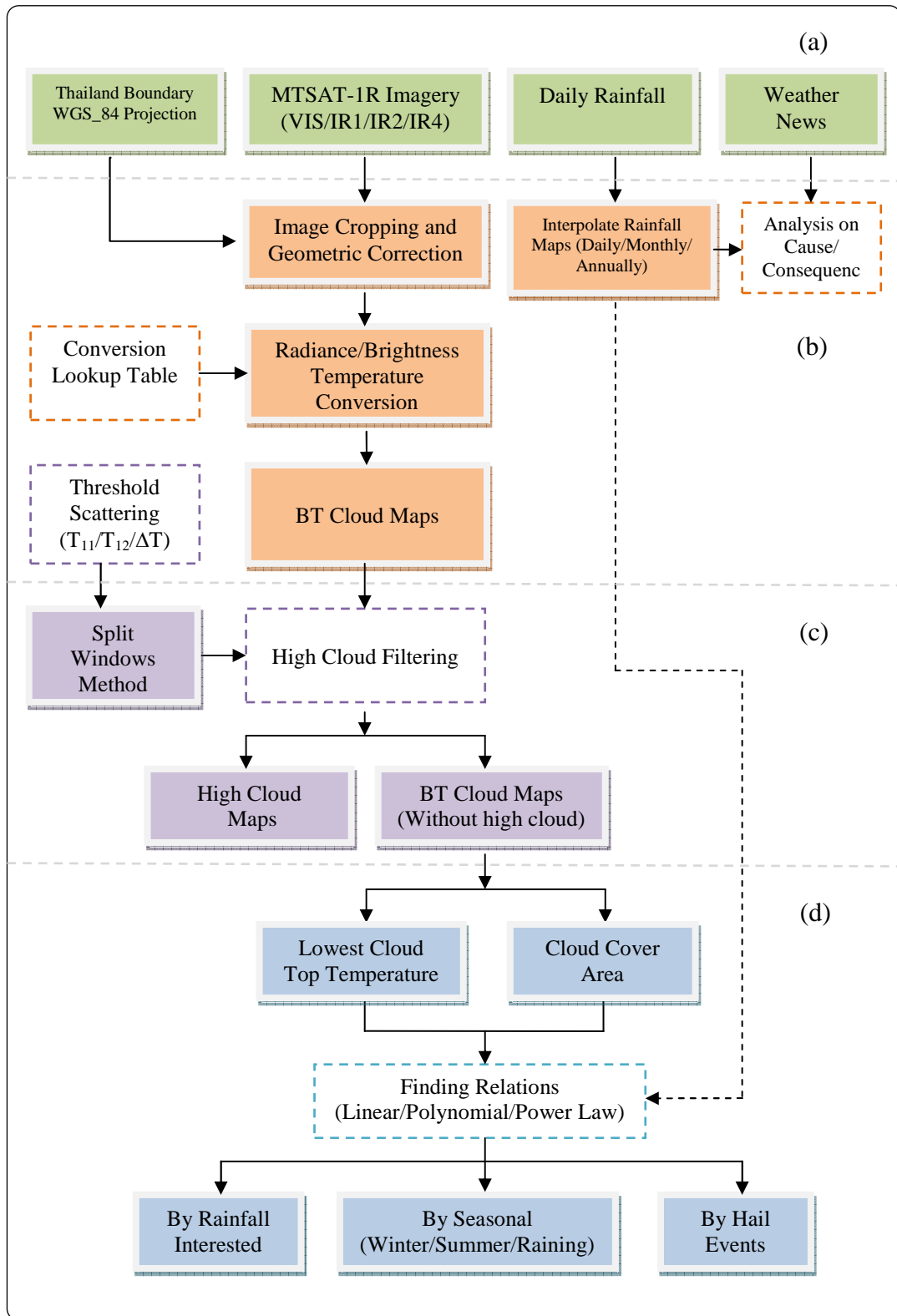


Figure 3.1 Flow chart of the study divided into 4 principal parts: (a) data collection (b) data map preparation, (c) cloud model development and (d) analysis and reporting.

Table 3.1 Information of the data usage.

Data type	Raw data format	Input format	Original source
Rainfall	Daily record from 116 TMD stations	Interpolated map (using IDW method)	Thai Meteorological Department (TMD)
Satellite imagery	MTSAT-1R (1 VIS and 4 TIR bands)	Cloud cover area and CTT maps	Kochi University, Japan
Boundary map	Province polygon	Country boundary	Department of Environmental Quality Promotion (DEQP)
Weather news	Official report	Details of the events	TMD, Department of Disaster Prevention and Mitigation (DDPM)

As this work needs large number of the classified cloud distributing and cloud top temperature (CTT) maps over the entire country in the analyzing process but the proper tools to operate this task effectively were still yet to find. As a consequence, at the beginning of the research period, most time was devoted to the development of such tool based on application of several existing computer programs like MATLAB, SML and ERDAS Macro. The result is the cloud classification model for MTSAT-1R imagery over Thailand as needed (see Section 3.3 for detail).

3.2 Data collection and data map preparation

All needed data for the study are described in Table 3.1 along with the original source of the referred data. However, most data have to be modified, or enhanced, and transformed into some proper formats that are capable of being used by the processing program or models. This is called data map preparation and details are as follows:

3.2.1 Rainfall map

The first stage of analyzing process performed was the examination of rainfall pattern over Thailand compared between years 2006 and 2007 based on the generated monthly, quarterly, and annual rainfall maps of those years. These maps were created by the interpolation of rainfall records from 116 weather stations locating around the country using the IDW interpolation method (see Figure 3.2 and Appendix C for more detail). These stations are responsible by the Thai Meteorological Department (TMD) and raw data were provided in the form of daily rainfall files (.xls spreadsheet). These received files need to be re-formatted before putting into ArcMap for further analysis. (See Figure 3.3 for example of the used rainfall file).

The daily rainfall data were subsequently accumulated to produce rainfall map at specific time period required; e.g. daily, monthly or annual. To assist the qualitative analysis, rainfall data were divided into several classes to represent different zones of intensity level on the rainfall map.

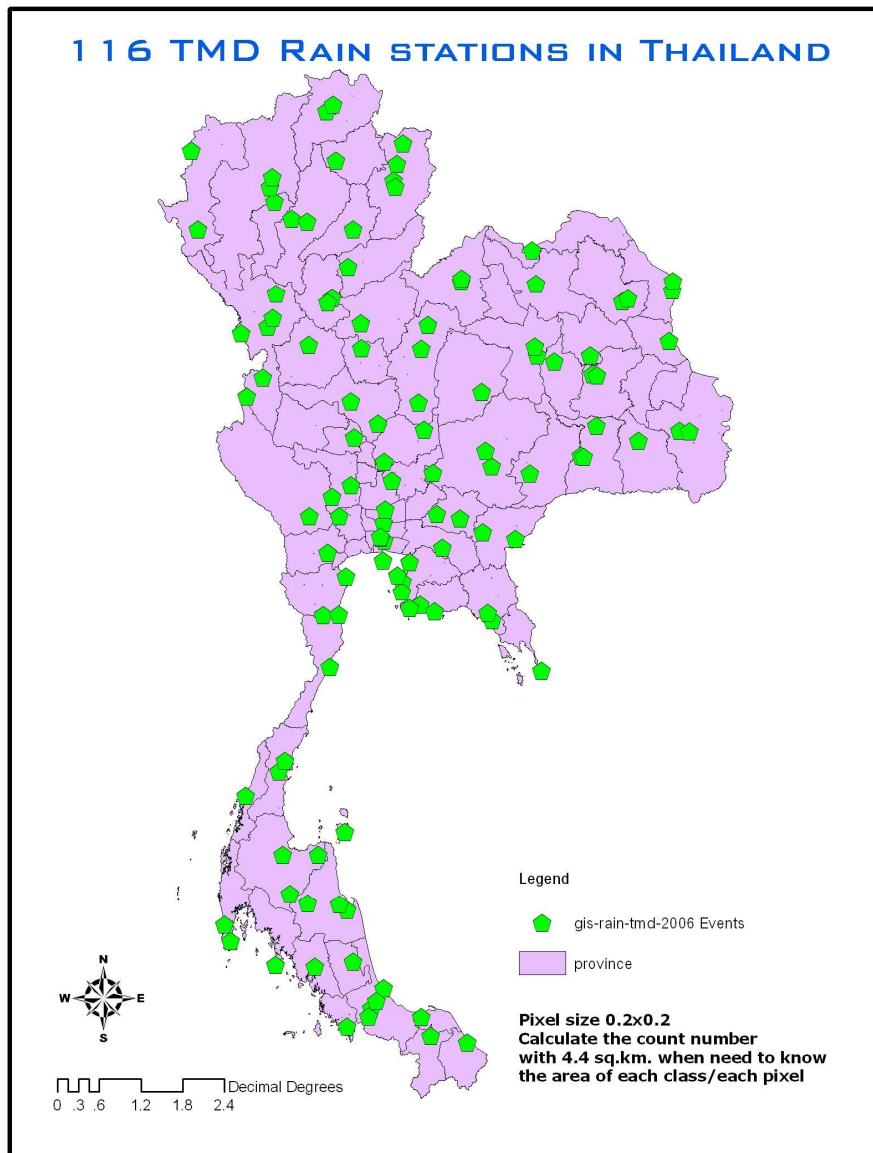


Figure 3.2 Location map of the 116 TMD weather stations in use.

	A	B	C	D	E	F	G	H
1	stn_name	stn_lat	stn_lon	stncod	year	month	dday	rain
336	Sawi Agromet	10.3333	99.1	517301	2006	12	6	158.2
337	Chumphon*	10.4833	99.1833	517201	2006	12	6	116.9
338	Kho Hong Agromet	7.0167	100.5	568301	2006	12	16	68.7
339	Yala Agromet	6.5167	101.283	581301	2006	12	20	67.1
340	Nakhon Si Thammarat*	8.4667	99.9667	552201	2006	12	16	63.8
341	Nakhon Si Thammarat*	8.4667	99.9667	552201	2006	12	15	60.1
342	Pattani Airport*	6.7833	101.15	580201	2006	12	16	55.8
343	Songkhla*	7.2039	100.605	568501	2006	12	16	48.3

Figure 3.3 Example of the used rainfall data files (before re-formatting).

Source: TMD (2009)

3.2.2 Cloud cover map

The cloud cover maps for some selected dates, or periods, were also prepared based on raw data of MTSAT-1R satellite images in the visible and infrared regions, which can be downloaded from the web site of Kochi University in Japan: <http://weather.is.kochi/archive-e.html>, under the supervision. However, at present, only hourly image files were available for the download. Ancillary data of the image; e.g. hour/date/year being taken or band, were given in the file's name as illustrated in Figure 3.4.

All five bands of the VISSR sensor (1 visible and 4 TIR in Table 2.9) are available for the download. The spatial resolution of the visible image is about 1 km (nadir) and the TIR image is about 4 km (nadir). Example of the satellite's visible image is shown in Figure 3.5.

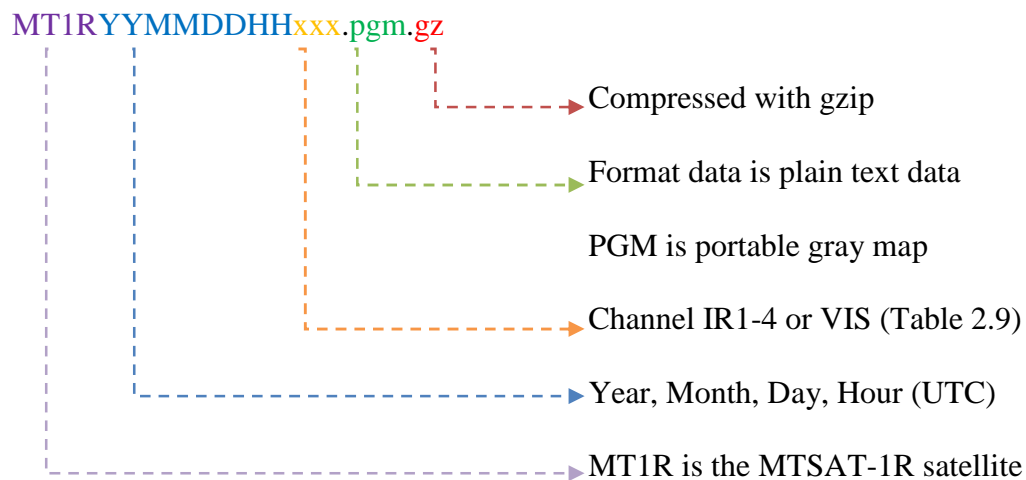


Figure 3.4 Structure of the MTSAT-1R filename

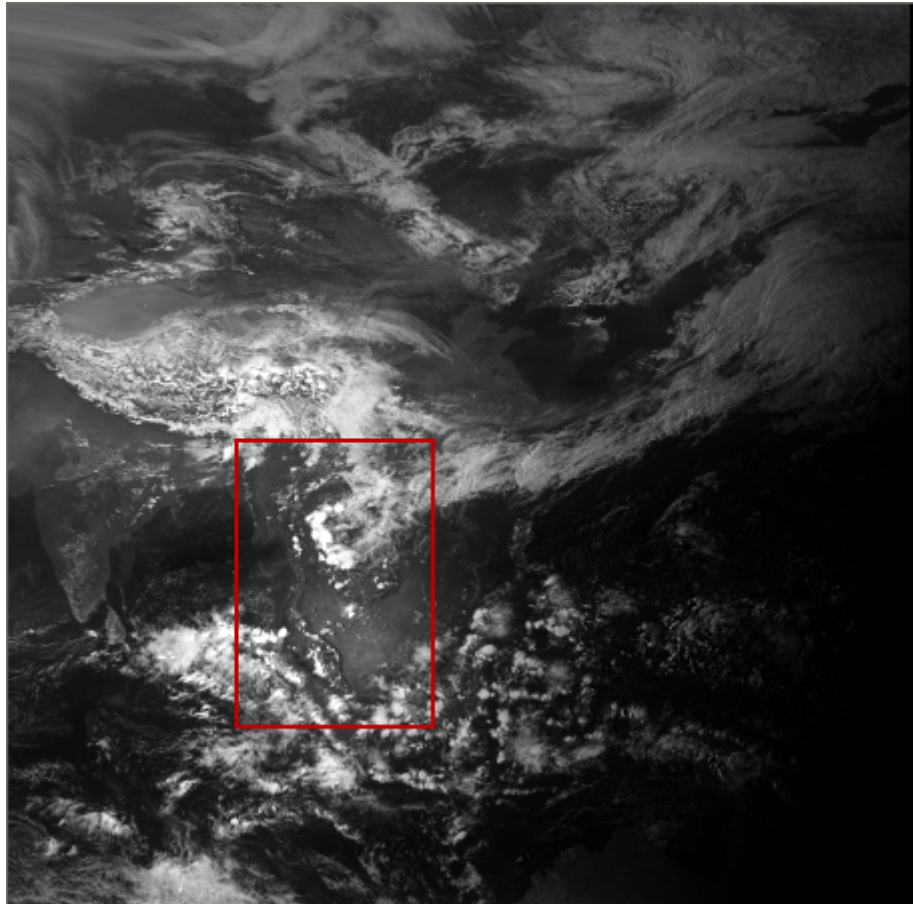


Figure 3.5 MTSAT-1R VIS image over the Pacific Ocean on 25 April 2007

Source: Kochi University (<http://weather.is.kochi/archive-e.html>)

Before putting in use, the original satellite images must be cropped to separate only the portion of area over Thailand for further study using the MATLAB program. These images were then geometrically corrected by the ERDAS program based on the WGS-84 projection and the country's boundary was then added to the cropped image. The boundary location was derived by dissolving the province polygon provided by the Department of Environmental Quality Promotion (DEQP).

The brightness values in gray scale 0-255 for TIR images were subsequently converted into the equivalent brightness temperature, or BT, (in Kelvin

unit) based on the standard look-up tables for the proper conversion of each TIR band provided by the satellite's responsible agency-JAXA. The BT images are needed for the classification of cloud types, especially the heavy-rain cloud (cumulonimbus) and cold/high cloud (e.g. cirrus), by the conventional methods like bi-spectral (along with VIS image) or split-window technique.

However, to evaluate relationship between rainfall and cloud top temperature, the non-precipitating cold clouds, like cirrus, must be screened off first otherwise they may be mistakenly classed as being rain-bearing cumulonimbus as their normal CTTs are rather indifferent. All the before mentioned procedure can be operated automatically using the developed model that is discussed later in Section 3.4.2.

3.3 Analyzing process

The first step of the planned analyzing process in this thesis was to examine variation in pattern of the seasonal rainfall and cloud distribution over Thailand in the selected years (2006 and 2007), and also, to identify the causal factors that influence the appearance of those observed rain and cloud maps. In the explanation, the priority was given to the main factors that are believed to dominate pattern of rainfall found in Thailand as discussed in Section 2.3.6, especially the monsoon systems.

The work in this part was focused on analyzing the seasonal cloud and rainfall distributing patterns as a whole based on their observed data during the years. For the rainfall, these are rainfall accumulated maps on monthly, seasonal, and annual basis. But for the cloud cover, these are temporal classified cloud maps during some chosen period (about 5 days) in each season (summer, rainy, and winter).

The second task was to analyze the relationship between rainfall intensity and cloud properties (cloud top temperature and cloud cover area) based on some chosen case studies. The used rainfall data (for each case) were gained from the 116 TMD stations mentioned earlier (Figure 3.2) and the corresponding CTT maps were derived from the developed model (see Section 3.4). The analysis was separated into three broad scenarios based on season, region, and rainfall intensity. Particular interest was given to the severe rainfall from the cumulonimbus cloud. The relationship was explained in proper linear form, polynomial form, or power-law regression form that most fit.

Main focus of the study was also placed upon the hail events which are good indicator for the presence of severe thunderstorms (from the cumulonimbus cloud). Information of hail events was gathered from official reports issued by the TMD and also the DDPM in 2006 and 2007 (see Table 3.2 for more detail).

Table 3.2 Reports of hail events in 2006 and 2007 from the TMD and DDPM

Date	Locations (Provinces)
14 March 2006	Lampang
7 April 2006	Nakhonratchasima, Buriram, Srisaket, Sakaew, Phetchaboon, Loey, Sakonnakorn
9 April 2006	Chiangmai
12 April 2006	Tak
13 April 2006	Sakonnakorn
14 April 2006	Chiangrai, Ubonratchathani
17 March 2007	Yasotorn, Kalasin
27 March 2007	Chanthaburi
3 April 2007	Kalasin, Khonkan, Roet, Srisaket
4 April 2007	Chachoengsao, Trang, Trad, Mahasarakham, Yasotorn, Roet, Lopburi
8 April 2007	Kanchanaburi, Tak, Sakaew
11 April 2007	Kanchanaburi, Chachoengsao, Chiangrai, Chiangmai, Nan, Prathumthani, Lampang, Surin, Uthaithani
18 April 2007	Khonkan, Chiangmai, Prae, Mahasarakham
19 April 2007	Chiangrai, Nan
24 April 2007	Nakhonpanom, Nongkai
25 April 2007	Nakhonsawan, Prae, Lampang, Srisaket, Surin, Utrดิต
27 April 2007	Trad, Tak, Pisanulok, Phetchaboon, Srisaket, Nongkai

3.4 Development of automatic cloud classification model

As this study need to use large number of the classified cloud distributing and CTT maps over the entire country in the analyzing process but the proper tools to operate this task effectively and conveniently was still yet to find. As a consequence, at the beginning of the research period, most time was devoted to the development of such tool for further use as required. There were three main steps in the formation of this required cloud classification model after the original satellite image files were downloaded form the host website (at Kochi University) which are:

- (1) Cropping and geometric correction of Thailand portion in the image,
- (2) Conversion from radiance files into equivalent brightness temperature file,
and
- (3) Classification of cloud types using the brightness temperature map.

3.4.1 Cropping and geometric correction of Thailand portion

As this study concerns only the rainfall and cloud distribution over Thailand territory while the original MTSAT-1R satellite images cover all the Pacific regions, where Thailand is located on the far left of the image, as seen in Figure 3.5 (or Figure 2.13 for GMS-5). As a result, all the downloaded images must be cropped to reduce their size to cover the Thailand portion only. This was succeeded by using MATLAB cropping module that is able to operate the cropping file by file through the entire source directory. The destination directory, band preference, or cropping location can also be specified on the module through the code-writing process (see appendix B).

Before cropping, each image file covers area between longitudes 70°E-160°E and latitudes 20°S-70°N. This comprises of about 1800x1800 pixels in total,

each pixel has $1/20 \times 1/20$ degree resolution, as shown in Figure 3.6. Downloaded data are normalized to 8 bits (256 levels).

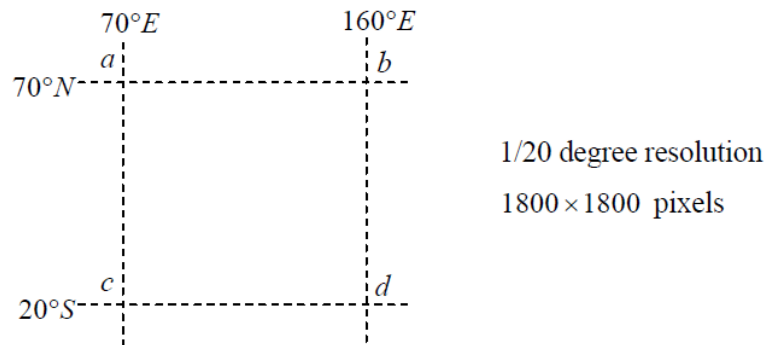


Figure 3.6 Original area cover of MTSAT-1R image

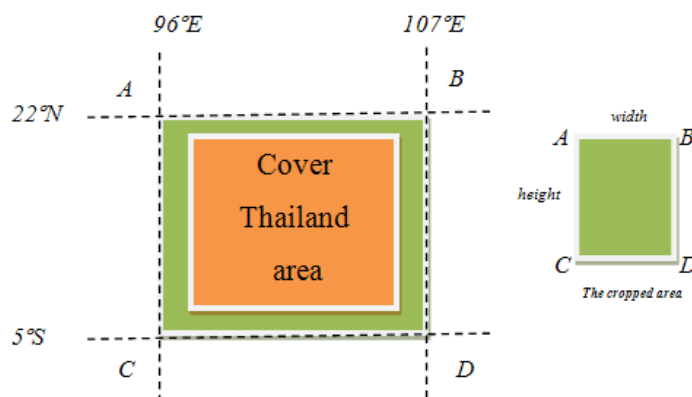
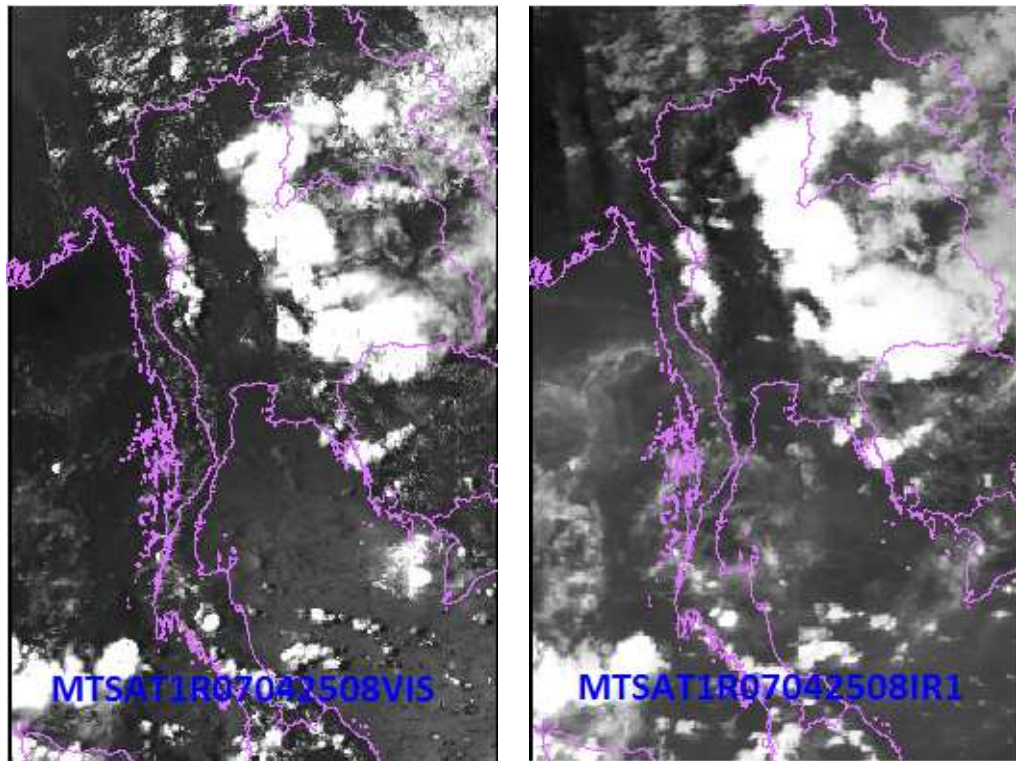


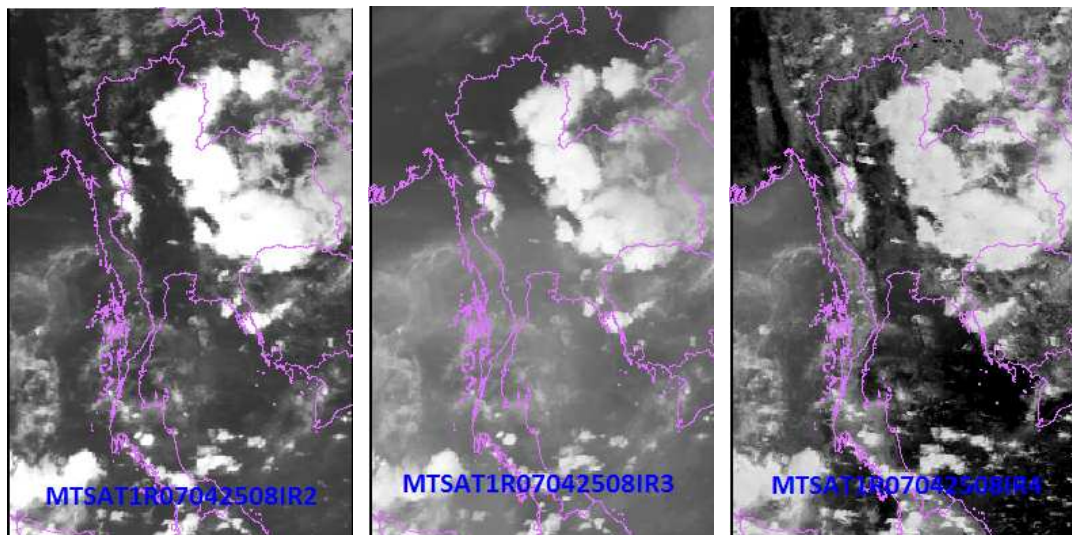
Figure 3.7 Cropping area cover of MTSAT-1R image

To crop Thailand portion off from the whole image, four specific coordinates close to Thai border were chosen and listed as position A, B, C and D, where their respective coordinates are: A (96°E , 22°N); B (107°E , 22°N); C (96°E , 5°S) and D (107°E , 5°S) as displayed in Figure 3.7. The cropped image now has 220×340 pixels. Examples of the cropped image files over Thailand are shown in Figure 3.8.



(a) Visible band

(b) IR1 band



(c) IR2 band

(d) IR3 band

(e) IR4 band

Figure 3.8 Examples of the cropped MTSAT-1R satellite image for Thailand portion in (a) visible band (at 0.55-0.90 μm), (b) IR1 band (at 10.3-11.3 μm), (c) IR2 band (at 11.5-12.5 μm), (d) IR3 band (at 6.5-7.0 μm) and (e) IR4 band (at 3.5-4.0 μm).

In order to make the Thailand study area in the cropped area, the following calculations are performed. The cropped image has 220x340 pixels. The cropped area is defined by the area *ABCD*.

The locations for the points *A*, *B*, *C* and *D* of the cropped area in Figure 3.7 with reference to the points *a*, *b*, *c* and *d* of the original area of the satellite image in Figure 3.6 can be calculated as follows:

$$A: (96^{\circ}\text{E}-70^{\circ}\text{E}, 70^{\circ}\text{N}-22^{\circ}\text{N}) = (26, 48)$$

$$B: (107^{\circ}\text{E}-70^{\circ}\text{E}, 70^{\circ}\text{N}-22^{\circ}\text{N}) = (37, 48)$$

$$C: (96^{\circ}\text{E}-70^{\circ}\text{E}, 70^{\circ}\text{N}-5^{\circ}\text{S}) = (26, 65)$$

$$D: (107^{\circ}\text{E}-70^{\circ}\text{S}, 70^{\circ}\text{N}-5^{\circ}\text{S}) = (37, 65)$$

In terms of pixels, the locations are defined as follows:

$$A: (26 \times 20, 48 \times 20) = (520, 960) \quad B: (37 \times 20, 48 \times 20) = (740, 960)$$

$$C: (26 \times 20, 65 \times 20) = (520, 1300) \quad D: (37 \times 20, 65 \times 20) = (740, 1300)$$

Then width and length are defined to size of *X* and size of *Y* as follows:

$$\text{size of width (X)} = 740 - 520 = 220 \text{ pixels}$$

$$\text{size of length (Y)} = 1300 - 960 = 340 \text{ pixels}$$

The variables will be used to entry in MATLAB crop programming. It is (*x*, *y*, *w*, *l*). In this study, the value of (*x*, *y*, *w*, *l*) is (520, 960, 220, 340).

These images were then geometrically corrected using the ERDAS program and based on the WGS-84 lat/long projection and the country's boundary was then added to the cropped image. The boundary was derived from the province polygon provided by the Department of Environmental Quality Promotion (DEQP).

3.4.2 Radiance conversion for BT mapping

To classify the cloud types on the satellite images, knowledge of the cloud top temperature (CTT) are necessary. For MTSAT-TIR imagery, this CTT map could be generated directly by using the standard look-up table for the radiance/BT conversion provided for each individual image (see Table 3.4 and Figure 3.9 for examples). The conversion table was formulated based on the Planck function and sensor's spectral response functions from which the approximated conversion formula is given as follows (MSC, 2009):

$$B_i(T_b) = 2hc^2V_i^3 / \exp \{hcv_i/k(a_{1i}+a_{2i}T_b) - 1\} \quad (3.1)$$

where B_i : sensor Planck function of channel i

T_b : brightness temperature

V_i : central wave number of channel i

a_{1i}, a_{2i} : band correction coefficients of channel i

h : Planck constant

k : Boltzmann constant

c : speed of light

values of the constants a_1 and a_2 for each band of MTSAT-1R are given in Table 3.3.

In this context, the brightness temperature T_b is the equivalent temperature at the surface of the objects under the observation (along the FOV line of sight) from which the measured radiance was first released.

Table 3.3 Values of the constants a_1 and a_2 for each MTSAT-1R band (MSC, 2009).

Channel	Wave number	Band correction coefficients	
	ν (cm ⁻¹)	a_1	a_2
IR1 (10.8 μm)	926.6118	0.3592380	0.9987587
IR2 (12.0 μm)	833.1675	0.1968675	0.9992525
IR3 (6.8 μm)	1482.2068	0.3785336	0.9991187
IR4 (3.8 μm)	2652.9316	2.3473427	0.9969755

Table 3.4 Example of the conversion table for TIR images of MTSAT-1R

Radiance Value	Equivalent brightness temperature (in Kevin unit)			
	IR1	IR2	IR3	IR4
0	329.941500	329.940000	299.967083	319.969643
1	329.625500	329.593333	299.799306	319.862024
2	329.309500	329.246667	299.631528	319.754405
3	328.993500	328.900000	299.463750	319.646786

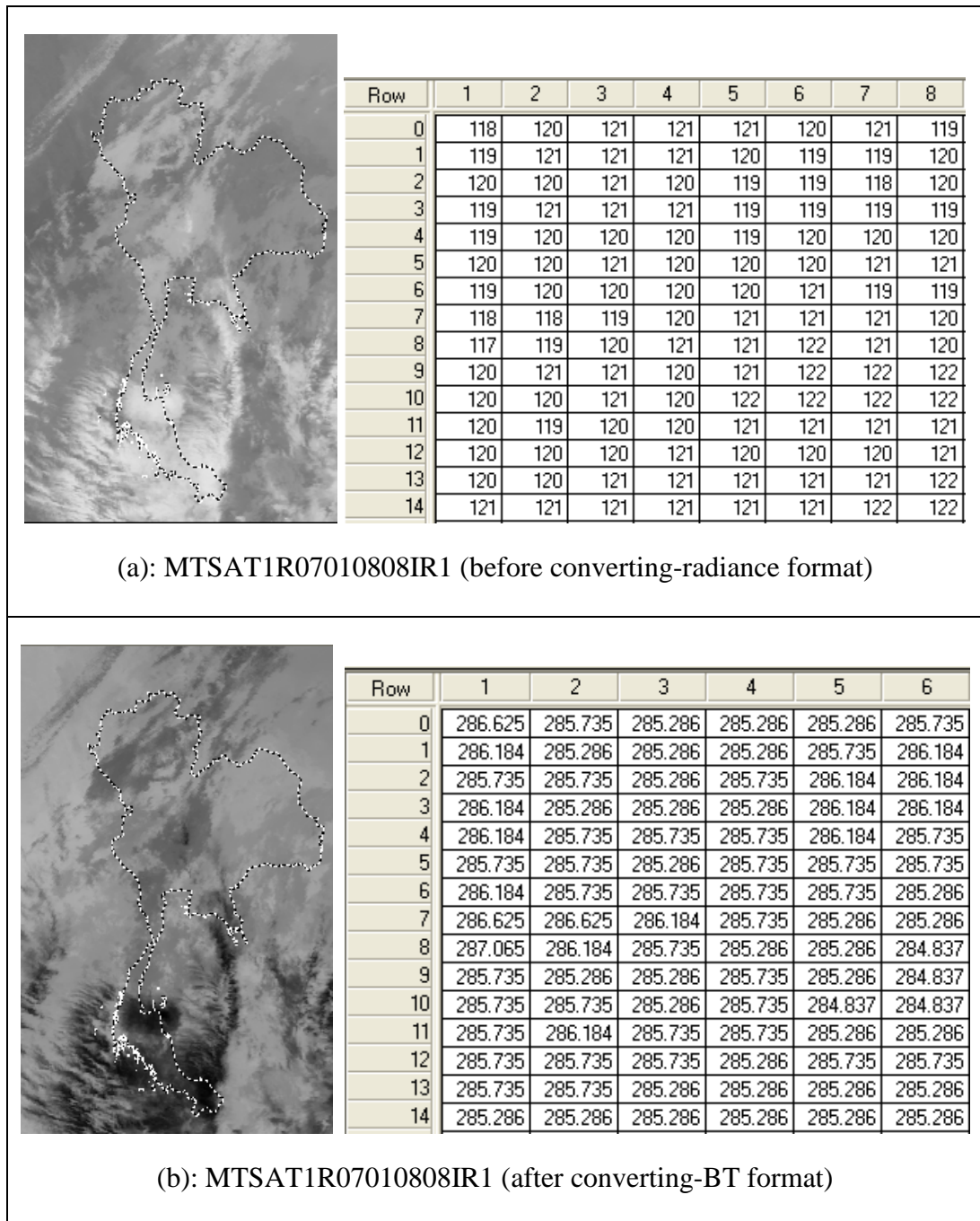


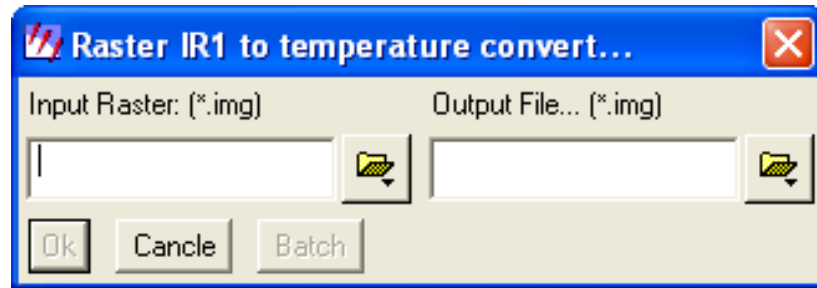
Figure 3.9 Examples of the MTSAT TIR image (a) before conversion-displayed as radiance image and (b) after conversion-displayed as equivalent BT image (in Kelvin unit).

To assist the automatic conversion from radiance image to corresponding BT image, the conversion module was developed based on the Spatial Modeler Language and ERDAS Macro Language. The module was created for general use with TIR images from any weather satellite where the conversion look-up table is available and was added as an extended utility tool in ERDAS menu. The GUI appearance of the module is shown in Figure 3.10. Note that, in the module, only the conversion of band IR1, IR2 and IR4 are available at present as they were needed in the analysis. However, the application for IR3 image could be implemented conveniently if required. The input file is radiance file (with DN = 0-255) and the output file is its equivalent BT file (in Kelvin unit).

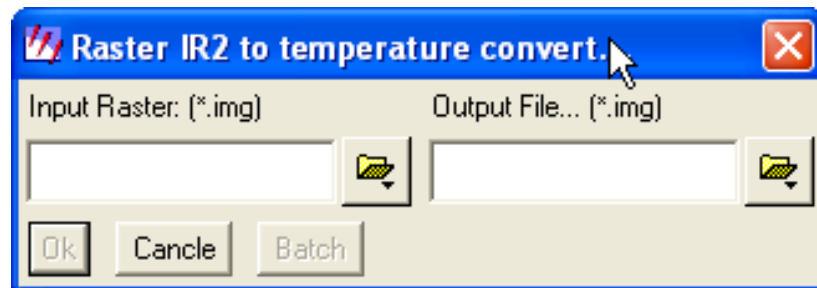
3.4.2.1 Classified CTT maps

The derived BT map was for all objects that appear on the satellite image. However, only the cloud section of the image that was of interest in the study therefore the BT threshold was set at 10°C in the formulation of cloud cover image. This makes most of the background objects on the Earth's surface being screened off the displayed map along with some warm clouds that have CTT greater than 10°C.

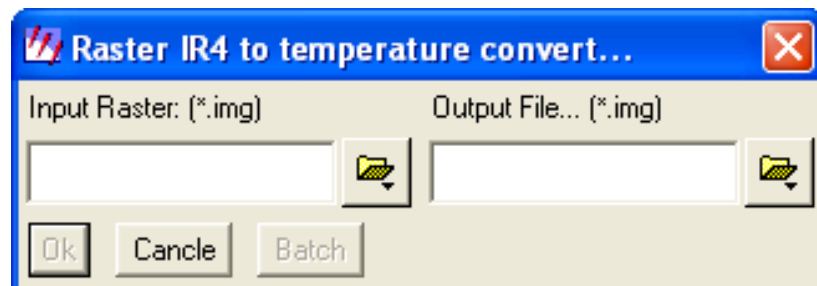
However, by setting threshold at this value, it can enable the detection of warm clouds that have CTT between 0 and 10°C and also the mixed cold/warm clouds that may have temperature between 0 and -20°C. The identification of cloud type on the image was still not performed at this stage but, generally, the clouds at temperature 10 to -20°C are usually the growing cumulus cloud, or some stratiform clouds, that might be able to produce a shower or light rainfall but not heavy rainfall. But clouds with temperature less than -40 or -50°C are likely to be rain-bearing cloud like cumulonimbus; however, these can be cold high clouds like cirrus also.



(a) GUI for the conversion of raster IR1



(b) GUI for the conversion of raster IR2



(c) GUI for the conversion of raster IR4

Figure 3.10 The GUI appearance of the derived radiance/BT conversion module

In this work, the brightness temperature data on used cloud images were classified into eight classes (at interval of 10°C) as described in Table 3.5 and some examples of the classified CTT maps are shown in Figure 3.11.

Table 3.5 The classification scheme of cloud top temperature map

Class	Range (in °C)	Range (in K)	Potential cloud types
1	0 to 10	273 to 283	Warm cloud like cumulus or stratus (that have only water droplets as main component)
2	-10 to 0	263 to 273	
3	-20 to -10	253 to 263	
4	-30 to -20	243 to 253	Mixed clouds (that have both water droplets and ice crystal as main components)
5	-40 to -30	233 to 243	
6	-50 to -40	223 to 233	Huge mixed cloud like cumulonimbus or cold high clouds (like cirrus or cirrostratus that have only ice crystal as main components)
7	-60 to -50	213 to 223	
8	< -60	< 213	

3.4.3 Cloud classification scheme

The final step of the model developing process was to classified type of clouds that appear on the satellite images (in form of the CTT map). The ultimate goal was to identify the existing cumulonimbus cloud for the further use in the analysis of cloud-rainfall relationship. This could be done using the bi-spectral or split window methods as described earlier in Section 2.5.1. But as the visible images are valid only during daytime when the sunlight is still strong while the TIR images are available both in daytime and nighttime, therefore the split-window method was chosen over the bi-spectral method in this thesis. In theory, both methods have the same fundamental principle, which is to establish some proper thresholds and apply them to the images for the classification of cloud types needed.

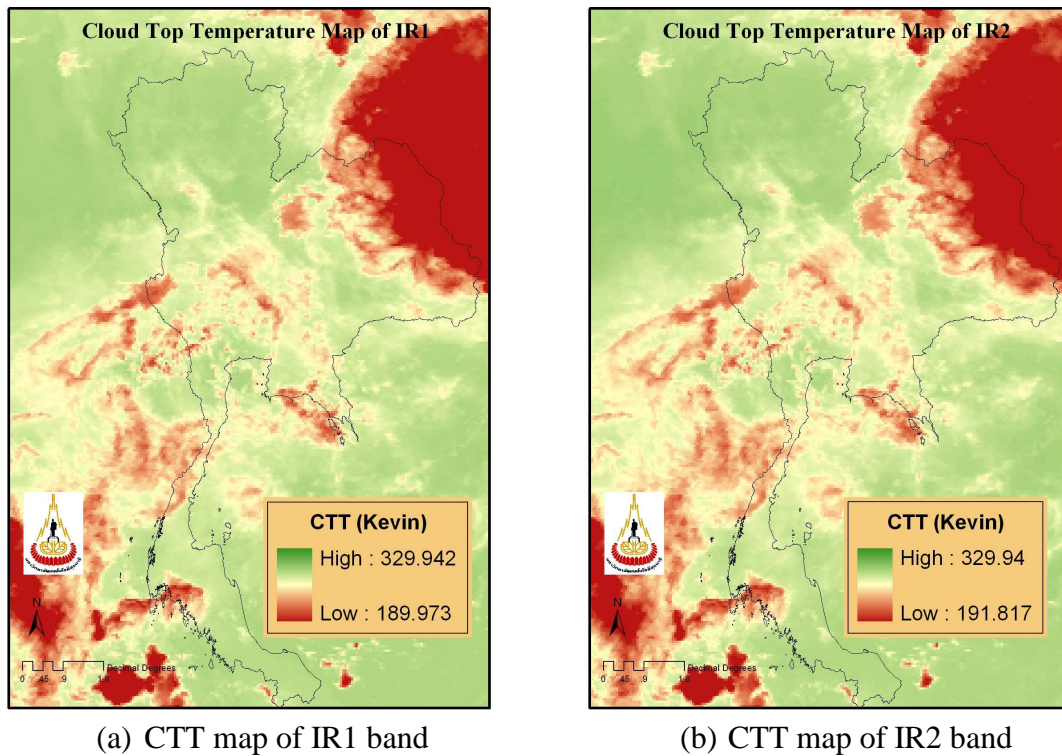


Figure 3.11 Examples of the classified CTT map over Thailand based on the MTSAT image of (a) band IR1 and (b) band IR 2 as shown in Figure 3.8. (Apr 25, 2007 UTC00 images)

In this study, data from band 1 and 2 of MTSAT-1R were selected for the use in split-window analysis as they are usable both in daytime and nighttime. However, at nighttime, the difference between BTs measured in the shortwave (center at $3.75 \mu\text{m}$) and longwave ($11 \mu\text{m}$) IR ($TB_{3.75} - TB_{11}$) can also be used to detect partial cloud or thin cloud within a sensor's field of view (FOV). The small or negative differences are observed only for the case where an opaque scene (such as thick cloud or the surface) fills the FOV and negative differences occur at night over extended clouds due to lower cloud emissivity at $3.75 \mu\text{m}$ channel.

Similarly, at nighttime, the $6.7 \mu\text{m}$ TIR channel can also be employed to identify the thick cumulonimbus cloud. The idea is that low clouds are buried in the

water vapor, and since the 6.7 μm channel sees temperature of the cooler water vapor present above the cloud, the satellite-measured temperature would be lower than the actual CTT. But, the same cloud when observed at 11 μm will yield temperature much closer to the true CTT. Therefore, the difference between the two measurements will be large. Conversely, for high and thick cloud, the values in this case are typically small (Kurino, 1997a, b).

3.4.3.1 High cloud filtering

One of the major problems normally found in the identification of cumulonimbus clouds on the satellite images is their appeared CTT range that still somewhat overlaps with the high and cold clouds (especially thin cirrus). Therefore, to reduce the confusion in the interpretation of further classification results, the high clouds must be screened off the map beforehand. Here, the threshold index for high cloud identification was set based on the observed difference in values of BT in the IR1 and IR2 bands for those clouds.

In this process, samples of high clouds were distinguished on the cloud map based on their apparent structure in visible image and the variation in spectral values in the IR1 and visible bands (low in visible and high in IR1). And to assure more about the validity of the selection, the images in use were chosen to be only in the early morning of winter days at which all other middle/low clouds still did not form much. Then, the BT values (cell-based basis) of those chosen samples in the IR1 and IR2 bands were assembled and some basic statistical parameters e.g. mean, range and SD were calculated. The calculation was also performed for ΔT ($T_{11} - T_{12}$) and results are given in Table 3.7 and Figure 3.12. From the data, thresholds for screening of high clouds (especially thin cirrus) are $T_{11} < 250 \text{ K}$ (-23°C) and $\Delta T > 1.5 \text{ K}$ (upper-

bound values of the variation). Applications of these thresholds are shown for examples in Figure 3.13a and 3.13b.

This screening process was also applied to the cumulonimbus cloud to ensure that the screened cirrus clouds (under the aforementioned thresholds) have less or no impact on the existing of actual cumulonimbus cloud on the images. And results of the calculation are illustrated in Table 3.6 along with the high cloud data. Data in the table could help us define potential thresholds for the classification of high clouds, middle or low clouds, and cumulonimbus clouds for Thailand like one seen in Figure 2.15, for example, threshold for separate cumulus from cumulonimbus should be around greater than 250 K for infrared 1.

Table 3.6 BT and ΔT statistics (in Kevin unit) for the high cloud and cumulonimbus cloud over Thailand (as observed by IR1 and IR2 channels of MTSAT-1R).

Cloud type	Parameter	Mean	Minimum	Maximum	SD
High clouds	IR1 (11 μm)	253.72	222.43	284.83	14.02
	IR2 (12 μm)	249.89	219.48	280.44	13.03
	ΔT	3.8	2.95	4.38	0.99
Cumulonimbus	IR1 (11 μm)	233.73	197.6	284.83	28.23
	IR2 (12 μm)	231.39	198.07	280.44	26.15
	ΔT	2.34	-0.47	4.38	2.07

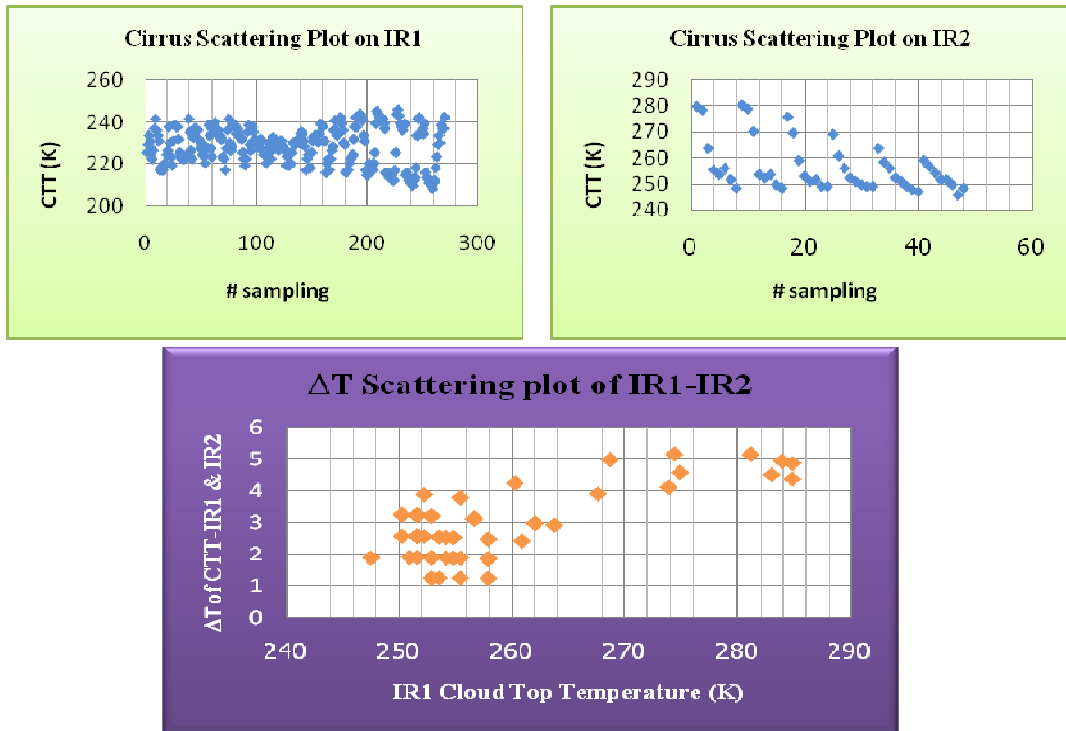


Figure 3.12 Scatter plots of IR1/IR2 BT and IR1/ ΔT of high cloud samples

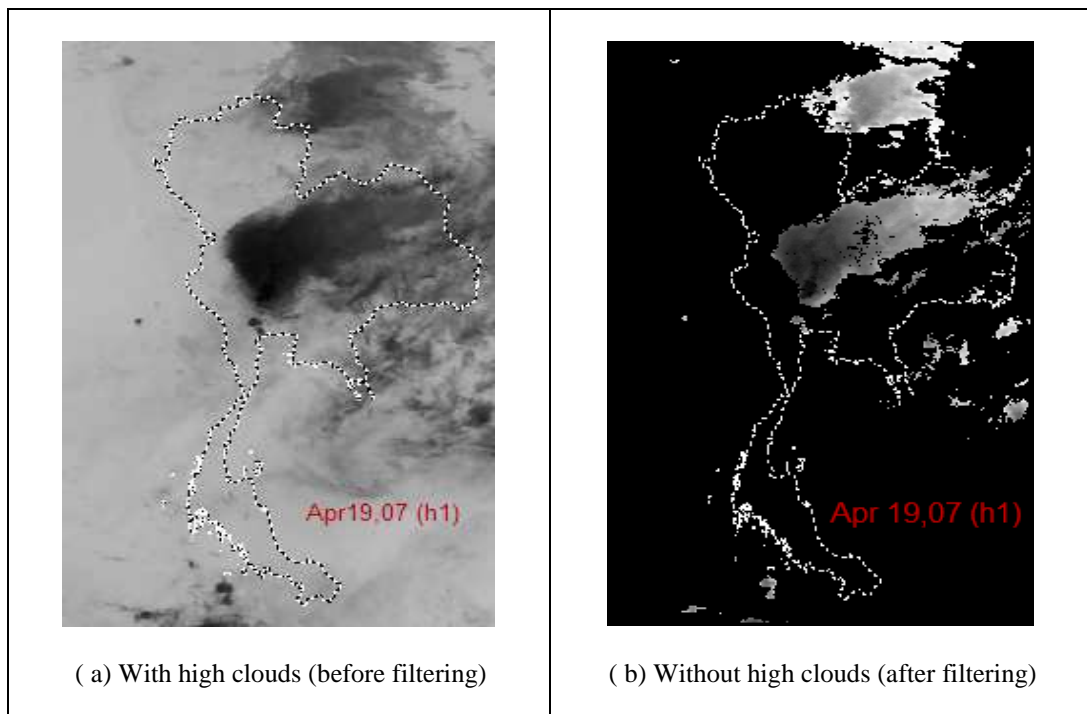


Figure 3.13a Examples of cloud images (a) with and (b) without high cloud appearance, example on Apr 19, 2007 (h1).

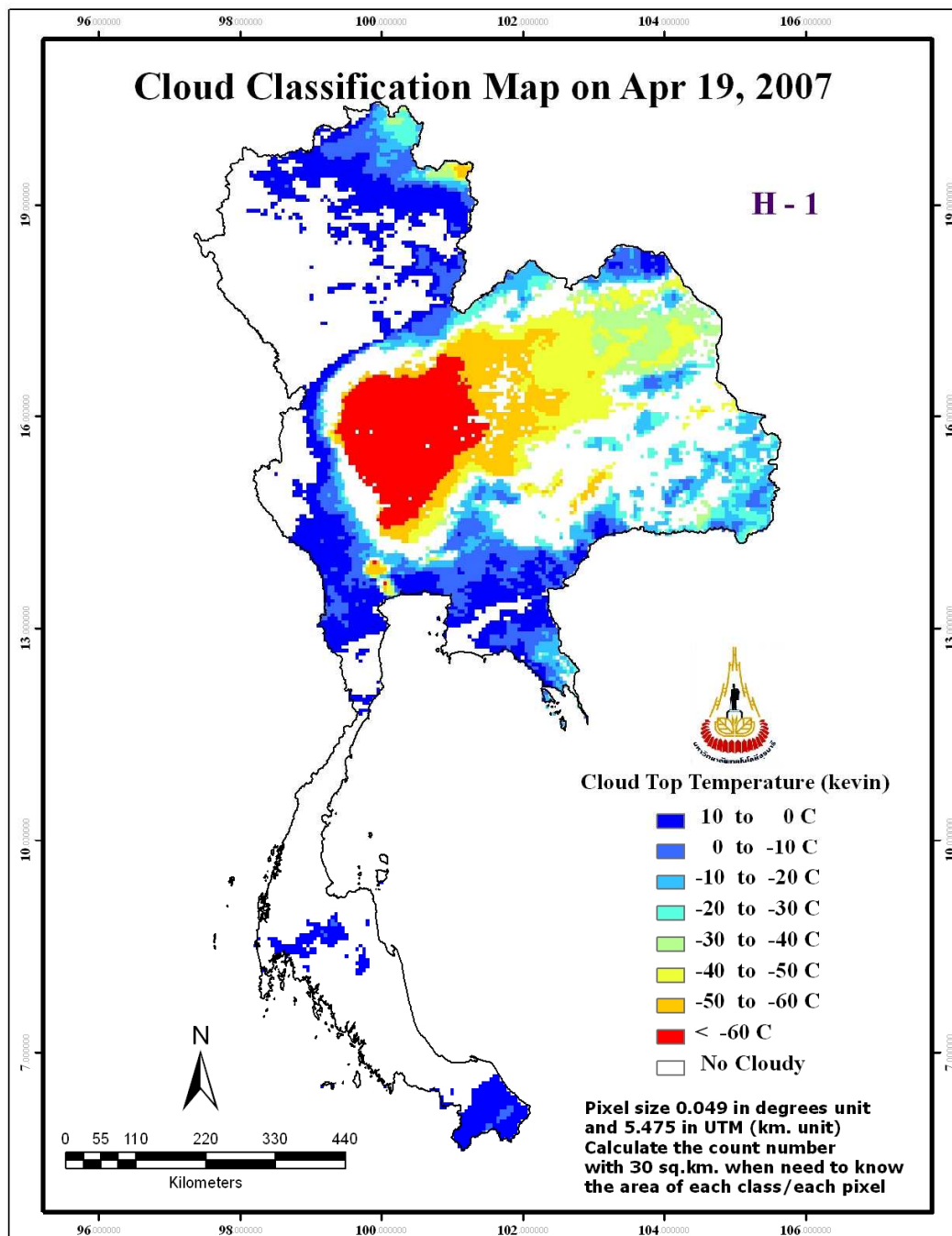


Figure 3.13b Example of cloud image after the high-cloud filtering process (without high cloud appearance) on April 19, 2007 (h1).

3.4.3.2 Development of the classification model

The main outcome of the needed classification model is cloud distribution map on which the potential high clouds are already filtered off the scene. As a result, only clouds (apart from high clouds) that have CTT less than 10°C will be identified and presented on the output cloud maps. The classification module was designed to fulfill this objective in which three main operating steps were devised:

- (1) Input MTSAT-1R image files band IR1 and IR2,
- (2) Filtering potential high clouds on the input images based on thresholds that are primarily set in the script (T_{11} and $\Delta T = T_{11} - T_{12}$), and
- (3) Generate the output cloud map files which are cirrus map, cirrus-filtered map, and all classified cloud maps (cloud with $CTT < 283$ K)

The operation at each step was controlled by the specific source codes written as SML/EML script and added as utility tool in ERDAS's Utilities section (see figure 3.14 and appendix A for more detail of how to use the modules). Though, the cirrus cloud and warm cloud maps were not needed in the analysis but they are necessary for the study of the Earth's energy budget and weather variation at regional or global scales.

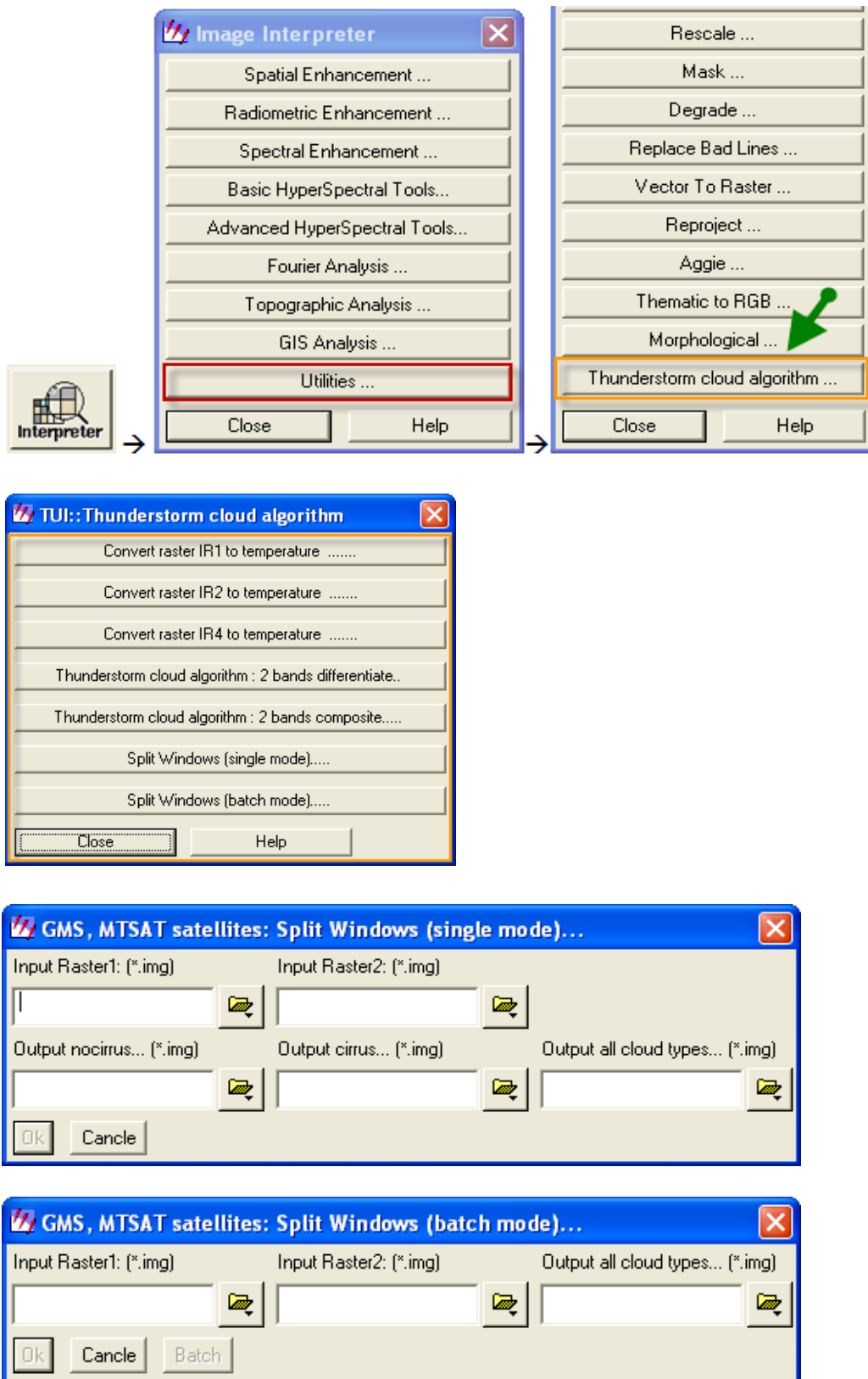


Figure 3.14: Step-by-step GUI of derive ERDAS module for cloud classification

CHAPTER IV

RESULTS AND DISCUSSION

4.1 Seasonal rainfall and cloud cover distribution patterns

The main purpose of this section is to examine pattern of rainfall and cloud cover distribution over Thailand during years 2006 and 2007 in relation with the main influencing factors being identified at each specified time period (at seasonal scale). The comparison between rainfall and cloud distribution patterns found in the study can inform us about their potential relation which is further quantified in more detail in Section 4.2.

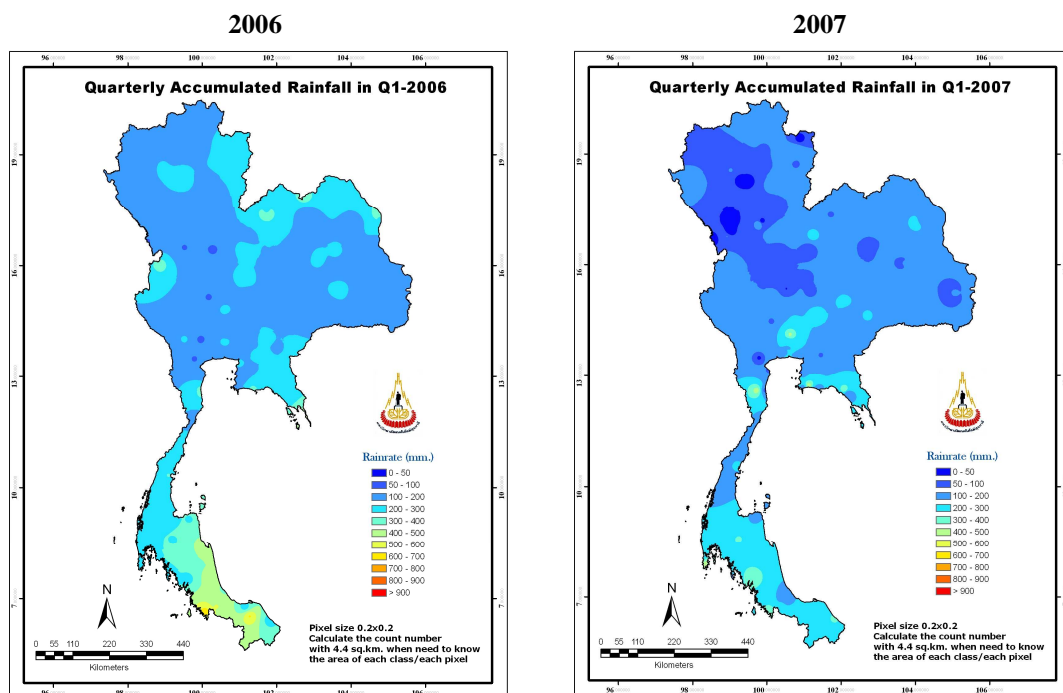
4.1.1 Seasonal rainfall distribution

As Thailand is located in the monsoon-dominated region, most rainfall is created from the monsoon-induced mechanisms. However, some other factors like the monsoon trough (or the ITCZ), the tropical cyclone, and the cold air mass moving south from the mainland China can also induce heavy rainfall from time to time whenever they reside in the country (as described in Section 2.3.3). The influence of these factors could be seen in the accumulated rainfall maps, especially when compared to the normal situation one.

To illustrate this fact here; the quarterly and annual rainfall maps of Thailand in years 2006 and 2007 are placed side by side to present their similarities and differences (Figures 4.1 and 4.2 and Table 4.1) and the causes of differences are

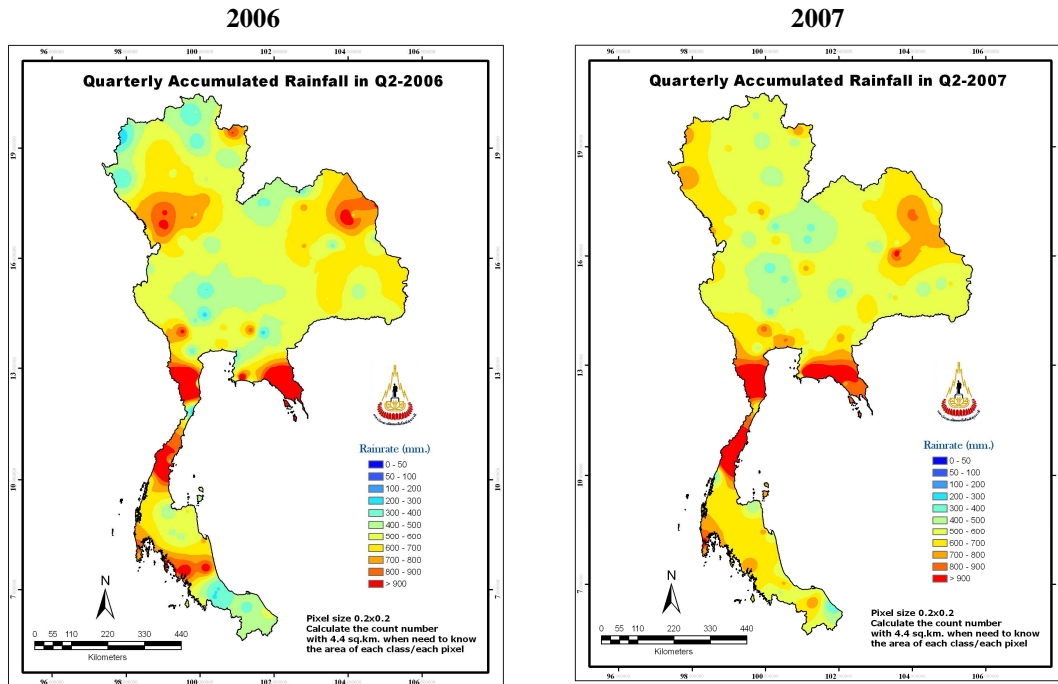
identified based on official weather reports of the TMD and DDPM during the concerned period.

It was found that, patterns of rainfall distribution in both years (Figure 4.1) are rather similar in general where high amount of rainfall (e.g. > 2,000 mm) appear in the south and in the eastern region (especially Chanthaburi and Trat Province). The relatively high rainfall areas also exist in the some part of northeastern region (upper right) and the western region (along the lower border). And, in average, the central region and upper north receive least rainfall amount in both years. Here, the seasonal rainfall pattern has been further divided into 4 periods and the detailed explanation is as follows.

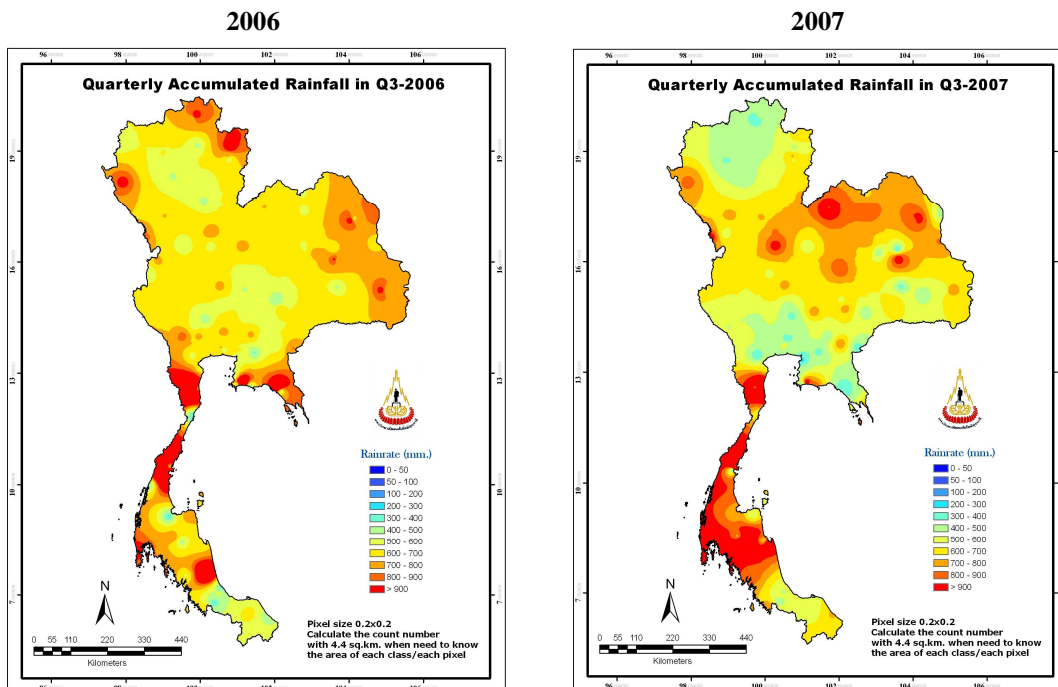


(a) First quarter: February-April

Figure 4.1 Pattern of rainfall distribution in periods: (a) February-April, (b) May-July, (c) August-October and (d) November-January

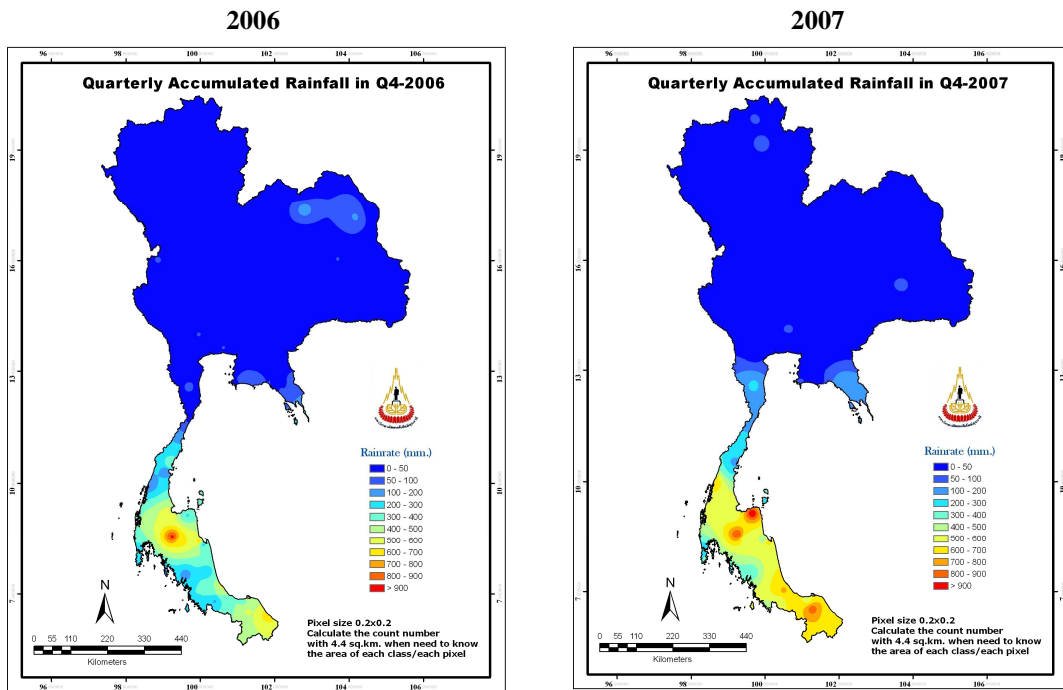


(b) Second quarter: May-July



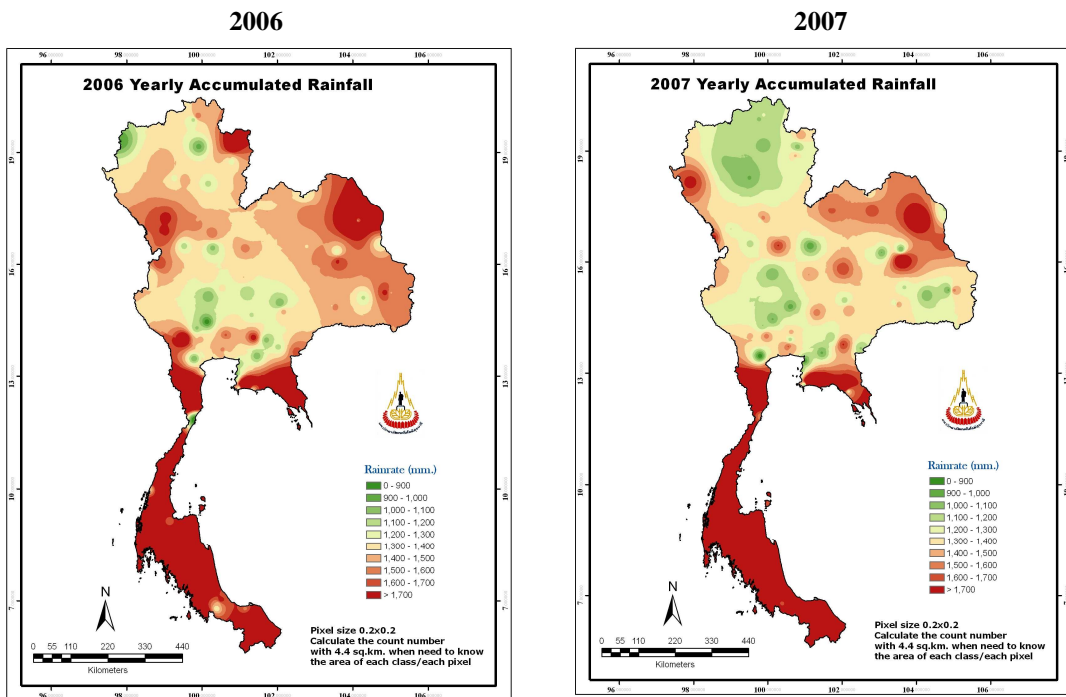
(c) Third quarter: August-October

Figure 4.1 (Continued)



(d) Fourth quarter: November-January

Figure 4.1 (Continued)



(a) 2006 map

(b) 2007 map

Figure 4.2 Annual rainfall maps for (a) 2006 and (b) 2007

Table 4.1 Monthly accumulated rainfall amount in 2006 and 2007

Period	Month	Monthly rainfall (mm)		Dominant causes
		2006	2007	
Quarter 1 (Feb-Apr)	February	4,933.80	1,216.70	Cold air mass (weather front), northeast monsoon (for the south), low pressure area (from the ocean), upper westerly wind, and local convection
	March	7,989.30	4,727.90	
	April	12,892.10	12,783.10	
	Total amount	25,815.20	18,727.70	
Quarter 2 (May-July)	May	24,087.80	31,610.10	Southwest monsoon, monsoon trough, tropical cyclone and low pressure area (from the ocean)
	June	21,566.40	20,058.30	
	July	25,186.70	21,988.90	
	Total amount	70,840.90	73,657.30	
Quarter 3 (Aug-Oct)	August	27,810.40	23,426.70	Southwest monsoon, monsoon trough, tropical cyclone and low pressure area (from the ocean)
	September	29,475.80	27,978.40	
	October	23,109.80	25,365.30	
	Total amount	80,396.00	76,770.40	
Quarter 4 (Nov-Jan)	November	5,424.10	7,576.20	Cold air mass (weather front), northeast monsoon (for the south), and local convection
	December	3,595.40	3,765.00	
	January	1,742.30	2,999.50	
	Total amount	10,761.80	14,340.70	
Annual average (mm)		1,619.09	1,581.86	-

4.1.1.1 First quarter: February to April

This is the beginning of summer time in the country where normal weather is mild and dry under the strong influence of the northeast monsoon that normally brings the cold and dry air from the Siberian High down to the tropical region. Rainfall occurred during this period is mostly due to the local convective process where it is generally seen in late afternoon or in the evening. Apart from this, cold air mass from China can also produce a considerable amount of rain fall along the weather front. However, the rain resulted from the aforementioned processes typically does not last long (often less than an hour) and pronounced heavy rainfall is rarely found in these situations

At this time, the northeast monsoon that moves across the Gulf of Thailand to the south will carry huge amount of air moisture to form heavy and widespread rainfall all over the eastern side of the middle and far south, especially on the windward side of the mountain. This sometimes results in the deadly flooding in some hit areas (Figure 4.3).

Another less known factor that sometimes could generate specula heavy rainfall during this period is the upper westerly wind that is moving eastward across the country (mostly in February or March) at high altitudes (typically 10-15 km). This wind was held responsible for heavy rains and serious flood seen in the south during mid-February 2006 (Figure 4.4). The low pressure areas formed over warmer ocean can also bring significant amount of rain to the coastal zone in March and April.

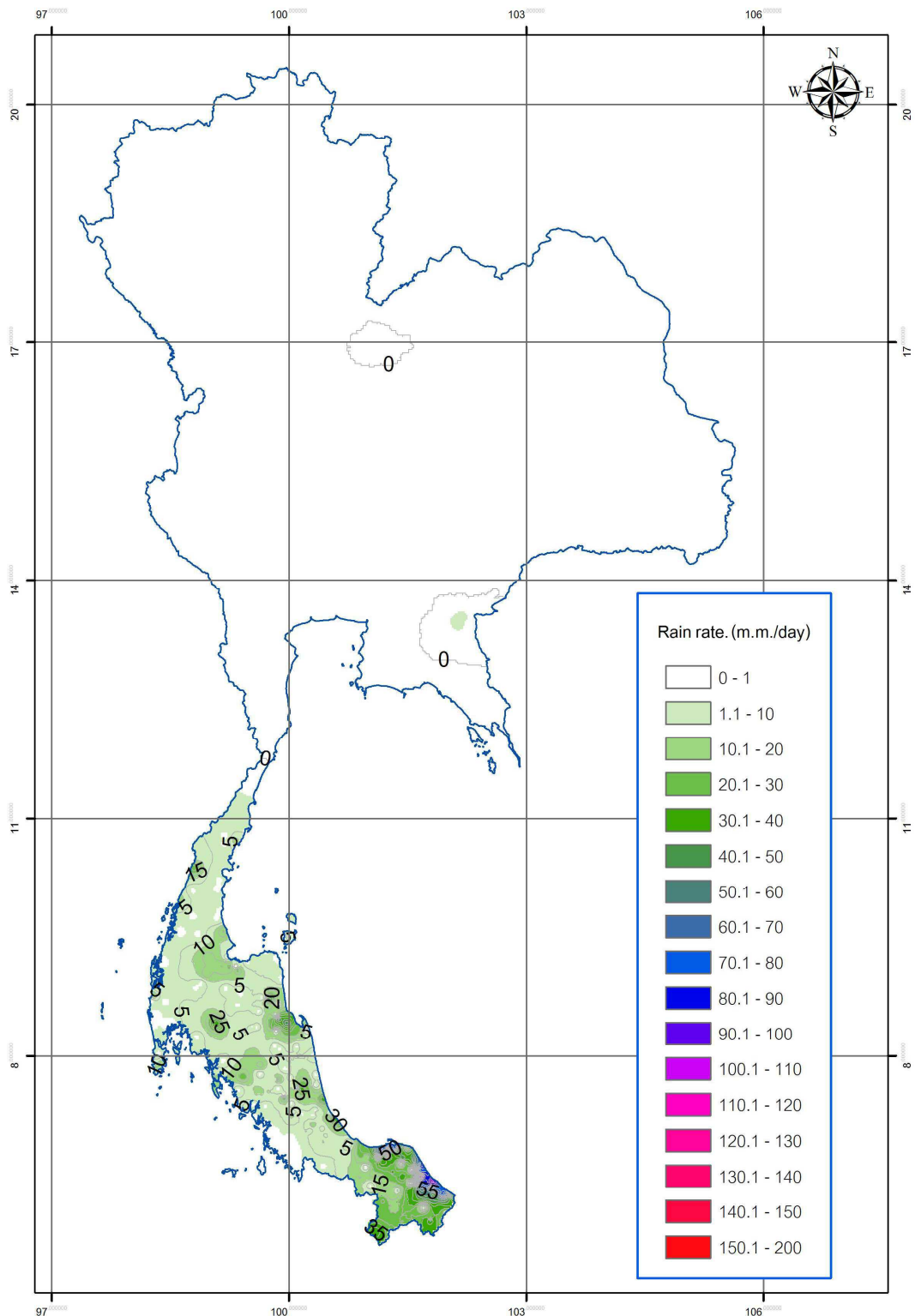


Figure 4.3 Rainfall map on 3 January 2006 when the strong northeast monsoon generated widespread rainfall in the south, especially on the eastern side and in the far south.

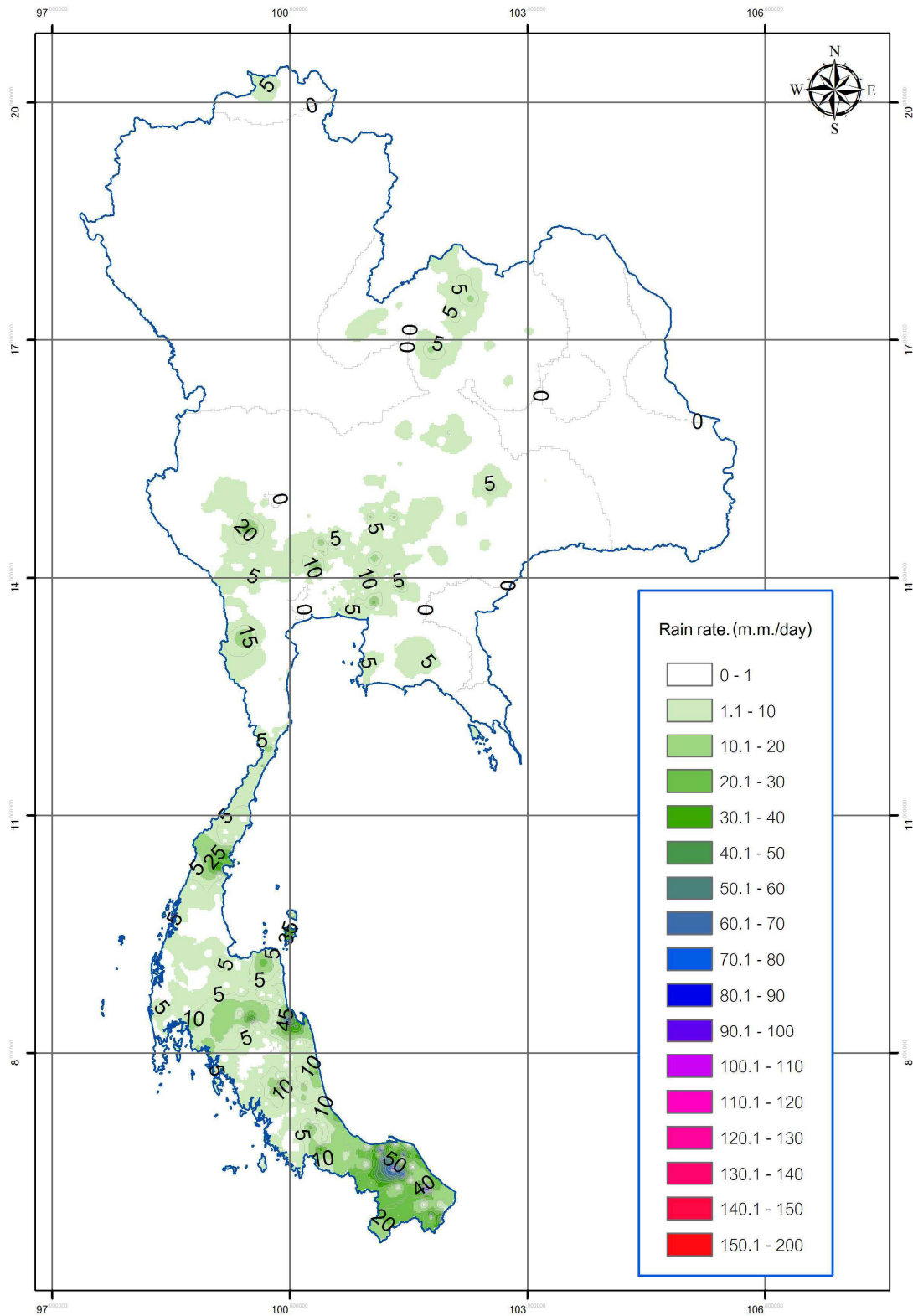


Figure 4.4 Rainfall map on 13 February 2006 when the strong upper westerly wind was moving across the south which caused heavy rainfall and flooding in some areas.

4.1.1.2 Second quarter: May to July

This is the beginning of the rainy, or monsoon, season that provides most of the rainfall to the country. At this period, the rains are generally contributed by the southwest monsoon and the monsoon trough. The southwest monsoon is the prime contributor to the rainfall observed all over the country, especially on eastern and western parts. During the rainy season, it will continuously carry moist air from the Indian Ocean into the country which is being main source of observed rains (Figure 4.5). Several severe heavy rains and floods were reported nationwide in both years (especially in 2007) in association to the prolonged intense southwest monsoon (Table 4.2).

Meanwhile the monsoon trough, a long stripe of the low pressure zone from the Equator which is moving up and down across the country every year, begins to enter the south in April and moves northward to the central and northern portion of the country in May and June respectively. Along the way, it can induce huge amount of rainfall within the occupied territory (lying mostly toward east-west direction) that sometimes results in serious flash flooding and great damages in many places as seen, for example, during 21-23 May 2006 in the lower northern region (Figure 4.6).

Apart from the two main sources of rain mentioned earlier, there are also some other factors that have potential to produce widespread rainfall in Thailand which are the tropical cyclone in the Pacific Ocean and the low pressure area in the Indian Ocean or the South China Sea. The tropical cyclone is a tremendous cyclonic system (of low pressure area) that can generate intense rainfall in vast area. Usually, it has been called in several names based on strength at each stage of the development which are (from weak to strong) the depression, tropical storm, and typhoon (or

hurricane) respectively. The area likely to have most impact from the tropical cyclone formed in the Pacific Ocean is the northeast as it is located closer to the cyclone path than all other parts of the country (Figure 4.7).

Table 4.2 Reports of severe floods and number of casualties in 2006 and 2007 (DDPM, 2009)

2006	Date	Location	Casualty	Main contributor
1	12-16 February	Middle/lower south	4	Upper westerly wind
2	21-23 May	Lower north	88	Monsoon trough
3	30 June-3 July	All regions	5	Southwest monsoon
4	13-18 August	Upper south and NE	-	Southwest monsoon
5	19-21 August	Upper north	2	Monsoon trough
6	September-October	All regions	347	Monsoon trough, Tropical cyclone
2007	Date	Location	Casualty	Main contributor
1	1-8 May	Upper south	-	Monsoon trough, Tropical cyclone
2	9-31 May	Upper Thailand	-	Monsoon trough, Southwest monsoon
3	25-30 June	All regions	-	Southwest monsoon
4	4-12 July	All regions	-	Southwest monsoon
5	20-22 July	All regions	-	Southwest monsoon
6	1-12 August	Upper Thailand	2	Southwest monsoon, Tropical cyclone
7	18-25 August	Middle south	-	Southwest monsoon
8	9-11 September	Lower north	6	Monsoon trough
9	26-30 September	All regions	-	Monsoon trough, Southwest monsoon
10	October	Upper Thailand	17	Tropical cyclone
11	20-24 October	Middle south	2	Monsoon trough
12	7-12 November	Middle south	-	Low depression area

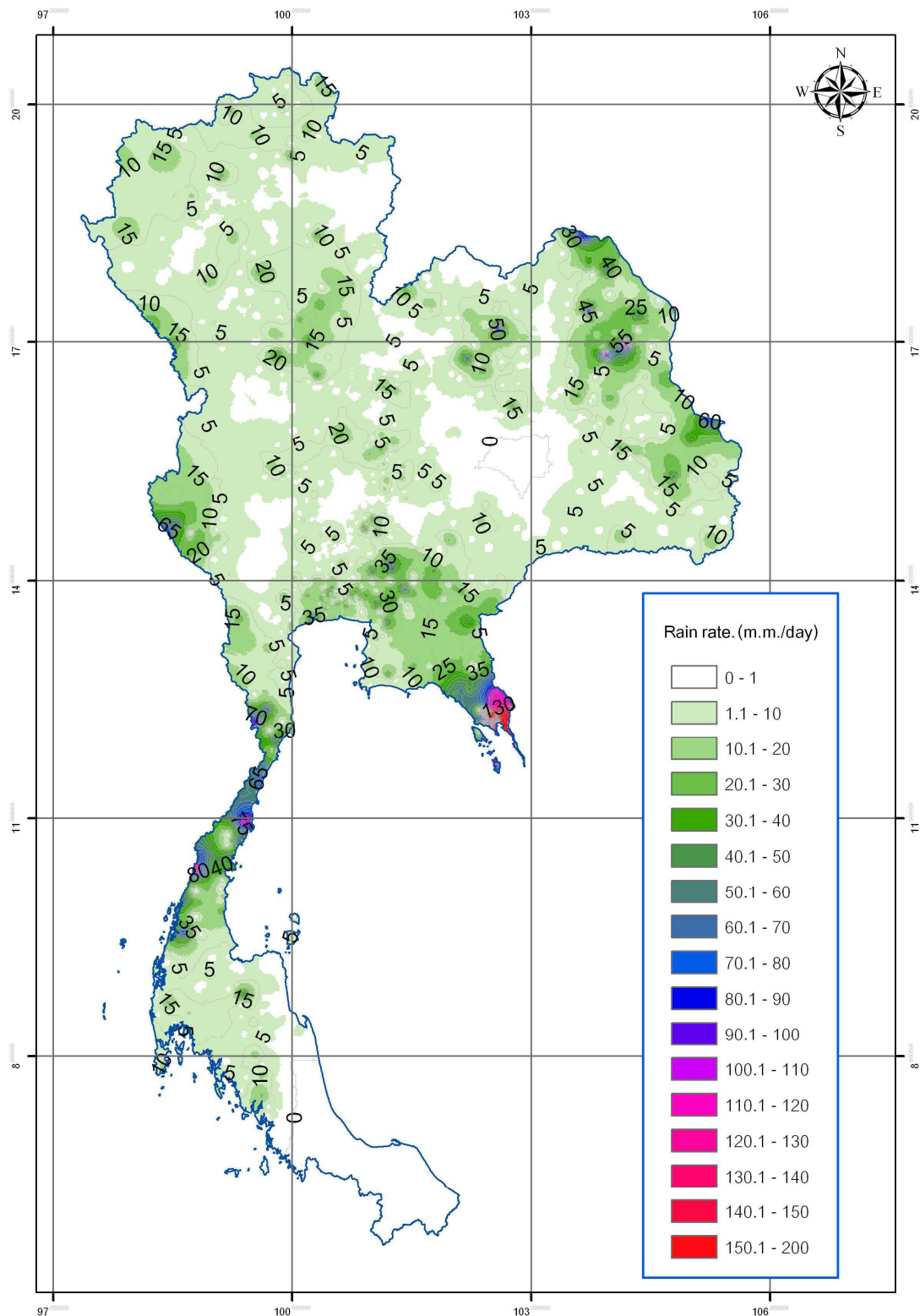


Figure 4.5 Rainfall map on 2 July 2006 when the strong southwest monsoon induced the widespread heavy rainfall and flooding in several places across the country.

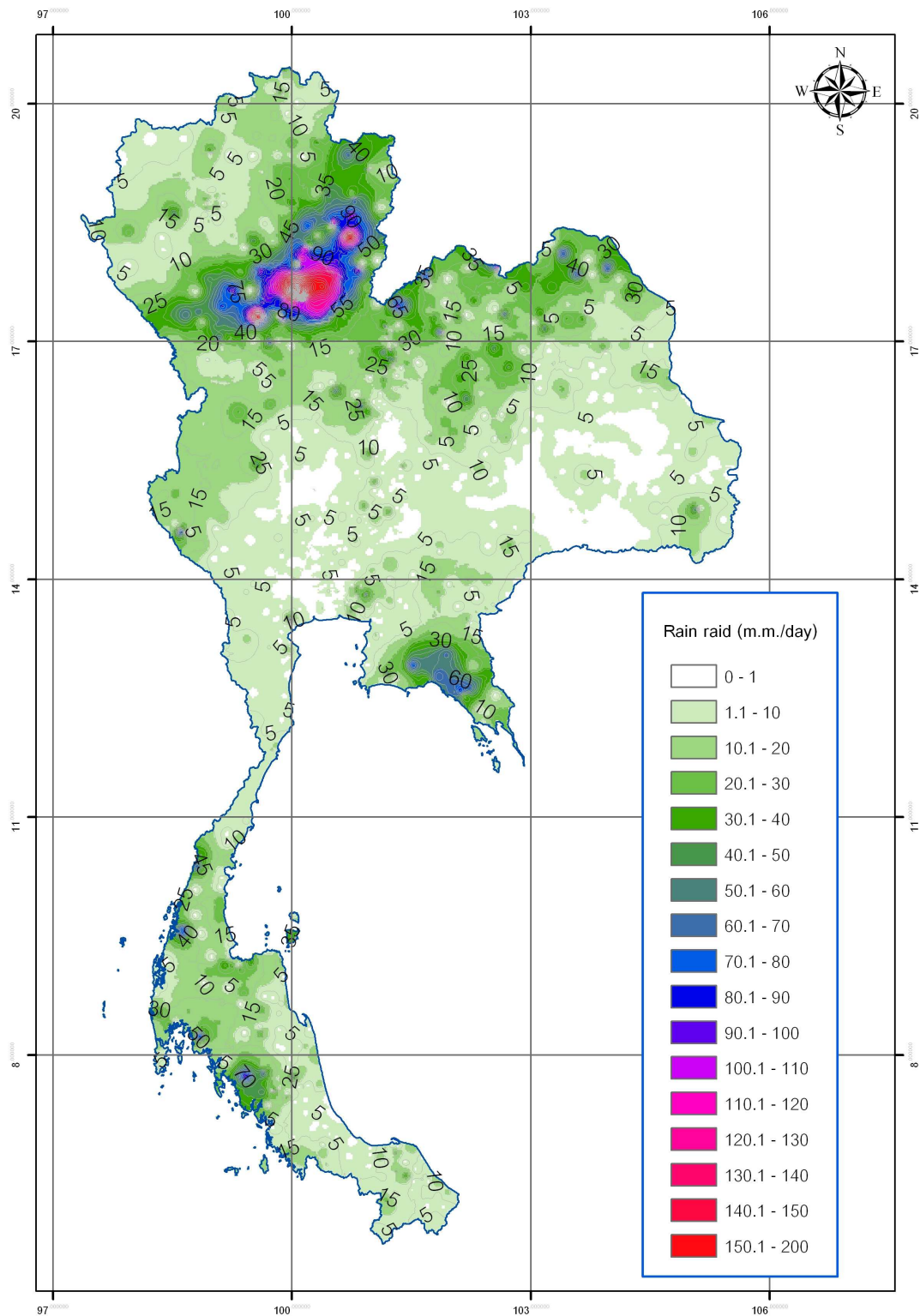


Figure 4.6 Rainfall map on 22 May 2006 when the strong monsoon trough induced the widespread heavy rainfall and flooding in several places in the lower-northern region.

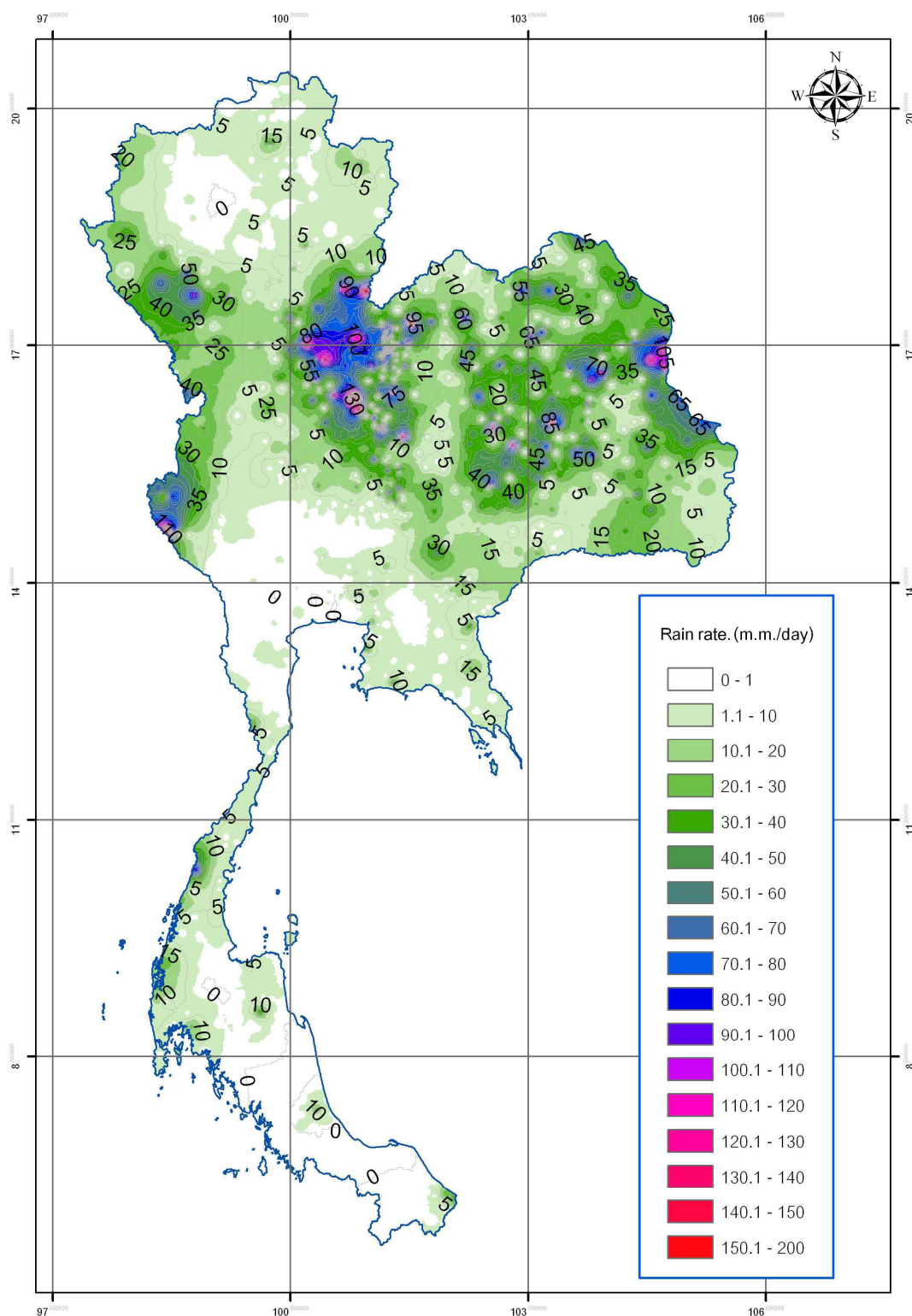


Figure 4.7 Rainfall map on 4 October 2007 when the tropical cyclone “Lekima” moved into the country and induced widespread heavy rainfall and flooding in several places in the lower-northern and northeastern regions of the country.

Most tropical cyclones moving into the country in the past are usually in form of depressions and tropical storms, and rarely in form of the true typhoon. In addition, the tropical cyclone can also form in the Indian Ocean where it is simply called as “cyclone” instead of “typhoon”. These cyclones are found less frequently than those in the Pacific region but could also produce heavy rains as they move closer to the country’s territory.

Whereas, the low pressure areas in the Indian Ocean or the South China Sea can occur from time to time due to the warmer sea water during this time that provides higher warm moisture for the atmosphere. This situation could lead to the development of low pressure area as a consequence. When these systems move ashore, they bring with them plenty of raw materials for the use in rain production later on (Figure 4.8).

4.1.1.3 Third quarter: August to October

This is the most intense period of rainfall in Thailand as most of rain contributors have gained significantly more strength during this season due to the warmer atmosphere and also warmer ocean (note that, this is summer time of the northern hemisphere). Rains may be notable reduced in July when the monsoon trough is away to southern China that leaves the southwest monsoon as sole contributor of rains found in the country. However, the monsoon trough will move southward back to the country once again in August till October and when encounter with the southwest monsoon; they can initiate large volume of rainfall amount over most parts of the country, especially on the windward side of the area and floods will eventually arise as a consequence (Figure 4.6).

In addition, the tropical cyclone in the Pacific Ocean and the low pressure area in the Indian Ocean or the South China Sea can be formed more productively at this period of the year due to the warmer ocean. For example, in October of both years, the typhoons (in its depression form) have caused widespread heavy rains and flood in many regions in the upper part of the country, especially in the lowlands situated close to the river.

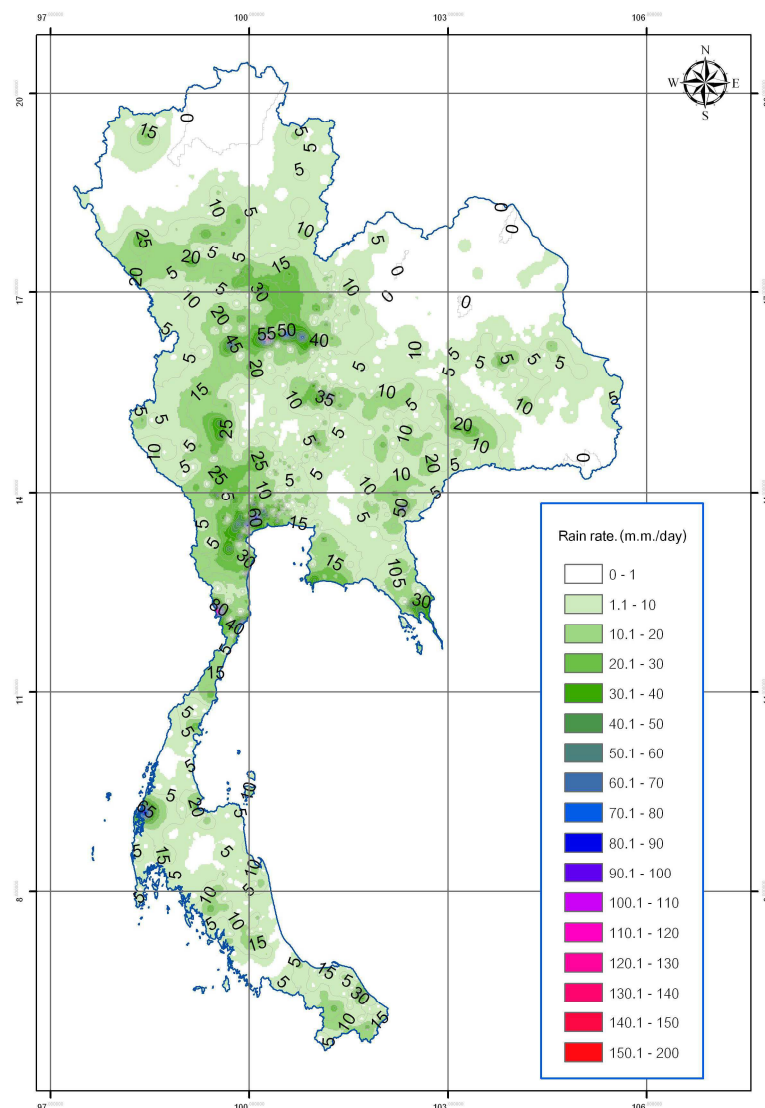


Figure 4.8 Rainfall map on 2 May 2007 as the low depression area from the Gulf of Thailand moved inland and induced widespread heavy rainfall in several regions of the country.

4.1.1.4 Fourth quarter: November to January

This is in the middle of wintertime for the northern hemisphere in which weather is relatively dry and the near-surface air is getting colder and less turbulent. The intense rainfall at this time is rarely found except in the south where the northeast monsoon can generate great amount of rains in the area. However, huge cold masses from China often move to occupy upper part of the country at this time which makes the atmosphere more stable and less rain is produced (except along the front where the air is very turbulent and many severe storms being developed as a consequence) (Figure 4.9).

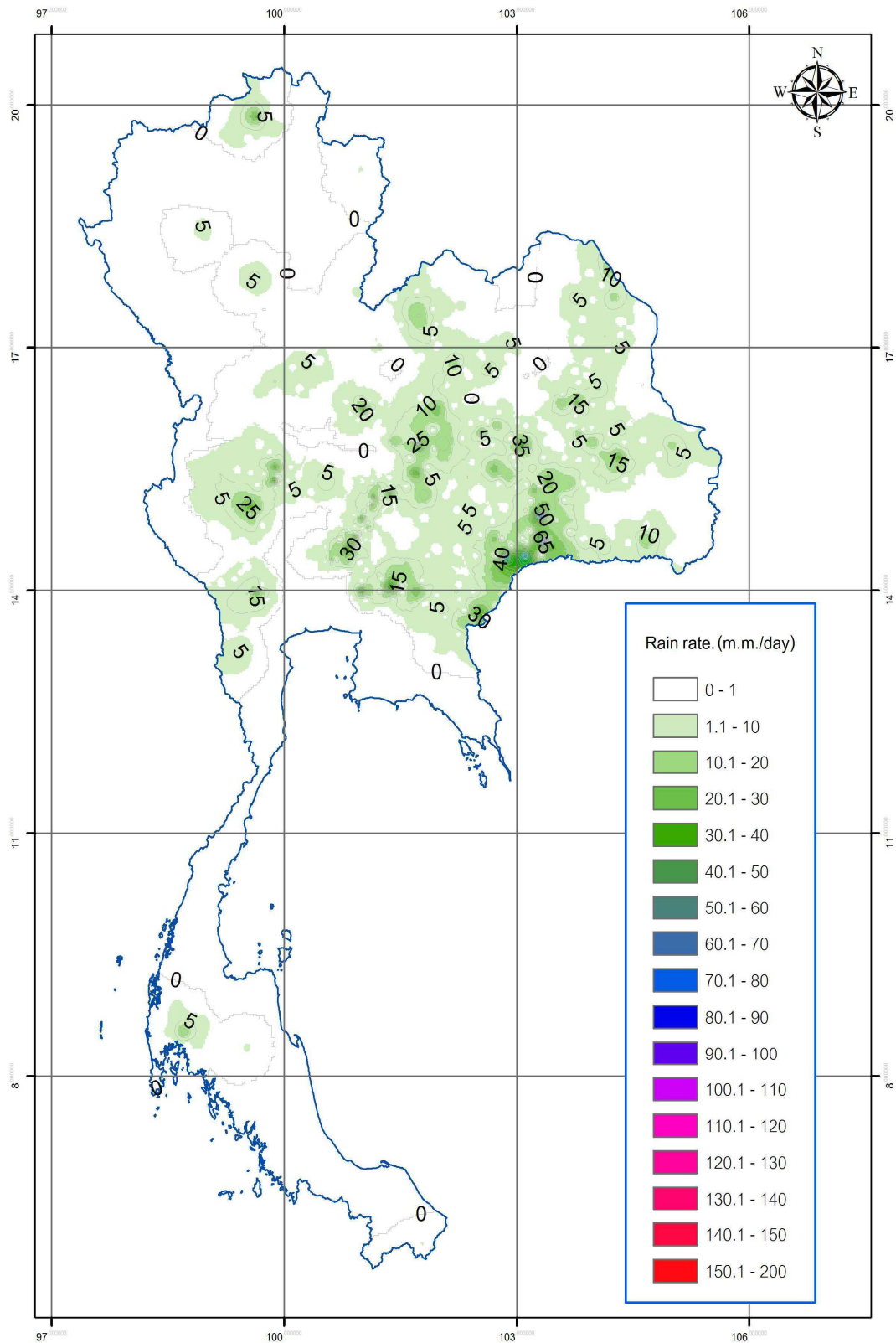


Figure 4.9 Rainfall map on 13 March 2006 when large cold mass moved to occupy upper part of the country and induced widespread rainfall along the weather front.

4.1.2 Seasonal cloud distribution

As already described in Section 4.1.1, the dominant contributors of rainfall seen in Thailand vary distinctively with time of the year (broadly at seasonal scale). Typically, in summer (mid-February to Mid-May), the major sources of rainfall are local convective mechanisms, the low pressure area coming from the ocean, the southwest monsoon, the monsoon trough and the cold air mass (weather front). In rainy season (mid-May to mid-October), they are the southwest monsoon, the monsoon trough and the tropical cyclone. And in wintertime (mid-October to mid-February), they are cold air mass (weather front), northeast monsoon (for the south), and local convection.

However, before the rain could be formed, the rain clouds must be developed first under the influence of these major contributors. Different types of clouds are responsible for the different pattern of rainfall intensity and duration. In this section, some examples of daily cloud distributing pattern (for different season) derived from the MTSAT-1R and their associated daily rainfall map are presented to gain prior knowledge of their relation before the more detailed analysis is performed in Section 4.2.

4.1.2.1 Cloud/rainfall in winter

To represent cloud/rainfall distributing pattern in winter, their data maps taken on 6-7 January 2007 were chosen for the analysis. On that dates, the massive cold air mass still occupied most areas in the upper part of the country, as a consequence, the weather was rather cold and calm and less clouds were able to form in the sky (as the atmosphere was relatively stable at that time) (Figure 4.11). The observed rainfall was mostly located in the lower part of the south due to the influence

of the strong northeast monsoon and no record of rainfall in the upper part of the country as seen in the rainfall map for 7 January (Figure 4.10). This map represents accumulated rainfall being collected within 24 hours during 7.00 am (6th Jan) to 6.00 am (7th Jan).

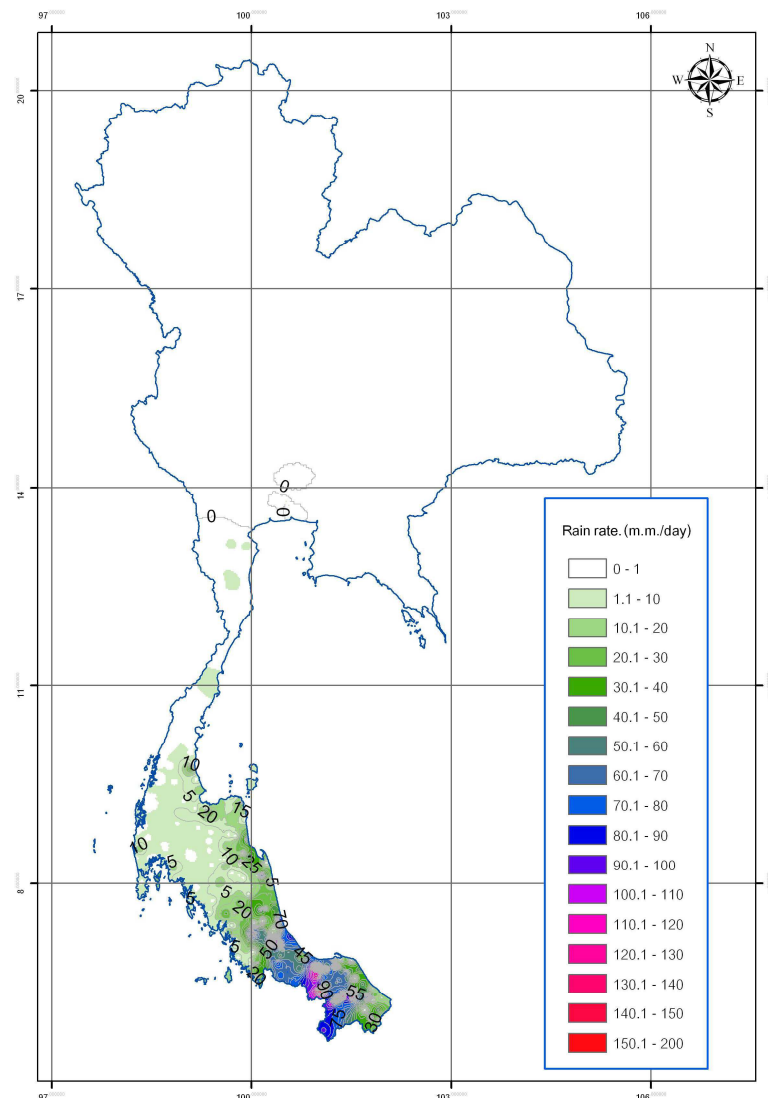


Figure 4.10 Rainfall map for 7 January 2007 when strong northeast monsoon generated widespread rainfall in the south, especially on the eastern side and in the far south. And, there was no record of rainfall measured in the upper part of the country. The rainfall data were collected within 24 hours during 7.00 am (6th Jan) to 6.00 am (7th Jan)

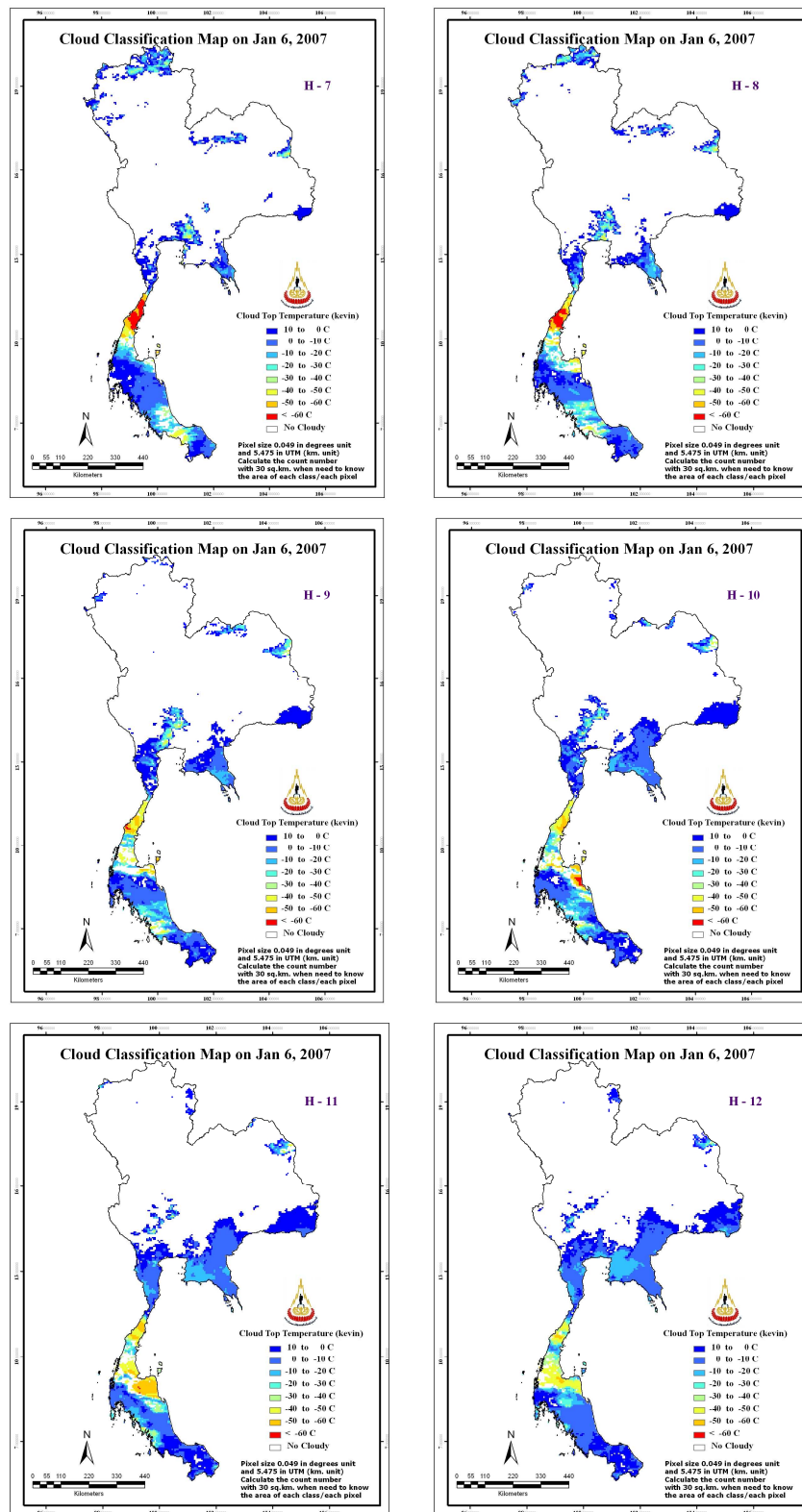


Figure 4.11 Hourly CTT maps (derived from MTSAT-1R images) for 6-7 January 2007 taken within 24 hours during 7.00 am (6th Jan) to 6.00 am (7th Jan).

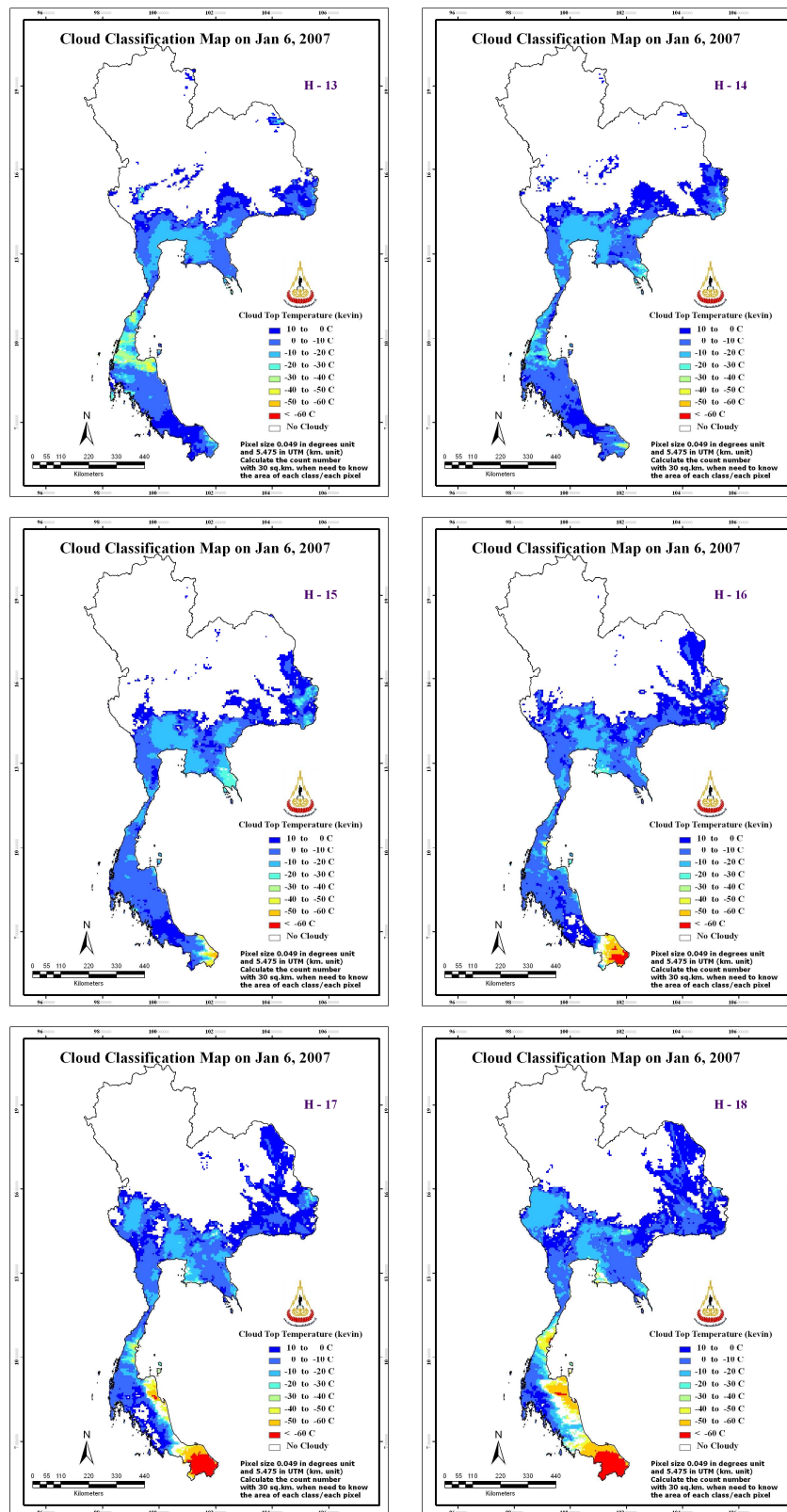


Figure 4.11 (Continued).

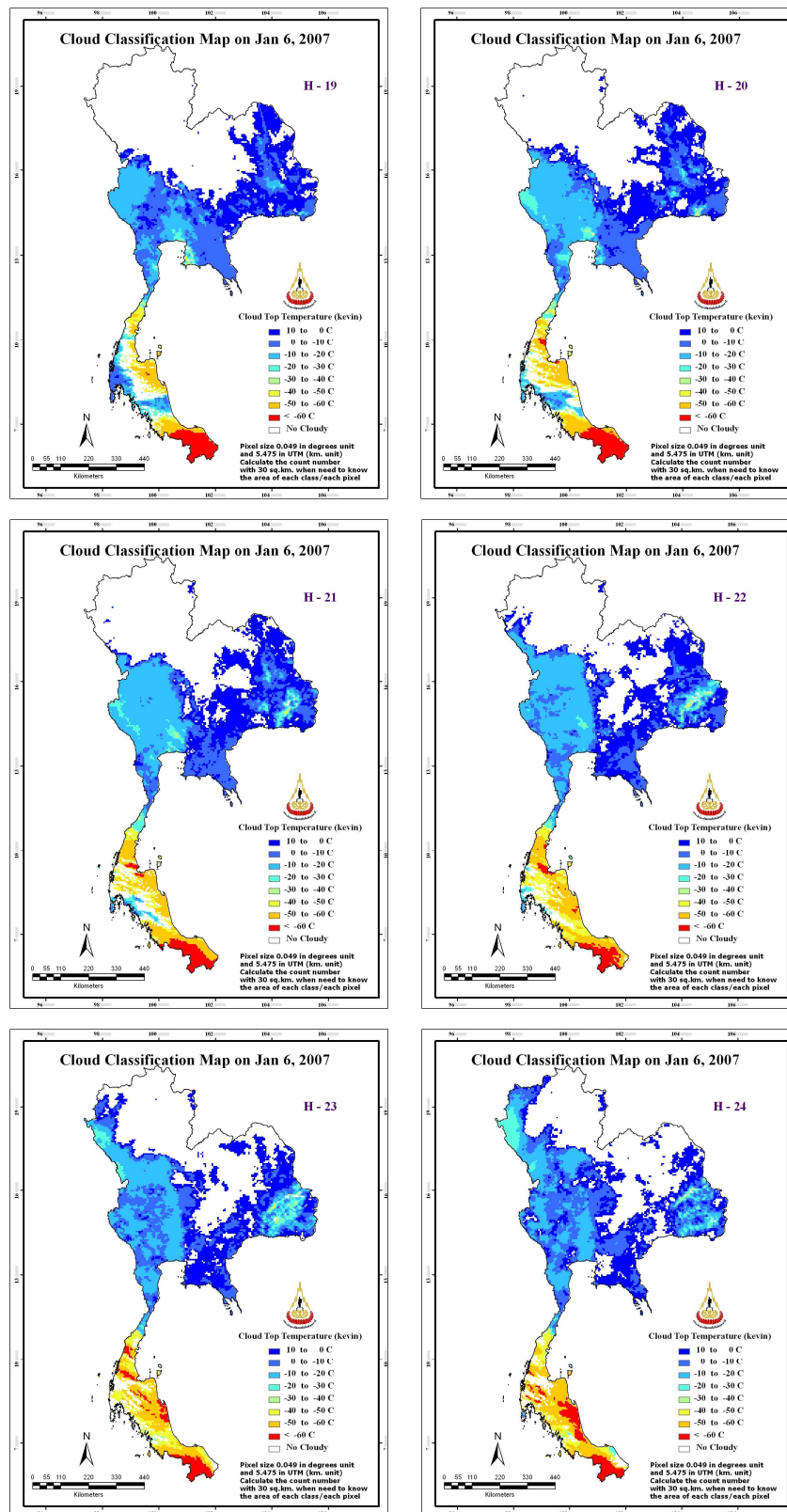


Figure 4.11 (Continued).

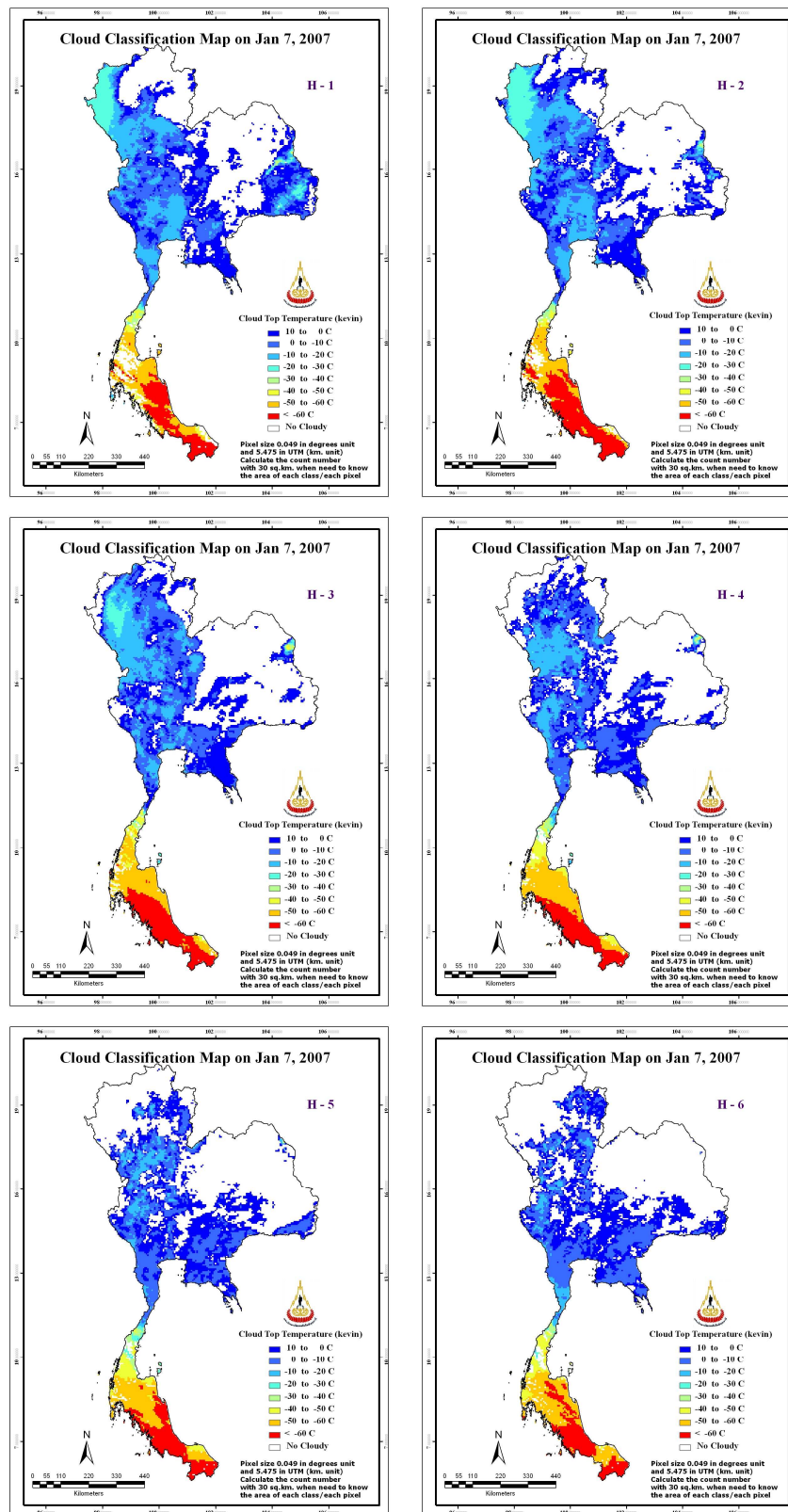


Figure 4.11 (Continued).

Table 4.3 Variation of CTT area coverage during 6-7 January 2007 (Figure 4.11)

Time order	Coverage area base on CTT class (km ²)									Cloud area (km ²)	Lowest temp (K)
	No cloud	10/0	0/-10	-10/-20	-20/-30	-30/-40	-40/-50	-50/-60	< -60		
06-H7	406,710	45,210	36,840	16,050	7,560	3,150	3,510	2,520	3,420	118,260	205.510
06-H8	407,640	39,330	36,840	17,520	10,740	3,840	3,930	2,670	2,460	117,330	204.042
06-H9	399,840	45,990	39,000	18,930	9,000	3,090	6,210	2,670	240	125,130	209.661
06-H10	386,430	49,380	48,750	19,350	7,080	3,990	5,910	3,450	630	138,540	209.661
06-H11	372,870	51,750	58,950	19,260	5,160	3,750	6,090	7,050	90	152,100	212.248
06-H12	357,600	54,120	71,760	22,230	5,100	4,260	9,000	900	-	167,370	219.285
06-H13	337,260	53,160	79,500	40,020	7,440	6,450	1,140	-	-	187,710	228.360
06-H14	326,400	58,950	87,330	46,140	5,280	660	180	30	-	198,570	222.431
06-H15	321,240	55,920	95,880	43,590	5,790	570	1,140	810	30	203,730	212.248
06-H16	305,010	68,250	105,240	36,060	2,490	270	1,290	4,050	2,310	219,960	206.935
06-H17	289,260	85,440	89,700	38,880	4,470	1,500	3,480	4,890	7,350	235,710	204.042
06-H18	267,810	80,310	92,760	48,240	6,870	2,250	6,270	10,590	9,870	257,160	202.515
06-H19	241,980	83,910	94,140	60,000	8,340	2,190	7,620	14,310	12,480	282,990	200.938
06-H20	217,860	89,910	79,860	79,740	13,410	2,970	8,580	19,080	13,560	307,110	200.938
06-H21	204,960	100,440	68,820	88,260	13,620	1,860	10,020	25,830	11,160	320,010	204.042
06-H22	200,250	98,340	68,130	93,840	7,410	1,770	16,380	29,190	9,660	324,720	204.042
06-H23	189,750	97,980	82,110	85,920	11,430	2,820	17,010	26,250	11,700	335,220	197.600
06-H24	183,570	97,740	99,960	73,020	13,980	2,220	11,550	28,980	13,950	341,400	193.975
07-H1	179,100	105,960	93,300	70,050	19,590	2,280	5,700	24,240	24,750	345,870	195.825
07-H2	178,650	108,240	82,620	71,400	22,020	2,040	2,610	21,240	36,150	346,320	197.600
07-H3	187,170	96,690	99,030	66,960	7,920	1,560	5,580	27,840	32,220	337,800	197.600
07-H4	208,560	111,150	92,040	45,750	1,260	2,250	8,580	28,980	26,400	316,410	200.938
07-H5	237,960	109,950	90,090	19,860	2,070	3,060	9,180	26,100	26,700	287,010	199.300
07-H6	246,570	114,300	85,320	13,650	540	1,800	8,220	29,940	24,630	278,400	199.300

Form the rainfall data in Figure 4.10 and cloud data in Figure 4.11 and Table 4.3; it is obvious that there were plenty of clouds observed in the sky during that 24-hr period especially at nighttime in the lower part of the country. However, in the north and upper northeast fewer clouds were seen due to the influence of stable air in cold mass territory. Majority of the clouds are potential warm cloud with temperature between 10 and -10°C and only small fraction that can be considered as being rain cloud (with temperature less than -30 or -40°C). However, the potential relationship of cloud top temperature and rain rate will be discussed more in Section 4.2.

4.1.2.2 Cloud/rainfall in summer

To represent cloud/rainfall distributing pattern in summer, their data maps taken on 18-19 April 2007 were chosen for the analysis. On that dates, the cold air mass was weaken and gave chance to the warm/moist air streams from the Thai Gulf and Andaman Sea to move into the central and lower northeastern region. This results in the formation of rain cloud along the weather front and by local convective process (Figure 4.12). Most cold clouds were developed during daytime and normally lasted just only few hours. But the longer-lasting cold cloud was seen at nighttime in the central area, where it could be visible for more than 10 hours. Most potential warm clouds (at temperature 10 to -10°C) were seen in the afternoon but some can last all night long. Hourly amount of the cloud cover at each temperature range is shown in Table 4.4. Also, amount of rain cloud (with temperature less than -30 or -40°C) is considerably higher than in wintertime, especially the amount of huge cumulonimbus cloud (e.g. at $\text{CTT} < -60^{\circ}\text{C}$).

The rainfall was mostly observed in the central and lower northeastern region due to strong influence of warm/moist air current as seen in the rainfall map for 19 April 2007 (Figure 4.13). This map represents accumulated rainfall being collected within 24 hours during 7.00 am (18th Apr) to 6.00 am (19th Apr).

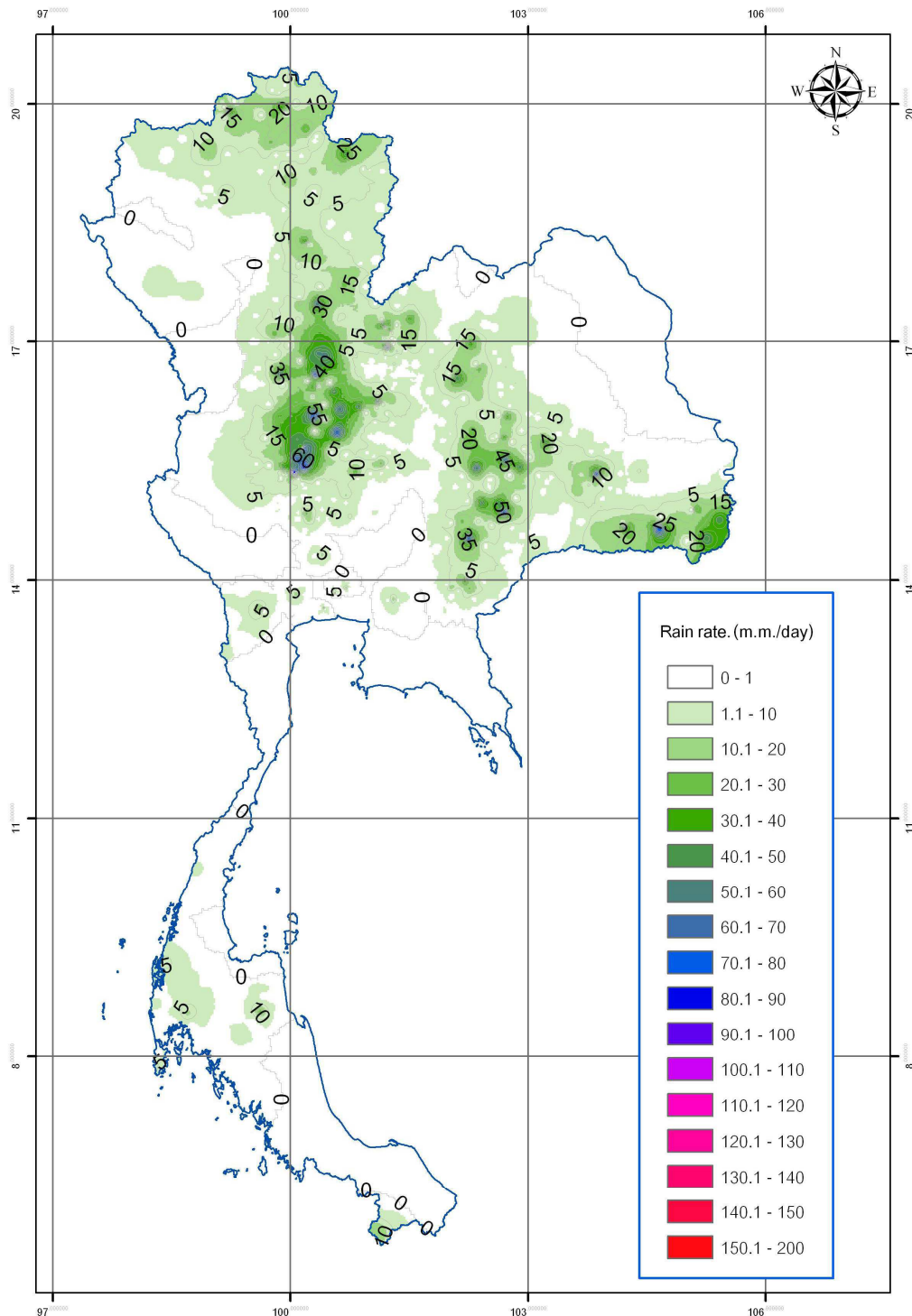


Figure 4.12 Rainfall map for 19 April 2007 when strong current of warm/moist air from the Thai Gulf and Andaman Sea to move into the central and lower northeastern region that had resulted of widespread rainfall within that area. The rainfall data were collected within 24 hours during 7.00 am (18th Apr) to 6.00 am (19th Apr)

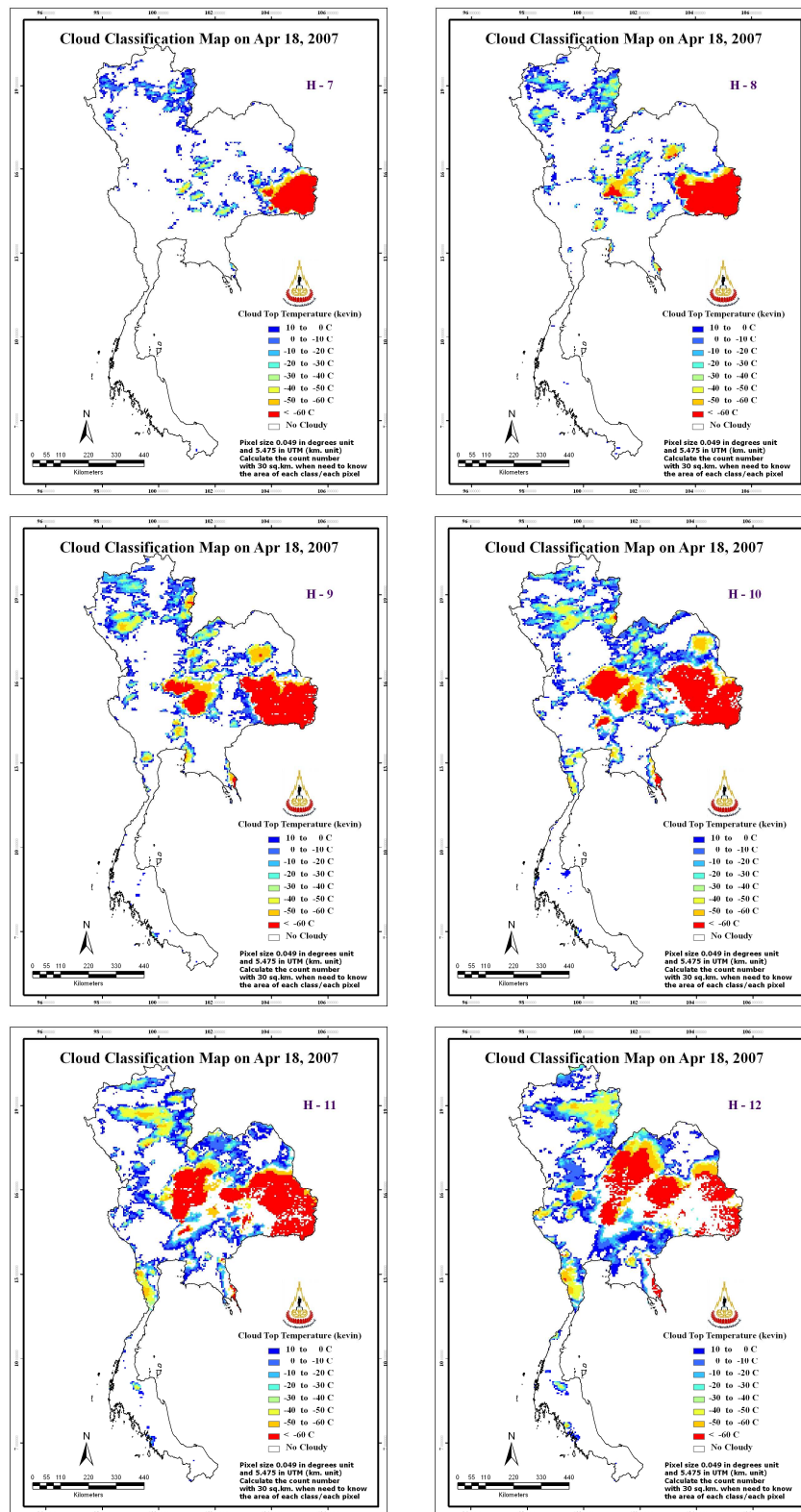


Figure 4.13 Hourly CTT maps (derived from MTSAT-1R images) for 18-19 April 2007 taken within 24 hours during 7.00 am (18^h Apr) to 6.00 am (19^h Apr).

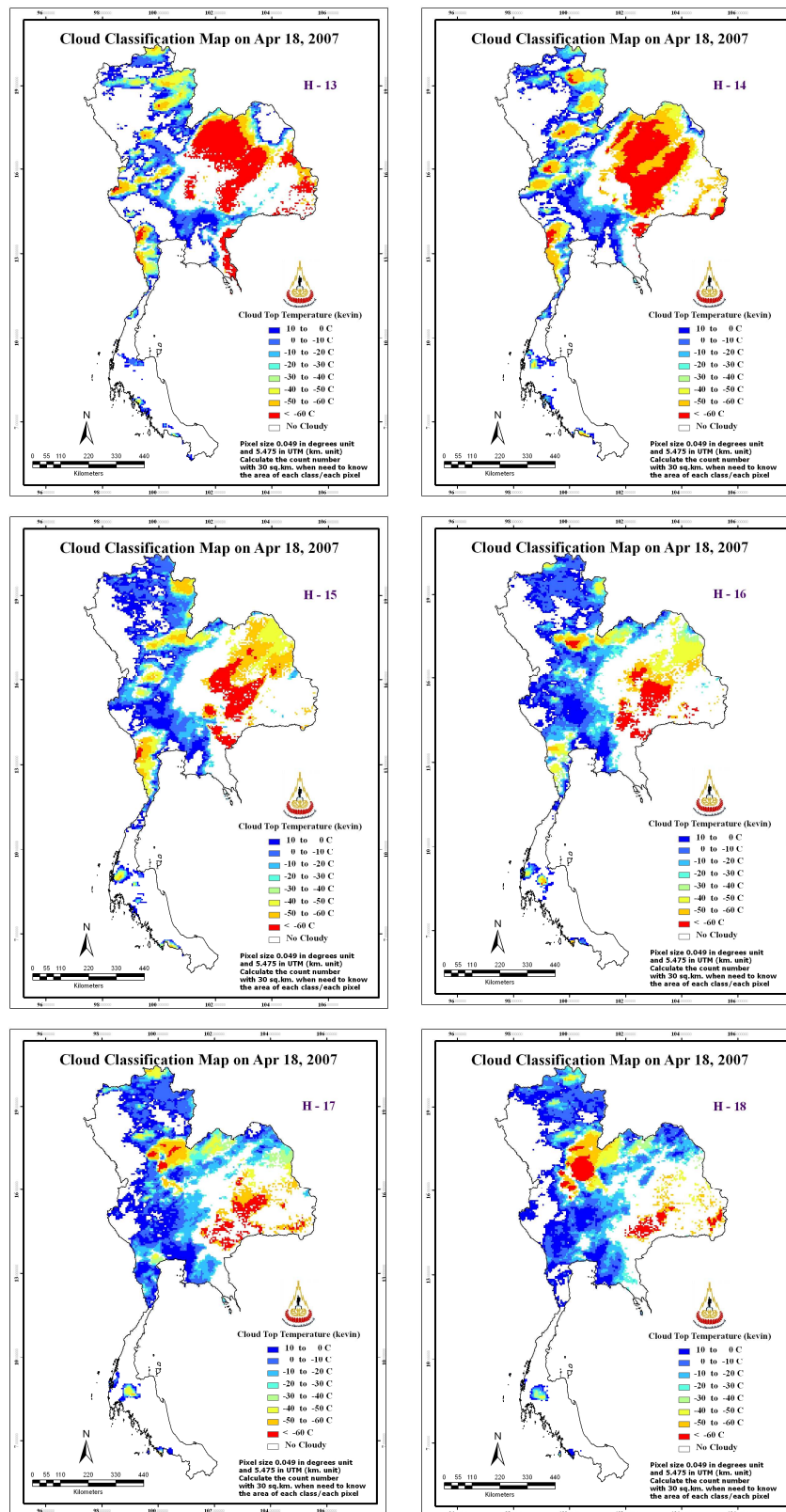


Figure 4.13 (Continued).

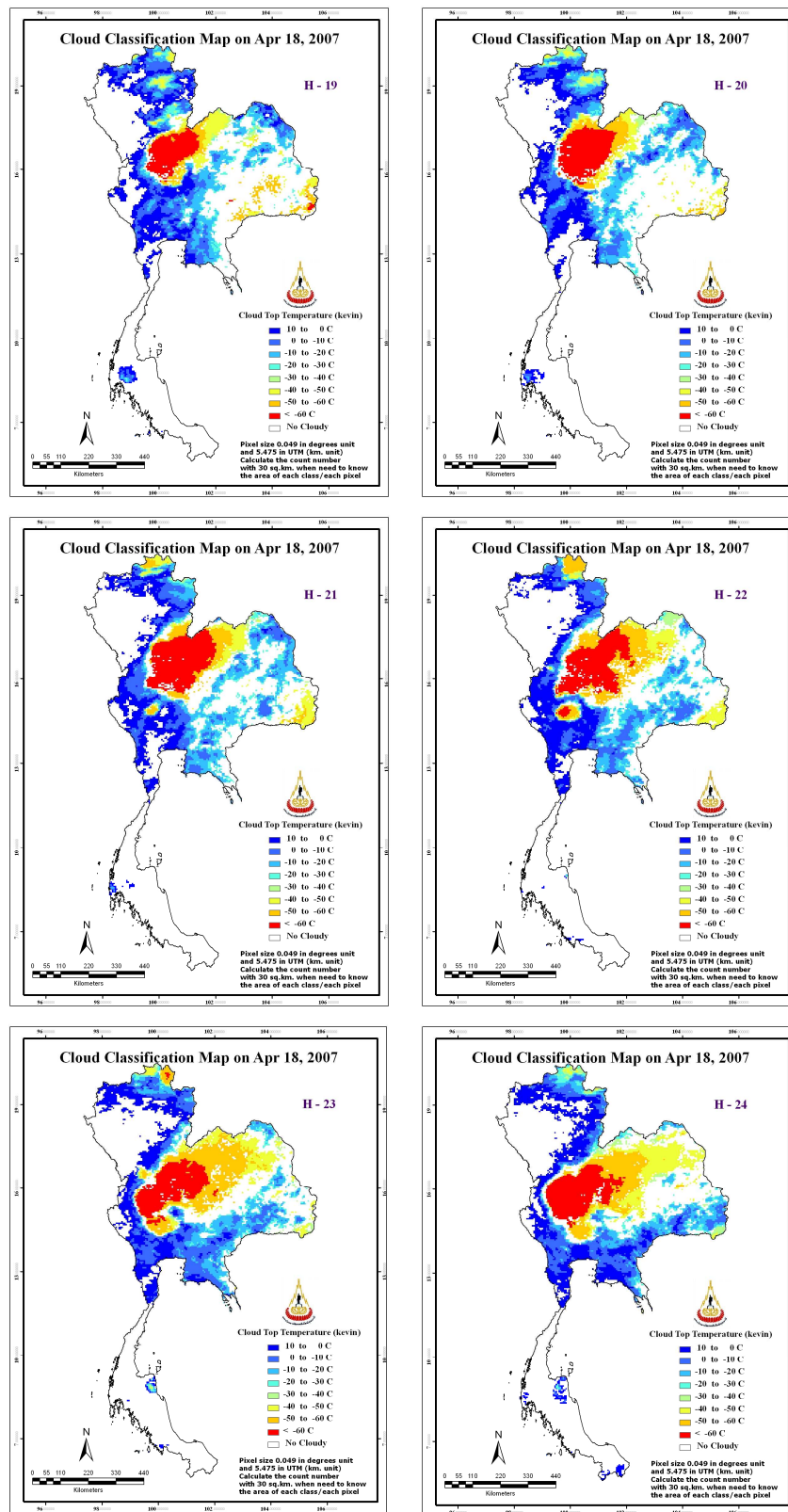


Figure 4.13 (Continued).

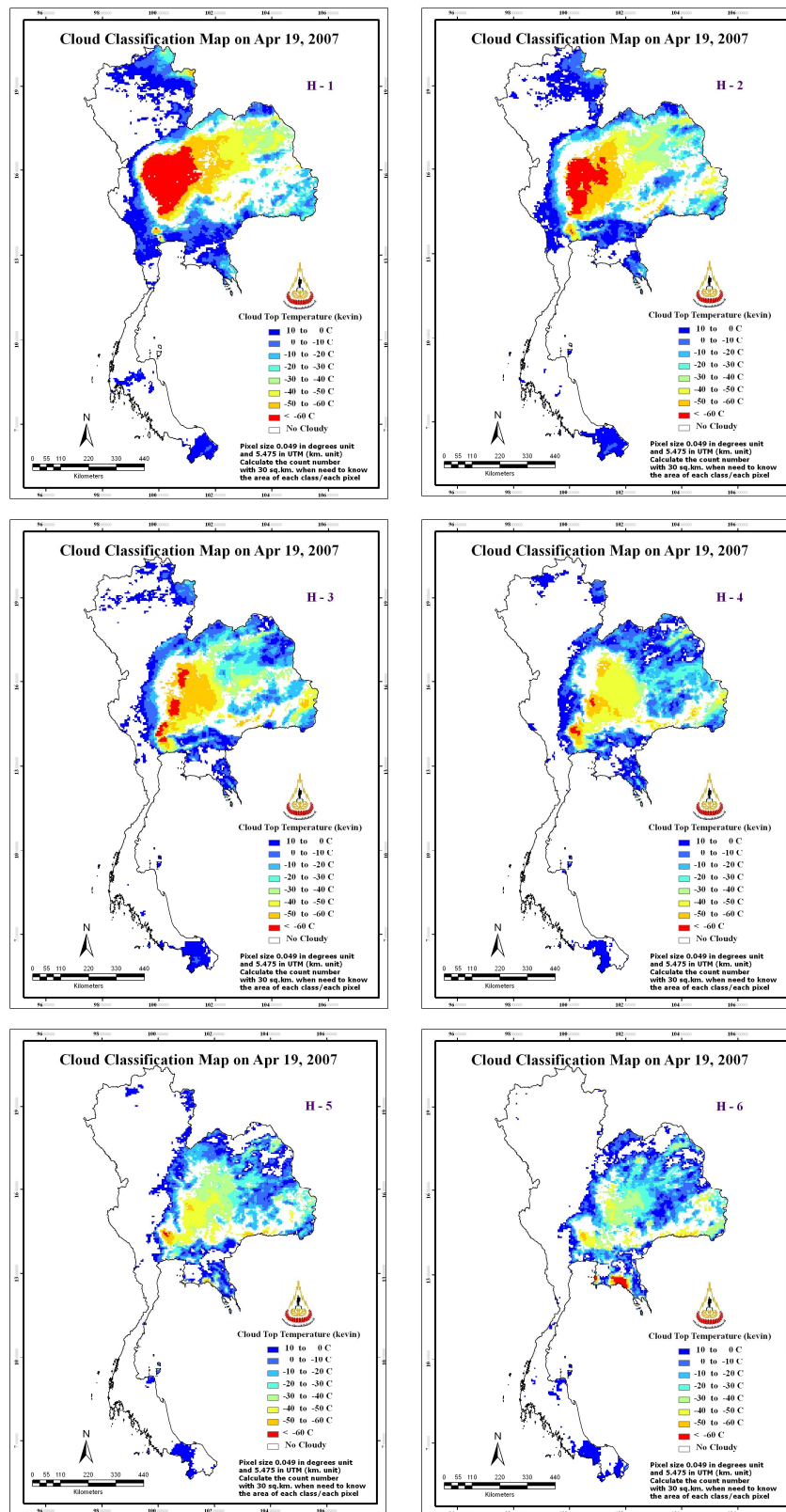


Figure 4.13 (Continued).

Table 4.4 Variation of CTT area coverage during 18-19 April 2007 (Figure 4.13)

Time order	Coverage area base on CTT class (km ²)									Cloud area (km ²)	Lowest temp (K)
	No cloud	10/0	0/-10	-10/-20	-20/-30	-30/-40	-40/-50	-50/-60	< -60		
18-H7	440,610	26,850	15,870	8,040	3,900	2,700	2,910	3,210	20,880	84,360	193.975
18-H8	396,150	28,800	17,880	12,540	9,450	8,280	10,320	8,490	33,060	128,820	187.808
18-H9	341,550	39,960	27,360	17,760	10,050	8,430	14,430	14,790	50,640	183,420	189.973
18-H10	302,400	43,500	37,560	25,560	14,490	10,260	14,370	14,820	62,010	222,570	192.028
18-H11	291,330	49,500	38,130	24,120	11,190	9,210	19,050	14,130	68,310	233,640	192.028
18-H12	289,410	45,810	39,960	23,310	12,990	11,190	24,330	19,350	58,620	235,560	192.028
18-H13	277,470	45,090	38,460	26,700	14,040	11,190	21,810	22,830	67,380	247,500	187.808
18-H14	242,490	51,030	38,790	28,500	12,930	7,980	22,890	56,460	63,900	282,480	192.028
18-H15	260,100	58,320	56,490	33,270	10,650	5,490	31,530	41,160	27,960	264,870	195.825
18-H16	266,460	60,060	66,810	37,020	16,020	11,160	27,270	19,620	20,550	258,510	197.600
18-H17	253,140	68,370	65,670	49,290	19,320	13,290	13,650	25,110	17,130	271,830	200.938
18-H18	263,520	66,210	69,090	47,670	19,230	7,410	14,160	20,760	16,920	261,450	197.600
18-H19	263,880	65,910	58,350	50,760	18,480	5,700	20,520	17,550	23,820	261,090	192.028
18-H20	263,130	57,960	53,400	55,770	21,420	7,140	17,250	15,870	33,030	261,840	192.028
18-H21	245,430	57,060	54,000	59,220	22,440	3,390	21,210	19,500	42,720	279,540	195.825
18-H22	241,350	63,090	50,670	48,600	18,030	4,560	20,370	36,840	41,460	283,620	195.825
18-H23	227,010	60,630	58,290	46,860	15,540	3,690	26,730	49,230	36,990	297,960	187.808
18-H24	221,520	76,380	56,040	38,130	15,720	7,770	37,140	33,540	38,730	303,450	193.975
19-H1	238,380	79,020	41,400	35,310	19,080	15,090	32,790	26,880	37,020	286,590	195.825
19-H2	253,500	72,150	36,210	36,600	22,380	25,440	30,390	27,780	20,520	271,470	202.515
19-H3	273,120	58,680	46,290	41,580	27,510	19,050	23,670	29,340	5,730	251,850	204.042
19-H4	287,520	60,300	50,820	43,380	21,270	10,080	39,240	11,160	1,200	237,450	205.510
19-H5	323,610	48,390	41,460	36,810	23,520	26,310	21,150	3,420	300	201,360	210.973
19-H6	334,770	48,840	39,390	37,770	27,060	21,600	11,340	2,310	1,890	190,200	202.515

4.1.2.3 Cloud/rainfall in monsoon season

To represent cloud/rainfall distributing pattern in monsoon season, the data maps taken on 16-17 August 2007 were chosen for the analysis. On that dates, the weather was under the influence of strong monsoon trough and the southwest monsoon which induced widespread heavy rainfall and floods in several areas, especially in the upper part of the country. The sky was cloudy all day long and many cold clouds were huge and lasted for several hours, however most clouds seen were potential warm clouds (at temperature 10 to -10°C) as described in Table 4.5.

Rainfall was mostly observed in the central, the western, and lower northeastern regions due to the moon trough and the southwest monsoon as seen in the rainfall map for 17 August 2007 (Figure 4.14). This map represents accumulated rainfall being collected within 24 hours during 7.00 am (16th Aug) to 6.00 am (17th Aug).

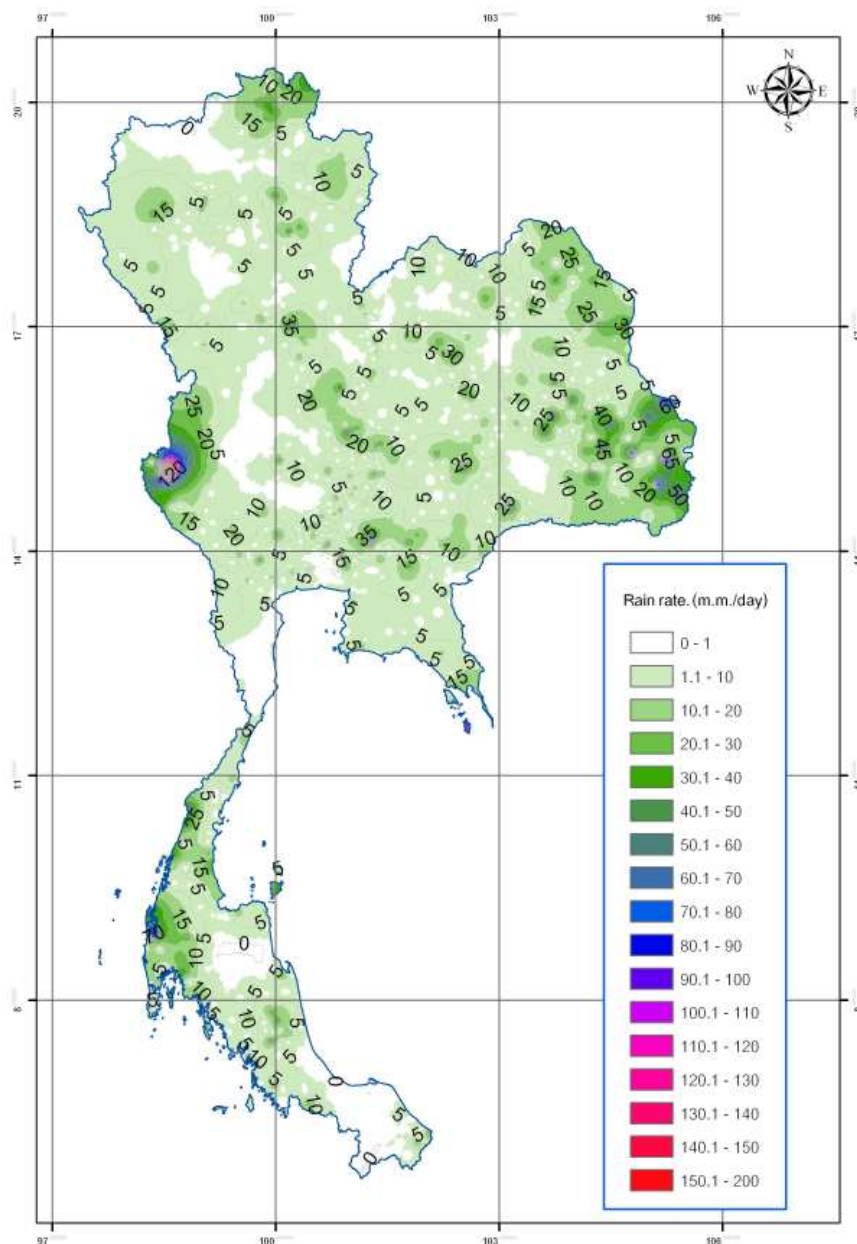


Figure 4.14 Rainfall map for 17 August 2007. The rainfall data were collected within 24 hours during 7.00 am (16th Aug) to 6.00 am (17th Aug).

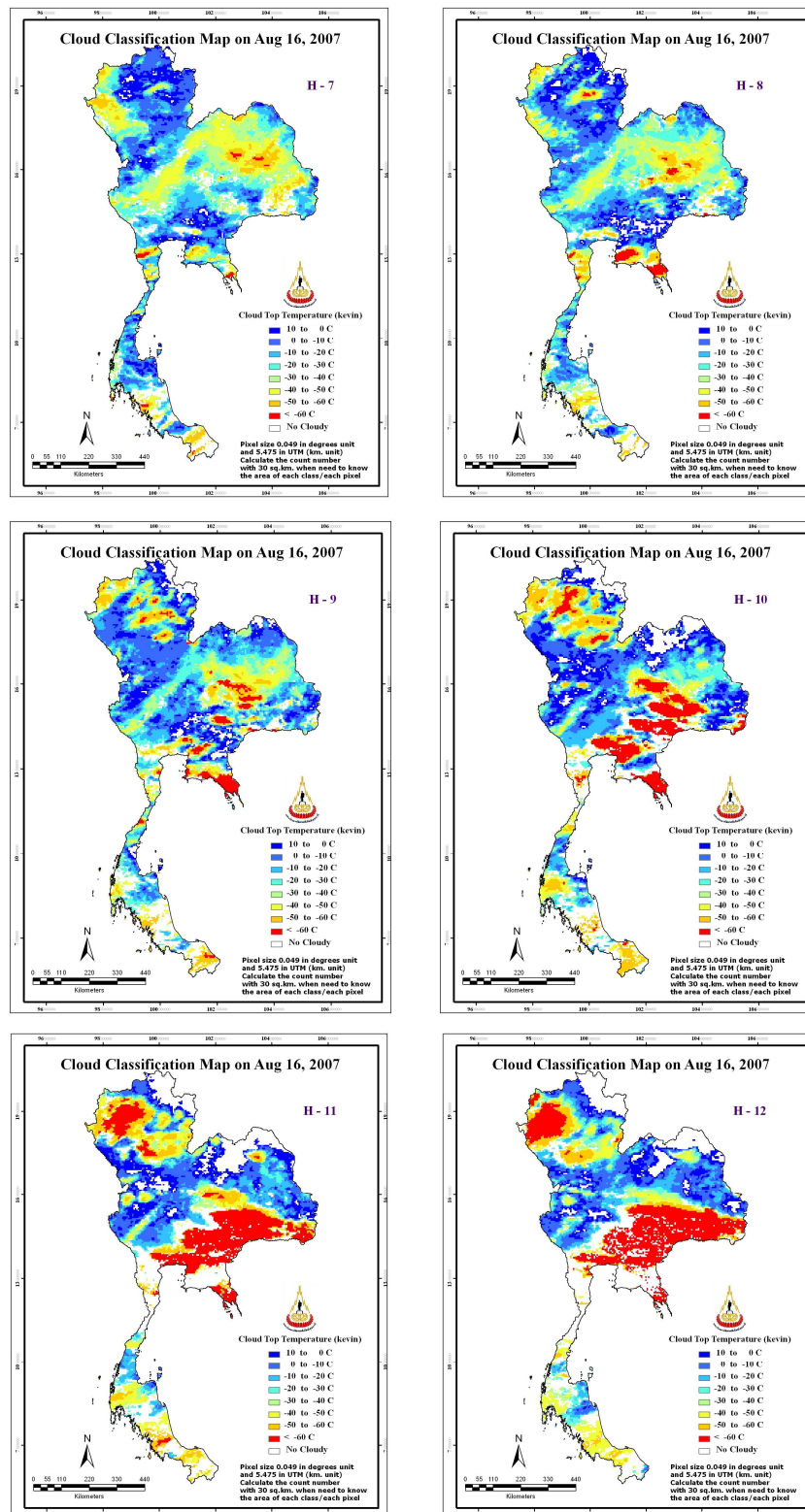


Figure 4.15 Hourly CTT maps (derived from MTSAT-IR images) for 16-17 August 2007 taken within 24 hours during 7.00 am (16th Aug) to 6.00 am (17th Aug).

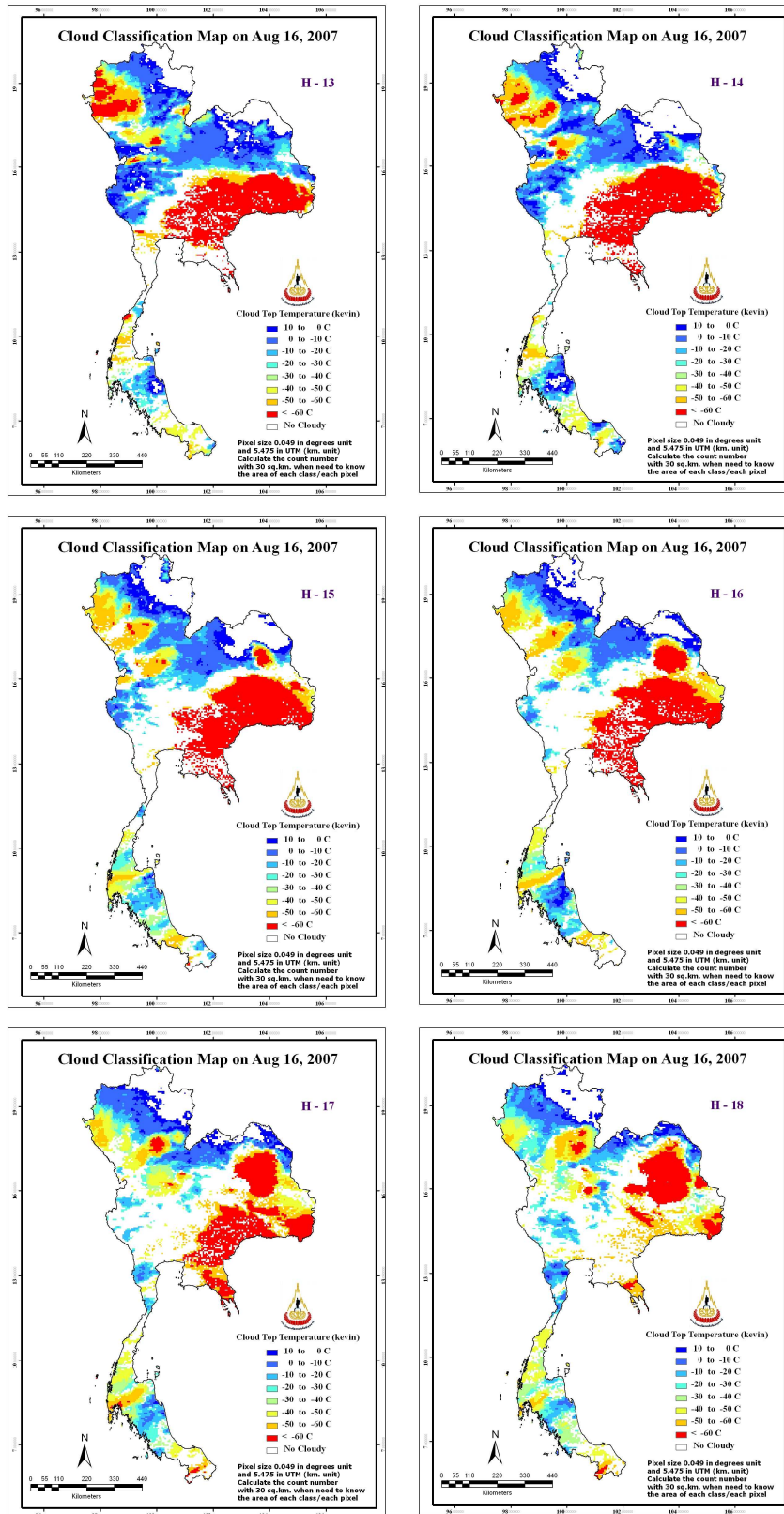


Figure 4.15 (Continued).

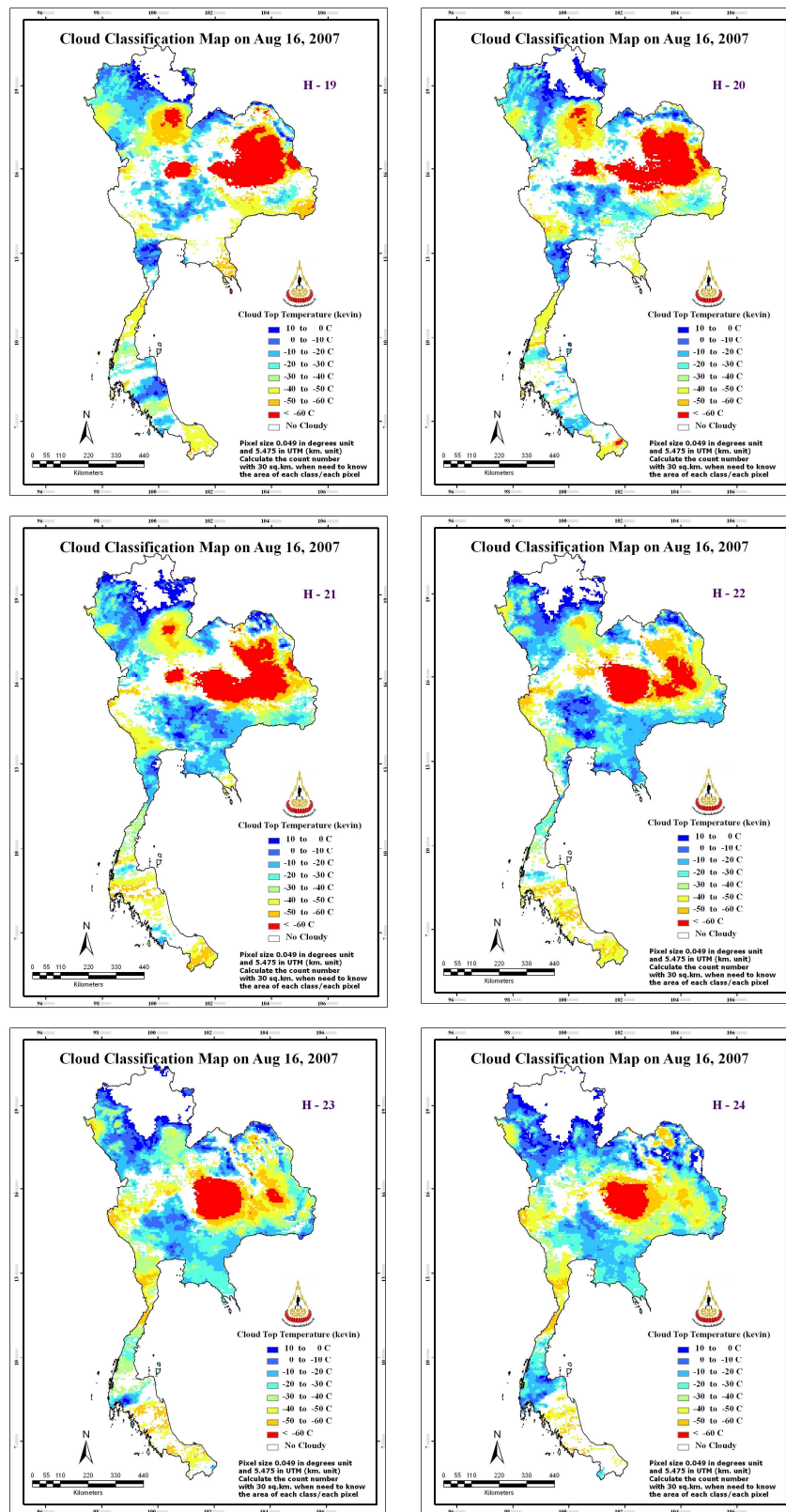


Figure 4.15 (Continued).

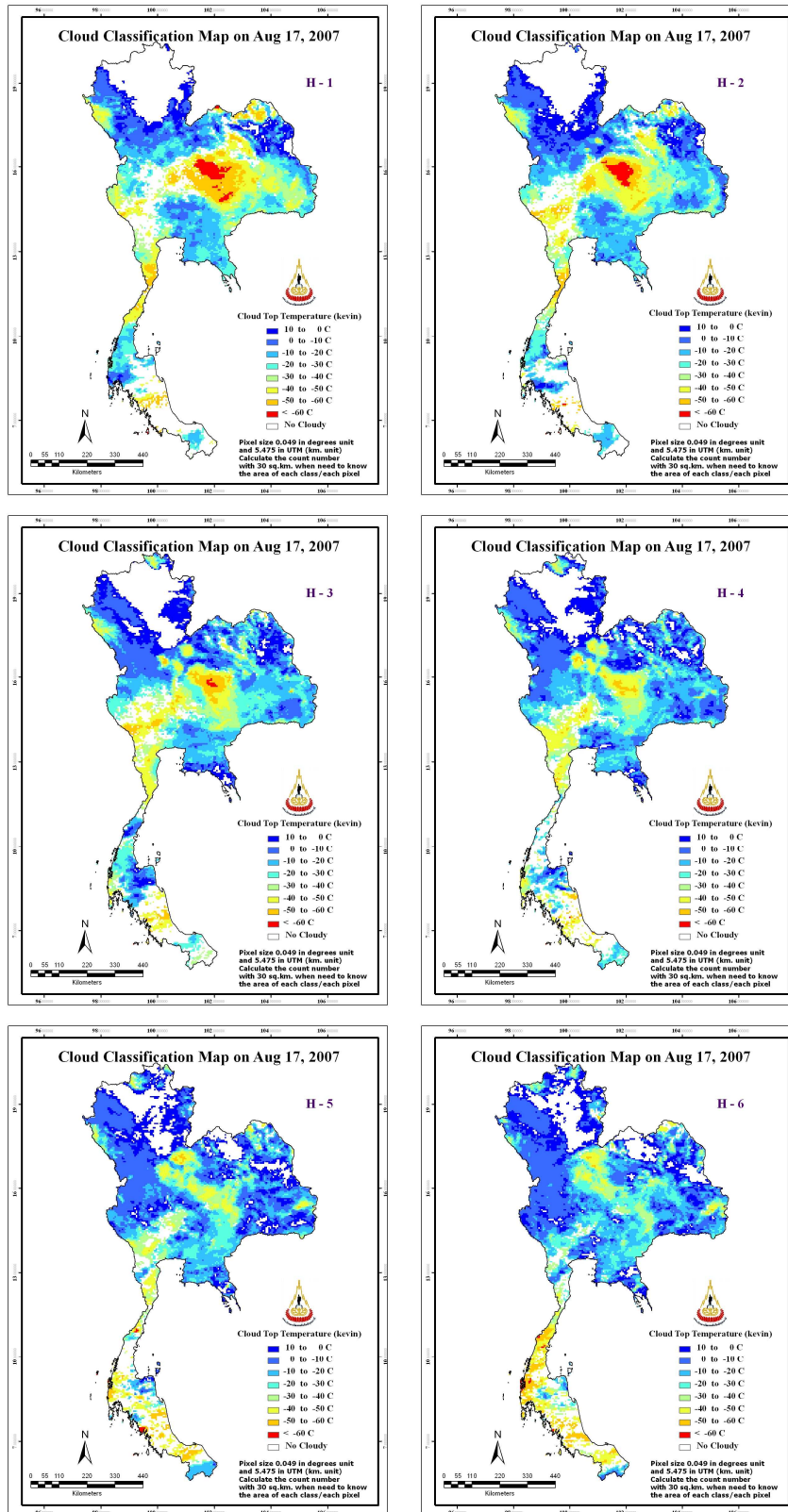


Figure 4.15 (Continued).

Table 4.5 Variation of CTT area coverage during 16-17 August 2007 (Figure 4.15)

Time order	Coverage area base on CTT class (km ²)									Cloud area (km ²)	Lowest temp (K)
	No cloud	10/0	0/-10	-10/-20	-20/-30	-30/-40	-40/-50	-50/-60	< -60		
16-H7	61,950	45,000	83,580	87,090	68,790	73,020	76,980	25,470	3,090	463,020	204.042
16-H8	64,500	47,430	95,250	85,140	71,790	69,690	58,650	24,150	8,370	460,470	199.300
16-H9	73,890	49,380	104,280	84,990	65,640	47,160	48,360	33,660	17,610	451,080	193.975
16-H10	110,280	68,880	77,490	63,600	42,930	24,270	39,000	49,470	49,050	414,690	187.808
16-H11	135,360	51,330	69,420	54,390	23,820	16,770	47,460	46,590	79,830	389,610	183.050
16-H12	143,160	42,060	76,110	51,330	28,380	23,010	39,990	29,820	91,110	381,810	185.505
16-H13	157,860	39,300	85,050	52,740	25,110	11,040	26,310	33,150	94,410	367,110	185.505
16-H14	177,570	37,440	68,940	50,430	22,410	11,430	24,030	36,510	96,210	347,400	187.808
16-H15	193,650	25,260	57,270	49,560	23,970	14,940	25,080	43,260	91,980	331,320	187.808
16-H16	203,220	26,490	51,420	37,350	21,750	15,210	34,950	45,960	88,620	321,750	187.808
16-H17	205,080	19,950	43,680	36,120	25,410	21,690	48,840	46,800	77,400	319,890	185.505
16-H18	215,880	14,130	34,200	50,160	35,220	27,240	51,480	47,610	49,050	309,090	187.808
16-H19	199,800	11,880	29,790	63,000	45,090	26,010	58,530	33,660	57,210	325,170	189.973
16-H20	197,220	16,140	30,540	60,150	50,790	26,490	55,950	28,200	59,490	327,750	189.973
16-H21	160,560	21,360	38,010	74,730	48,870	30,390	60,090	36,900	54,060	364,410	185.505
16-H22	149,520	20,070	38,880	84,870	51,210	39,600	61,920	41,130	37,770	375,450	189.973
16-H23	158,400	15,120	35,940	69,450	69,150	54,810	55,680	37,620	28,800	366,570	192.028
16-H24	148,140	22,950	44,760	86,820	68,910	40,020	62,490	30,630	20,250	376,830	199.300
17-H1	149,040	30,030	61,020	86,220	67,440	42,780	48,390	32,340	7,710	375,930	199.300
17-H2	130,860	43,590	79,980	93,570	65,250	42,930	44,820	18,060	5,910	394,110	200.938
17-H3	112,620	55,290	91,650	89,670	73,620	42,420	44,880	14,040	780	412,350	205.510
17-H4	111,390	60,540	107,130	104,670	56,940	38,640	39,930	5,670	60	413,580	209.661
17-H5	107,610	73,410	125,490	89,460	49,530	39,390	31,680	7,710	690	417,360	200.938
17-H6	97,440	72,000	129,510	89,730	61,080	34,650	26,640	12,840	1,080	427,530	204.042

4.2 Relationship between rainfall and cloud properties

In theory, the intensity of rainfall amount depends directly on type of cloud where most heavy rainfall is from cumulonimbus cloud and light rain normally from the stratiform cloud. As these clouds naturally locate at different altitude, therefore, their usual CTT tend to be distinguishable on satellite TIR images where cumulonimbus clouds have significantly lower CTT as their top surface situate much higher compared to the stratiform cloud, or other middle or low clouds.

As a result, it is possible to identify the cumulonimbus cloud based on data of CTT and this knowledge can be related to the potential amount of the observed rainfall later on. Also, amount of potential rain clouds as a whole (not only cumulonimbus) can be linked to rainfall observed each day which is also discussed in detail in this section.

4.2.1 Rainfall intensity and CTT

The first study was conducted to examine general characteristics of the lowest hourly CTT on the used MTSAT-1R satellite images (on the seasonal basis) and amount of maximum daily rainfall observed in the country that was classified into 5 groups: 0-20, 20-40, 40-60, 60-80, 80-100 and >100 mm. The classes represent days with light rainfall to very heavy rainfall respectively. Also, data of the recorded “hail” days are displayed as a comparison, as hail can originate from the cumulonimbus cloud only, therefore, in the hail days, there must have the cumulonimbus cloud presented in the satellite images.

From Figure 4.16, it can be primarily concluded that sign of the cold cloud appearance (e.g. clouds with temperature less than 240 K) are more pronounced in rainy season than in summer or winter. Also, for heavier rain day, the less CTT values were normally found especially in summer (where the CTT as low as 175 K could be found). This means some clouds on that day grow much higher than usual.

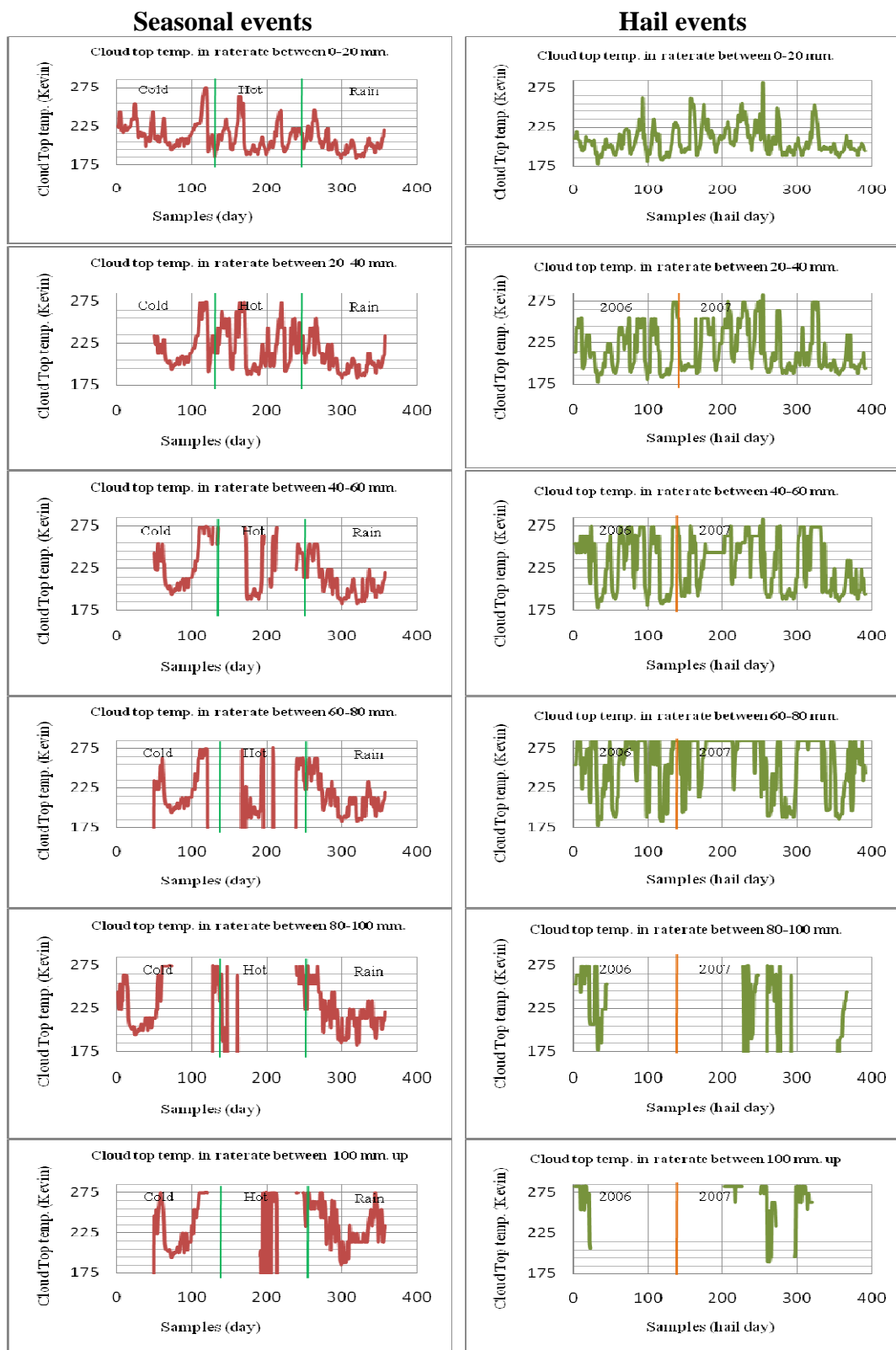


Figure 4.16 Data of the minimum hourly CCT on the used MTSAT-1R satellite images on different season and also for the chosen “hail” days in 2006 and 2007.

Table 4.6 Statistics of the lowest CTT (in Kevin unit) for seasonal and hail events

Statistics	Winter	Summer	Rainy	Hail-06	Hail-07
Minimum	197.60	193.98	185.51	183.05	173.53
Maximum	274.39	281.16	282.09	279.27	282.09
Mean	218.79	222.61	219.73	224.50	217.53
SD	13.87	22.55	20.12	25.38	21.46

For the hail days (occurring in summer), the CTTs can become spectacularly low, e.g. < 200 K, in a very short period of time. This could indicate about the rapid growing of cumulonimbus cloud (under the unstable air) which is an original source of the hail event found. This is quite contrast to the forming of cumulonimbus cloud in the winter which is rather taking more time than in summer or rainy season. And, as seen in Table 4.6, the minimum CTT for hail in 2006 was 183.05 K and 2007 was 173.53 K, this means that hail event might be found on days that have CTT less than about 183 K (about -90°C).

4.2.2 Rainfall estimation using lowest CTT

Amount of rain rate is long known to be related of the CTT of the rain clouds where the lower CTT indicate the higher amount of rainfall created (as discussed in Chapter II). However, based on several previous studies, pattern of this relationship is still subject to the time period and places of the study. In Thailand, most studies on this issue focused mainly of the cloud/rainfall relationship base on data at some selected stations (normally less than 20 stations). Therefore, in principle, their results still cannot explain the variety of the cloud/rainfall relationship in Thailand as a whole. To gain more knowledge of this relationship in wider scope, more stations covering wider area and longer time-span of rain/cloud record are needed, which is significantly fulfilled in this study.

Here, the relationship between cloud/rainfall in Thailand (on seasonal basis) was investigated based on data of minimum CTT in the specified period and total rainfall amount observed during that period from a number of weather stations across Thailand.

The assumption here is that, the lower the CTT, the higher amount of rainfall observed. The overall results of the study were shown in Figure 4.17.

It could be seen in Figure 4.17 that, the relationships between rainfall amount and lowest CTT found in the analysis still did not exhibit a clear pattern where the highest correlation of 0.6277 was seen in rainy season but in summer and winter, the correlation level was still rather low (less than 0.5). This means the CTT value alone cannot be used as sole indicator of the rainfall amount observed each day. Some other factors, like type of cloud or period of being cold cloud should also be taken into consideration.

However, in rainy season, the CTT was found to be correlated best to the observed rainfall amount and the relation was applied to predict rainfall amount on 16 August 2007 to test its validity in rainfall prediction. Results of the study are shown in Table 4.7 where most predicted values were lower than the real observed ones about 30%.

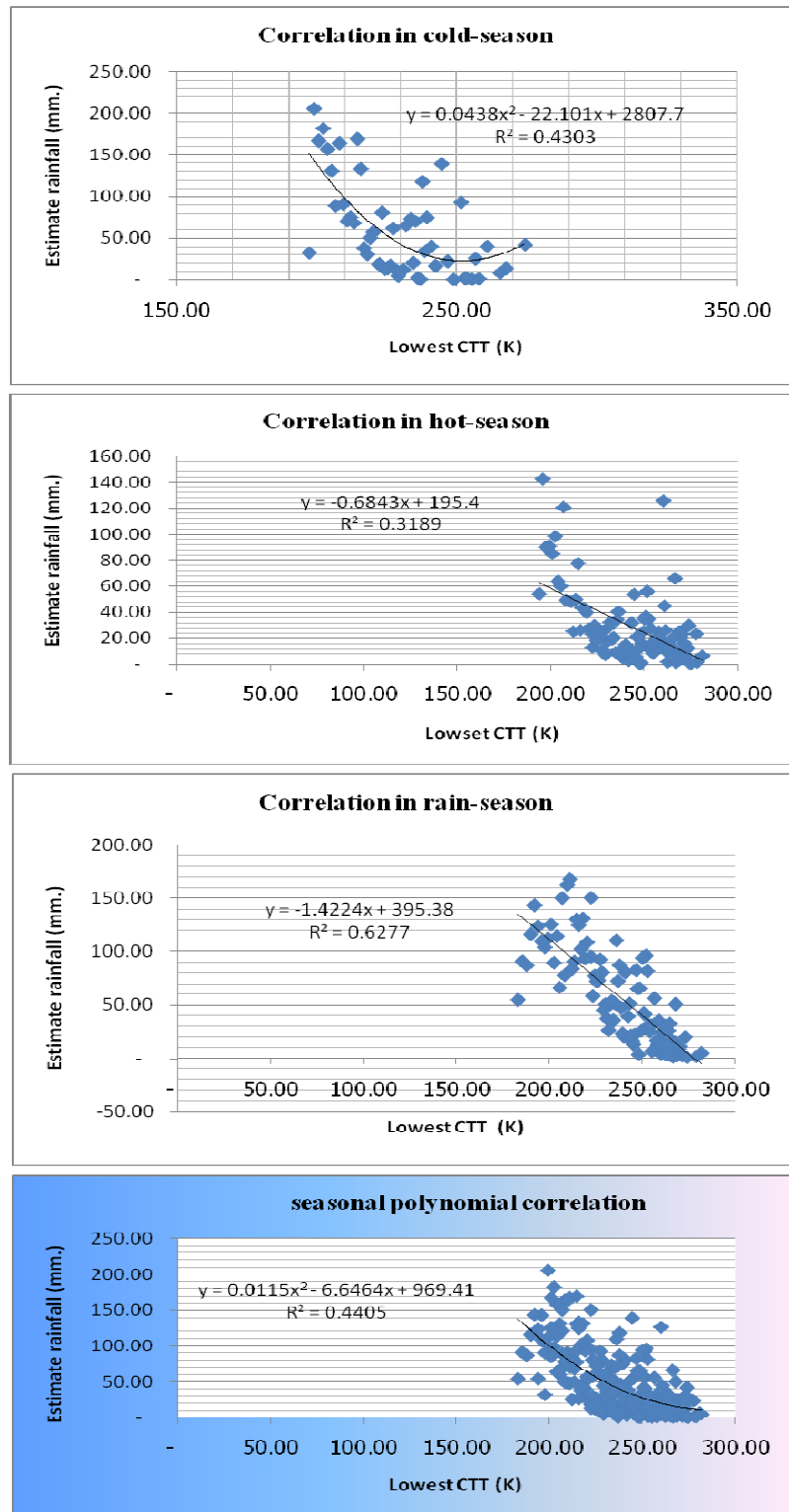


Figure 4.17 Relationship between rainfall amounts and lowest CTT in different season based on data from several stations across Thailand.

Table 4.7 Application of the cloud/rainfall relationship (as described in Figure 4.17) for rainfall prediction on 16 August 2007 (the relation is $y = -1.4224x + 395.38$)

Lowest CTT (K)	Rainfall amount (mm)		% Error	% Accuracy
	Actual	Predicted		
232.86	50.00	64.16	-35.84	64.16
231.98	26.00	65.41	-34.59	65.41
231.10	36.60	66.67	- 33.33	66.67
230.20	50.00	67.94	- 32.06	67.94
229.29	44.50	69.25	-30.75	69.25
228.36	80.30	70.56	-29.44	70.56
227.43	92.30	71.89	-28.11	71.89
226.46	73.00	73.26	-26.74	73.26
225.49	72.30	74.64	-25.36	74.64
224.50	77.20	76.05	-23.95	76.05
223.50	57.80	77.48	-22.52	77.48
	Average		-29.34	70.66

4.2.3 Rainfall intensity and cloud cover area

As mentioned earlier, not only the CTT which is being crucial indication of rainfall amount observed each day, the amount of cloud cover is also another main factors. Here, the relationship between the observed daily rainfall and average amount of cloud cover in each day taken from the satellite images is investigated. To achieve this objective, several cases were examined based on level of the rainfall intensity and the recorded hail days. Results are shown in Figure 4.18.

From the obtain results, it is clearly seen that the amount of observed daily rainfall has high correlation with the amount of cloud cover seen each day, with $r^2 > 0.8$ in all cases especially on the days with heavy rainfall (e.g. > 80 mm). High correlation was also found for the hail days (with $r^2 = 0.8915$). As the cloud cover here

includes all types of cloud seen on the satellite image, this high correlation might indicate that most types of clouds, should have contribution to the rainfall observed each day.

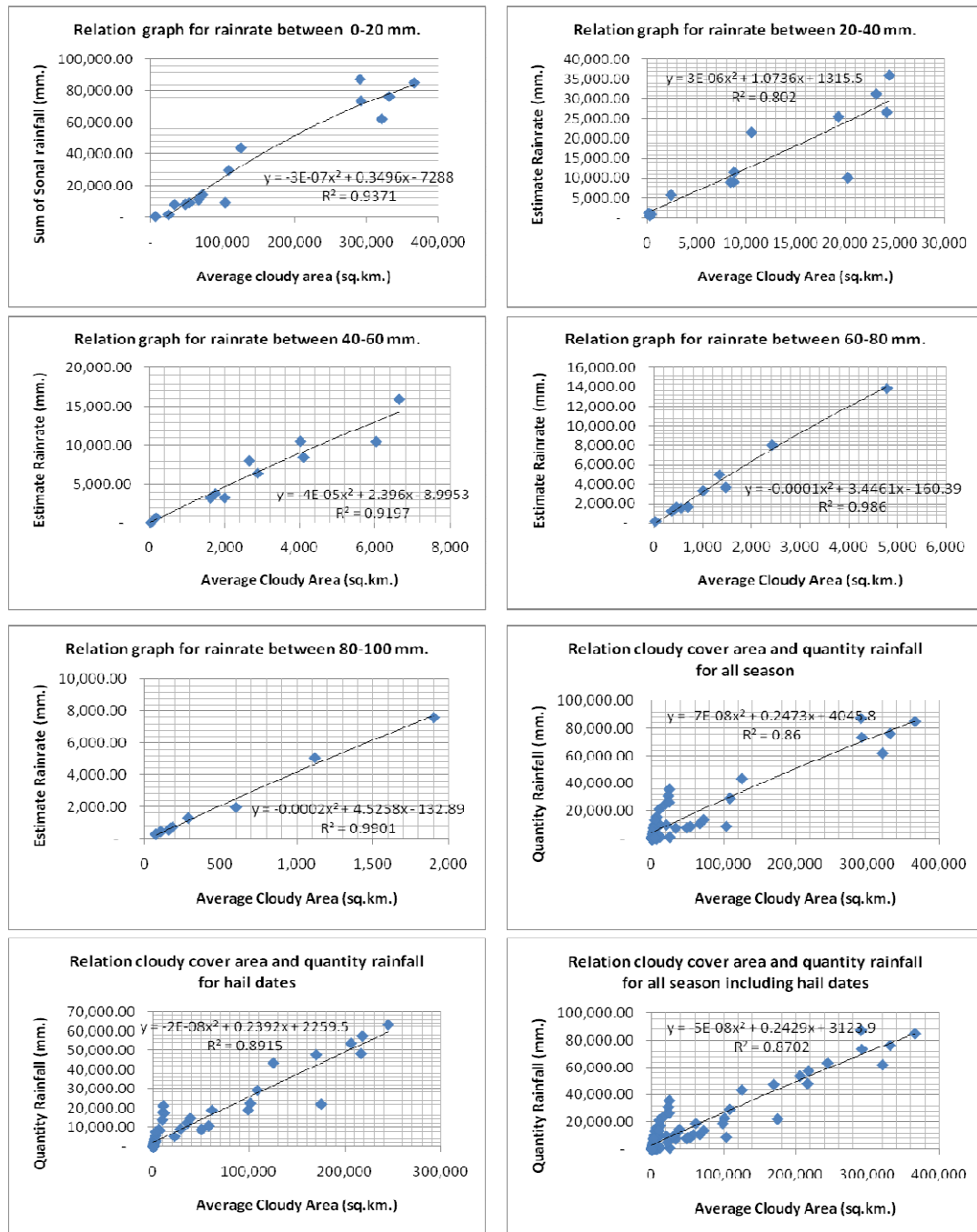


Figure 4.18 The relationship between average daily cloud cover and the total amount of observed rainfall for different levels of rainfall intensity and the hail days.

CHAPTER V

CONCLUSION AND RECOMMENDATION

5.1 Conclusions and recommendation

The main objective of this study is to analyze the relationship between rainfall intensity and the associated cloud properties (cloud top temperature and cloud cover area) in Thailand based on the selected case studies occurring during years 2006 and 2007. In addition, the classified cloud data was also applied for the study of seasonal cloud and rainfall distribution during those specified years.

To achieve the required tasks, the automatic cloud classification model was developed first based on the observed cloud top temperature (CTT) seen on the TIR image (IR-1 band) of MTSAT-1R satellite. And to reduce the confusion between cold high clouds, like cirrus, and the rain-bearing cumulonimbus cloud, the potential high clouds were filtered off at the beginning of the classifying process using split-window technique in which the threshold temperatures $T_{11} < 250 \text{ K}$ (-23°C) and $\Delta T > 1.5 \text{ K}$ ($T_{11} - T_{12}$) were employed in according to values being analyzed from cloud samples. The CTT maps were then generated and all clouds with CTT greater than 10°C were identified on maps and used to describe pattern of cloud distribution and to find the relationship with the rainfall amount observed at the same geographical locations.

From the analysis of seasonal cloud and rainfall distribution and knowledge of weather information provided from the responsible agencies, it can be concluded that patterns of seasonal cloud and rainfall distribution in Thailand are product of the

combined effects among several main driving factors. In summer, these are the local convective system, the cold airmass, the monsoon trough, the westerly wind, and the low pressure area from the ocean. In rainy season, these are the monsoon trough, the southwest monsoon, the tropical cyclone and the low pressure area from the ocean. And in winter, these are the cold air mass (weather front), northeast monsoon (for the south), and local convection. Most observed floods occurred in rainy season as results of the strong monsoon trough, the southwest monsoon, the tropical cyclone. But all reported hails were observed in March and April of each year.

In general, less cloud cover was seen in wintertime due to the more stable air, especially the rain cloud. In summer, most observed rain clouds were developed and dissipated in short time period (within few hours) and cloud top temperature can decrease as low as 175 K. These very cold clouds are normally associated to the great cumulonimbus cloud which is source of the hail event found in summer. During rainy season, clouds are more visible all day long, especially the cold cloud that can last for a considerable period of time (up to 8-10 hours).

The analysis on proper relationship between daily measured rainfall across the country and the corresponding cloud top temperature indicated that the relationships between rainfall amount and observed CTT found still did not exhibit a clear pattern where the highest correlation of 0.6277 was seen in rainy season but in summer and winter, the correlation level was still rather low (less than 0.5). This means the CTT value alone cannot be used as sole indicator of the rainfall amount observed each day.

In addition, it is clearly seen from the study that the amount of the total daily rainfall has high correlation with the amount of cloud cover area seen each day, with $r^2 > 0.8$ in all cases especially on the days with heavy rainfall (e.g. > 80 mm) or on the

hail days (with $r^2 = 0.8915$). As the cloud cover here includes all types of cloud seen on the satellite image, this high correlation might indicate that most types of clouds, should have contribution to the rainfall observed each day.

Though, some satisfied outcome have been achieved in this study, especially the automatic cloud classification model for the TIR weather satellite images and the high correlation between cloud cover area and total rainfall amount, however, there are still many interesting issues that need to be investigated more. For examples:

(1) The relationship between cloud top temperature and rainfall accumulated in shorter time period; for examples, within 3hr or 6hr, and at more specific locations;

(2) The applicability of free data from some other weather satellites, especially TRMM, in the study of rain and cloud relationship in the country;

(3) The developing pattern of rain clouds in different season and the relations between their properties, e.g. size, area cover, CTT, or the period of being cold clouds.

(4) Take some other factors, like type or thickness of cloud body or period of being cold clouds into the consideration for the analysis of cloud and rain relationship.

(5) The relationship between cloud top temperature and rainfall accumulated in other weather satellites or on MTSAT-1R on other infrared bands.

REFERENCES

REFERENCES

- ชนิด ชาญหาญ (2545). การประมาณปริมาณน้ำฝนด้วยดาวเทียมสำหรับกรุงเทพมหานครในช่วงมรสุมตะวันตกเฉียงใต้. วิทยานิพนธ์ปริญญาวิศวกรรมศาสตรมหาบัณฑิต สถาบันเทคโนโลยีพระจอมเกล้าเจ้าคุณทหารลาดกระบัง.
- ธีระพงษ์ เสาวภาคย์ (2539). การประเมินน้ำฝนที่ทำให้เกิดอุทกภัยจากข้อมูลดาวเทียมอุตุนิยมวิทยา. วิทยานิพนธ์ปริญญาโทมหาวิทยาลัยเกษตรศาสตร์.
- มณฑล จิตเอื้ออารีกุล (2546). การประมาณปริมาณฝนด้วยดาวเทียมสำหรับกรุงเทพมหานครในช่วงมรสุมตะวันออกเฉียงเหนือ. มหาวิทยาลัยเกษตรศาสตร์.
- Adhikari, N.B. and Nakamura, K. (2002). Detectable rain range of spaceborne Ka-band radar estimated from TRMM precipitation radar data. **Journal of Atmospheric and Oceanic Technology**. 19(11): 1878-1885.
- Adler, R.F. and Negri, A.J. (1988). A satellite infrared technique to estimate tropical convective and stratiform rainfall. **Journal of Applied Meteorology**. 27: 30-51.
- Ahrens, C.D. (2000). **Meteorology Today 6th Edition**. California. Brooks/Cole.
- American Meteorology Society. (2009). Glossary of Meteorology [On-line]. Available: <http://amsglossary.allenpress.com/glossary>.
- Arkin, P.A. (1979). The relationship between fractional coverage of high cloud and rainfall accumulations during GATE over the B-scale array. **Monthly Weather Review**. 106: 1153-1171.

- Arkin, P.A. and Meisner, B.N. (1987). The relationship between large-scale convective rainfall and cold cloud over the Western Hemisphere during 1982-84. **Monthly Weather Review**. 115: 51-74.
- Arkin, P.A. and Janowiak (1991). Analysis of the global distribution of precipitation. **Dynamic Atmosphere Oceans**. 16: 5-16.
- Barrett, E.C. and Martin, D.W. (1981). **The Use of Satellite Data in Rainfall Monitoring**. London: Academic Press.
- Berg, W., Olson, W., Ferraro, R., Goodman, S.J. and LaFontaine, F.J. (1998). An assessment of the first and second-generation Navy operational precipitation retrieval algorithms. **Journal of Atmosphere Science**. 55: 1558-1575.
- Bellon, A., Lovejoy, S. and Austin, G.L. (1980). Combining satellite and radar data for the short-range forecasting of precipitation. **Monthly Weather Review**. 108: 1554-1556.
- Budhakooncharoen, S. (2004). Rainfall estimate for flood management using meteorological data from satellite imagery. **In the Proceeding of the International Conference on Freshwater**. Bonn, Germany. 4 - 6 December.
- Cooper, S., Ecuyer, T.L. and Stephens, G. (2003). The impact of explicit cloud boundary information on ice cloud microphysical property retrievals from infrared radiances. **Journal of Geophysical Research**. 108(D3): 4107.
- Davis, G. (2007). History of the NOAA satellite program. **Journal of Applied Remote Sensing**. 1(012504): 1-18.

Dioszeghy, M. and Fejes, E. (1995). Cloud classification derived from Meteosat data involving the standard deviation fields of the brightness values. **Advances in Space Research**. 16(10): 33-36.

Department of Disaster Prevention and Mitigation (2009). [On-line]. Available: <http://www.disaster.go.th/dpm>.

Fan, Y. and Changsheng, L. (1997). Man-Computer interactive method on cloud classification based on bispectral satellite imagery. **Advances in Atmospheric Sciences**. 14(3): 389-398.

Ferraro, R.R., Grody, N.C. and Marks, G.F. (1994). Effects of surface conditions on rain identification using the SSM/I. **Remote Sensing Review**. 11: 195-209.

Griffith, C.G., Woodley, W.L., Grube, P.G. Martin, D.W., Stout, J. and Sikdar, D.N. (1978) Rain estimation from geosynchronous satellite imagery-visible and infrared studies. **Monthly Weather Review**. 106: 1153-1171.

Grimes, D. *et al.* (1999). Optimal areal rainfall estimation using raingauges and satellite data. **Journal of Hydrology**. 222: 93-108.

Hamblyn, R. (2001). The Invention of Clouds: **How an Amateur Meteorologist Forged the Language of the Skies**. Ohio. Farrar Straus & Giroux.

Hayasaka, T. (1996). Recent studies on satellite remote sensing of clouds in Japan. **Advances in Space Research**. 18(7): 29-36.

- Inoue, T. (1985). On the temperature and effective emissivity determination of semitransparent cirrus clouds by bispectral measurements in the 10 μm window region. **Journal of Meteorology Society Japan**. 63: 88-98.
- Inoue, T. (1987a). A cloud type classification with NOAA 7 split-window measurements. **Journal of Geophysical Research**. 92: 3991-4000.
- Inoue, T. (1987b). An instantaneous delineation of convective rainfall area using split window data of NOAA-7 AVHRR. **Journal of Meteorology Society Japan**. 65: 469-481.
- Inoue, T. (1989). Features of clouds over the tropical pacific during northern hemispheric winter derived from split window measurements. **Journal of Meteorology Society Japan**. 67: 621-637.
- Inoue, T. (1997). Detection of rain-bearing convective systems using cloud information derived from split window. **In Proceeding of the Meteorological Satellite Data Users' Conference**. 173-182.
- Inoue, T. (2004). Development of a technique to define the life stage of deep convection using the split window data of GOES. **The 2nd TRMM International Science Conference**.
- Inoue, T. (2006). Features of cloud types over the Bay of Bengal using split window measurements and TRMM satellite data. **Meteorological Society of Japan**. 2: 41-44.

- Islam, M.N. and Wahid, C.M. (2003). Adaptation of a technique to estimate rainfall from satellite data in Bangladesh. **Sri Lanka Journal of Physics**. 4: 1-9.
- Japan Meteorological Agency. (2009). Monitoring the earth from the MTSAT [On-line]. Available: <http://mscweb.kishou.go.jp/index.htm>.
- Japan Aerospace Exploration Agency (2009). The TRMM Satellite Observes Global Precipitation Distribution and Contribution to Understanding the machines of Climate Change [On-line]. Available: http://www.eorc.jaxa.jp/TRMM/index_e.htm.
- Jobard, I. and Desbois, M. (1992). A method combining infrared and microwave satellite radiances for the estimation of tropical rain. **In Proceeding Of the 6th Conference Satellite Meteorology and Oceanography**. 264-267.
- King, P.W.S. *et al.* (1995). The role of visible data in improving satellite rainrate estimates. **Journal of Applied Meteorology**. 34: 1608-1621.
- Kochi University of Japan (2009). [On-line]. Available: <http://weather.is.kochi-u.ac.jp/index-e.html>.
- Kumar, M.R. and Prasad, T.G. (1997). Annual and interannual variation of precipitation over the tropical Indian Ocean. **Journal of Geophysical Research**. 102(C8): 519-527.
- Kurino, T. (1997a). A satellite infrared technique for estimating “Deep/Shallow” convective and stratiform precipitation. **Advances in Space Research**. 19(3): 511-514.

- Kurino, T. (1997b). A Rainfall Estimation with the GMS-5 Infrared Split-window and Water Vapour Measurements. **Meteorology Center Technique Note**. Meteorological Satellite Centre, Japan Meteorology Agency. 33: 91-101.
- Laing, A.G., Fritsch, J.M. and Negri, A.J. (1994). Estimation of rainfall from mesoscale convective system in Africa using geostationary infrared and passive microwave data. **In Proceeding of the 7th Conference Satellite Meteorology and Oceanography**. 40-42.
- Levizzani, V. *et al.* (1996). Investigating a SSM/I microwave algorithm to calibrate METEOSAT infrared instantaneous rainrate estimates. **Meteorology Application**. 3: 5-17.
- Levizzani, V. (1999). Convective rain from a satellite perspective: Achievements and challenges. **SAF Training Workshop-Nowcasting and Very Short Range Forecasting**. Madrid. 25: 75-84.
- Levizzani, V. (2000). Satellite rainfall estimates: a look back and a perspective. **In Proceeding of The 2000 EUMETSAT Meteorological Satellite Data User**.
- Levizzani, V., Amorati, R. and Meneguzzo, F. (2002). A Review of Satellite-based Rainfall Estimation Methods. [On-line]. Available: <http://www.isao.bo.cnr.it/~meteosat>.
- Luke Howard (1772-1864). [On-line]. Available: <http://www.weatheronline.co.uk/reports/wxfacts/Cloud-classification.htm>.

- Lutgens, F.K. and Tarbuck, E.J. (1998). **The Atmosphere: An Introduction to Meteorology 7th Edition**. London. Prentice-Hall International, Inc.
- Massons, J., Domingo, D. and Grau, J. (1996). Automatic Classification of VIS-IR Meteosat images. **Journal of Computers & Geosciences**. 22(10): 1137-1146.
- Meteorological Satellite Center (2009). [On-line]. Available: <http://mscweb.kishou.go.jp/index.htm>.
- Mohammedberhan, N. (1998). **Satellite based rainfall estimation over Eritrea**. Master Thesis. Department of Meteorology. The University of Reading.
- National Aeronautics and Space Administration-Cloud and Radiation (2009). The Earth's Climate System Constantly Adjusts. [On-line]. Available: <http://earthobservatory.nasa.gov/Features/Clouds>.
- National Aeronautics and Space Administration-GOES (2009). [On-line]. Available: <http://www.goes.noaa.gov>.
- National Aeronautics and Space Administration-MODIS (2009). [On-line]. Available: <http://modis.gsfc.nasa.gov>.
- National Aeronautics and Space Administration-TRMM (2009). [On-line]. Available: <http://trmm.gsfc.nasa.gov>.
- National Geophysical Data Center (2006). SSM/I-Microwave Imager. [On-line]. Available: <http://www.ngdc.noaa.gov/dmsp/sensors/ssmi.html>.
- O'Sullivan, F. *et al.* (1990). Rain estimation from infrared and visible GOES satellite data. **Journal of Applied Meteorology**. 29(3): 209-223.

- Petty, G.W. (1995). The status of satellite-based rainfall estimation over land. **Remote Sensing Environment**. 51: 125-137.
- Scofield, R.A. (1987). The NESDIS operational convective precipitation technique. **Monthly Weather Review**. 115: 1773-1792.
- Stull, R.B. (2000). **Meteorology for Scientists and Engineers 2nd Edition**. California: Brooks/Cole.
- Sumner, G. (1988). **Precipitation Process and Analysis**. John Wiley & Sons, Inc. New York. The Both Press.
- Thai Meteorological Department (2009). [On-line]. Available: <http://www.tmd.go.th>.
- The European Organisation for the Exploitation of Meteorological Satellites (2009). Monitoring weather and climate from space. [On-line]. Available: <http://www.eumetsat.int/Home/index.htm>.
- Thorne, V., Coakley, P., Grimes, D. and Dugdale, G. (2001). Comparison of TAMSAT and CPC rainfall estimates with rainfall for southern Africa. **International Journal of Remote Sensing**. 22(10): 1951-1974.
- Tsonis, A.A. and Isaac, G.A. (1985). On a new approach for instantaneous rain area delineation in the midlatitudes using GOES data. **Journal of Climate and Applied Meteorology**. 24(11): 1208-1218.
- Tsonis, A.A. (1987). Determining rainfall intensity and type from GOES imagery in the midlatitudes. **Remote Sensing of Environment**. 21(1): 29-36.

- Todd M.C. *et al.* (1995). Satellite identification of rain days over the upper Nile river basin using an optimum infrared rain/no-rain threshold temperature model. **Journal of Applied Meteorology**. 34(12): 2600-2611.
- Tucker, M.R. and Sear, C.B. (2001). A comparison of Meteosat rainfall estimation techniques in Kenya. **Meteorological Applications**. 8: 107-117.
- Turk, F.J., Marzano, F.S. and Smith, E.A. (1998a). Combining geostationary and SSM/I data for rapid rain rate estimation and accumulation. **In Processing of the 9th Conference Satellite Meteorology and Oceanography**. 462-465.
- Turk, F.J., Marzano, F.S. and Smith, E.A. (1998b). Using coincident SSM/I and infrared satellite data for rapid updates of rainfall. **In Proceeding of IGARSS'98-Sensing and Managing the Environment Symposium**. 3-9.
- Udomchoke, V. and Aungsuratana, P. (1995). The Rainfall Estimation using Remote Sensing in Thailand. [On-line]. Available: https://pindex.ku.ac.th/file_search/WE60.doc.
- United State Geological Survey-Advanced Very High Resolution Radiometer (2009). [On-line]. Available: <http://eros.usgs.gov/products/satellite/avhrr.php>.
- Vicente, G.A. and Anderson, J.R. (1994). A new rain retrieval technique that combines geosynchronous IR and MW polar orbit data for hourly rainfall estimates. **In Proceeding of the 7th Conference Satellite Meteorology and Oceanography**. 34-37.

- Vicente, G.A., Scofield, R.A. and Menzel, W.P. (1998). The operational GOES infrared rainfall estimation technique. **Bulletin of the American Meteorological Society**. 79: 1883-1898.
- Wilheit, T.T. *et al.* (1994). Algorithms for the retrieval of rainfall from passive microwave measurements. **Remote Sensing Review**. 11:163-194.
- World Climate Research Program (1996). Assessment of Global Precipitation Products. [On-line]. Available: <http://www.wmo.ch/pages/prog/wcrp/documents/AssessmentGlobalPrecipitationReport.pdf>.
- World Meteorological Organization (1956). **International Cloud Atlas**. Geneva. Abridged Atlas.1: 50-62.

APPENDICES

APPENDIX A

USER MANUAL OF CLOUD MODEL

Introduction

The ERDAS MTSAT-1R Cloud model is designed to support cloud analysis. It is developed by using Spatial Modeler Language (SML) and ERDAS Macro Language (EML). They run within ERDAS environment.

Copyright Notice

Copyright © 2009 by Suranaree University of Technology

Developer

- Miss. Pornthip Bumrunklang
- Email : *paragon09@hotmail.com; tui.pornthip@gmail.com*
- Cell Phone: 6686-2512999
- Home Phone: 6644-211524

System Requirement

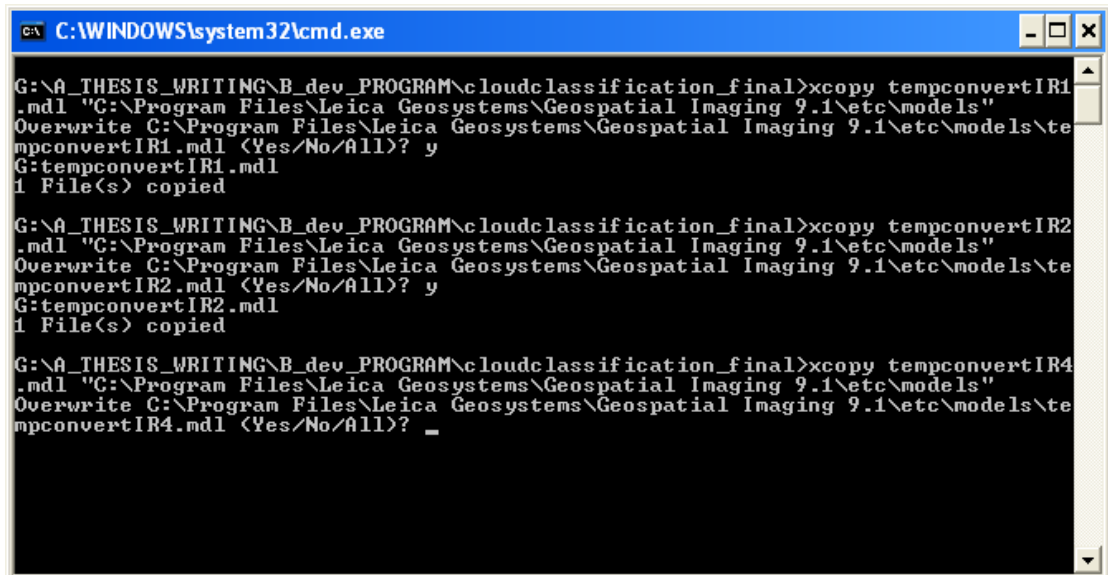
- Operating System: any windows versions that support ERDAS 9.x up

Data Format

- IMG
- TIF
- Any raster formats that able to run on ERDAS software

Installation step

1. Run or Double click *install.bat* in windows command session or window explorer session, see example as Figure A.1



```

C:\WINDOWS\system32\cmd.exe

G:\A_THESIS_WRITING\B_dev_PROGRAM\cloudclassification_final>xcopy tempconvertIR1
.mdl "C:\Program Files\Leica Geosystems\Geospatial Imaging 9.1\etc\models"
Overwrite C:\Program Files\Leica Geosystems\Geospatial Imaging 9.1\etc\models\te
mpconvertIR1.mdl <Yes/No/All>? y
G:tempconvertIR1.mdl
1 File(s) copied

G:\A_THESIS_WRITING\B_dev_PROGRAM\cloudclassification_final>xcopy tempconvertIR2
.mdl "C:\Program Files\Leica Geosystems\Geospatial Imaging 9.1\etc\models"
Overwrite C:\Program Files\Leica Geosystems\Geospatial Imaging 9.1\etc\models\te
mpconvertIR2.mdl <Yes/No/All>? y
G:tempconvertIR2.mdl
1 File(s) copied

G:\A_THESIS_WRITING\B_dev_PROGRAM\cloudclassification_final>xcopy tempconvertIR4
.mdl "C:\Program Files\Leica Geosystems\Geospatial Imaging 9.1\etc\models"
Overwrite C:\Program Files\Leica Geosystems\Geospatial Imaging 9.1\etc\models\te
mpconvertIR4.mdl <Yes/No/All>? _

```

Figure A.1 Show the installation step

2. Type "Y" or "A" to replace if there are existing files.
3. Then SML and EML MTSAT-1R cloud models will be installed into your ERDAS software under Interpreter main menu, see as Figure A.2

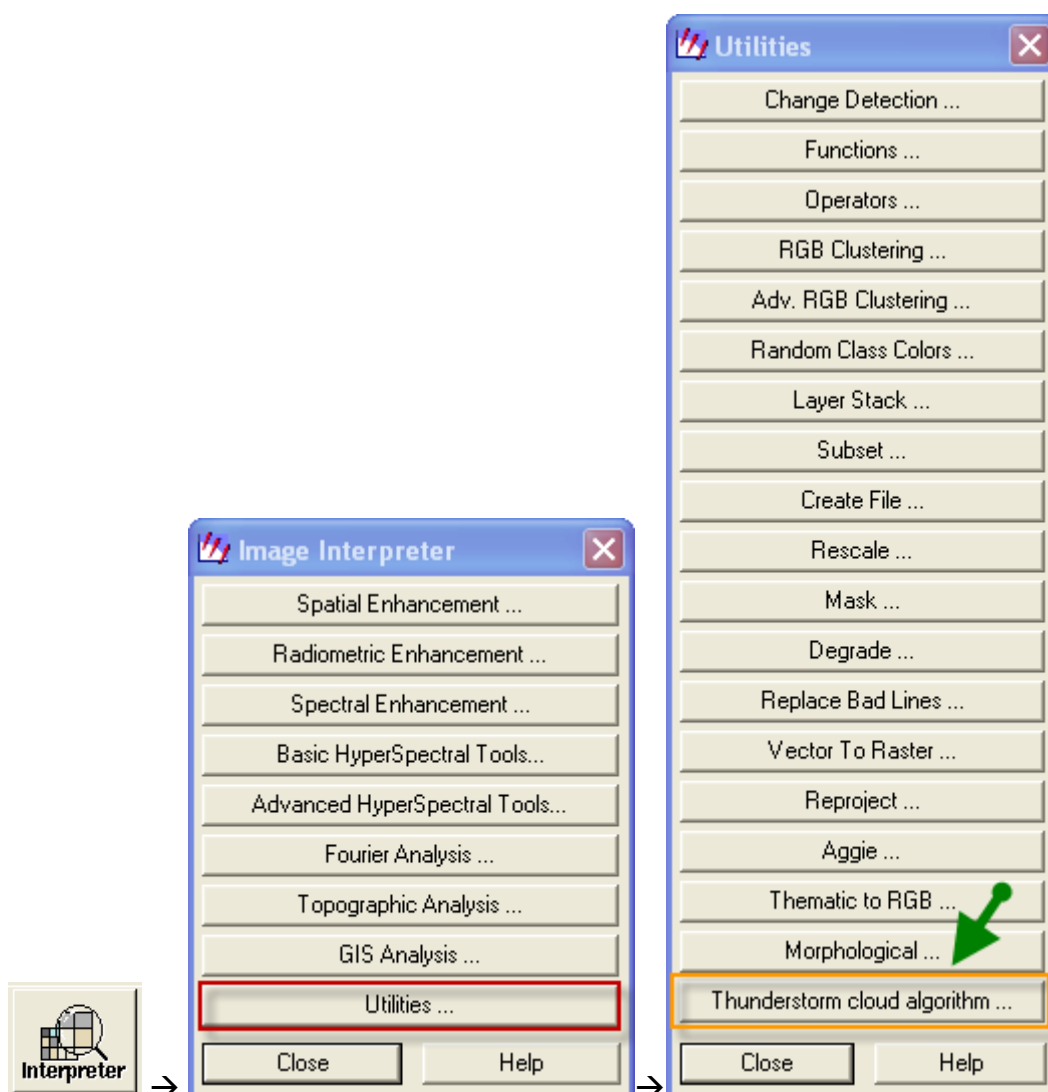


Figure A.2 Show the Interpreter main menu, the Utilities menu and the Thunderstorm cloud algorithm menu.

4. Then click at “Thunderstorm cloud algorithm” to access any MTSAT-1R cloud model, see as Figure A.3

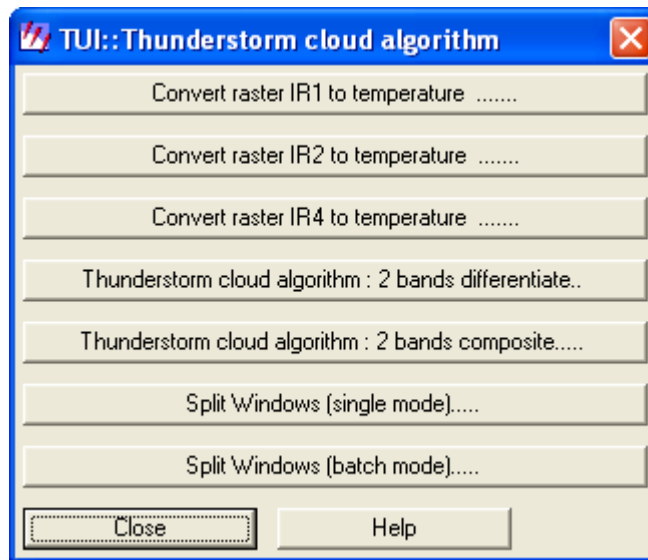


Figure A.3 Show the TUI:Thunderstorm cloud algorithm

Converting raster IR1 to Temperature step

1. Click at “Convert raster IR1 to Temperature” when you want to convert IR1 satellite image from grey scale to temperature (Kevin)

2. Click at  button when you want to select the raster image by directly into each directory. Input IR1 satellite image into “Input” box and typing output file name (.img) into “Output” box, as Figure A.4

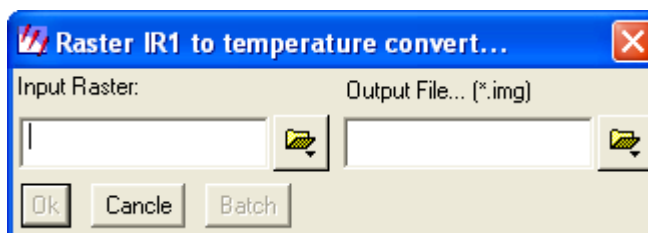


Figure A.4 Show raster IR1 to temperature converting window

Converting raster IR2 to Temperature step

1. Click at “Convert raster IR2 to Temperature” when you want to convert IR2 satellite image from grey scale to temperature (Kevin)

2. Click at  button when you want to select the raster image by directly into each directory. Input IR2 satellite image into “Input” box and type output file name (.img) into “Output” box, as Figure A.5

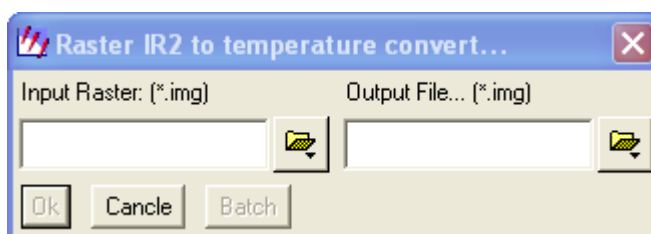


Figure A.5 Show raster IR2 to temperature converting window

Converting raster IR4 to Temperature step

1. Click at “Convert raster IR4 to Temperature” when you want to convert IR4 satellite image from grey scale to temperature (Kevin)

2. Click at  button when you want to select the raster image directly into each directory. Input IR4 satellite image into “Input” box and typing output file name (.img) into “Output” box, as Figure A.6



Figure A.6 Show raster IR4 to temperature converting window

Thunderstorm cloud 2 band composition step

1. Click at “Thunderstorm cloud 2 band composition” when you want to composite 2 raster satellite images (after converting to temperature).

2. Click at  button when you want to select the raster raster image directly into each directory. Input IR1 satellite image into “Input IR1” box, Input IR4 satellite image into “Input IR4” box and type output file name (.img) into “Output” box, as Figure A.7



Figure A.7 Show thunderstorm cloud 2 band composition window

3. Enter temperature no. (Kevin) at “Filter temperature” when you want to filter grid value. After doing raster composition, the result will get all grid values which there are value less than filter temperature number.

4. Leave filter temperature no. as default, if no need to filter

Thunderstorm cloud 2 band differentiate step

1. Click at “Thunderstorm cloud 2 band differentiate” when you want to get 2 different raster satellite images (after converting to temperature).

2. Click at  button when you want to select the raster image directly into each directory. Input IR1 satellite image into “Input IR1” box, Input IR4 satellite

image into “Input IR4” box and type output file name (.img) into “Output” box, as Figure A.8

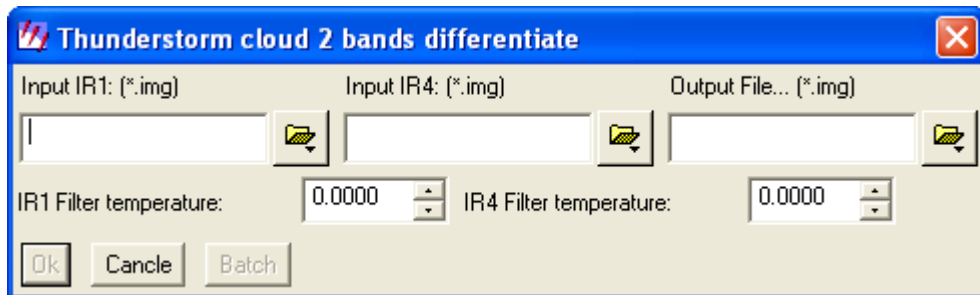


Figure A.8 Show thunderstorm cloud 2 band differentiate window

3. Enter temperature no. (Kevin) at “IR1 Filter temperature” when you want to filter IR1 grid value. The result will filter IR1 before doing differentiation (by getting all grid values that there is value less than IR1 filter temperature number)

4. Enter temperature no. (Kevin) at “IR4 Filter temperature” when you want to filter IR4 grid value. The result will filter IR4 before doing differentiation (by getting all grid values that there is value less than IR4 filter temperature number)

5. Leave filter temperature no. as default, if no need to filter

GMS, MTSAT satellite: Split windows (single mode) step

1. Click at “Split windows (single mode)” when you want to run split windows from 2 raster satellite images (after converting to temperature).

Notes: Split windows technique will get different of T_{IR1} (11 μm) and T_{IR2} (12 μm) and T_{IR1} for detecting cirrus cloud.

2. Click at  button when you want to select the raster image directly into each directory, see as Figure A.9 and detail as below.

- Input IR1 satellite image into “Input Raster 1” box

- Input IR2 satellite image into “Input Raster 2” box
- Type output file name (.img) into three output boxes.
 - Type no cirrus cloud output name at “Output nocirrus” box.
 - Type cirrus cloud output name at “Output cirrus” box
 - Type rain cloud output name at “Output warmcloud” box

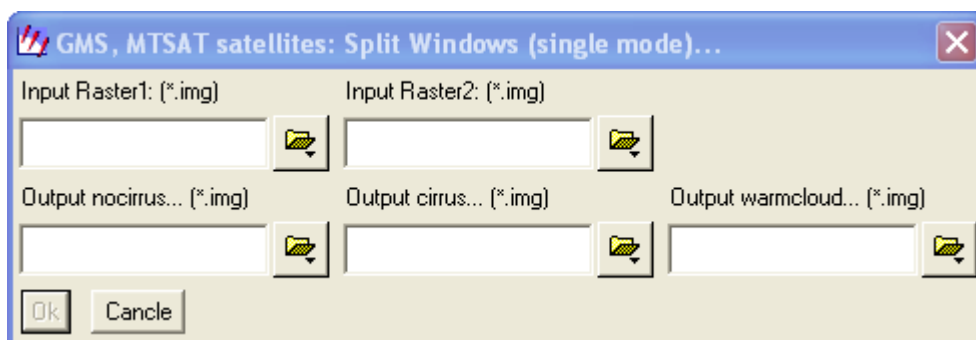


Figure A.9 Show GMS, MTSAT satellite: Split Windows (single mode) window

GMS, MTSAT satellite: Split windows (batch mode) step

1. Click at “Split windows (batch mode)” when you want to run split windows from 2 raster satellite images (after converting to temperature) in batch mode. The batch mode allows you to run several files in batch processing.

Notes: Split windows technique will get different T_{IR1} (11 μm), T_{IR2} (12 μm), and T_{IRI} for detecting cirrus cloud.

2. Click at  button when you want to select the raster image directly into each directory, see as Figure A.10 and detail as below.

- Input IR1 satellite image into “Input Raster 1” box
- Input IR2 satellite image into “Input Raster 2” box
- Type rain cloud output name at “Output warmcloud” box



Figure A.10 Show GMS, MTSAT satellite: Split Windows (batch mode) window

Sample of how to run ERDAS batch script

Step 1: Select input 2 raster files as needed and type the output name. See Figure A.11 as below.



Figure A.11 Show batch process step#1

Step 2: Select “Modified commands automatically” option, then click “Next”. See Figure A.12 as below.

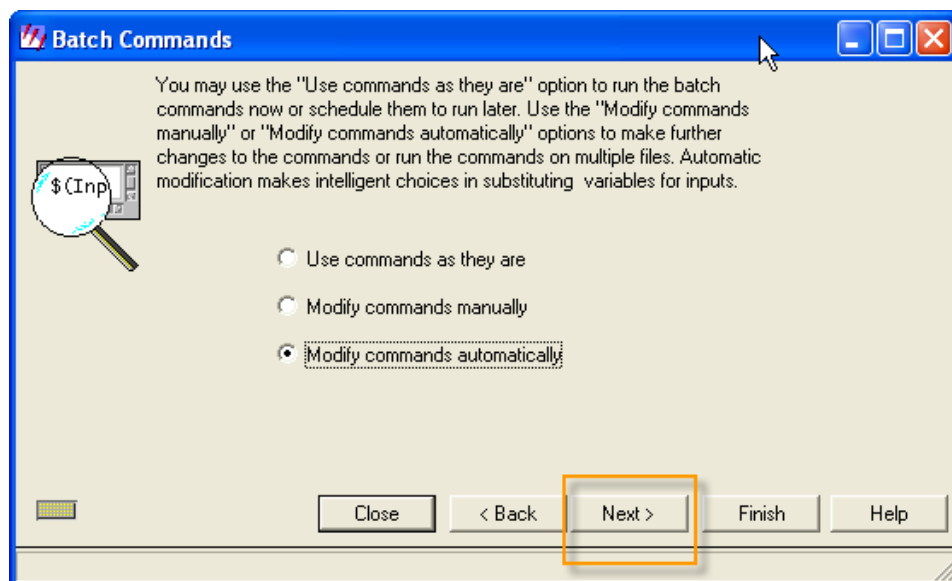


Figure A.12 Show batch process step#2

Step 3: At “Variables” tab, select temp1 variable, and then go to change type from “Auto” mode to “User” mode. Then click “Next” to go to next step. See Figure A.13 as below.

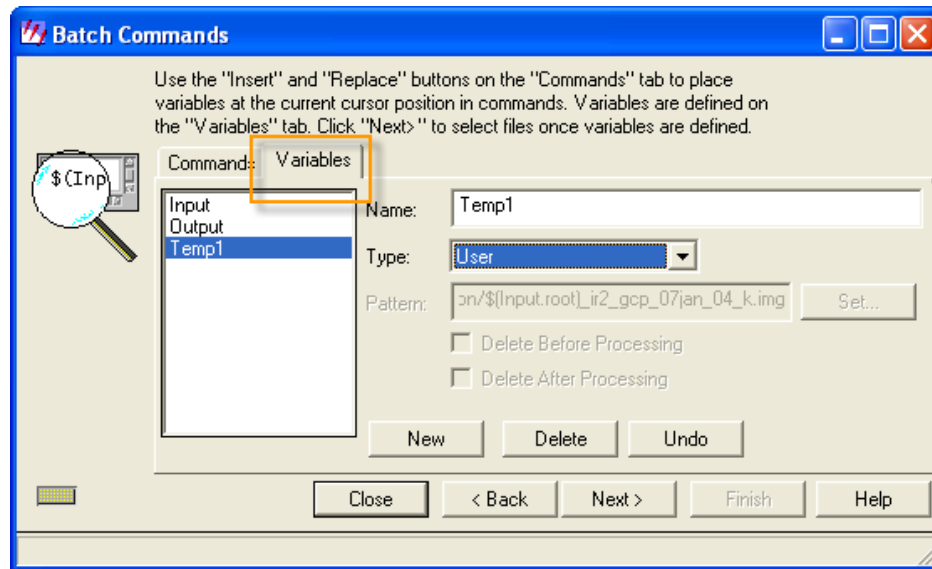


Figure A.13 Show batch process step#3

Step 4: At arrow “1” select each variable, and then click  to select multi-files. Do the same direction for “Input” variable and “Temp1” variable. See Figure A.14 as below.

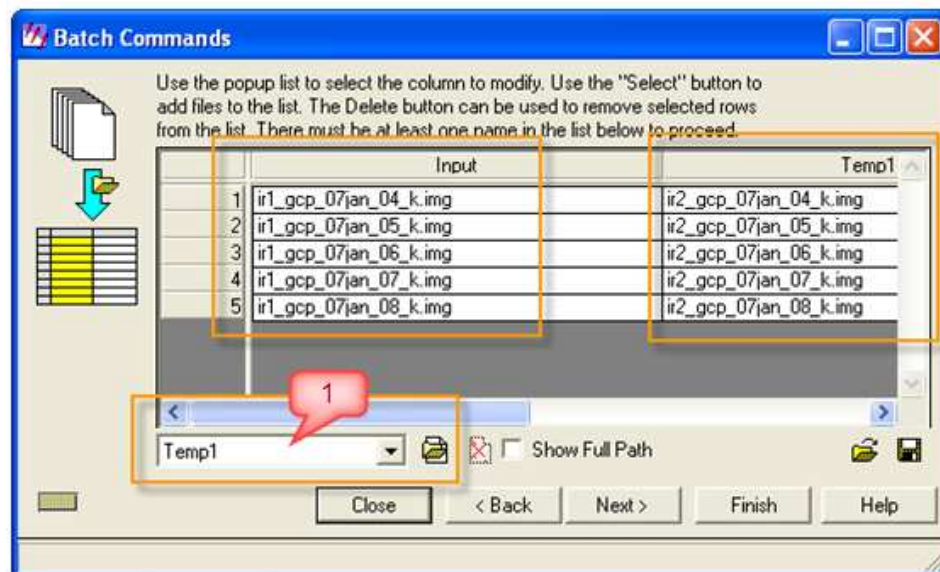


Figure A.14 Show batch process step#4

Step 5: Select “Starting Processing Now” if you want to start immediately. Select “Start Processing Later At.” when you need to set schedule. See Figure A.15 as below.

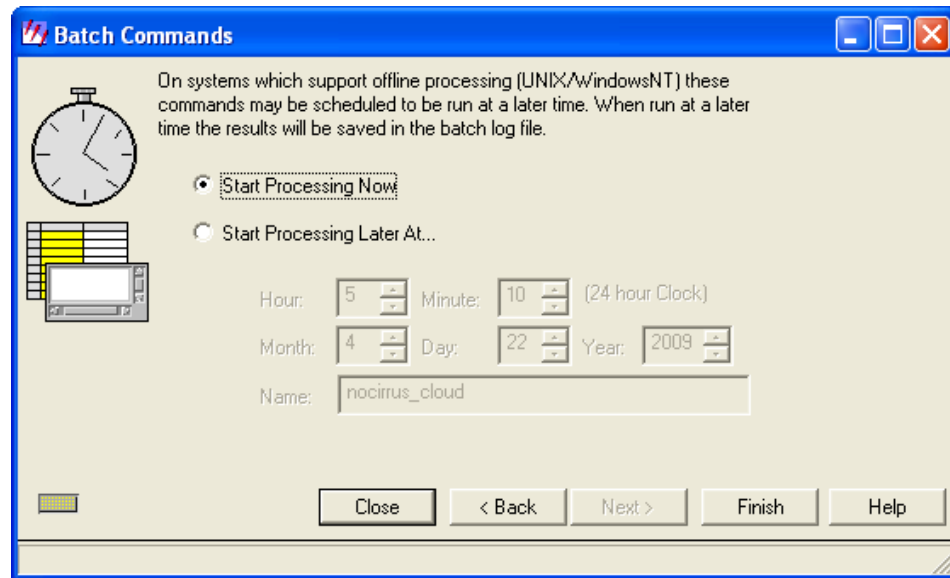


Figure A.15 Show batch process step#5

Step 6: All will be done and finished. Good luck when running.

APPENDIX B

SAMPLE OF MATLAB CROP PROGRAMMING

Filename: pgm_crop_workIR1.m

Coding: See box below (Box B.1).

```
%*****  
%***** Author : Ms. Pornthip Bumrungklang *****  
%***** Program name : pgm_crop_workIR1.m *****  
%***** Modify date : 8 April 2007 *****  
%***** Description : Use for cropping IR1 from MTSAT-1R satellite image by directory **  
%*****  
clear all;  
close all;  
clc;  
outputDir = './outputIR1c';  
%delete output folder  
[status,message,messageid] = rmdir(outputDir,'s');  
disp(message);  
%create output folder  
[status,message,messageid] = mkdir(outputDir);  
disp(message);  
%read pgm file from folder  
pgmDir = input('Input your pgm directory: ','s');  
calFile = input('Input your cal file: ','s');  
x=500;  
y=960;  
w=221;  
h=341;  
isFilter = 0;  
tempFilter = -40;  
if(strcmp(input('Do you want to filter [yes|no]: ','s'),'yes'))  
    isFilter = 1;  
    tempFilter = input('Input filter temperature : ');  
end  
%cal lon and lat  
startLon = (x/20)+70;  
startLat = abs((y/20)-70);  
endLon = ((x+w)/20)+70;  
endLat = abs(((y+h)/20)-70);  
%check cal file  
calFID = fopen(calFile, 'r');  
tline = fgetl(calFID);
```

Box B.1 Show the pgm_crop_workIR1.m code

```

ir1Temp = zeros(256,2);
ir2Temp = zeros(256,2);
ir3Temp = zeros(256,2);
ir4Temp = zeros(256,2);
j = 1;
while ischar(tline)
    line = textscan(tline, '%s','delimiter', ' ');
    keys = line{:};
    if strcmp(keys{2}, 'Temperature')
        len = length(keys);
        pix = str2double(strtrim(keys{len-2}));
        val = str2double(strtrim(keys{len}));
        if strcmp(keys{1}, 'IR1')
            ir1Temp(j,1) = pix;
            ir1Temp(j,2) = val;
        end
        if strcmp(keys{1}, 'IR2')
            ir2Temp(j,1) = pix;
            ir2Temp(j,2) = val;
        end
        if strcmp(keys{1}, 'IR3')
            ir3Temp(j,1) = pix;
            ir3Temp(j,2) = val;
        end
        if strcmp(keys{1}, 'IR4')
            ir4Temp(j,1) = pix;
            ir4Temp(j,2) = val;
        end
        j = j + 1;
    end
    tline = fgetl(calFID);
end
fclose(calFID);
pgmFiles = dir(fullfile(pgmDir, '*.pgm'));
for i=1:length(pgmFiles)
    pgmName = pgmFiles(i).name;
    disp(strcat('==> ',pgmName));

    ir = regexp(pgmName, 'IR[0-9]', 'match');
    ir = ir{1,1};
    pgmCrop = imcrop(imread(fullfile(pgmDir,pgmName)),[x y w h]);

    %save pgmCrop to file
    imwrite(pgmCrop,fullfile(outputDir,strep(pgmName, '.pgm', '_crop.pgm')));
    [cropH,cropW] = size(pgmCrop);
    xyGrey = zeros(cropW*cropH,3);
    latRef = zeros(cropH,cropW);
    lonRef = zeros(cropH,cropW);
    idx = 1;
    lat = startLat;
    for yP=1:cropH
        lon = startLon;
        for xP=1:cropW

```

Box B.1 (Continued)

```

latRef(yP,xP) = lat;
lonRef(yP,xP) = lon;

xyGrey(idx,1) = lat;
xyGrey(idx,2) = lon;
xyGrey(idx,3) = pgmCrop(yP,xP);
idx = idx + 1;
lon = lon + 0.05;
end
        lat = lat - 0.05;
end

%pgmDouble = im2double(pgmCrop);
pgmDouble = double(pgmCrop);

%replace temperature
if strcmp(ir,'IR1')
    pixTemp = ir1Temp;
end
if strcmp(ir,'IR2')
    pixTemp = ir2Temp;
end
if strcmp(ir,'IR3')
    pixTemp = ir3Temp;
end
if strcmp(ir,'IR4')
    pixTemp = ir4Temp;
end
for xP=1:cropW
    for yP=1:cropH
        val = pgmDouble(yP,xP);
        for k=1:length(pixTemp)
            if val == pixTemp(k,1)
                %disp(pgmDouble(yP,xP));
                %disp(pixTemp(k,2));
                %disp(pixTemp(k,2)-273);
                c = pixTemp(k,2) - 273;
                if(isFilter && c > tempFilter)
                    c = 0;
                end
                pgmDouble(yP,xP) = c;
                %disp(pgmDouble(yP,xP));
            end
        end
    end
end
    %save pgmDouble to file
    [doubleH,doubleW] = size(pgmDouble);
end
clear all;
close all;
disp('Done');

```

Box B.1 (Continued)

Filename: pgm_crop_workIR2.m

Coding: See box below (Box B.2).

```

%*****
%***** Author : Ms. Pornthip Bumrungklang *****
%***** Program name : pgm_crop_workIR2.m *****
%***** Modify date : 8 April 2007 *****
%***** Description : Use for cropping IR2 from MTSAT-1R satellite image by directory **
%*****
clear all;
close all;
clc;

outputDir = './outputIR2c';
%delete output folder
[status,message,messageid] = rmdir(outputDir,'s');
disp(message);

%create output folder
[status,message,messageid] = mkdir(outputDir);
disp(message);

%read pgm file from folder
pgmDir = input('Input your pgm directory: ','s');
calFile = input('Input your cal file: ','s');
x=500;
y=960;
w=221;
h=341;

isFilter = 0;
tempFilter = -40;
if(strcmp(input('Do you want to filter [yes|no]: ','s'),'yes'))
    isFilter = 1;
    tempFilter = input('Input filter temperature : ');
end
%cal lon and lat
startLon = (x/20)+70;
startLat = abs((y/20)-70);
endLon = ((x+w)/20)+70;
endLat = abs(((y+h)/20)-70);
%check cal file
calFID = fopen(calFile, 'r');
tline = fgetl(calFID);
ir1Temp = zeros(256,2);
ir2Temp = zeros(256,2);
ir3Temp = zeros(256,2);
ir4Temp = zeros(256,2);
j = 1;
while ischar(tline)

```

Box B.2 Show the pgm_crop_workIR2.m code

```

line = textscan(tline, '%s','delimiter', ' ');
keys = line{:};
if strcmp(keys{2}, 'Temperature')
    len = length(keys);
    pix = str2double(strtrim(keys{len-2}));
    val = str2double(strtrim(keys{len}));
    if strcmp(keys{1}, 'IR1')
        ir1Temp(j,1) = pix;
        ir1Temp(j,2) = val;
    end
    if strcmp(keys{1}, 'IR2')
        ir2Temp(j,1) = pix;
        ir2Temp(j,2) = val;
    end
    if strcmp(keys{1}, 'IR3')
        ir3Temp(j,1) = pix;
        ir3Temp(j,2) = val;
    end
    if strcmp(keys{1}, 'IR4')
        ir4Temp(j,1) = pix;
        ir4Temp(j,2) = val;
    end
    j = j + 1;
end
tline = fgetl(calFID);
fclose(calFID);

pgmFiles = dir(fullfile(pgmDir, '*.pgm'));
for i=1:length(pgmFiles)
    pgmName = pgmFiles(i).name;
    disp(strcat('==> ',pgmName));

    ir = regexp(pgmName, 'IR[0-9]', 'match');
    ir = ir{1,1};

    pgmCrop = imcrop(imread(fullfile(pgmDir,pgmName)),[x y w h]);

    %save pgmCrop to file
    imwrite(pgmCrop,fullfile(outputDir,strep(pgmName, '.pgm', '_crop.pgm')));
    [cropH,cropW] = size(pgmCrop);
    xyGrey = zeros(cropW*cropH,3);
    latRef = zeros(cropH,cropW);
    lonRef = zeros(cropH,cropW);
    idx = 1;
    lat = startLat;
#for loop

    for yP=1:cropH
        lon = startLon;
        for xP=1:cropW
            latRef(yP,xP) = lat;
            lonRef(yP,xP) = lon;
        end
    end
end

```

Box B.2 (Continued)

```

xyGrey(idx,1) = lat;
xyGrey(idx,2) = lon;
xyGrey(idx,3) = pgmCrop(yP,xP);
idx = idx + 1;
lon = lon + 0.05;
end
        lat = lat - 0.05;
end

%pgmDouble = im2double(pgmCrop);
pgmDouble = double(pgmCrop);

%replace temperature
if strcmp(ir,'IR1')
    pixTemp = ir1Temp;
end
if strcmp(ir,'IR2')
    pixTemp = ir2Temp;
end
if strcmp(ir,'IR3')
    pixTemp = ir3Temp;
end
if strcmp(ir,'IR4')
    pixTemp = ir4Temp;
end
for xP=1:cropW
    for yP=1:cropH
        val = pgmDouble(yP,xP);
        for k=1:length(pixTemp)
            if val == pixTemp(k,1)
                %disp(pgmDouble(yP,xP));
                %disp(pixTemp(k,2));
                %disp(pixTemp(k,2)-273);
                c = pixTemp(k,2) - 273;
                if(isFilter && c > tempFilter)
                    c = 0;
                end
                pgmDouble(yP,xP) = c;
                %disp(pgmDouble(yP,xP));
            end
        end
    end
end

%save pgmDouble to file
[doubleH,doubleW] = size(pgmDouble);

end
clear all;
close all;
disp('Done');

```

Box B.2 (Continued)

APPENDIX C

DATA PREPARATION AND MANIPULATION

Table C.1 Rainfall re-formatting data in year 2006

St_code	X	Y	ST_NAME_E	JAN	FEB	MAR	APR	MAY	JUN	JUL	AUG	SEP	OCT	NOV	DEC	SUM
583201	101.816667	6.416667	NaraThiwas	210.20	54.50	158.70	49.10	245.90	163.00	110.70	59.50	159.50	241.50	247.10	190.40	1,890.10
581301	101.283333	6.516667	Yaal Agro	89.80	236.70	149.40	218.80	147.80	76.00	157.00	168.70	239.70	245.50	154.60	265.20	2,149.20
580201	101.150000	6.783333	Pattani	114.90	108.40	88.30	45.90	140.20	153.30	113.30	111.60	231.90	199.20	130.10	141.90	1,579.00
570201	100.083333	6.650000	Satun	9.70	174.60	244.70	220.80	144.70	188.90	208.80	69.70	256.50	331.50	191.10	38.40	2,079.40
568502	100.433333	6.916667	Hatyai	29.70	96.90	164.70	164.20	170.10	48.60	75.30	49.10	278.60	108.20	70.40	157.40	1,413.20
568501	100.604722	7.203889	Songkla	69.50	119.30	106.70	126.60	143.30	197.70	41.70	36.50	91.40	171.00	303.80	189.10	1,596.60
568401	100.394167	6.795556	Sadao	24.40	174.80	113.40	224.40	138.30	87.60	57.10	43.00	178.90	85.20	79.70	77.00	1,283.80
568301	100.500000	7.016667	Kho Hong Agro	53.20	145.80	147.80	192.60	165.50	71.60	53.40	87.40	301.40	146.90	155.50	261.70	1,782.80
567201	99.616667	7.516667	Trang	44.80	20.70	65.20	177.30	365.30	279.40	341.80	303.50	185.70	100.80	78.20	30.10	1,992.80
566201	99.050000	7.533333	Ko Lanta	26.50	18.80	117.80	71.00	333.30	445.60	335.40	365.70	282.90	169.70	95.00	38.70	2,300.40
564202	98.3167	8.1167	Phuket Airport*	15.90	3.00	128.30	90.80	286.60	381.90	186.70	252.40	448.40	329.50	140.40	88.00	2,351.90
564201	98.400000	7.883333	Phuket	20.50	9.10	185.80	93.40	242.00	297.00	213.70	168.80	353.80	354.60	82.60	132.30	2,153.60
560301	100.166667	7.583333	Pattalung Agro	140.70	97.30	140.40	191.80	455.50	118.40	409.80	664.80	593.60	547.00	70.60	37.80	3,467.70
552401	99.511944	8.431944	Chawang	80.80	139.20	31.10	164.20	133.50	317.70	18.10	44.60	157.50	268.60	313.40	244.20	1,912.90
552301	100.083333	8.333333	Nakhon Sithamarat Agro	151.80	218.90	42.50	156.10	215.20	310.70	211.70	245.70	297.90	141.80	82.30	30.60	2,105.20
552201	99.966667	8.416667	Nakhon Sithamarat	194.30	319.50	48.20	95.20	186.50	277.60	33.10	64.60	185.10	365.50	284.10	155.50	2,209.20
551401	99.255000	8.565833	Prasaeng	78.00	48.70	128.70	116.10	177.30	262.20	38.90	211.00	224.30	340.30	417.80	422.50	2,465.80
551301	99.663056	9.138889	Surat Thani Agro	91.50	90.60	77.40	126.50	216.80	187.70	197.20	231.30	226.90	260.90	120.60	80.60	1,908.00
551203	100.050000	9.466667	Ko Samui	67.80	219.60	38.70	131.50	268.40	43.40	89.90	188.30	216.60	255.10	215.10	82.10	1,816.50

Table C.1 (Continued)

St_code	X	Y	ST_NAME_E	JAN	FEB	MAR	APR	MAY	JUN	JUL	AUG	SEP	OCT	NOV	DEC	SUM
551203	100.050000	9.466667	Ko Samui	67.80	219.60	38.70	131.50	268.40	43.40	89.90	188.30	216.60	255.10	215.10	82.10	1,816.50
551202	99.151944	9.135556	Surat Thani	58.70	107.90	52.50	109.90	152.50	137.40	120.70	87.60	195.50	66.60	353.30	166.40	1,609.00
532201	98.616667	9.983333	Ranong	16.30	29.60	39.90	148.30	141.00	429.90	78.80	111.30	165.20	165.80	79.60	21.20	1,426.90
517301	99.100000	10.333333	Sawi Agro	27.60	188.50	42.90	70.10	654.00	92.40	763.20	999.30	685.10	720.60	39.50	53.20	4,336.40
517201	99.183333	10.483333	Chumporn	18.60	121.60	51.60	111.80	243.90	176.10	340.00	357.50	175.90	212.00	103.40	257.10	2,169.50
501201	102.881500	11.778306	Khlong Yai	45.40	206.20	129.80	277.50	198.50	633.80	313.30	366.00	206.00	271.90	62.40	185.80	2,896.60
500301	99.733333	12.583333	Nong Phlap	4.90	1.00	135.80	70.90	460.20	171.50	2,061.90	1,163.40	739.80	693.50	51.70	0.00	5,554.60
500202	99.960000	12.586111	Hua Hin	22.90	1.30	247.00	128.90	171.40	129.80	137.40	53.00	633.30	84.00	2.90	9.90	1,621.80
500201	99.833333	11.833333	Prachap Khirikhan	0.00	10.70	91.30	66.40	72.50	93.50	95.60	106.10	115.30	75.00	0.10	35.00	761.50
480301	102.173167	12.508639	Phlew Agro	2.00	124.50	24.90	143.00	187.30	734.60	230.10	214.80	192.30	98.10	12.80	36.50	2,000.90
480201	102.107444	12.608139	Chantaburi	0.00	59.40	60.10	101.70	583.40	509.00	705.90	414.60	559.10	501.10	40.30	0.00	3,534.60
478301	101.133333	12.733333	Huai Pong Agro	0.10	71.50	71.50	58.40	466.20	171.80	585.10	626.30	581.00	829.70	90.70	1.30	3,553.60
478201	101.345833	12.634722	Rayong	12.00	142.90	78.60	132.10	283.80	102.50	120.50	65.00	256.70	92.90	61.20	16.30	1,364.50
465201	100.066667	13.150000	Petchaburi	0.00	9.60	17.20	82.40	265.50	218.30	115.30	116.90	268.70	172.30	2.30	11.80	1,280.30
459205	100.875833	13.076944	Laem Chabong	0.00	8.80	38.90	32.60	98.00	185.30	85.50	64.50	148.30	197.70	2.40	20.80	882.80
459204	100.983333	12.683333	Sattahip	0.00	36.10	24.90	102.40	201.90	209.00	119.90	102.80	345.70	137.80	38.60	0.20	1,319.30
459203	100.869444	12.920000	Pattaya	0.00	45.40	101.00	17.90	242.60	155.40	90.70	104.60	217.50	83.00	9.00	17.90	1,085.00
459202	100.806139	13.161083	Ko Sichang	0.00	3.40	53.20	12.00	174.40	189.20	54.90	137.30	374.90	122.30	74.40	0.60	1,196.60
459201	100.985667	13.353917	Chonburi	0.00	81.50	34.40	126.60	155.80	87.30	76.70	121.40	291.30	96.90	31.10	0.00	1,103.00
455601	100.605000	13.919167	Don Muang	5.80	9.30	103.00	141.40	205.60	203.70	106.30	136.50	217.20	301.60	20.90	0.40	1,451.70
455301	100.616670	13.666670	Bang Na Agro	0.70	17.10	47.00	55.60	310.10	223.50	120.60	59.60	228.60	190.30	60.20	4.80	1,318.10
455203	100.568056	13.706944	Bangkok Port	2.50	38.70	90.20	41.80	137.10	293.90	168.50	154.60	451.80	144.40	14.90	0.40	1,538.80
455201	100.560000	13.726389	Bangkok	0.90	38.90	74.50	37.50	239.70	278.10	150.60	96.90	294.30	306.60	26.40	0.90	1,545.30
451301	99.966667	14.016667	Kampaeng Saen	2.60	17.80	22.60	38.60	250.10	162.50	149.70	71.10	317.30	336.80	42.90	7.20	1,419.20
450201	99.533333	14.016667	Kanchana Buri	1.40	50.70	54.20	108.40	399.10	36.30	491.60	472.40	235.00	138.00	44.20	3.10	2,034.40
440401	102.035972	13.790389	Sakaew	0.00	37.70	125.40	26.30	169.60	197.20	83.50	29.20	318.50	174.60	16.30	0.20	1,178.50
440201	102.507639	13.687333	Aranyaprathet	2.00	31.90	86.00	114.20	185.70	133.70	240.70	275.80	361.30	166.80	33.90	0.40	1,632.40
436401	102.717866	14.633033	Nang Rong	0.00	22.90	93.50	42.80	105.20	42.20	361.30	250.90	287.00	87.80	3.40	6.10	1,303.10
432401	103.679167	15.319444	Tha Tum	0.00	0.00	42.00	203.90	274.20	193.20	190.40	164.50	170.30	150.50	13.30	0.00	1,402.30

Table C.1 (Continued)

St_code	X	Y	ST_NAME_E	JAN	FEB	MAR	APR	MAY	JUN	JUL	AUG	SEP	OCT	NOV	DEC	SUM
432301	103.449175	14.892429	Surin Agro	0.00	0.50	71.40	85.50	101.00	224.80	258.60	271.70	110.80	245.00	9.30	0.00	1,378.60
432201	103.495894	14.875478	Surin	0.00	0.10	91.50	105.10	179.80	225.60	276.50	432.00	97.90	158.90	14.50	0.00	1,581.90
431401	102.164842	14.739511	Chok Chai	0.00	34.70	41.20	101.10	169.70	130.20	290.00	346.60	145.40	163.90	7.60	0.30	1,430.70
431301	101.318144	14.643880	Pak Chong	0.70	22.50	50.50	121.70	127.10	248.10	104.80	73.20	160.80	271.50	10.20	0.00	1,191.10
431201	102.076667	14.962778	Nakhon Ratchasima	0.00	4.30	42.00	145.60	206.80	60.60	145.40	115.80	140.40	147.80	7.50	1.40	1,017.60
430401	101.707972	13.984500	Kabin buri	0.00	0.00	95.00	120.50	109.90	98.20	66.40	61.40	241.30	255.40	3.50	5.80	1,057.40
430201	101.372889	14.049361	Prachin Buri	0.00	9.30	85.90	100.80	266.60	102.00	470.50	159.00	337.80	235.20	12.40	0.00	1,779.50
429201	100.599444	13.377222	Bangkok Pilot	1.90	19.30	67.20	41.70	182.00	118.30	311.80	158.20	334.00	204.90	0.20	2.30	1,441.80
426401	101.190861	15.264944	Bau Chum	0.00	11.40	144.70	23.90	128.80	247.20	55.20	146.80	203.00	141.20	14.40	0.00	1,116.60
426201	100.616667	14.800000	Lopburi	0.00	8.80	68.50	154.60	166.50	179.30	111.10	169.10	156.80	189.20	28.40	0.00	1,232.30
425301	99.866667	14.300000	U Thong Agro	0.00	25.10	94.50	15.40	184.40	113.00	86.80	93.20	334.80	116.50	0.00	18.00	1,081.70
425201	100.133333	14.466667	Suphanburi	0.00	31.70	17.80	78.50	131.80	78.10	60.70	60.20	198.40	163.90	16.80	1.50	839.40
424301	99.797500	13.487222	Ratchaburi Agro	0.00	17.90	13.20	61.60	122.50	181.70	42.20	78.10	335.50	151.90	2.50	9.40	1,016.50
423301	101.457833	13.565806	Chacoeng Sao Agro	0.00	30.50	101.20	85.70	202.60	137.90	82.90	24.30	150.90	214.70	0.00	0.00	1,030.70
419301	100.633333	14.116667	Prathumtani Agro	1.30	2.60	134.80	49.60	220.50	219.60	193.60	195.20	404.00	164.10	9.00	22.10	1,616.40
415301	100.727778	14.533333	Ayutthaya Agro	0.00	4.20	84.60	53.90	153.10	184.60	171.80	117.40	377.60	167.50	14.50	0.00	1,329.20
409301	104.284313	15.108578	Sri Saket Agro	0.00	4.60	41.70	91.20	144.10	72.10	216.40	72.80	309.00	219.60	15.10	0.00	1,186.60
407501	104.871347	15.245708	Ubon Ratcha Thani	0.00	6.80	1.70	187.10	204.70	157.80	227.40	457.30	161.90	338.10	4.30	0.00	1,747.10
407301	105.019593	15.240489	Ubon Agro	0.00	14.00	2.10	87.00	85.00	215.90	325.50	344.80	198.40	177.20	42.40	0.90	1,493.20
405301	103.616667	16.066667	Roi Et Agro	0.00	22.60	87.20	58.90	87.10	115.70	397.50	486.40	235.10	228.90	35.60	0.10	1,755.10
405201	103.683333	16.050000	Roi Et	0.00	23.00	56.40	70.40	189.40	194.70	318.40	282.10	216.00	211.20	56.20	0.00	1,617.80
403201	102.024263	15.807336	Chaiyaphum	0.00	9.60	57.10	44.00	178.50	66.00	333.40	214.20	105.60	295.20	11.80	0.00	1,315.40
402301	100.183333	15.150000	Chai Nat Agro	0.00	3.70	13.10	73.20	80.00	144.50	73.60	185.00	284.20	151.00	0.90	0.00	1,009.20
400301	100.530514	15.349714	Tak Pha Agro	0.00	3.10	38.40	67.70	49.60	275.70	138.90	104.00	462.30	178.70	0.00	0.00	1,318.40
400201	100.135500	15.669972	Nakhon Sawan	0.00	65.90	5.80	112.20	164.50	214.90	179.30	195.40	272.90	176.30	3.10	0.00	1,390.30
388401	103.588333	16.332500	Kamalasai	0.00	15.40	102.70	106.70	74.60	190.10	105.00	158.00	258.00	218.30	8.50	0.00	1,237.30
387401	103.068056	16.247222	Kosum Phisai	0.00	31.70	99.20	142.00	121.60	201.10	216.00	237.10	183.30	314.80	11.20	0.00	1,558.00
386301	100.285504	16.437768	Pichit	0.00	7.00	41.20	34.20	94.50	150.60	156.70	151.40	226.10	194.80	7.20	0.00	1,063.70
383201	104.725054	16.543050	Mukdahan	0.00	33.80	37.80	73.60	202.80	123.80	148.20	176.20	335.90	135.60	1.60	0.00	1,269.30

Table C.1 (Continued)

St_code	X	Y	ST_NAME_E	JAN	FEB	MAR	APR	MAY	JUN	JUL	AUG	SEP	OCT	NOV	DEC	SUM
381301	102.823212	16.337759	Taphra Agro	0.00	38.20	16.30	88.80	186.30	216.40	315.80	267.10	147.70	178.50	14.20	0.00	1,469.30
381201	102.785677	16.462551	Khon Kaen	0.00	34.10	7.00	81.10	163.30	209.00	305.60	238.60	214.10	133.30	0.80	0.00	1,386.90
380201	99.526938	16.486638	Kampaeng Phet	0.00	14.20	6.80	73.30	174.80	195.30	176.40	189.40	150.60	173.30	5.80	0.00	1,159.90
379402	101.108333	15.656944	Wichian Buri	0.00	23.70	153.30	94.20	273.30	162.20	135.70	180.30	264.50	108.90	5.30	0.00	1,401.40
379401	101.246667	16.773611	Lom Sak	0.00	26.40	69.00	72.50	143.40	119.90	249.50	240.30	178.90	238.90	0.70	0.00	1,339.50
379201	101.150000	16.433333	Phetchabun	0.00	21.90	43.20	176.10	159.00	219.80	156.70	195.20	350.90	183.50	32.60	0.00	1,538.90
378201	100.275881	16.796395	Phitsanulok	0.00	19.70	46.90	79.00	219.30	198.10	205.70	251.20	423.20	119.50	2.50	0.00	1,565.10
376401	98.865556	16.015833	Umphang	0.00	7.60	136.90	216.30	191.80	161.40	203.30	182.30	280.30	256.60	55.40	0.00	1,691.90
376301	98.933333	16.750000	Doi Musor Agro	0.00	6.30	21.50	136.70	322.50	207.20	309.40	288.10	316.10	70.80	13.90	0.00	1,692.50
376203	99.053056	17.233333	Phumibol Dam	0.00	2.40	1.40	128.00	278.70	276.10	357.20	242.00	285.10	176.30	10.70	0.00	1,757.90
376202	98.550833	16.659167	Mae Sot	0.00	0.10	30.30	64.70	355.60	213.90	46.80	162.20	437.90	240.70	0.00	0.00	1,552.20
376201	99.009833	16.877972	Tak	0.00	8.50	41.10	78.50	237.60	150.10	612.20	267.80	260.90	110.40	0.00	0.00	1,767.10
373301	99.866667	17.166667	Sri Samrong Agro	0.00	26.20	7.60	136.90	312.70	262.30	108.20	87.30	342.40	188.90	16.80	0.00	1,489.30
373201	99.800000	17.100000	Sukhothai	0.00	14.30	9.90	96.70	304.00	286.20	226.30	204.70	274.80	160.80	0.00	0.00	1,577.70
357301	104.769772	17.277857	NKP-Agro	0.00	58.60	147.10	89.90	274.80	202.20	246.10	211.00	379.60	251.30	1.20	0.00	1,861.80
357201	104.778596	17.412086	Nakpon Phanom	0.00	24.00	185.40	161.00	142.80	260.40	533.70	588.80	91.90	215.10	9.10	0.00	2,212.20
356301	104.050000	17.116667	Sakol Nakhon	0.00	5.10	64.50	125.60	143.40	265.10	846.20	714.20	52.80	244.00	53.30	0.00	2,514.20
356201	104.133246	17.156535	Sakol Nakhon	0.00	12.00	33.40	107.30	160.90	165.50	297.50	391.90	85.10	152.90	130.00	0.00	1,536.50
354201	102.805853	17.378622	Udon Thani	0.00	4.00	72.80	45.80	210.90	149.40	358.50	274.00	91.50	218.80	130.30	0.00	1,556.00
353301	101.729767	17.409350	Loei Agro	0.00	43.20	71.90	266.40	133.90	88.80	225.80	409.00	138.30	139.10	5.90	0.00	1,522.30
353201	101.730646	17.452893	Loei	0.00	16.10	56.90	182.80	170.30	71.30	82.50	176.10	221.10	311.50	1.30	0.00	1,289.90
352201	102.747349	17.865132	Nong Khai	0.00	5.00	76.40	263.60	163.30	123.50	70.50	171.90	141.90	275.60	0.10	0.00	1,291.80
351201	100.095658	17.624801	Uttaradit	0.00	22.10	19.30	109.40	125.80	313.30	309.10	195.40	103.40	172.90	0.00	0.00	1,370.70
331402	100.886111	19.408056	Thung Chang	0.00	10.50	80.10	120.50	538.20	72.30	294.10	387.70	341.40	215.50	0.00	0.00	2,060.30
331401	100.802500	19.110556	Tha Wang Pha	0.00	9.40	94.00	155.10	189.90	106.60	348.30	885.10	158.70	61.40	0.00	0.00	2,008.50
331301	100.750000	18.866667	Nan Agro	0.00	33.30	60.30	185.70	163.90	97.60	142.20	477.50	188.20	68.60	0.00	0.00	1,417.30
331201	100.777778	18.779722	Nan	0.00	21.70	15.60	182.40	235.20	46.90	167.00	431.20	45.00	57.60	0.00	0.40	1,203.00
330201	100.166667	18.166667	Phrae	0.00	0.60	19.90	118.70	278.70	110.20	107.40	343.20	132.00	66.30	0.00	0.00	1,177.00
329201	99.033333	18.566667	Lamphun	0.00	0.00	6.00	209.20	320.70	122.40	244.20	254.80	146.80	182.40	0.00	2.30	1,488.80

Table C.1 (Continued)

St_code	X	Y	ST_NAME_E	JAN	FEB	MAR	APR	MAY	JUN	JUL	AUG	SEP	OCT	NOV	DEC	SUM
328301	99.283333	18.316667	Lampang Agro	0.00	17.20	51.60	149.70	177.50	235.10	155.50	240.10	157.40	73.30	0.90	0.00	1,258.30
328201	99.506623	18.278337	Lampang	0.00	16.80	43.00	174.40	268.90	175.70	209.00	266.60	223.00	69.80	0.00	0.00	1,447.20
327501	98.972552	18.771273	Chiang Mai	0.00	0.00	18.00	206.70	313.60	180.40	179.80	293.40	170.50	100.60	0.00	0.00	1,463.00
327301	99.000000	18.916667	Mae Jo Agro	0.00	0.90	23.60	112.10	219.50	176.00	269.30	341.40	194.80	69.90	0.00	0.00	1,407.50
310201	99.920000	19.156111	Phayao	0.00	2.70	38.30	130.50	246.90	63.20		228.30	202.40	53.00	0.00	0.00	965.30
303301	99.782778	19.870833	Chaing Rai Agro	0.00	34.40	44.40	60.90	163.70	144.30		306.20	221.80	176.80	0.70	2.00	1,155.20
303201	99.881389	19.961389	Chaing Rai	0.00	17.90	27.30	129.90	187.20	218.00		535.90	323.00	127.10	0.00	7.90	1,574.20
300202	97.933333	18.166667	Mae Sariang	0.00	0.00	53.60	75.70	207.40	94.90		483.40	329.20	129.20	0.00	0.00	1,373.40
300201	97.833333	19.300000	Mae Hong Son	0.00	0.90	13.00	113.00	76.10	158.80		259.70	148.80	109.90	13.70		893.90

Table C.2 Rainfall re-formatting data in year 2007

St_code	X	Y	ST_NAME_E	JAN	FEB	MAR	APR	MAY	JUN	JUL	AUG	SEP	OCT	NOV	DEC	SUM
583201	101.816667	6.416667	NaraThiwas	130.50	55.10	142.90	109.80	112.80	67.30	138.00	183.20	173.80	351.80	200.70	268.10	1,934.00
581301	101.283333	6.516667	Yaal Agro	203.50	1.20	117.40	98.00	384.10	197.00	216.20	106.60	118.60	327.40	109.40	539.60	2,419.00
580201	101.150000	6.783333	Pattani	179.80	0.00	78.10	166.90	170.50	109.20	222.90	98.10	138.30	316.10	139.60	229.20	1,848.70
570201	100.083333	6.650000	Satun	82.40	39.30	108.10	191.20	84.00	200.60	303.90	321.20	146.10	294.90	237.00	148.40	2,157.10
568502	100.433333	6.916667	Hatyai	176.30	0.00	65.50	93.00	131.70	309.80	194.00	26.50	184.90	351.70	223.60	276.40	2,033.40
568501	100.604722	7.203889	Songkla	316.00	7.30	70.60	90.00	203.00	113.60	146.60	38.00	169.00	363.80	217.10	169.80	1,904.80
568401	100.394167	6.795556	Sadao	186.90	0.00	85.70	134.40	97.10	156.50	212.70	65.40	74.20	261.10	143.30	186.70	1,604.00
568301	100.500000	7.016667	Kho Hong Agro	217.00	9.10	91.80	67.40	257.10	249.20	225.80	52.90	68.70	351.60	251.20	263.40	2,105.20
567201	99.616667	7.516667	Trang	73.30	3.10	164.00	212.70	187.50	275.10	272.00	285.00	172.90	412.50	157.00	79.60	2,294.70
566201	99.050000	7.533333	Ko Lanta	28.70	4.40	26.30	155.30	166.70	265.60	266.50	215.50	325.70	375.20	175.60	68.80	2,074.30
564202	98.3167	8.1167	Phuket Airport*	28.40	4.80	34.60	193.90	359.10	391.40	205.70	548.80	284.80	317.00	141.10	43.30	2,552.90
564201	98.400000	7.883333	Phuket	27.80	0.10	97.40	379.20	328.00	142.30	273.80	444.30	533.90	374.50	250.40	28.70	2,880.40
561201	98.252222	8.684167	Takuapa	30.10	61.80	137.60	269.60	387.20	365.10	122.10	403.00	461.40	291.50	129.70	85.50	2,744.60
560301	99.511944	8.431944	Chawang	263.00	3.50	83.90	151.40	175.70	116.80	362.70	706.60	605.00	375.90	193.90	40.60	3,079.00

Table C.2 (Continued)

St_code	X	Y	ST_NAME_E	JAN	FEB	MAR	APR	MAY	JUN	JUL	AUG	SEP	OCT	NOV	DEC	SUM
552401	100.083333	8.333333	Nakhon Sithamarat Agro	25.80	24.70	129.50	111.40	287.10	160.50	83.60	60.00	798.20	328.30	312.50	288.90	2,610.50
552301	99.966667	8.416667	Nakhon Sithamarat	182.30	2.70	75.70	161.10	320.40	174.00	250.40	232.20	163.80	281.30	168.80	87.50	2,100.20
552201	99.255000	8.565833	Prasaeng	211.40	5.70	133.60	173.40	261.90	188.00	176.30	108.10	255.80	420.10	475.50	215.10	2,624.90
551401	99.663056	9.138889	Surat Thani Agro	51.80	31.10	107.00	47.70	137.80	135.10	126.80	104.20	92.60	315.90	619.50	297.90	2,067.40
551301	100.050000	9.466667	Ko Samui	109.30	0.00	40.20	109.40	335.20	183.10	197.70	117.60	196.90	187.60	105.30	49.40	1,631.70
551203	99.151944	9.135556	Surat Thani	89.50	7.00	75.60	141.80	330.20	149.50	144.60	40.00	240.70	447.40	373.60	56.60	2,096.50
551202	98.616667	9.983333	Ranong	41.30	0.00	37.80	69.60	185.10	108.60	75.10	20.00	201.80	725.60	520.60	141.60	2,127.10
532201	99.100000	10.333333	Sawi Agro	0.20	4.00	91.00	80.20	555.50	598.30	235.90	62.10	77.70	280.40	216.50	76.70	2,278.50
517301	99.183333	10.483333	Chumporn	16.50	0.00	75.60	134.60	244.60	120.40	698.30	697.30	525.60	665.30	117.10	5.50	3,300.80
517201	102.881500	11.778306	Khlong Yai	44.00	1.50	20.80	212.20	426.70	182.80	236.30	177.40	343.50	570.20	137.00	59.30	2,411.70
501201	99.733333	12.583333	Nong Phlap	65.30	150.90	42.50	253.30	462.10	411.10	366.80	127.60	150.00	602.80	160.90	32.80	2,826.10
500301	99.960000	12.586111	Hua Hin	15.80	0.00	3.30	74.00	400.70	124.30	1,067.60	759.00	613.90	674.20	97.70	0.10	3,830.60
500202	99.833333	11.833333	Prachap Khirikhan	0.60	0.00	19.60	170.80	375.70	84.00	140.80	109.30	380.40	128.40	119.70	1.70	1,531.00
500201	102.173167	12.508639	Phlew Agro	0.30	10.60	5.80	96.20	581.10	40.50	98.30	66.80	103.80	186.40	142.60	0.30	1,332.70
480301	102.107444	12.608139	Chantaburi	15.60	27.90	56.30	293.20	648.70	437.70	188.60	76.30	115.80	142.60	149.10	0.20	2,152.00
480201	101.133333	12.733333	Huai Pong Agro	19.10	26.40	161.90	272.10	578.40	548.20	853.30	460.30	291.20	279.10	7.30	0.00	3,497.30
478301	101.345833	12.634722	Rayong	9.50	2.90	7.20	139.10	334.90	176.90	851.90	299.80	424.50	144.10	13.10	0.00	2,403.90
478201	100.066667	13.150000	Petchaburi	9.40	0.00	1.60	85.90	416.30	227.80	209.50	75.00	428.10	91.70	61.60	0.00	1,606.90
465201	100.875833	13.076944	Laem Chabong	0.00	0.00	0.30	46.10	274.30	52.70	192.70	128.00	220.20	76.90	15.60	0.00	1,006.80
459205	100.983333	12.683333	Sattahip	3.80	10.20	66.00	98.60	181.10	124.50	164.50	119.00	129.10	195.30	63.90	0.00	1,156.00
459204	100.869444	12.920000	Pattaya	20.00	7.20	135.50	93.70	353.60	132.10	95.30	79.00	240.30	96.70	4.10	0.00	1,257.50
459203	100.806139	13.161083	Ko Sichang	4.20	5.60	69.20	64.10	224.50	93.40	105.20	55.10	159.30	148.20	74.10	0.00	1,002.90
459202	100.985667	13.353917	Chonburi	0.00	0.00	0.00	111.60	175.80	170.50	135.50	80.20	125.70	39.20	28.90	0.80	868.20
459201	100.605000	13.919167	Don Muang	2.80	0.30	14.80	234.10	238.60	216.10	122.10	92.50	156.20	49.50	8.30	0.00	1,135.30
455601	100.616670	13.666670	Bang Na Agro	0.40	1.50	45.80	159.00	294.90	258.90	220.70	51.90	309.10	81.10	4.90	0.00	1,428.20
455301	100.568056	13.706944	Bangkok Port	1.80	0.00	34.30	180.30	241.90	360.00	255.20	106.80	217.30	132.00	2.30	0.00	1,531.90
455203	100.560000	13.726389	Bangkok	19.00	0.10	9.60	150.30	255.30	206.10	333.50	144.30	202.90	301.40	35.00	0.00	1,657.50
455201	99.966667	14.016667	Kampaeng Saen	29.90	0.00	12.70	143.10	309.50	268.20	277.30	120.10	246.50	128.80	13.90	0.00	1,550.00
451301	98.6364	15.7422	Thong Pha Phum*	7.00	0.00	16.90	151.30	260.00	149.20	267.90	147.00	244.40	225.90	17.60	0.00	1,487.20

Table C.2 (Continued)

St_code	X	Y	ST_NAME_E	JAN	FEB	MAR	APR	MAY	JUN	JUL	AUG	SEP	OCT	NOV	DEC	SUM
450401	99.533333	14.016667	Kanchana Buri	0.00	0.40	54.80	116.30	292.10	241.70	146.20	183.10	206.50	164.60	14.40	0.00	1,420.10
450201	102.035972	13.790389	Sakaew	14.00	0.00	1.80	170.70	306.60	95.50	328.80	366.80	197.00	225.50	0.80	0.00	1,707.50
440401	102.507639	13.687333	Aranyaprathet	9.40	4.10	30.20	120.50	268.70	130.30	139.80	76.30	133.70	147.30	32.80	0.00	1,093.10
440201	102.717866	14.633033	Nang Rong	4.00	4.80	15.90	189.00	326.10	206.90	146.30	97.60	199.60	146.80	26.80	0.00	1,363.80
436401	103.679167	15.319444	Tha Tum	0.00	0.70	12.50	111.60	286.30	158.20	169.70	98.70	163.50	110.20	77.70	0.00	1,189.10
432401	103.449175	14.892429	Surin Agro	0.00	24.40	34.80	98.20	121.40	80.10	196.20	157.30	236.80	205.20	19.10	0.00	1,173.50
432301	103.495894	14.875478	Surin	0.20	4.40	12.80	109.90	410.80	78.50	215.00	267.80	253.70	182.90	1.50	0.00	1,537.50
432201	102.164842	14.739511	Chok Chai	0.00	21.10	38.30	100.00	313.60	94.10	163.40	312.00	224.10	209.00	2.70	0.00	1,478.30
431401	101.318144	14.643880	Pak Chong	0.00	11.60	100.30	144.60	232.50	87.30	209.60	275.80	262.50	221.50	1.10	0.00	1,546.80
431301	102.076667	14.962778	Nakhon Ratchasima	0.00	94.10	56.30	87.70	163.00	101.60	59.70	183.70	233.20	165.10	14.10	0.00	1,158.50
431201	101.707972	13.984500	Kabin buri	0.00	0.00	94.30	53.30	254.30	106.30	150.80	229.20	105.10	125.60	18.40	0.00	1,137.30
430401	101.372889	14.049361	Prachin Buri	0.00	14.30	29.50	129.10	260.40	115.80	132.20	157.00	149.20	231.20	1.30	0.00	1,220.00
430201	100.599444	13.377222	Bangkok Pilot	5.20	14.90	2.00	228.00	402.40	182.20	132.20	104.80	291.20	105.00	16.90	0.00	1,484.80
429201	101.190861	15.264944	Bau Chum	0.70	0.00	6.00	68.70	154.80	186.40	218.80	215.80	264.10	217.40	1.70	0.00	1,334.40
426401	100.616667	14.800000	Lopburi	0.00	0.00	18.00	85.60	252.60	63.30	75.60	126.00	274.10	60.80	2.30	0.00	958.30
426201	99.866667	14.300000	U Thong Agro	0.00	0.00	0.10	102.00	259.60	151.90	129.60	110.20	194.40	144.10	4.90	0.00	1,096.80
425301	100.133333	14.466667	Suphanburi	10.30	0.00	0.00	87.00	174.80	99.30	74.30	70.90	367.40	108.70	0.40	0.00	993.10
425201	99.797500	13.487222	Ratchaburi Agro	0.00	0.00	0.00	41.70	232.60	101.60	151.10	140.70	59.50	101.10	13.90	0.00	842.20
424301	101.457833	13.565806	Chacoeng Sao Agro	1.10	0.00	0.90	90.60	335.20	107.40	57.80	58.10	121.10	192.60	6.00	14.50	985.30
423301	100.633333	14.116667	Prathumtani Agro	0.40	23.50	155.00	248.30	259.90	115.20	133.00	218.30	83.40	117.60	77.60	0.00	1,432.20
419301	100.727778	14.533333	Ayutthaya Agro	0.40	0.00	0.10	224.10	239.60	168.10	195.70	58.30	221.50	76.80	22.80	0.00	1,207.40
415301	104.284313	15.108578	Sri Saket Agro	0.00	0.00	21.10	130.30	213.30	93.60	143.60	116.70	185.70	118.70	6.00	0.00	1,029.00
409301	104.871347	15.245708	Ubon Ratcha Thani	0.00	0.50	16.20	37.30	256.40	110.70	51.00	126.50	303.40	63.40	17.20	0.00	982.60
407501	105.019593	15.240489	Ubon Agro	0.00	2.70	85.40	20.00	319.10	152.10	153.60	296.60	224.20	278.60	1.20	0.00	1,533.50
407301	103.616667	16.066667	Roi Et Agro	0.50	0.20	41.80	33.50	485.80	195.40	388.60	498.10	314.80	231.50	12.60	0.00	2,202.80
405301	103.683333	16.050000	Roi Et	0.50	22.10	60.60	25.30	244.30	151.30	314.30	437.20	278.10	185.00	10.80	0.00	1,729.50
405201	102.024263	15.807336	Chaiyaphum	5.20	28.20	61.10	78.50	287.00	190.30	108.80	391.30	333.70	173.60	33.00	0.00	1,690.70
403201	100.183333	15.150000	Chai Nat Agro	0.00	16.60	52.30	50.70	107.70	192.70	145.50	318.30	173.70	193.00	7.20	0.00	1,257.70
402301	100.530514	15.349714	Tak Pha Agro	0.00	0.90	7.10	40.80	159.30	124.80	94.30	284.30	298.30	154.80	0.30	0.00	1,164.90

Table C.2 (Continued)

St_code	X	Y	ST_NAME_E	JAN	FEB	MAR	APR	MAY	JUN	JUL	AUG	SEP	OCT	NOV	DEC	SUM
400301	100.135500	15.669972	Nakhon Sawan	6.90	0.40	0.10	58.90	161.60	159.90	50.70	35.50	346.00	196.20	2.90	0.00	1,019.10
400201	103.588333	16.332500	Kamalasai	0.00	0.00	6.40	110.80	256.90	141.00	170.70	60.20	93.40	157.40	0.50	0.00	997.30
388401	103.068056	16.247222	Kosum Phisai	0.10	6.60	47.00	84.90	161.30	62.40	188.40	63.80	178.00	184.00	17.20	0.00	993.70
387401	100.285504	16.437768	Pichit	0.00	8.10	46.50	17.20	323.10	82.60	243.20	410.90	274.60	292.70	7.00	0.00	1,705.90
386301	104.725054	16.543050	Mukdahan	0.00	31.50	0.60	77.00	358.20	231.00	177.60	275.90	354.90	179.80	4.00	0.00	1,690.50
383201	102.823212	16.337759	Taphra Agro	0.00	6.90	43.10	10.70	160.20	190.40	141.20	296.70	242.30	91.10	25.30	0.00	1,207.90
381301	102.785677	16.462551	Khon Kaen	0.00	7.80	59.70	9.80	231.30	129.20	167.00	297.80	211.60	270.90	0.90	0.00	1,386.00
381201	99.526938	16.486638	Kampaeng Phet	0.00	59.10	9.60	22.80	228.10	120.60	85.40	225.50	212.60	193.40	14.10	0.00	1,171.20
380201	101.108333	15.656944	Wichian Buri	0.20	2.00	4.10	85.60	300.40	223.50	199.10	313.30	186.40	172.10	14.90	0.00	1,501.60
379402	101.246667	16.773611	Lom Sak	0.00	16.40	18.00	213.80	187.20	50.30	148.70	89.40	334.40	259.30	4.10	0.00	1,321.60
379401	101.150000	16.433333	Phetchabun	0.00	2.00	3.10	46.30	204.00	109.20	68.90	114.40	254.60	134.00	1.80	0.00	938.30
379201	100.275881	16.796395	Phitsanulok	0.00	38.10	20.00	109.40	233.10	89.40	40.10	225.70	296.80	287.20	0.90	0.00	1,340.70
378201	98.865556	16.015833	Umphang	0.00	23.80	38.70	118.90	343.00	117.70	69.00	212.10	248.10	213.90	1.10	0.00	1,386.30
376401	98.933333	16.750000	Doi Musor Agro	0.00	0.00	39.80	61.70	221.40	134.10	296.50	150.40	183.30	208.30	3.00	3.20	1,301.70
376301	99.053056	17.233333	Phumibol Dam	0.00	0.00	0.60	18.60	309.00	118.70	184.70	155.90	332.40	254.10	1.80	0.00	1,375.80
376203	98.550833	16.659167	Mae Sot	0.00	0.00	0.00	24.20	475.90	115.40	138.30	248.10	272.30	447.80	10.50	0.00	1,732.50
376202	99.009833	16.877972	Tak	0.00	0.00	15.80	0.70	352.60	185.60	21.30	83.60	302.60	210.00	23.90	0.00	1,196.10
376201	99.866667	17.166667	Sri Samrong Agro	0.00	0.00	0.00	22.30	422.00	115.90	264.70	315.10	204.00	219.60	0.00	0.00	1,563.60
373301	99.800000	17.100000	Sukhothai	0.00	14.60	27.50	99.50	364.00	129.50	29.10	58.90	249.80	290.90	0.50	0.00	1,264.30
373201	104.769772	17.277857	NKP Agro	0.00	0.10	22.80	119.10	322.50	205.50	75.80	193.20	207.10	60.30	1.80	0.00	1,208.20
357301	104.778596	17.412086	Nakpon Phanom	0.00	26.40	53.80	104.60	162.40	268.10	71.60	172.40	224.10	89.40	8.10	0.00	1,180.90
357201	104.050000	17.116667	Sakol Nakhon	0.00	20.70	69.40	186.10	216.40	424.60	227.20	448.40	138.20	274.40	3.20	4.80	2,013.40
356301	104.133246	17.156535	Sakol Nakhon	0.00	27.90	101.70	16.00	248.30	173.80	355.00	497.30	222.50	278.30	0.90	0.00	1,921.70
356201	102.805853	17.378622	Udon Thani	0.00	39.00	67.10	38.80	219.10	246.50	150.20	332.80	329.70	228.20	5.70	0.00	1,657.10
354201	101.729767	17.409350	Loei Agro	0.00	11.90	7.00	31.40	171.20	159.50	172.30	498.00	369.30	228.10	7.10	0.00	1,655.80
353301	101.730646	17.452893	Loei	0.00	40.10	10.10	125.80	188.90	249.80	74.00	223.70	351.50	285.40	3.20	0.00	1,552.50
353201	102.747349	17.865132	Nong Khai	0.00	13.60	6.90	138.60	152.20	236.00	130.20	244.90	207.30	228.30	1.30	0.00	1,359.30
352201	100.095658	17.624801	Uttaradit	0.00	2.00	16.20	46.40	237.90	232.00	89.10	190.80	299.20	159.70	0.00	0.00	1,273.30
351201	100.886111	19.408056	Thung Chang	0.00	0.00	1.00	25.00	363.90	244.80	164.10	305.40	209.40	155.00	3.70	0.00	1,472.30

Table C.2 (Continued)

St_code	X	Y	ST_NAME_E	JAN	FEB	MAR	APR	MAY	JUN	JUL	AUG	SEP	OCT	NOV	DEC	SUM
331402	100.802500	19.110556	Tha Wang Pha	0.00	0.00	9.50	153.10	175.00	157.00	82.30	136.60	249.50	87.70	1.80	0.00	1,052.50
331401	100.750000	18.866667	Nan Agro	0.00	0.00	18.20	96.90	214.00	160.10	218.90	277.10	214.50	227.50	4.80	0.00	1,432.00
331301	100.777778	18.779722	Nan	0.00	0.00	24.90	64.90	171.50	216.90	182.70	177.60	254.70	149.60	11.70	0.00	1,254.50
331201	100.166667	18.166667	Phrae	0.00	4.60	21.30	114.90	208.00	131.20	88.10	200.00	227.80	169.80	2.00	0.00	1,167.70
330201	99.033333	18.566667	Lamphun	0.10	10.00	14.70	78.90	240.50	122.00	163.80	196.10	138.60	118.30	0.40	0.00	1,083.40
329201	99.283333	18.316667	Lampang Agro	0.00	0.00	4.90	27.00	289.70	139.90	87.90	191.80	205.10	81.10	0.10	0.00	1,027.50
328301	99.506623	18.278337	Lampang	0.00	0.00	0.00	31.50	298.70	151.40	55.70	74.80	268.60	86.90	22.30	0.00	989.90
328201	98.972552	18.771273	Chiang Mai	0.00	1.30	5.40	85.20	332.70	80.40	137.10	137.60	147.50	63.40	12.50	0.00	1,003.10
327501	99.000000	18.916667	Mae Jo Agro	0.00	0.00	0.00	56.00	393.50	130.10	100.10	200.30	189.90	84.90	13.70	0.00	1,168.50
327301	99.920000	19.156111	Phayao	0.00	0.00	12.40	82.90	275.20	112.80	74.60	153.20	213.70	64.60	73.50	0.00	1,062.90
310201	99.782778	19.870833	Chaing Rai Agro	0.00	0.10	1.10	195.40	215.10	128.40	133.40	138.50	146.50	58.10	65.40	0.00	1,082.00
303301	99.881389	19.961389	Chaing Rai	0.00	0.80	46.80	131.50	246.40	189.30	135.10	166.00	136.40	138.70	22.10	0.00	1,213.10
303201	97.933333	18.166667	Mae Sariang	0.00	1.40	28.90	213.80	342.00	280.80	174.00	139.10	363.80	221.00	43.30	0.00	1,808.10
300202	97.933333	18.166667	Mae Sariang	0.00	0.00	0.00	31.90	275.10	186.40	201.00	308.50	419.30	194.90	51.10	0.00	1,668.20
300201	97.833333	19.300000	Mae Hong Son	0.00	0.00	1.00	49.00	236.10	280.40	217.30	196.20	216.10	114.90	49.60	0.00	1,360.60

Table C.3 TMD rain-stations

ST_CODE	LONGITUDE	LATITUDE	ST_NAME_ENG	TYPE_ST2	TYPE_ST1
300201	97.83333333	19.30000000	Mae Hong Son	Observmet	1
300202	97.93333333	18.16666667	Mae Sariang	Observmet	1
303201	99.88138889	19.96138889	Chaing Rai	Observmet	1
303301	99.78277778	19.87083333	Chaing Rai Agro	Agromet	2
310201	99.92000000	19.15611111	Phayao	Observmet	1
327301	99.00000000	18.91666667	Mae Jo Agro	Agromet	2
327501	98.97255242	18.77127349	Chiang Mai	Observmet	1
328201	99.50662315	18.27833712	Lampang	Observmet	1
328202	99.24471617	17.63632357	Thern	Observmet	1
328301	99.28333333	18.31666667	Lampang Agro	Agromet	2
329201	99.03333333	18.56666667	Lamphun	Observmet	1
330201	100.16666667	18.16666667	Phrae	Observmet	1
331201	100.77777778	18.77972222	Nan	Observmet	1
331301	100.75000000	18.86666667	Nan Agro	Agromet	2
331401	100.80250000	19.11055556	Tha Wang Pha	Hydromet	3
331402	100.88611111	19.40805556	Thung Chang	Hydromet	3
351201	100.09565771	17.62480080	Uttaradit	Observmet	1
352201	102.74734855	17.86513209	Nong Khai	Observmet	1
353201	101.73064649	17.45289266	Loei	Observmet	1
353301	101.72976673	17.40934968	Loei Agro	Agromet	2
354201	102.80585289	17.37862229	Udon Thani	Observmet	1
356201	104.13324594	17.15653539	Sakol Nakhon	Observmet	1
356301	104.05000000	17.11666667	Sakol Nakhon	Agromet	2
357201	104.77859616	17.41208553	Nakpon Phanom	Observmet	1
357301	104.76977170	17.27785707	Nakpon Phanom Agro	Agromet	2
373201	99.80000000	17.10000000	Sukhothai	Observmet	1
373301	99.86666667	17.16666667	Sri Samrong Agro	Agromet	2
376201	99.00983333	16.87797222	Tak	Observmet	1
376202	98.55083333	16.65916667	Mae Sot	Observmet	1
376203	99.05305556	17.23333333	Phumibol Dam	Observmet	1
376301	98.93333333	16.75000000	Doi Musor Agro	Agromet	2
376401	98.86555556	16.01583333	Umphang	Hydromet	3
378201	100.27588069	16.79639518	Phitsanulok	Observmet	1
379201	101.15000000	16.43333330	Phetchabun	Observmet	1
379401	101.24666667	16.77361111	Lom Sak	Hydromet	3
379402	101.10833333	15.65694444	Wichian Buri	Hydromet	3
380201	99.52693820	16.48663759	Kampaeng Phet	Observmet	1
381201	102.78567731	16.46255136	Khon Kaen	Observmet	1
381301	102.82321215	16.33775890	Taphra Agro	Agromet	2
383201	104.72505391	16.54304981	Mukdahan	Observmet	1
386301	100.28550446	16.43776774	Pichit	Agromet	2
387401	103.06805556	16.24722222	Kosum Phisai	Hydromet	3
388401	103.58833333	16.33250000	Kamalasai	Hydromet	3
400201	100.13550000	15.66997222	Nakhon Sawan	Observmet	1
400301	100.53051353	15.34971356	Tak Pha Agro	Agromet	2
402301	100.18333333	15.15000000	Chai Nat Agro	Agromet	2
403201	102.02426255	15.80733597	Chaiyaphum	Observmet	1
405201	103.68333333	16.05000000	Roi Et	Observmet	1
405301	103.61666667	16.06666667	Roi Et Agro	Agromet	2
407301	105.01959300	15.24048900	Ubon Ratcha Thani Agro	Agromet	2

Table C.3 (Continued)

ST_CODE	LONGITUDE	LATITUDE	ST_NAME_ENG	TYPE_ST2	TYPE_ST1
407501	104.87134695	15.24570823	Ubon Ratcha Thani	C_Met	5
409301	104.28431332	15.10857761	Sri Saket Agro	Agromet	2
415301	100.72777778	14.53333333	Ayutthaya Agro	Agromet	2
417201	101.38333333	14.21666667	Nakhonnayok	Observmet	1
419301	100.63333333	14.11666667	Prathumtani Agro	Agromet	2
423301	101.45783333	13.56580556	Chacoeng Sao Agro	Agromet	2
424301	99.79750000	13.48722222	Ratchaburi Agro	Agromet	2
425201	100.13333333	14.46666667	Suphanburi	Observmet	1
425301	99.86666667	14.30000000	U Thong Agro	Agromet	2
426201	100.61666667	14.80000000	Lopburi	Observmet	1
426401	101.19086111	15.26494444	Bau Chum	Hydromet	3
429201	100.59944444	13.37722222	Bangkok Pilot	Observmet	1
429601	100.76750000	13.68638889	Suwanphum		1
430201	101.37288889	14.04936111	Prachin Buri	Observmet	1
430401	101.70797222	13.98450000	Kabin buri	Hydromet	3
431201	102.07666667	14.96277778	Nakhon Ratchasima	Observmet	1
431301	101.31814420	14.64387953	Pak Chong	Agromet	2
431401	102.16484249	14.73951101	Chok Chai	Hydromet	3
432201	103.49589407	14.87547755	Surin	Observmet	1
432301	103.44917536	14.89242911	Surin Agro	Agromet	2
432401	103.67916667	15.31944444	Tha Tum	Hydromet	3
436201	103.23333333	15.23333333	Burirum	Observmet	1
436401	102.71786571	14.63303268	Nang Rong	Hydromet	3
440201	102.50763889	13.68733333	Aranyaprathet	Observmet	1
440401	102.03597222	13.79038889	Sakaew	Hydromet	3
450201	99.53333333	14.01666667	Kanchana Buri	Observmet	1
450202	98.63638889	14.74222222	Thongphaphum	Observmet	1
451301	99.96666667	14.01666667	Kampaeng Saen	Agromet	2
455201	100.56000000	13.72638889	Bangkok	Observmet	1
455301	100.61667000	13.66667000	Bang Na Agro	Agromet	2
455601	100.60500000	13.91916700	Don Muang	Observmet	1
459201	100.98566667	13.35391667	Chonburi	Observmet	1
459202	100.80613889	13.16108333	Ko Sichang	Observmet	1
459203	100.86944444	12.92000000	Pattaya	Observmet	1
459204	100.98333333	12.68333333	Sattahip	Observmet	1
465201	100.06666667	13.15000000	Petchaburi	Observmet	1
478201	101.34583333	12.63472222	Rayong	Observmet	1
478301	101.13333333	12.73333333	Huai Pong Agro	Agromet	2
480201	102.10744444	12.60813889	Chantaburi	Observmet	1
480301	102.17316667	12.50863889	Phlew Agro	Agromet	2
500201	99.83333333	11.83333333	Prachap Khirikhan	Observmet	1
500202	99.96000000	12.58611111	Hua Hin	Observmet	1
500301	99.73333333	12.58333333	Nong Phlap	Agromet	2
501201	102.88150000	11.77830556	Khlong Yai	Observmet	1
517201	99.18333333	10.48333333	Chumporn	Observmet	1
517301	99.10000000	10.33333333	Sawi Agro	Agromet	2
532201	98.61666667	9.98333333	Ranong	Observmet	1
551202	99.15194444	9.13555556	Surat Thani	Observmet	1
551203	100.05000000	9.46666667	Ko Samui	Observmet	1
551301	99.66305556	9.13888889	Surat Thani Agro	Agromet	2

Table C.3 (Continued)

ST_CODE	LONGITUDE	LATITUDE	ST_NAME_ENG	TYPE_ST2	TYPE_ST1
551401	99.25500000	8.56583333	Prasaeng	Hydromet	3
552201	99.96666667	8.41666667	Nakhon Sithamarat	Observmet	1
552301	100.08333333	8.33333333	Nakhon Sithamarat Agro	Agromet	2
552401	99.51194444	8.43194444	Chawang	Hydromet	3
560301	100.16666667	7.58333333	Pattalung Agro	Agromet	2
561201	98.25222222	8.68416667	Takuapa	Observmet	1
564201	98.40000000	7.88333333	Phuket	Observmet	1
564501	98.31444444	8.11666667	Phuket	C_Met	5
566201	99.05000000	7.53333333	Ko Lanta	Observmet	1
566202	98.90666667	8.06250000	Krabi	Observmet	1
567201	99.61666667	7.51666667	Trang	Observmet	1
568301	100.50000000	7.01666667	Kho Hong Agro	Agromet	2
568401	100.39416667	6.79555556	Sadao	Hydromet	3
568501	100.60472222	7.20388889	Songkla	C_Met	5
568502	100.43333333	6.91666667	Hatyai	Observmet	1
570201	100.08333333	6.65000000	Satun	Observmet	1
580201	101.15000000	6.78333333	Pattani	Observmet	1
581301	101.28333333	6.51666667	Yaal Agro	Agromet	2
583201	101.81666667	6.41666667	NaraThiwas	Observmet	1

CURRICULUM VITAE

Name: Pornthip Bumrungklang (Ms.)

Place of Birth: Nakhonratchasima, Thailand

Contact: *paragon09@hotmail.com; tui.pornthip@gmail.com*

Education Background:

- | | |
|-----------|---|
| 1989-1992 | B.Sc. Computer Science
The University of Thai Chamber of Commerce
Bangkok, Thailand |
| 1995-1999 | M.Sc. Remote Sensing
Suranaree University of Technology
Nakhonratchasima, Thailand |
| 2003-2008 | Ph.D. Geoinformatics
Suranaree University of Technology
Nakhonratchasima, Thailand |

Conference:

1. การประชุมวิชาการ – การแผนที่และภูมิสารสนเทศแห่งชาติ ประจำปี 2549 กรุงเทพฯ:
SATELLITE CLOUD CLASSIFICATION TECHNIQUE BY USING MTSAT-1R
IMAGERY
2. 2nd SUT GRADUATE CONFERENCE 2009: AN ANALYSIS OF
SEASONAL THUNDERSTORM CLOUD DISTRIBUTION AND ITS RELATION
TO OCCURANCE RAINFALL IN THAILAND USING REMOTELY-SENSED
DATA.